WCAP-13963 - Rev. 1

SCALING LOGIC FOR THE CORE MAKEUP TANK TEST

L. E. Hochreiter
K. G. Serafini
D. Aumiller

Westinghouse Electric Corporation
Energy Systems
P. O. Box 355
Pittsburgh, Pennsylvania 15230

AP600 DOCUMENT COVER SHEET

TDC: _____ IDS: I _____ S _____

Form 58202G(5/94)

AP600 CENTRAL FILE USE ONLY:

0058.FRM

RFS#: RFS ITEM #:

AP600 DOCUMENT NO.	REVISION NO.		ASSIGNED TO
MT01-TGR-001	1	Page 1 of (XXX)	

ALTERNATE DOCUMENT NUMBER: WCAP-13963 WORK BREAKDOWN #: 2.6.18.2

DESIGN AGENT ORGANIZATION: WESTINGHOUSE

TITLE: SCALING LOGIC FOR THE CORE MAKEUP TANK TEST

ATTACHMENTS:	DCP #/REV. INCORPORATED IN THIS DOCUMENT REVISION: N/A
CALCULATION/ANALYSIS REFERENCE:	

ELECTRONIC FILENAME	ELECTRONIC FILE FORMAT	ELECTRONIC FILE DESCRIPTION
U:\1628W.WPF	WordPerfect 5.2 WINDOWS	DOCUMENT TEXT AND FIGURES
U:\1628.FRM	WordPerfect 5.2 WINDOWS	COVER SHEET

☐ WESTINGHOUSE PROPRIETARY CLASS 2

This document contains information proprietary to Westinghouse Electric Corporation; it is submitted in confidence and is to be used solely for the purpose for which it is furnished and returned upon request. This document and such information is not to be reproduced, transmitted, disclosed or used otherwise in whole or in part without prior written authorization of Westinghouse Electric Corporation, Energy Systems Business Unit, subject to the legends contained hereof.

☐ WESTINGHOUSE PROPRIETARY CLASS 2C

This document is the property of and contains Proprietary Information owned by Westinghouse Electric Corporation and/or its subcontractors and suppliers. It is transmitted to you in confidence and trust, and you agree to treat this document in strict accordance with the terms and conditions of the agreement under which it was provided to you.

☒ WESTINGHOUSE CLASS 3 (NON PROPRIETARY)

COMPLETE 1 IF WORK PERFORMED UNDER DESIGN CERTIFICATION OR COMPLETE 2 IF WORK PERFORMED UNDER FOAKE.

1 ☒ **DOE DESIGN CERTIFICATION PROGRAM** – GOVERNMENT LIMITED RIGHTS STATEMENT [See page 2]

Copyright statement: A license is reserved to the U.S. Government under contract DE-AC03-90SF18495.

☐ DOE CONTRACT DELIVERABLES (DELIVERED DATA)

Subject to specified exceptions, disclosure of this data is restricted until September 30, 1995 or Design Certification under DOE contract DE-AC03-90SF18495, whichever is later.

EPRI CONFIDENTIAL: NOTICE: 1 ☒ 2 ☐ 3 ☐ 4 ☐ 5 ☐ CATEGORY: A ☒ B ☐ C ☐ D ☐ E ☐ F ☐

2 ☐ **ARC FOAKE PROGRAM** – ARC LIMITED RIGHTS STATEMENT [See page 2]

Copyright statement: A license is reserved to the U.S. Government under contract DE-FC02-NE34267 and subcontract ARC-93-3-SC-001.

☐ ARC CONTRACT DELIVERABLES (CONTRACT DATA)

Subject to specified exceptions, disclosure of this data is restricted under ARC Subcontract ARC-93-3-SC-001.

ORIGINATOR	SIGNATURE/DATE	
L. E. Hochreiter	L E Hochreiter	1/30/95
AP600 RESPONSIBLE MANAGER	**SIGNATURE***	**APPROVAL DATE**
E. H. Novendstern	E H Novendstern	1-31-95

*Approval of the responsible manager signifies that document is complete, all required reviews are complete, electronic file is attached and document is released for use.

Form 58202G(5/94)

LIMITED RIGHTS STATEMENTS

DOE GOVERNMENT LIMITED RIGHTS STATEMENT

(A) These data are submitted with limited rights under government contract No. DE-AC03-90SF18495. These data may be reproduced and used by the government with the express limitation that they will not, without written permission of the contractor, be used for purposes of manufacturer nor disclosed outside the government; except that the government may disclose these data outside the government for the following purposes, if any, provided that the government makes such disclosure subject to prohibition against further use and disclosure:
   (I) This "Proprietary Data" may be disclosed for evaluation purposes under the restrictions above.
   (II) The "Proprietary Data" may be disclosed to the Electric Power Research Institute (EPRI), electric utility representatives and their direct consultants, excluding direct commercial competitors, and the DOE National Laboratories under the prohibitions and restrictions above.

(B) This notice shall be marked on any reproduction of these data, in whole or in part.

ARC LIMITED RIGHTS STATEMENT:

This proprietary data, furnished under Subcontract Number ARC-93-3-SC-001 with ARC may be duplicated and used by the government and ARC, subject to the limitations of Article H-17.F. of that subcontract, with the express limitations that the proprietary data may not be disclosed outside the government or ARC, or ARC's Class 1 & 3 members or EPRI or be used for purposes of manufacture without prior permission of the Subcontractor, except that further disclosure or use may be made solely for the following purposes:

This proprietary data may be disclosed to other than commercial competitors of Subcontractor for evaluation purposes of this subcontract under the restriction that the proprietary data be retained in confidence and not be further disclosed, and subject to the terms of a non-disclosure agreement between the Subcontractor and that organization, excluding DOE and its contractors.

DEFINITIONS

CONTRACT/DELIVERED DATA — Consists of documents (e.g. specifications, drawings, reports) which are generated under the DOE or ARC contracts which contain no background proprietary data.

EPRI CONFIDENTIALITY / OBLIGATION NOTICES

NOTICE 1: The data in this document is subject to no confidentiality obligations.

NOTICE 2: The data in this document is proprietary and confidential to Westinghouse Electric Corporation and/or its Contractors. It is forwarded to recipient under an obligation of Confidence and Trust for limited purposes only. Any use, disclosure to unauthorized persons, or copying of this document or parts thereof is prohibited except as agreed to in advance by the Electric Power Research Institute (EPRI) and Westinghouse Electric Corporation. Recipient of this data has a duty to inquire of EPRI and/or Westinghouse as to the uses of the information contained herein that are permitted.

NOTICE 3: The data in this document is proprietary and confidential to Westinghouse Electric Corporation and/or its Contractors. It is forwarded to recipient under an obligation of Confidence and Trust for use only in evaluation tasks specifically authorized by the Electric Power Research Institute (EPRI). Any use, disclosure to unauthorized persons, or copying this document or parts thereof is prohibited except as agreed to in advance by EPRI and Westinghouse Electric Corporation. Recipient of this data has a duty to inquire of EPRI and/or Westinghouse as to the uses of the information contained herein that are permitted. This document and any copies or excerpts thereof that may have been generated are to be returned to Westinghouse, directly or through EPRI, when requested to do so.

NOTICE 4: The data in this document is proprietary and confidential to Westinghouse Electric Corporation and/or its Contractors. It is being revealed in confidence and trust only to Employees of EPRI and to certain contractors of EPRI for limited evaluation tasks authorized by EPRI. Any use, disclosure to unauthorized persons, or copying of this document or parts thereof is prohibited. This Document and any copies or excerpts thereof that may have been generated are to be returned to Westinghouse, directly or through EPRI, when requested to do so.

NOTICE 5: The data in this document is proprietary and confidential to Westinghouse Electric Corporation and/or its Contractors. Access to this data is given in Confidence and Trust only at Westinghouse facilities for limited evaluation tasks assigned by EPRI. Any use, disclosure to unauthorized persons, or copying of this document or parts thereof is prohibited. Neither this document nor any excerpts therefrom are to be removed from Westinghouse facilities.

EPRI CONFIDENTIALITY / OBLIGATION CATEGORIES

CATEGORY "A" — (See Delivered Data) Consists of CONTRACTOR Foreground Data that is contained in an issued reported.

CATEGORY "B" — (See Delivered Data) Consists of CONTRACTOR Foreground Data that is not contained in an issued report, except for computer programs.

CATEGORY "C" — Consists of CONTRACTOR Background Data except for computer programs.

CATEGORY "D" — Consists of computer programs developed in the course of performing the Work.

CATEGORY "E" — Consists of computer programs developed prior to the Effective Date or after the Effective Date but outside the scope of the Work.

CATEGORY "F" — Consists of administrative plans and administrative reports.

TABLE OF CONTENTS

TABLE OF CONTENTS (Cont.)

LIST OF FIGURES

LIST OF FIGURES (Cont.)

LIST OF FIGURES (Cont.)

LIST OF FIGURES (Cont.)

LIST OF TABLES

ACRONYMS

ADS	Automatic depressurization system
CL	Cold leg
CMT	Core makeup tank
DAS	Data acquisition system
DVI	Direct vessel injection
IRWST	In-containment refueling water storage tank
L/D	Length over diameter
LOCA	Loss-of-coolant accident
MSLB	Main steamline break
RNS	Normal residual heat removal system
PCT	Peak cladding temperature
PIRT	Phenomena identification and ranking table
PRHR	Passive residual heat removal
PWR	Pressurized water reactor
RCP	Reactor coolant pump
RCS	Reactor coolant system
RTD	Resistance temperature detector
S	Safety injection signal
SGTR	Steam generator tube rupture
SSAR	Standard Safety Analysis Report
S/WR	Steam/water reservoir
TC	Thermocouple

ACKNOWLEDGEMENTS

The authors would like to acknowledge the excellent work performed by Dr. Jośe Reyes of Oregon State University in establishing clear guidelines and scaling criteria for complex two-phase flow system behavior. His scaling report on the AP600 low-pressure integral systems effects tests was used as a guide in this report. The authors also acknowledge the help and support given by E. J. Piplica, L. E. Conway, J. P. Cunningham, J. C. Butler, M. Roidt, B. E. Rarig, and L. G. McSwain in preparing and reviewing this report.

SUMMARY

The design and scaling logic of the Westinghouse core makeup tank (CMT) test has been performed to assess the test facility capability of representing the important thermal-hydraulic phenomena for CMT operation. The expected CMT phenomena have been identified in a phenomena identification and ranking table (PIRT) for the thermal-hydraulic processes that are expected to be of importance for the CMT. Estimates of the various expected phenomena are made and compared between the experiment and the prototype CMT. Scaling distortions of the CMT test are also described and assessed relative to the expected behavior of the AP600.

This revision of the CMT scaling report reflects the AP600 design changes that impact the CMT. Also, specific review comments made by the Nuclear Regulatory Commission (NRC) and Advisory Committee on Reactor Safeguards (ACRS) are addressed.

1.0 INTRODUCTION

1.1 Purpose

The purpose of this report is to establish that the CMT test will produce the necessary data to develop and verify the computer code models used to assess CMT performance for the AP600 design. The CMT test is a scaled, separate effects test in which the boundary conditions are controlled over a wide range to produce thermal-hydraulic conditions of interest for computer code verification.

Since the test is not full scale, compromises can exist between the test data and the application of the data to the AP600. The purposes of this document are to develop the scaling logic that supports the application of the data for code assessment; show that the key thermal-hydraulic phenomena of interest are reproduced in the test facility; and show that the test facility can be operated and controlled over a sufficiently broad range that captures all CMT modes of operation.

1.2 CMT Design and Operation

The AP600 design utilizes passive methods to perform core and containment cooling functions for a postulated loss-of-coolant accident (LOCA). The CMT, shown in Figure 1.2-1, is an important feature of the AP600 passive safety system. Each tank stores 2000 $ft.^3$ of cold borated water at reactor coolant system (RCS) pressure, which can be gravity-injected into the RCS to provide reactivity control and core cooling. The CMTs provide the same function as the high-pressure safety injection system in existing pressurized water reactors (PWRs), with the difference being that current plants require the availability of ac power to perform their safety function, whereas the CMTs perform this function using only gravity-driven flows.

The CMTs are connected to the RCS, as shown in Figure 1.2-1, by normally open isolation valves on the cold leg balance line and normally closed isolation valves on the CMT discharge line. The CMT discharge valves open on an safeguards (S-) signal and remain open. The CMTs are maintained at full system pressure by the cold leg balance line. During normal operation, the CMTs, as well as the cold leg balance line, are water solid.

The CMTs perform another safety function in addition to providing coolant and boron to the RCS. As the tanks continue to drain, they indicate that an unrecoverable LOCA has occurred. When approximately 33 percent of the tank liquid has drained, the CMT level sensing device activates the first stage of the automatic depressurization system (ADS), and the plant begins a controlled blowdown through the ADS valves into the in-containment refueling water storage tank (IRWST). The second- and third-stage ADS valves open on timers after the first stage has actuated. If the CMTs continue to drain and the CMT liquid volume reaches 20 percent, the fourth-stage ADS valves, which are located on the hot legs, open, providing a large vent path directly to containment to depressurize the RCS to containment pressure. During the RCS depressurization, the CMTs continue to add coolant to the RCS to maintain continued core cooling during the depressurization.

Each AP600 CMT, shown in Figure 1.2-2, is a 2000-ft.^{3} tank with hemispherical heads and a cylindrical shell. The hemispherical heads are stainless-steel-clad carbon steel (3/8-in. stainless cladding) with a total thickness of 4.6 in. The cylindrical portion of the tank is also stainless-steel-clad and is a total of 7.78-in. thick. The top of the tank is located 28 ft. above the RCS cold legs, providing a gravity head to drive the flow into the reactor vessel downcomer. The cold leg balance line is attached to the top of the CMT, and the drain line is at the bottom. The drain line is connected through an isolation valve and two check valves to the direct vessel injection (DVI) line. The cold leg balance line is an 8-in. Schedule 160 pipe with an inside diameter of 6.82 in. There is a normally open isolation valve near the top of this balance line. The AP600 piping schematic for the CMT and its balance line is shown in Figure 1.2-3.

The CMT design includes a diffuser that is located in the CMT inlet nozzle. The diffuser for the plant is shown in Figure 1.2-4 and consists of a pipe that extends into the CMT liquid and has flow holes to distribute the incoming cold leg balance line hot liquid or steam flow. The bottom of the diffuser is sealed so that the incoming flow enters the CMT horizontally in a radial direction through the flow holes. The purpose of the diffuser is to prevent the deep penetration of a steam jet into the CMT, which would result in good condensation. The radial flow limits mixing to the upper portion of the CMT liquid so that the condensation rates and duration are reduced. The scaling of this diffuser from the plant to the test facility is discussed in Section 3.2 of this report.

There are two modes of CMT operation for the CMTs: recirculation and draining. During the initial phase of a small-break LOCA, steam line break, or steam generator tube rupture (SGTR) event, the RCS inventory is at or near its steady-state value. When an S-signal occurs (typically low pressurizer pressure), the reactor coolant pumps (RCPs) trip and the CMT discharge isolation valve opens. A liquid circuit exists since the cold leg balance line is liquid-filled to the top of the CMT, and there is gravity-driven flow from the CMT to the reactor vessel and return flow from the cold leg to the top of the CMT. This is the recirculation phase of CMT operation. The colder, denser CMT water drives flow into the reactor vessel because of the density difference between the CMT water and the cold leg balance line (approximately 20 percent with reactor cold leg temperature at 550°F and CMT water at 120°F). Figure 1.2-5, from the *AP600 Standard Safety Analysis Report* (SSAR) calculations, shows the calculated CMT flow during the recirculation period for a 2-in. diameter cold leg break. This flow will continue and steadily decrease as the colder CMT water is replaced by hotter water from the balance line, thereby decreasing the gravity draining head. As the break continues to drain the RCS, the cold leg balance line begins to void, as seen in Figure 1.2-6; the recirculation flow path is broken; and the CMT drains as the water volume is replaced by steam from the cold leg. This begins the draining mode of the CMT. The CMT injection flow rate is larger in this mode because of the greater density difference between the colder CMT water and the steam or two-phase mixture in the balance line.

As a result of the recirculation mode, a hot, liquid layer is formed at the top of the CMT. This will reduce the steam condensation when the CMT transitions into the draining mode: the hot liquid layer

can flash as the RCS depressurizes, causing mixing and reducing the effects of condensation in the CMT. The thickness of this hot liquid layer is dependent upon the duration of the recirculation mode.

If the break is larger, the recirculation period is reduced because the cold leg balance line will void more rapidly, breaking natural circulation. In these cases, the hot liquid layer in the CMT will be less or may not exist. For large-break LOCAs, there is no recirculation period since the entire RCS voids quickly. The accumulators begin injecting very early in a large-break LOCA transient and have sufficient gas pressure to close the check valves in the CMT discharge line until the accumulators have completely injected their liquid inventory. The CMTs will begin injection after the accumulators are empty. By this time, the reactor vessel is refilled, the core peak cladding temperature (PCT) has been reached, and most, if not all, of the core has been quenched.

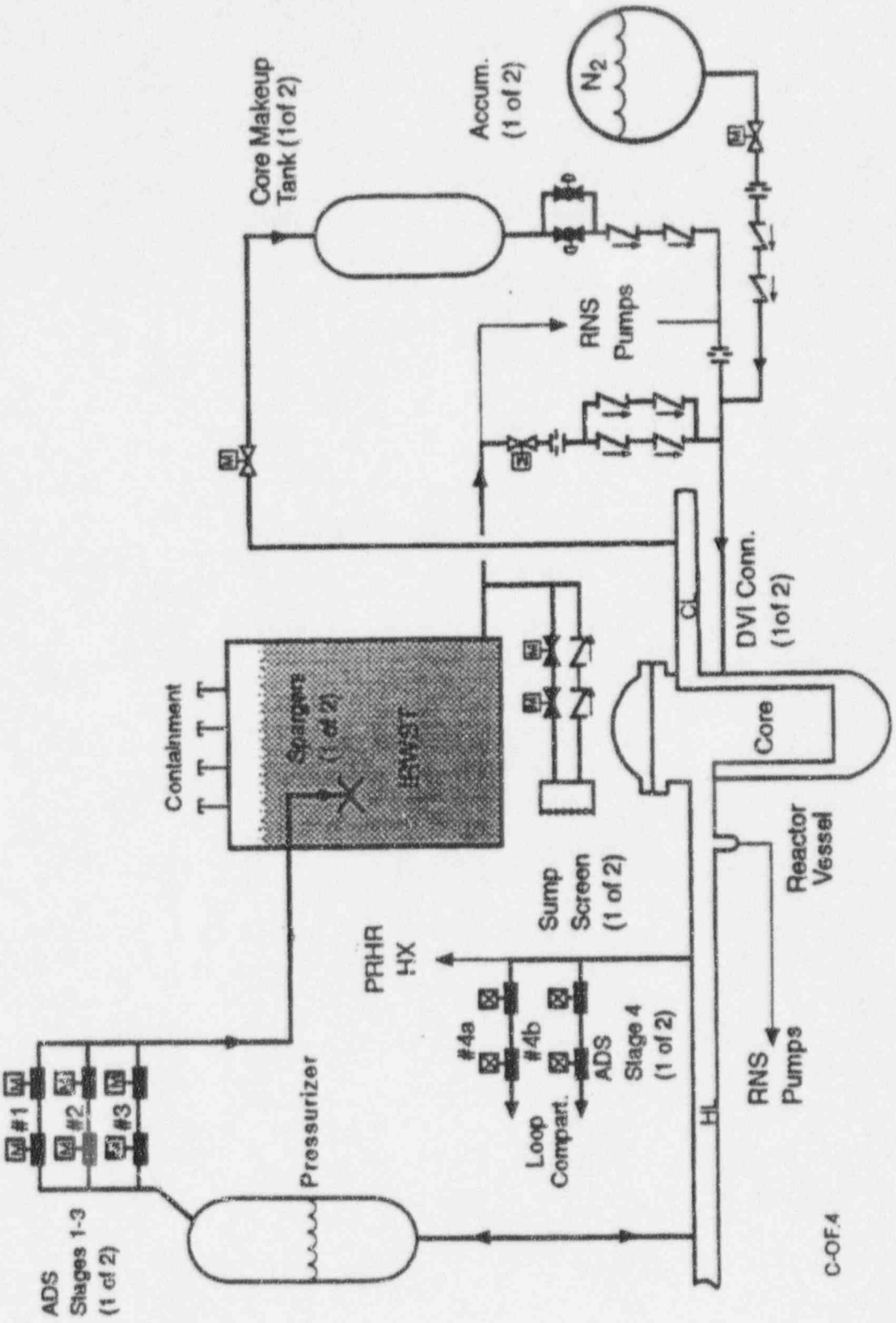

Figure 1.2-1 AP600 Passive Safety System Design

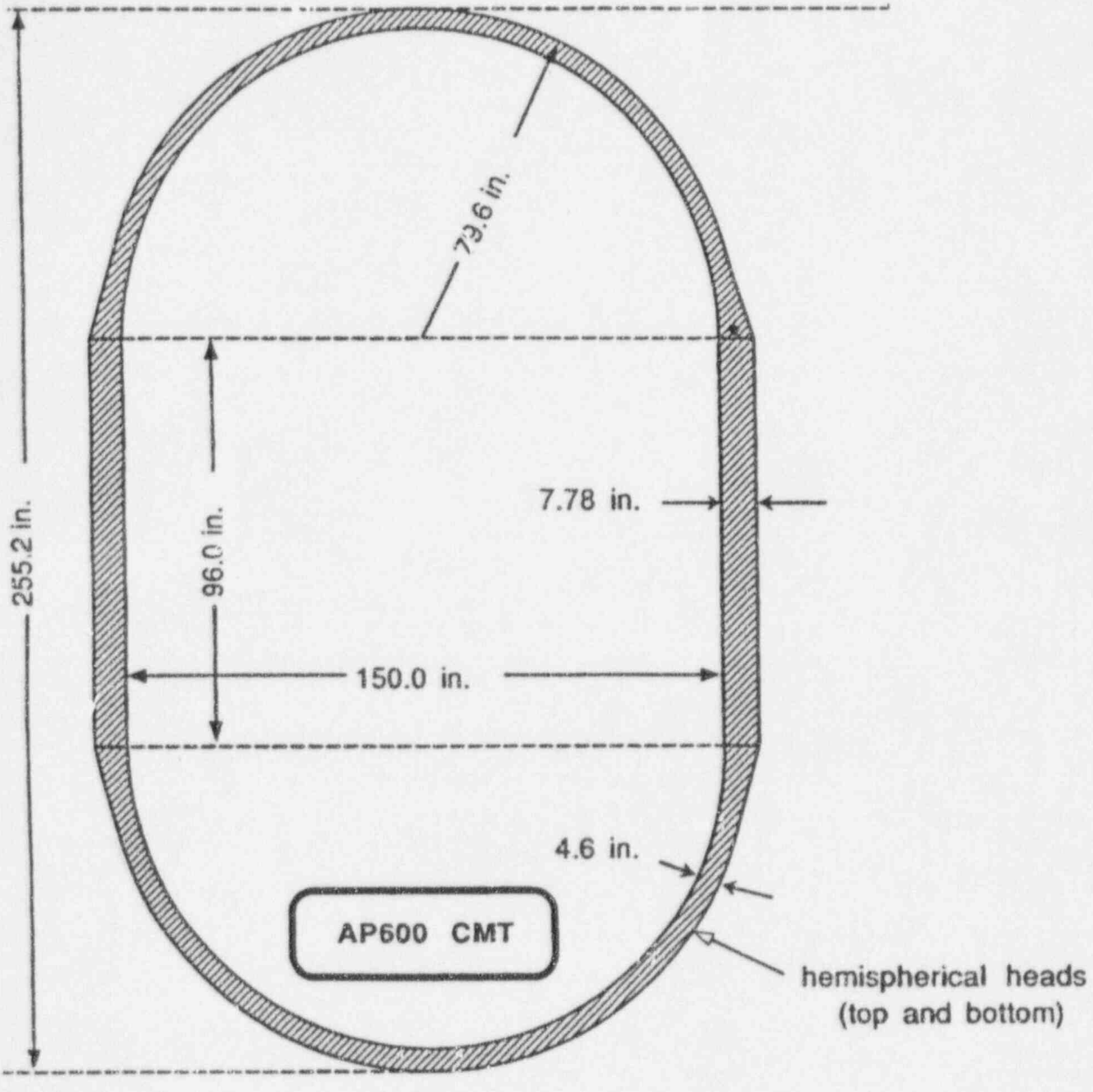

Figure 1.2-2 AP600 Core Makeup Tank

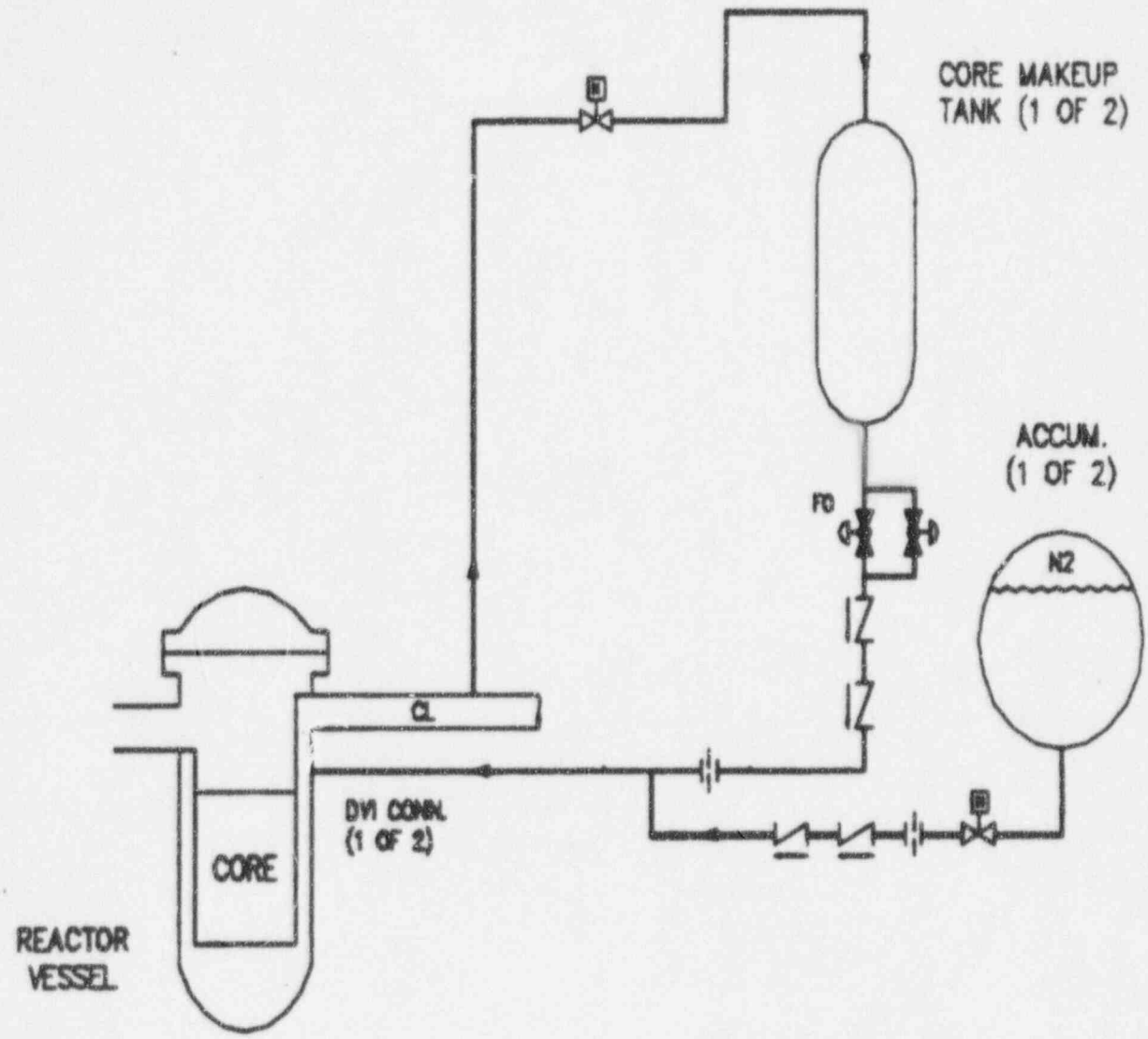

Figure 1.2-3 AP600 CMT Piping Layout

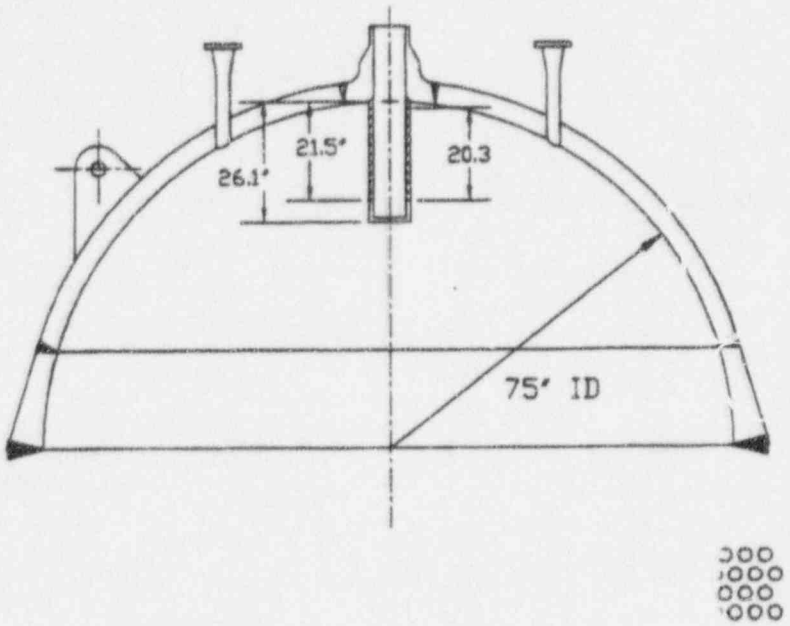

Figure 1.2-4 Plant CMT Diffuser

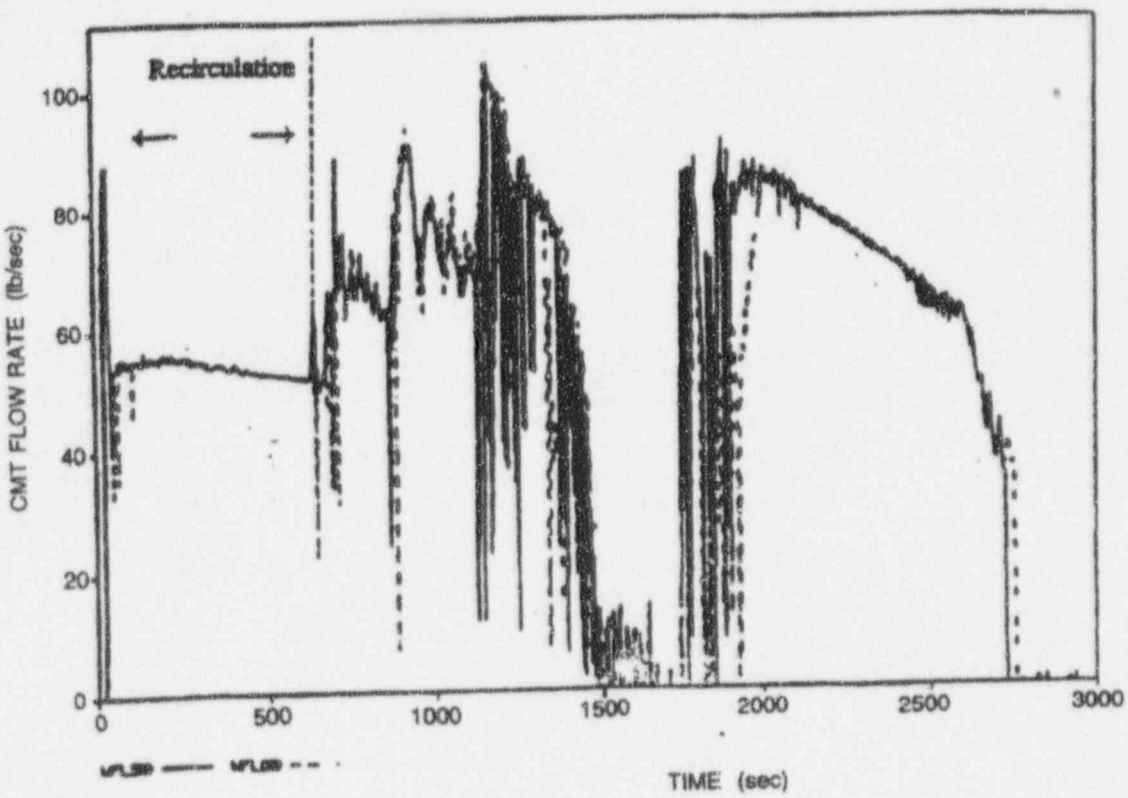

Figure 1.2-5 AP600 SSAR Calculation of CMT Draining Flow for 2-In. Cold Leg Break

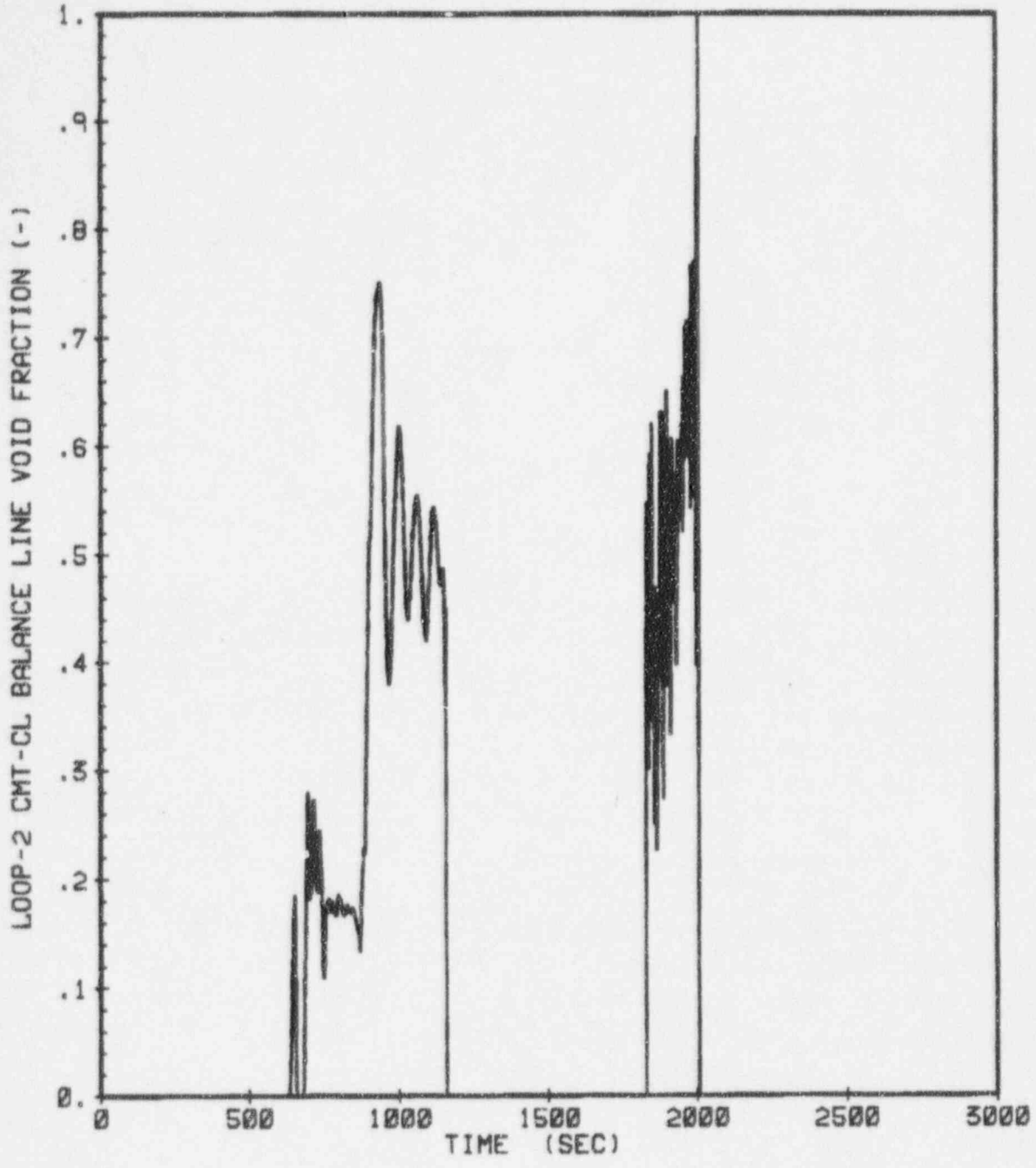

Figure 1.2-6 Cold Leg Balance Line Void Fraction for 2-in. Cold Leg Break

1.3 Description of the CMT Test Facility

The Westinghouse CMT test facility consists of an instrumented test vessel that simulates the CMT and a liquid/steam reservoir that simulates the remainder of the RCS. Connecting lines are provided to supply steam and/or liquid to the top of the CMT, as well as a drain line to allow flow out of the bottom of the CMT. A source of saturated steam, consisting of a high-pressure steam generator and accumulator, is connected to the liquid/steam reservoir. The test apparatus is shown schematically in Figure 1.3-1. A data acquisition system (DAS) is provided to record signals from thermocouples, pressure sensors, and flow meters.

The CMT test vessel is a vertically mounted, uninsulated carbon steel pressure vessel with an inside height of 115 in. The cylindrical portion of the vessel is constructed of 24-in. Schedule 160 pipe with an inside diameter of 19.312 in. and a wall thickness of 2.34 in. The pipe is capped on either end with 2:1 semi-elliptical heads with a wall thickness of 2.5 in. The height of the heads represents only about 4 percent of the total tank height. The vessel is elevated above the liquid/steam reservoir water level so that the gravity draining head is equivalent to that for the AP600 CMTs.

The steam/water reservoir (S/WR) is a vertically mounted, insulated carbon steel pressure vessel. The reservoir acts as the source of steam and/or liquid flow to the CMT and accommodates the CMT liquid discharge. The location of the reservoir permits simple gravity drain of the CMT test vessel through the discharge line. The reservoir supplies saturated liquid or steam to the top of the CMT test vessel through two steam lines. The reservoir is connected to a saturated steam source consisting of a high-pressure steam generator and accumulators. A pressure control valve between the steam accumulators and the S/WR allows the reservoir pressure to be maintained at any desired pressure over the range of 20 to 2250 psia.

The CMT test facility piping simulates the primary features of the plant RCS cold leg to CMT balance line and discharge line piping from the bottom of the CMT to the reactor vessel. The three primary CMT test facility piping runs are referred to as steam line no. 1, steam line no. 2, and the CMT discharge line; all three piping runs are constructed of 1.5-in., Schedule 160 seamless carbon steel pipe.

Steam line no. 1 represents the RCS cold leg balance line and is used to supply steam to the CMT for selected matrix tests. Steam line no. 1 is routed vertically from the S/WR upper head to a high point so no condensation can be trapped in the line; steam line no. 1 is connected to a S/WR nozzle, which is flush with the inside surface of the vessel. A 3-in. vortex flowmeter section is installed in the vertical portion of steam line no. 1 to provide a measurement of the steam flow to the CMT. As the vortex flowmeter is rated for a maximum operating pressure of 1500 psig, a 1.5-in., Schedule 160 piping spoolpiece is installed in place of the flow section for tests conducted at higher pressures. From the high point, steam line no. 1 slopes slightly downward to the CMT inlet and is designed and supported such that, as the pipe is heated during testing, the run will remain sloped towards the CMT. A 2-in. globe valve is provided in steam line no. 1 to permit isolation of steam flow through steam

line no. 1 during test operation. A 2-in. gate valve is also installed between the CMT and the globe valve to permit isolation of the CMT from the steam supply.

Steam line no. 2 also represents the RCS cold leg to CMT balance line. Steam line no. 2 is routed from the S/WR to the CMT such that it intersects with steam line no. 1 approximately 2 ft. upstream of the CMT inlet elbow. Steam line no. 2 extends 4 ft. into the S/WR so its end is below the "HI" reservoir water level setpoint but above the "LOW" reservoir water level setpoint; adjusting the S/WR liquid level allows either liquid or steam to flow through steam line no. 2. A 2-in. globe valve is provided in steam line no. 2 for flow isolation during test operations. A 3-in. vortex flowmeter section can also be installed in steam line no. 2 to provide a measurement of the steam flow to the CMT; a 1.5-in., Schedule 160 piping spoolpiece is installed in place of the flow section to permit testing at pressures higher than 1500 psig.

Steam line no. 2 is heat-traced and insulated from the S/WR to the "tee" with steam line no. 1. The trace heating provides sufficient power to heat the piping to saturation temperature over the full range of test pressures. The pipe run is also insulated with 4 in. of high-temperature fiberglass insulation.

Steam line no. 1 and steam line no. 2 intersect at a tee upstream of the CMT inlet elbow. A triple-flange arrangement is used at the CMT inlet nozzle to permit installation of the CMT steam distributor, which is designed to redirect and reduce the velocity of steam as it enters the CMT. The CMT steam distributor inlet nozzle used during testing is shown in Figure 1.3-2.

A 0.5-in. drain line is provided on the downstream or CMT side of the steam line no. 2 isolation valve. This drain line connects to the CMT discharge line returning to the S/WR and is used to ensure that no condensate collects in the vertical run that intersects with steam line no. 1.

Vents are provided in the steam line piping to provide for simulation of ADS depressurization; the vents are also used to trace heat the piping and vent condensate collected during facility startup.

The CMT test vessel discharge line represents the CMT discharge/direct vessel injection (DVI) line in the AP600. The CMT discharge line connects to a flanged nozzle in the center of the lower CMT head and runs vertically downward to within 12 in. of the floor and horizontally back to the S/WR. As the CMT drains by gravity, no portion of the discharge piping is located above the level of the CMT outlet.

A manual 1.5-in. globe valve is located in the vertical run near floor level. This valve can be used to preset the discharge line resistance to obtain a predetermined draindown rate or to isolate the CMT discharge line. Normally, the globe valve is set to its full-open position and the CMT discharge line isolation valve is then adjusted to provide the remaining line resistance necessary to achieve the desired drain rate for a specific test.

The CMT drain rate is measured using a 1-in. turbine flowmeter with a range of 2 to 75 gpm, located in the horizontal section of the discharge line. Since steam flow is detrimental to the turbine bearings, the turbine flowmeter is located in the lowest section of the discharge line so the flowmeter is always full of water as the CMT drains.

A single full-port swing check valve is installed in the discharge line downstream of the turbine flowmeter. The check valve is installed such that it prevents backflow from the S/WR to the CMT. A 2-in. isolation valve, similar to those installed in steam lines no. 1 and no. 2, is installed in the discharge line downstream of the check valve. The isolation valve is used to initiate the tests by allowing water to drain from the CMT.

The CMT vessel is highly instrumented with 5 sets of wall thermocouples, 41 fluid thermocouples, and 7 differential pressure cells for level measurements. The CMT wall temperature measurements consist of four sets located in the CMT cylindrical shell and one set located on the upper head. Each of the four sets located in the cylindrical shell consists of five thermocouples radially located with respect to the CMT inner wall surface; the thermocouples are positioned at the inner wall surface 0.125, 0.500, and 1.500 in. from the wall inner surface and at the wall outer surface. The inner and outer surface thermocouples are brazed into grooves cut into the CMT wall surfaces. The thermocouples within the vessel wall are placed in flat-bottomed holes and peened into place using copper disks to provide good thermal response. The set of wa" hermocouples located in the CMT upper head consists of two thermocouples: one at the vessel wall inner surface and the other at the wall outer surface adjacent to the inside wall thermocouple. All CMT wall thermocouples in a given set are located at the same axial position so a radial temperature profile can be measured through the CMT wall and can be fitted numerically to calculate the inner wall heat flux.

The fluid thermocouples are arranged in groups to detect thermal stratification and the presence of a hot liquid layer. Thermocouples are located at different radial positions at selected elevations within the tank. The differential pressure cells are arranged in levels to obtain the collapsed liquid level within the tank so the transient tank inventory can be measured.

There are also liquid flow measurements on the CMT discharge, absolute pressure cells on the tank and piping, as well as pressure drop measurements on the steam lines that have been calibrated to obtain steam flow. Pressure measurements and controls also exist on the steam supply system.

The CMT instrumentation is designed to provide the necessary measurements to calculate a transient mass and energy balance for the facility.

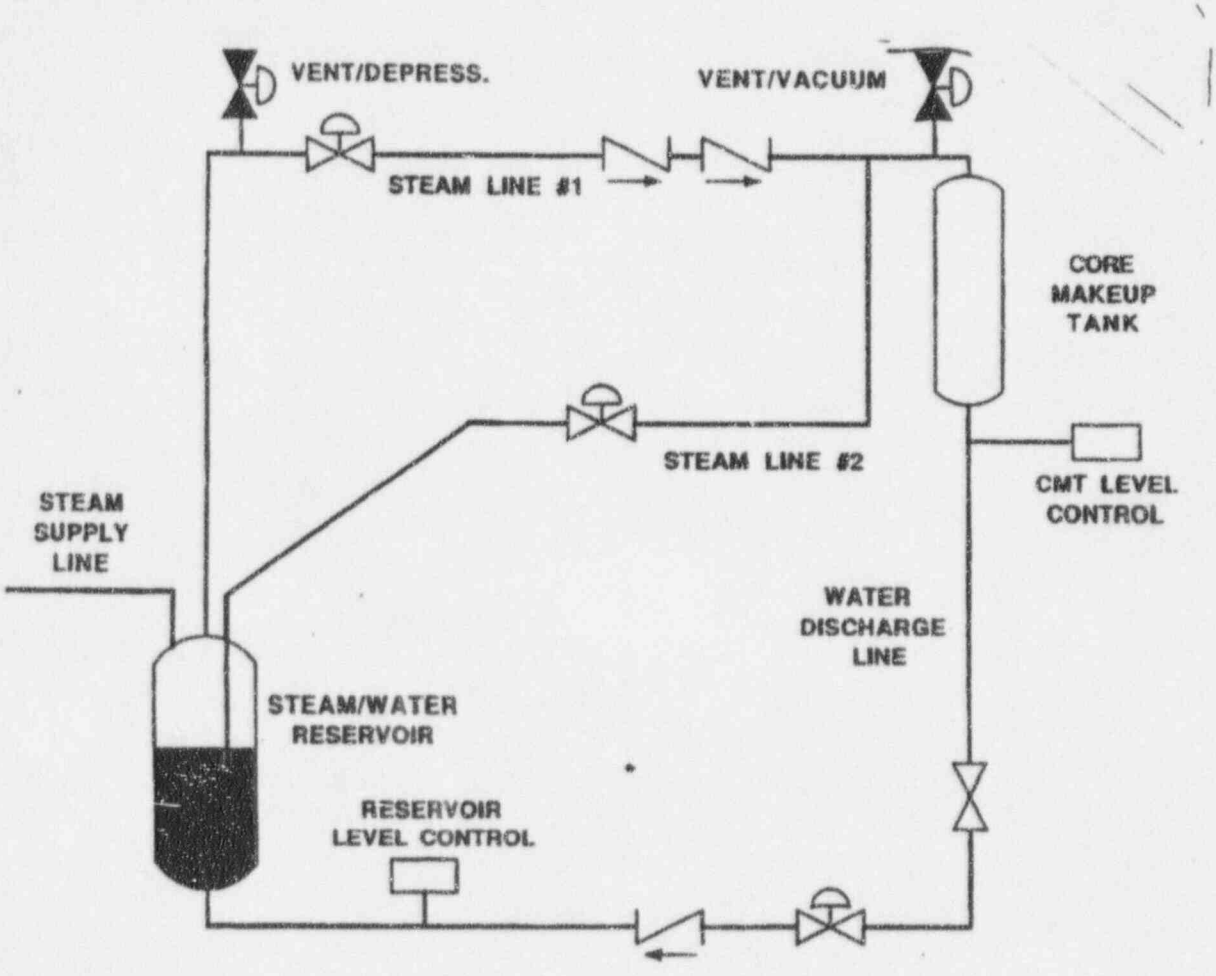

Figure 1.3-1 AP600 CMT Test Facility

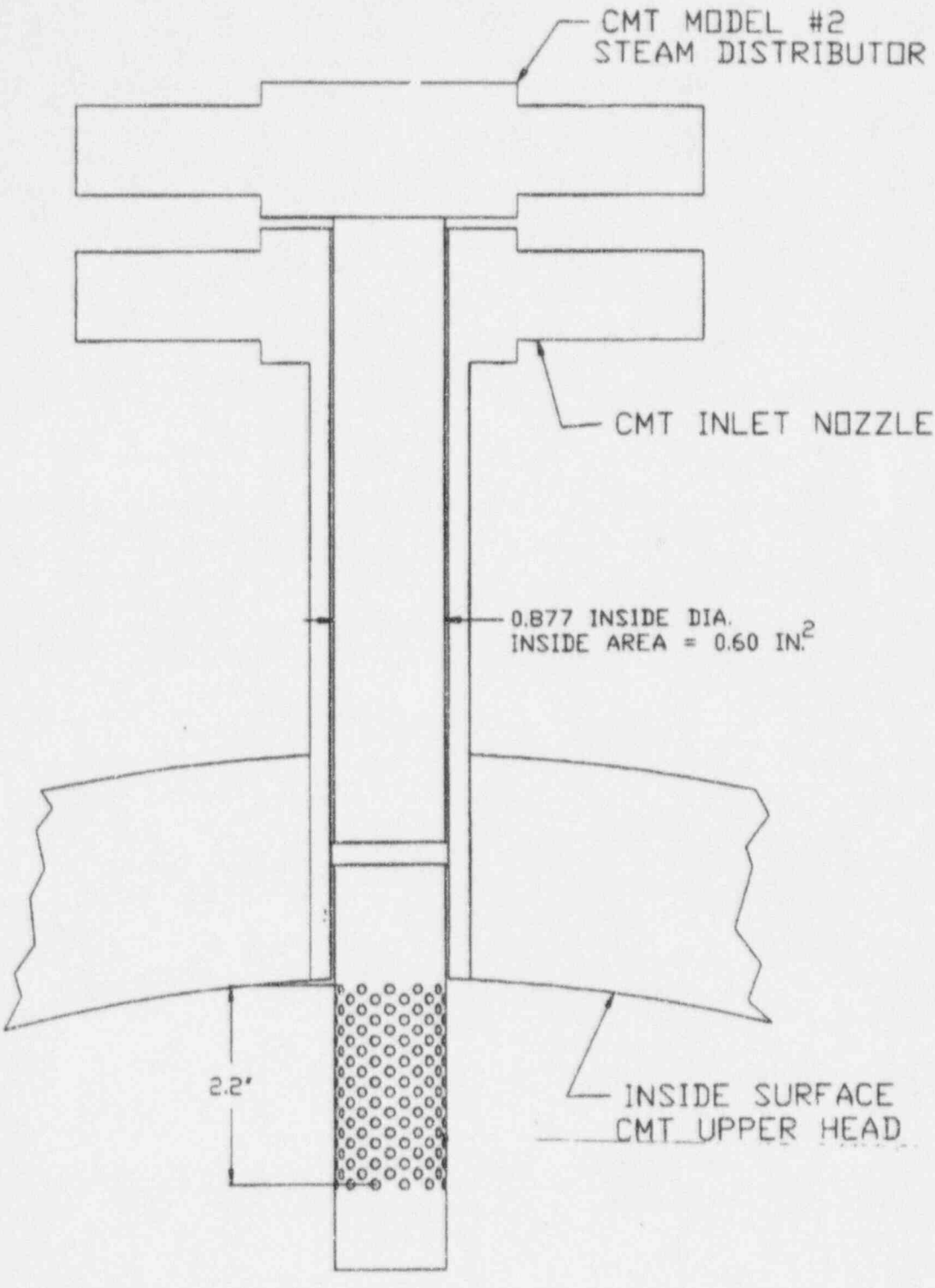

Figure 1.3-2 Steam Distributor Used in CMT Tests

1.4 Phenomena Identification and Ranking Table (PIRT) for the CMT

This section identifies and discusses the thermal-hydraulic phenomena captured by the CMT test and provides the ranking of those phenomena. These phenomena are grouped into two modes of operation for the CMT: recirculation and draining.

1.4.1 CMT Recirculation Thermal-Hydraulic Phenomena

The CMT recirculation is driven by the density difference between the cold CMT water and the hot cold leg balance line water. The recirculation provides colder, denser water to the reactor vessel from the CMT, and is replaced by hot, less dense cold leg water from the balance line. There is a net mass transfer from the CMT to the RCS due to the density difference, as well as a net energy transfer from the RCS back to the CMT. The rates of energy and mass transfer will depend on the buoyant differences and the hydraulic resistances in the flow path. The recirculating flow continuously diminishes with time as the CMT heats up and the buoyant head decreases. As the cold leg piping and cold leg balance line void, the buoyant head increases, thereby increasing the discharge flow as the tank begins to drain. Both single-phase and two-phase recirculation will occur for small-break LOCAs. Single-phase recirculation will occur for steam line breaks and steam generator tube ruptures.

CMT wall heat transfer occurs during recirculation as the hot fluid from the cold leg balance line transfers heat to the initially cold CMT walls. The heat transfer from the hot recirculating fluid to the colder CMT walls will heat the walls, and at the same time, cool the recirculating fluid. Circulation patterns within the hot liquid layer will be established, whereby the cooler water at the walls flows downward and mixes within the layer. The CMT walls heat up as the flow recirculates, and the potential for large wall condensation to occur is reduced when the CMT drains. Also, if the CMT walls become fully heated and the RCS depressurizes, heat transfers from the CMT walls back to the fluid in the tank. Because the walls are thick, the amount of heat transfer to the walls will be scenario-dependent.

Fluid mixing occurs at the top of the CMT during the recirculational phase of the transient. The hot liquid from the cold leg balance line will be injected into the CMT through the diffuser at the top of the CMT and will mix with the initially cold water in the CMT. A stratified hot liquid layer develops so the draining behavior is one dimensional in nature, and conduction effects between fluid layers are negligible while the convection effects appear to dominate.

As recirculation continues during a small-break LOCA, the cold leg balance lines begin to void and a two-phase mixture enters the CMTs. Depending on how long recirculation has occurred, the temperature of the CMT wall and the mixed liquid layer at the top of the CMT is dependent upon the duration of the recirculation phase. If the liquid layer and the CMT walls are hot, there will be limited condensation, the vapor will collect at the top of the CMT, the natural circulation flow path will be broken, and draining will begin. If the walls and liquid are cold, condensation will occur, drawing

more two-phase mixture up the balance line to the CMT, water recirculation can be re-established, and intermittent recirculation can occur.

1.4.2 CMT Draining Phenomena

The CMT draining is the flow of liquid from the bottom of the CMT with a corresponding decrease in the water volume in the CMT. As the CMT begins to drain, it can uncover CMT metal surfaces, which may be cold or warm depending upon the duration of the recirculation phase. Depending upon the wall temperature, various amounts of steam will be condensed. The thick CMT walls will soon become conduction-limited so the condensation rate is determined by the CMT wall temperature distribution, surface area, thickness, and degree of preheating during the recirculation phase.

Direct or contact condensation can also occur in the CMT water and on the steam/water interface as the tank drains. The amount of condensation will be a function of the water temperature, and the velocity of the steam as it mixes with the CMT water, and the flow of condensate from the walls to the liquid interface. The thickness of a hot liquid layer will also influence the interfacial condensation, since it will tend to insulate the colder CMT water from the steam flow. The location of the liquid level relative to the CMT inlet diffuser also influences the amount of condensation since the steam flows radially from the diffuser and mixes with the CMT liquid layer, increasing the amount of condensation. If the liquid is subcooled, the rapid condensation increases and draws more steam flow into the CMT. As the CMTs continue to drain, all of the above effects, which enhance interfacial heat transfer, diminish, and a thicker, warm liquid layer forms both from the direct interfacial heat transfer and from the tank wall condensate. This layer of hot condensate can later flashes during RCS depressurization when the later stages of the ADS valves open and the CMT depressurizes. The flashing will further enhance the mixing in this hot layer and pressurizes the top of the CMT so the delivery is increased. Once the additional cold CMT wall area is exposed, the additional steam generated from the flashing condenses and is recycled back to the liquid layer.

As the CMT drains there will be some liquid-to-liquid mixing; however, this effect is believed to be small since the system is in a thermally stable operating mode with the hot layer on the top. Also, as the CMT drains, heat is transferred from the hotter liquid layer to the CMT walls by convection. The amount of heat transfer that occurs depends upon the thickness of the hotter layer, its temperature, the draining rate, and the CMT wall initial temperature. If the convection from the hot liquid layer heats the CMT walls, the condensation heat transfer from the steam is reduced once the walls uncover.

1.4.3 CMT PIRT of Key Thermal-Hydraulic Phenomena

From the above discussion, a PIRT can be generated for the CMT. This is similar to the CMT phenomena table developed by Cozzuol, Fisher, and Boucher[1] and the PIRT developed by J. Reyes[2] for the AP600 low-pressure integral test at Oregon State University. The relative ranking is given for different accident scenarios in which the CMTs play an important role. The PIRT for the CMT phenomena is given in Table 1.4-1. As seen from the table, different scenarios are dominated by

different CMT operating modes. The large-break LOCA CMT behavior is dominated by the CMT draining behavior since recirculation does not have an opportunity to occur. Conversely, the CMT behavior for the main steam line break (MSLB) and steam generator tube rupture (SGTR) events is dominated by the recirculation phase of CMT operation since only a small amount, if any, CMT draindown occurs.

Depending upon the break size, the small-break LOCA spans both modes of operation of the CMT. For small breaks of 4 in. or less, there is ample recirculation in the CMT such that a thick, heated liquid layer forms. For larger small breaks of 6 to 10 in., such as the double-ended guillotine of the cold leg balance line, the RCS quickly depressurizes and the recirculation time period is significantly reduced. For breaks of this size and larger, the recirculation is very limited, and condensation can occur as the CMT drains. Thus, for the large-break model the recirculation period is important and a MSLB and STGR model could be less precise for the draindown period is less important. However, the small-break LOCA code must be able to model both CMT operational modes.

TABLE 1.4-1
PHENOMENA IDENTIFICATION AND RANKING TABLE (PIRT) FOR THE AP600 CMT

Phenomena	Large-Break LOCA	Small-Break LOCA	MSLB	SGTR
CMT Draining Effects				
• Condensation on cold thick steel surfaces	H	H	L	L
• Transient conduction in CMT walls	H	H	L	L
• Interfacial condensation on CMT water surface	H	H	M	M
• Dynamic effects of steam injection and mixing with CMT liquid and condensate	H	H	M	M
• Thermal stratification and mixing of warmer condensate with colder CMT water	H	H	M	M
CMT Recirculation				
• Natural circulation of CMT and cold leg balance leg	L	H	H	H
• Liquid mixing of cold leg balance leg, condensate, and CMT liquid	L	H	H	H
• Flashing effects of hot CMT liquid layer	L	H	L	L
• CMT wall heat transfer	L	M	M	M

Notes:
L = low importance
M = medium importance
H = high importance

2.0 CMT RECIRCULATION BEHAVIOR SCALING ASSESSMENT

In the recirculation mode of operation, the cold borated CMT water is replaced with hot water that flows up the cold leg balance line to the top of the CMT. The CMT remains full during this period. Flow continues until the CMT is fully heated and the natural circulation driving head decreases to zero.

2.1 CMT Recirculation Behavior

Both top-down and bottom-up scaling analyses have been performed to assess the capability of the CMT test to provide the key thermal-hydraulic data for the CMT recirculation period. This section will develop the governing equations and examine the scaling differences between the AP600 plant CMT and the CMT test facility to ensure that the key thermal-hydraulic phenomena presented in the PIRT are captured in the CMT test.

2.1.1 CMT Recirculation Behavior—Top-Down Analysis

Natural circulation behavior has been examined by Reyes for the Oregon State University AP600 low-pressure integral system effects tests. The general governing equations derived for the top-down scaling for single-phase recirculation are applicable for the single-phase recirculation of the CMT. The generalized system of equations that describe the natural circulation behavior is given in Equations 2.1-1 to 2.1-5, as:

Mass:

$$\frac{d}{dt}\left(\rho_f V_f\right) = \Delta\left[\rho_f Q_f\right] \tag{2.1-1}$$

Momentum:

$$\frac{d}{dt}\left(\rho_f U_f V_f\right) = \Delta\left[\rho_f U_f Q_f\right] + \beta_v g \rho_f \Delta T_f \ell a_c - \frac{\rho_f U_f Q_f}{2}\left(\frac{f L_f}{D_h} + K\right) \tag{2.1-2}$$

Energy:

$$\frac{d}{dt}\left(\rho_f C_{vf} T_f V_f\right) = \Delta\left[\rho_f C_{pf} T_f Q_f\right] + H_s A_s \left(T_s - T_f\right)\Big|_{Boundary} \tag{2.1-3}$$

Solid energy equation:

$$-k_s A_s \left(\frac{dT_s}{dx} \right)_{Boundary} = H_s A_s (T_s - T_\ell)|_{Boundary} \qquad (2.1\text{-}4)$$

Boundary condition:

$$\frac{d}{dt} (\rho_s C_{vs} T_s V_s) = H_s A_s (T_s - T_\ell)|_{Boundary} + q_s \qquad (2.1\text{-}5)$$

The nomenclature for these equations is provided in Section 8.1.

If these equations are normalized on their initial conditions and any boundary conditions designated with the subscript 0, the normalized equations expressed with the superscript + symbol become:

Mass:

$$\tau_{\ell,0} \frac{d}{dt} \left(\rho_\ell^+ V_\ell^+ \right) = \Delta \left[\rho_\ell^+ Q_\ell^+ \right] \qquad (2.1\text{-}6)$$

Momentum:

$$\tau_{\ell,0} \frac{d}{dt} \left(\rho_\ell^+ U_\ell^+ V_\ell^+ \right) = \Delta \left[\rho_\ell^+ U_\ell^+ Q_\ell^+ \right] + \Pi_{Ri} (\beta_T \rho_\ell \Delta T_\ell g a_c)^+ - \Pi_F \left(\frac{\rho_\ell^+ U_\ell^+ Q_\ell^+}{2} \right) \left(\frac{f\ell}{D_h} + K \right)^+ \qquad (2.1\text{-}7)$$

Energy:

$$\frac{\tau_{\ell,0}}{\gamma_0} \frac{d}{dt} \left(\rho_\ell^+ C_{v\ell}^+ T_\ell^+ V_\ell^+ \right) = \Delta \left[\rho_\ell^+ C_{p\ell}^+ T_\ell^+ Q_\ell^+ \right] + \Pi_{St} \Theta H_s^+ A_s^+ (T_s - T_\ell)^+|_{Boundary} \qquad (2.1\text{-}8)$$

Solid energy equation:

$$\frac{\tau_{s,0}}{\Theta_s} \frac{d}{dt} \left(\rho_s^+ C_{vs}^+ T_s^+ V_s^+ \right) = H_s^+ A_s^+ (T_s - T_\ell)^+|_{Boundary} + \Pi_{qt} q_s^+ \qquad (2.1\text{-}9)$$

Boundary condition:

$$-k_s^* A_s^* \left.\frac{dT_s^*}{dx^*}\right|_{Boundary} = \Pi_{Bi} \Theta_s H_s^* A_s^* \left(T_s - T_\ell\right)^* \Big|_{Boundary} \tag{2.1-10}$$

The characteristic Π time constant ratios are given below as:

Liquid residence time:

$$\tau_{\ell,0} = \frac{V_{\ell,0}}{Q_{\ell,0}} \tag{2.1-11}$$

and the solid-structure-specific frequency:

$$\frac{1}{\tau_{s,0}} = \frac{H_{s,0}}{\rho_{s,0} C_{vs,0} \delta} \tag{2.1-12}$$

The governing equations are time-dependent mass, momentum, and energy balances for the CMT. By examining the relative importance of the different terms in these equations, the system of equations can be simplified for the CMT recirculation phase of behavior. The drain rates for the plant CMT are estimated to be small relative to the mass inventory in the tank. The tank drains over several hundred-to-thousands of seconds, so that the liquid residence time is very large. Calculated recirculation flow rates for the plant are typically 50 lbm/sec, or 0.8 ft.^{3}/sec. Therefore, using Equation 2.1-11, the time to drain the 2000-ft.^{3} CMT is 2500 seconds. The problem is not highly time-dependent, and the temporal term in the momentum equation can be ignored; therefore, a quasi-steady state can be assumed.

The time constant for the solid-structure specific frequency given in Equation 2.1-12 will be different for the plant CMT and the CMT test due to the different wall thicknesses. Assuming that the heat transfer and fluid properties are the same, the test wall time constant, which is the inverse of Equation 2.1-12, is approximately 1/3 that of the plant CMT. As a result, the test CMT wall heats faster and has less thermal inertia than the plant walls. The heat transfer to the walls continues for a longer time period than in the plant CMT wall. The hot recirculated CMT liquid in the plant will cool to temperatures below that in the test due to the continued heat transfer to the walls. This has a secondary effect on the recirculation behavior of the test CMT relative to the plant CMT.

Characteristic time ratios:

$$\Pi_{Ri} = \frac{\beta_{T,0} g \Delta T_0 \ell}{U_0^2}$$ Richardson number (2.1-13)

$$\Pi_F = \left(\frac{f\ell}{D_h} + K \right)$$ Friction number (2.1-14)

$$\Pi_{St} = \frac{H_{s,0} A_{s,0}}{C_{pl,0} \rho_{l,0} U_{l,0} a_{c,0}}$$ Stanton number (2.1-15)

$$\Pi_{qll} = \frac{q_{s,0}\ \ell_0}{U_{l,0} \rho_{s,0} C_{vs,0} (T_s - T_l)_0 V_{s,0}}$$ Liquid heat source ratio (2.1-16)

$$\Pi_q = \frac{q_{s,0}}{H_{s,0} A_{s,0} (T_s - T_l)_0}$$ Heat source ratio (2.1-17)

$$\Pi_{Bi} = \frac{H_{s,0} \delta}{k_{s,0}}$$ Biot number (2.1-18)

Temperature ratios:

$$\Theta = \frac{(T_s - T_l)_0}{T_{l,0}} \qquad \Theta_s = \frac{(T_s - T_l)_0}{T_{s,0}}$$ (2.1-19)

Specific heat ratio:

$$\gamma_{l,0} = \frac{C_{pl,0}}{C_{vl,0}}$$ (2.1-20)

To preserve the recirculation flow behavior between the plant CMT and the test, the ratios of the Richardson numbers, which represent the buoyant driving head, and the Friction numbers, which represent the hydraulic losses in the system, must be preserved. Therefore, these ratios become:

$$\frac{\Pi_{Ri})_m}{\Pi_{Ri})_p} = 1 = \Pi_{Ri})_R$$ (2.1-21)

$$\frac{\Pi_F)_m}{\Pi_F)_p} = 1 = \Pi_F)_R \qquad (2.1\text{-}22)$$

where the subscript m refers to the CMT test and the subscript p refers to the plant. The momentum flux term shown in Equation 2.1-7 will be dependent on the resulting flow rate and the temperatures simulated in the test relative to the plant CMT. The preservation of the dimensionless Richardson and Friction groups will preserve the flow between the model and the plant CMT. Performing the tests at prototypical temperature and pressure conditions will preserve the fluid density differences and hence, the momentum flux.

Therefore, the momentum balance becomes a balance between the buoyant forces and the frictional forces given as:

$$\Delta\left[\rho_i^* Q_i^*\right] = 0 \qquad (2.1\text{-}23)$$

and:

$$\Delta\left[\rho_i^* U_i^* Q_i^*\right] + \Pi_{Ri}\ (\beta_T g \rho_i \Delta T_i \ell a_c)^* = \Pi_F \left[\frac{\rho_i^* U_i^* Q_i^*}{2}\right]\left(\frac{f\ell}{D_h} + K\right)^* \qquad (2.1\text{-}24)$$

Since the fluid properties and the height of the CMT test relative to the plant are preserved and the friction and form losses are also preserved, the $\Pi_{F)_R}$ and $\Pi_{Ri)_R}$ is close to one. Therefore, the test gives recirculation performance similar to the plant. The bottom-up scaling analysis and calculations verifies the CMT test recirculation performance relative to the plant CMT.

2.1.2 CMT Recirculation Behavior—Bottom-Up Scaling Analysis

The bottom-up scaling analysis calculates the recirculation performance of both the plant and the CMT test to verifying that similarity of performance exists between the two CMTs. Figure 2.1-1 shows a sketch of the CMT test relative to the plant. Note that the actual pipe routing is not fully represented in this sketch.

The assumptions used in this analysis are:

- Single-phase recirculation
- One-dimensional flow
- Linear interpolation of the density gradient in the CMT
- Linear interpolation of the density gradient in the CMT test reservoir
- Essentially zero velocity in the reactor vessel downcomer annulus

- Loss coefficients are independent of Reynolds number
- Quasi-steady-state conditions

The generalized mechanical energy balance equation (see Bennett and Meyer)[3] is given as:

$$\frac{\Delta P}{\rho} + \frac{\Delta U_b^2}{2g_c} + \left(\frac{f\ell}{D_h} + K\right)\frac{U_b^2}{2g_c} + \frac{g}{g_c}\Delta L + W_s = 0 \qquad (2.1\text{-}25)$$

where W_s is the rate of shaft work and is set to zero. Since the starting point and end point of the calculations are the same, then:

$$\frac{\Delta P}{\rho} = 0 \qquad (2.1\text{-}26)$$

Expanding Equation 2.1-25 around the piping network and using the component density gives:

$$\frac{\rho_2 U_{DVI}^2}{2g_c} - \frac{\rho_1 U_{CL}^2}{2g_c} + \left(K_{CL_n} + \frac{f\ell}{D_h}\right)_{CL}\rho_1\frac{U_{CL}^2}{2g_c} + \left(K_T + K_{CMT_n} + \frac{f\ell}{D_h}\right)_{BL}\rho_1\frac{U_{BL}^2}{2g_c} + \left(K_{CMT_{ex}} + K_{CKV} + K_{DVI_n} + \frac{f\ell}{D_h}\right)_{DVI}\rho_2\frac{U_{DVI}^2}{2g_c} + \frac{g}{g_c}\rho_1 L - \frac{g}{g_c}\rho_2 L = 0 \qquad (2.1\text{-}27)$$

where ρ_1 is the hot RCS and balance line flow, and ρ_2 is the cold CMT fluid density state.

The form loss coefficients and velocities are defined in the nomenclature in Section 8.1. The pressure loss of the inlet diffuser is included in the nozzle loss for the CMT.

Equation 2.1-27 can be further simplified, noting that the volume flow is preserved:

$$U_{CL}A_{CL} = U_{BL}A_{BL} = U_{DVI}A_{DVI} = Q_4 \qquad (2.1\text{-}28)$$

Transposing the gravity-head term to the left side of the equation and using Equation 2.1-28, the system Equation 2.1-27 becomes:

$$\frac{g}{g_c}L(\rho_2 - \rho_1) = \frac{Q_t^2}{2g_c}\left\{\left[\left[K_{CL_N} + \frac{f\ell}{D_h}\right)_{CL} - 1\right]\frac{\rho_1}{A_{CL}^2} + \right.$$

$$\left[K_T + K_{CMT_N} + \frac{f\ell}{D_h}\right)_{BL}\Bigg]\frac{\rho_1}{A_{BL}^2} + \qquad (2.1\text{-}29)$$

$$\left.\left[K_{CMT_{ex}} + K_{CKV} + K_{DVI_N} + \frac{f\ell}{D_h}\right)_{DVI}\Bigg]\frac{\rho_2}{A_{DVI}^2}\right\}$$

As the CMT recirculates, the top of the CMT will fill with the less dense, hot fluid from the cold leg at density ρ_1. Recirculation will end when all of the denser liquid, ρ_2, has been replaced with the less dense ρ_1 fluid. To represent the decrease in the driving head, the buoyant term becomes:

$$\frac{g}{g_c}\left[\left\{(L - L_1)\rho_2 + L_1\rho_1\right\} - \rho_1 L\right] \qquad (2.1\text{-}30)$$

which simplifies to:

$$\frac{g}{g_c}\left[(L - L_1)(\rho_2 - \rho_1)\right] \qquad (2.1\text{-}31)$$

where L_1 is the height of less dense liquid ρ_1 in the CMT, and L is the overall height. This expression has the correct limits since at the beginning of recirculation, L_1=0, and the full driving head is available, while when L_1=L, there is no driving head and recirculation ends.

The value of L_1 can be calculated as:

$$L_1 = \int_0^t \frac{\dot{m}(t)\,dt}{\rho_1 A_{CMT}} \qquad (2.1\text{-}32)$$

where A_{CMT} is a function of L_1 for the CMT heads and $\dot{m}(t)$ is the mass flow into the CMT. Equation 2.1-32 must be solved in an iterative fashion for the CMT head volume but can be directly solved for the cylindrical portion.

A similar calculation is used for the S/WR in the CMT test since the volume is much smaller than the volume of the reactor system. In this case, the driving head will also decrease as the reservoir fills with the denser ρ_2 fluid. This will result in a faster decreasing circulation rate for the CMT test, relative to the plant. In the plant, the cold CMT water that enters the downcomer can fall or flow downward to the core inlet. There is less of a chance that it would act to diminish the driving head, as in the CMT test.

The hydraulic resistances for the experiment were measured in the pre-operational tests and were found to be very close to standard textbook values. The current design values for the plant CMT balance line and DVI line resistances were used, as well as an estimate for the reverse flow cold leg nozzle loss and the DVI nozzle expansion. Equations 2.1-29, 2.1-31, and 2.1-32 were programmed for the plant CMT and the test facility.

Figure 2.1-2 shows the mean flow rate as a function of time for the plant CMT balance line circuit. Figure 2.1-3 shows the development of the hot, less dense fluid level in the CMT as it recirculates. The dominant terms in the plant CMT mass flow equation are the form losses in the circuit. The frictional terms are second-order effects.

The same figures are shown for the CMT test facility. Figure 2.1-4 shows the mass flow rate as a function of time for the CMT test circuit. Figure 2.1-5 shows the development of the hot liquid layer in the CMT test vessel. The dominant terms in the CMT test are the line frictional losses since there are many more length over diameters (L/Ds) in the test facility than in the plant.

The dimensionless ratio of interest in the recirculation phase is the mass flux ratio (ρv) in the cold leg balance line. Since full-height and full-pressure simulation is preserved, this ratio is close to unity if the resistances were maintained between the test and the plant.

Figure 2.1-6 show the recirculation mass flux ratio of the CMT test to the plant at 1100 psia. As the figure indicates, the CMT recirculates at ~90 percent of the mass flux of the plant; then as time increases, it decreases to ~80 percent. This is due to the increase in the cold level in the test reservoir, which decreases the test driving head relative to the plant. As a result, the mass flow decreases at a faster rate in the test than in the plant. The calculated hot liquid layers in the CMT test reservoir and the plant CMT are shown in Figure 2.1-7 at 1100 psia. Similar response occurs for the first 250 seconds between the test and plant, after which the hot liquid layer builds up faster in the test than in the plant. Figures 2.1-6 and 2.1-7 are repeated at 2250 psia conditions in Figures 2.1-8 and 2.1-9 for high-pressure performance of the CMTs (more typical of operational transients), and similar behavior is observed.

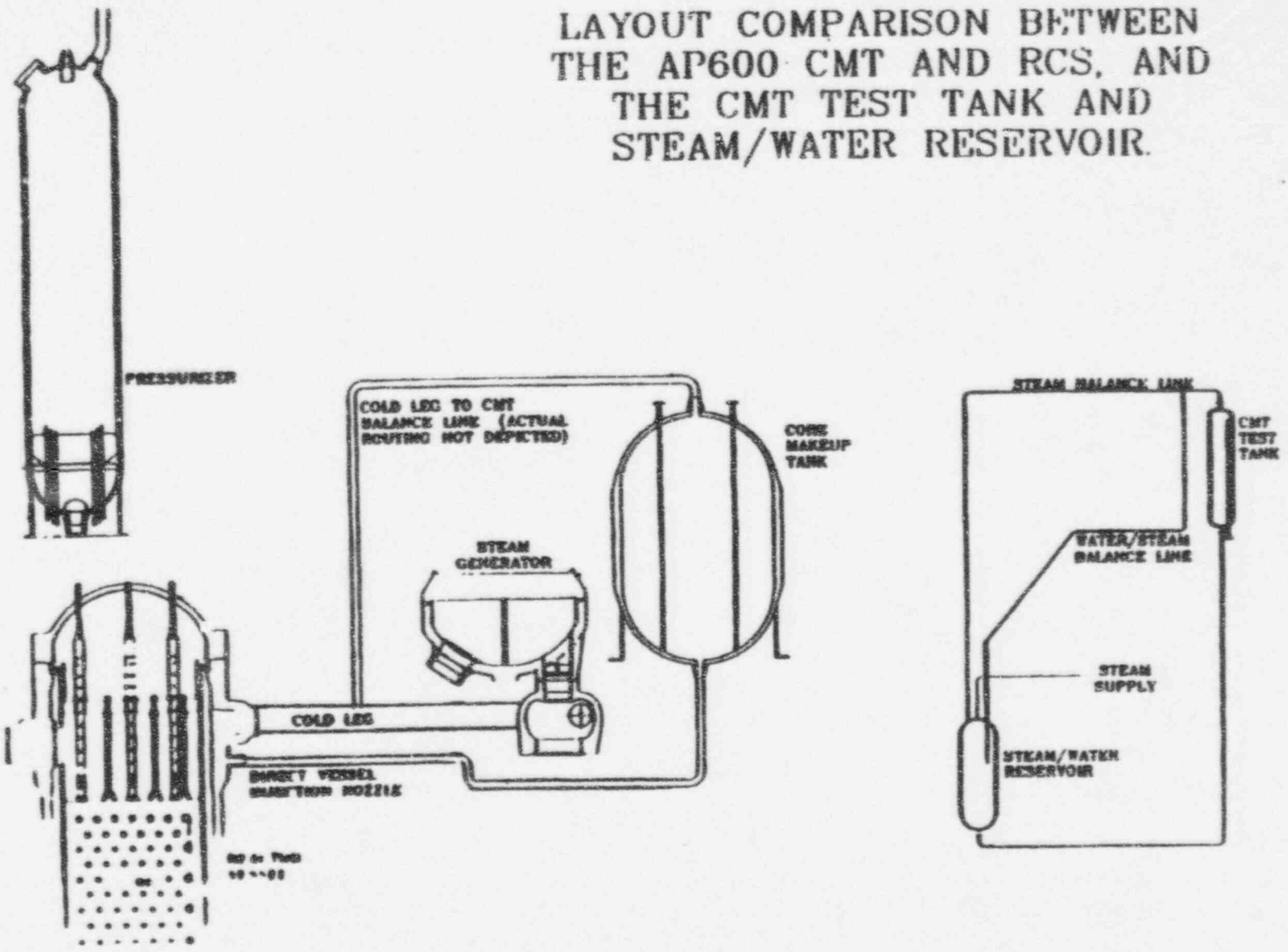

Figure 2.1-1 CMT Test Facility and AP600 Plant

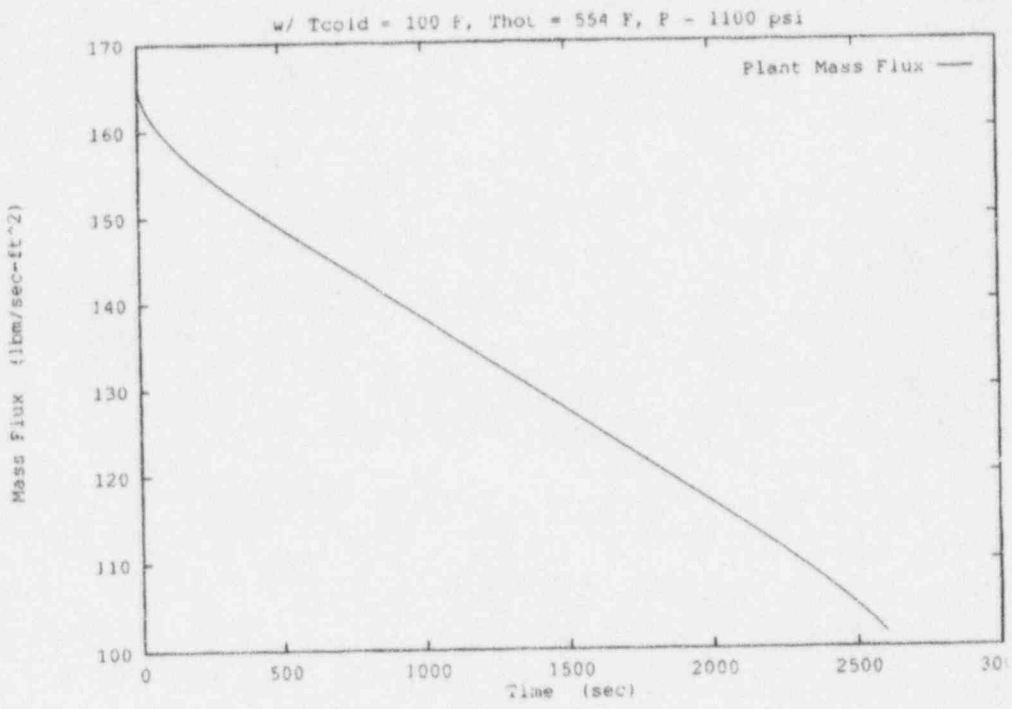

Figure 2.1-2 Calculated Recirculation Flow for the AP600 Plant CMT at 1100 psia

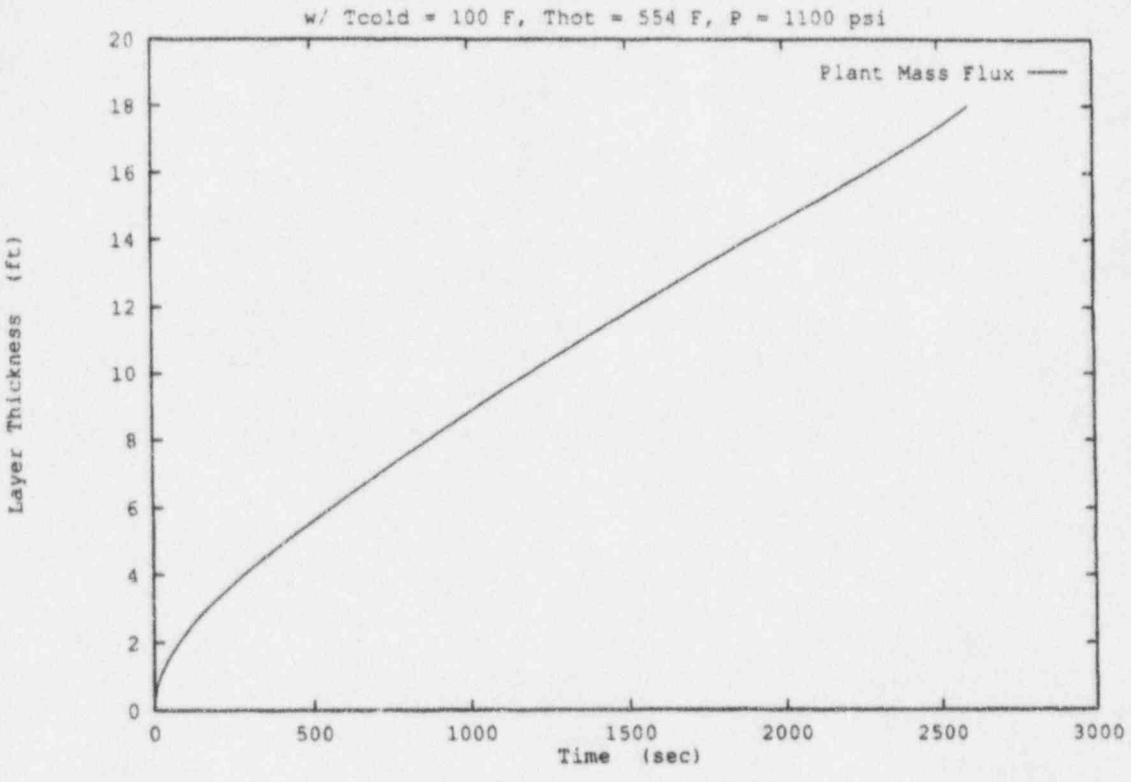

Figure 2.1-3 Calculation of the Hot Liquid Layer Thickness for the AP600 Plant CMT at 1100 psia

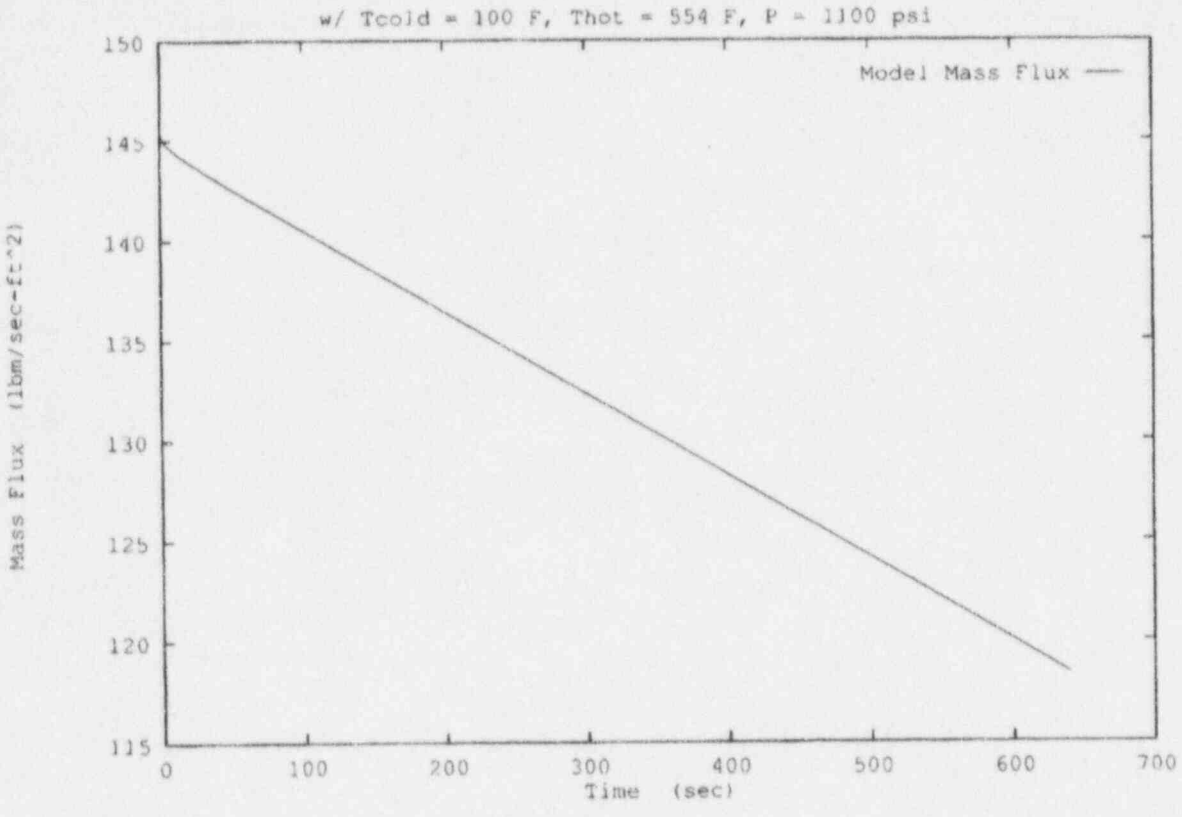

Figure 2.1-4 Calculated Recirculation Flow for the CMT Test Facility at 1100 psia

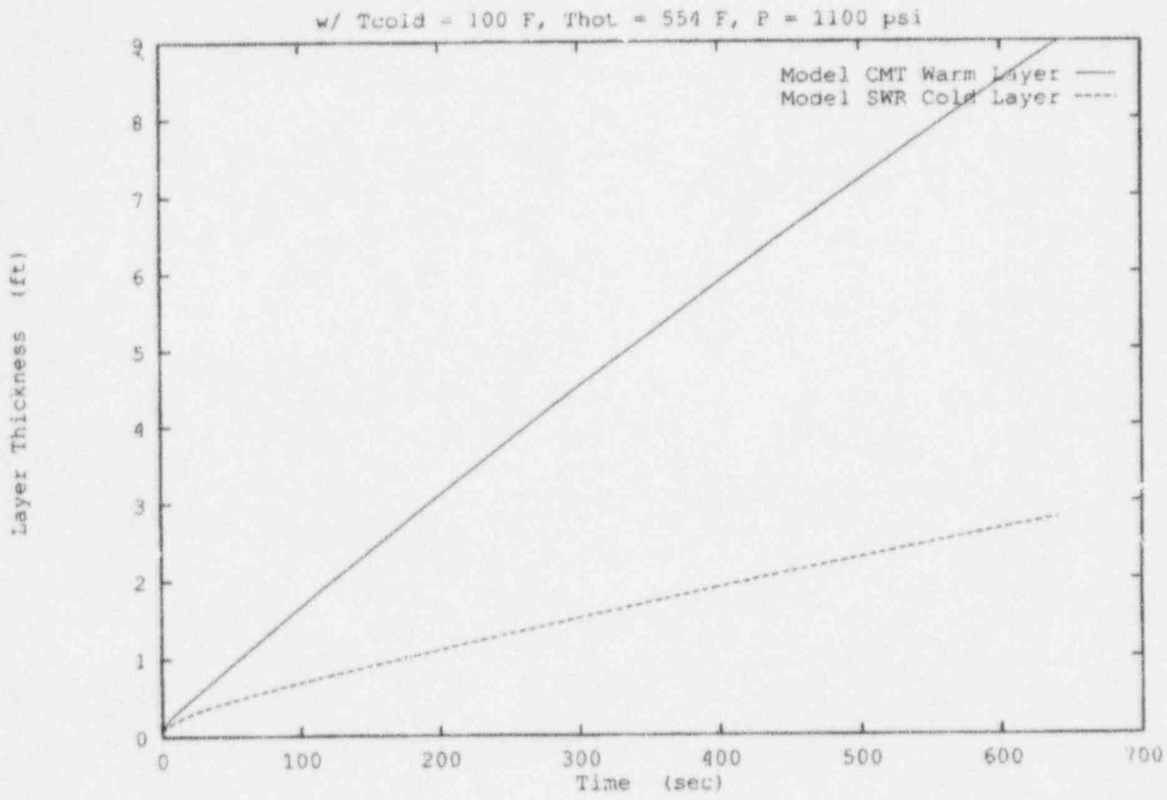

Figure 2.1-5 **Calculation of the Hot Liquid Layer Thickness for the CMT Test Facility and Cold Liquid Layer Thickness in the Reservoir at 1100 psia**

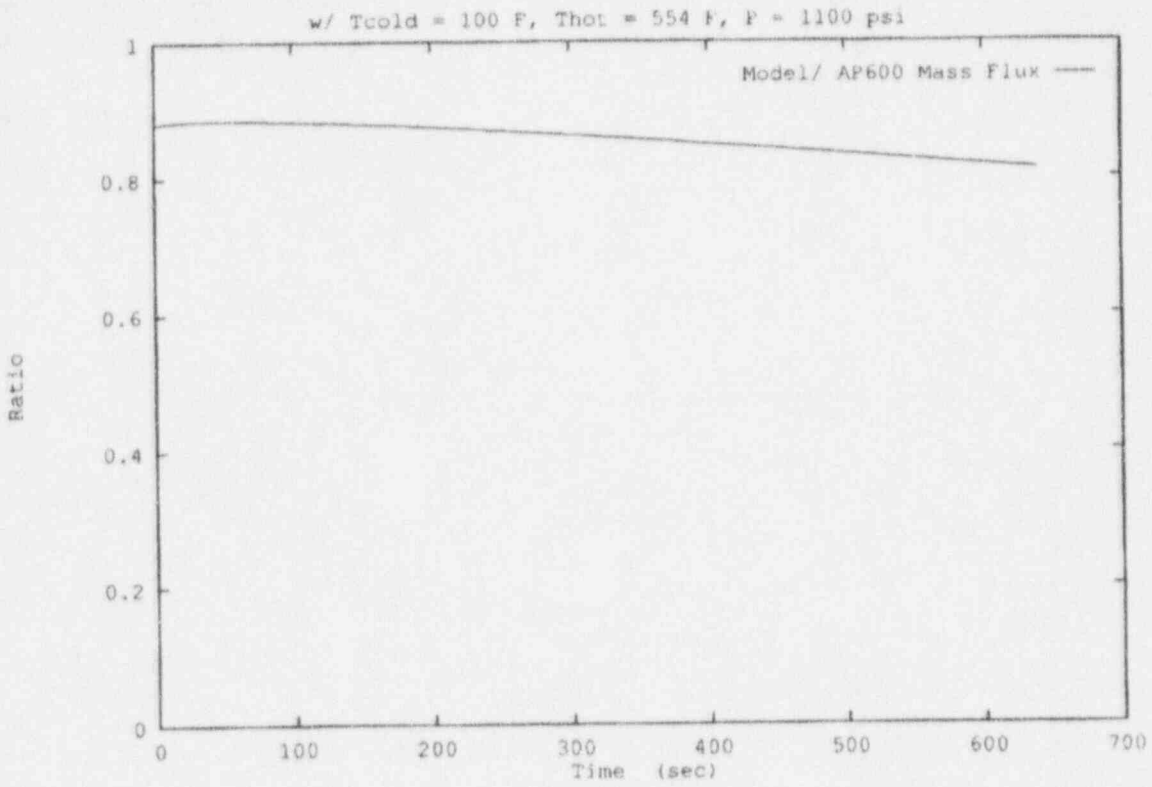

Figure 2.1-6 Recirculation Ratio of the CMT Test to the AP600 Plant CMT at 1100 psia

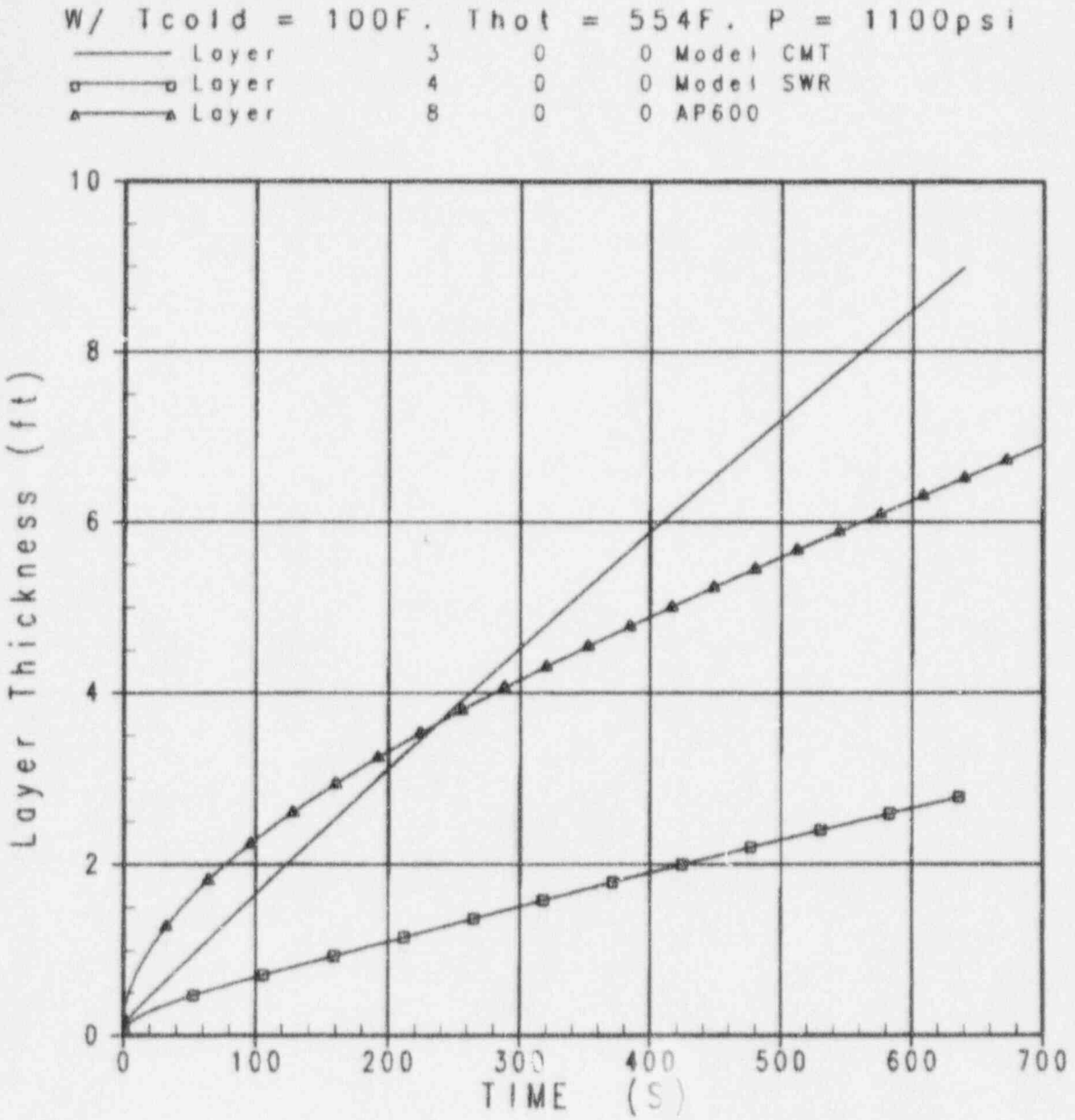

Figure 2.1-7 Comparison of the Hot Layer Thickness of the CMT Test and the AP600 Plant CMT at 1100 psia

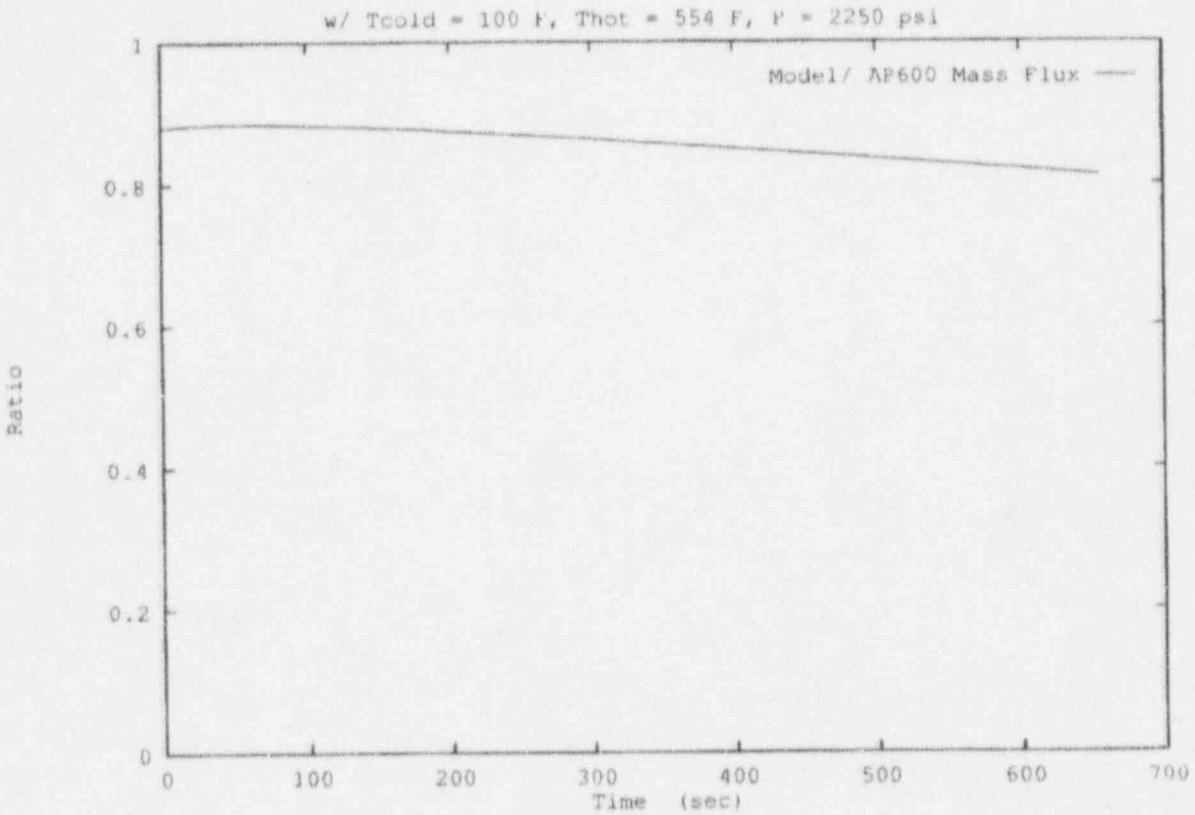

Figure 2.1-8 Recirculation Ratio of the CMT Test to the AP600 Plant CMT at 2250 psia

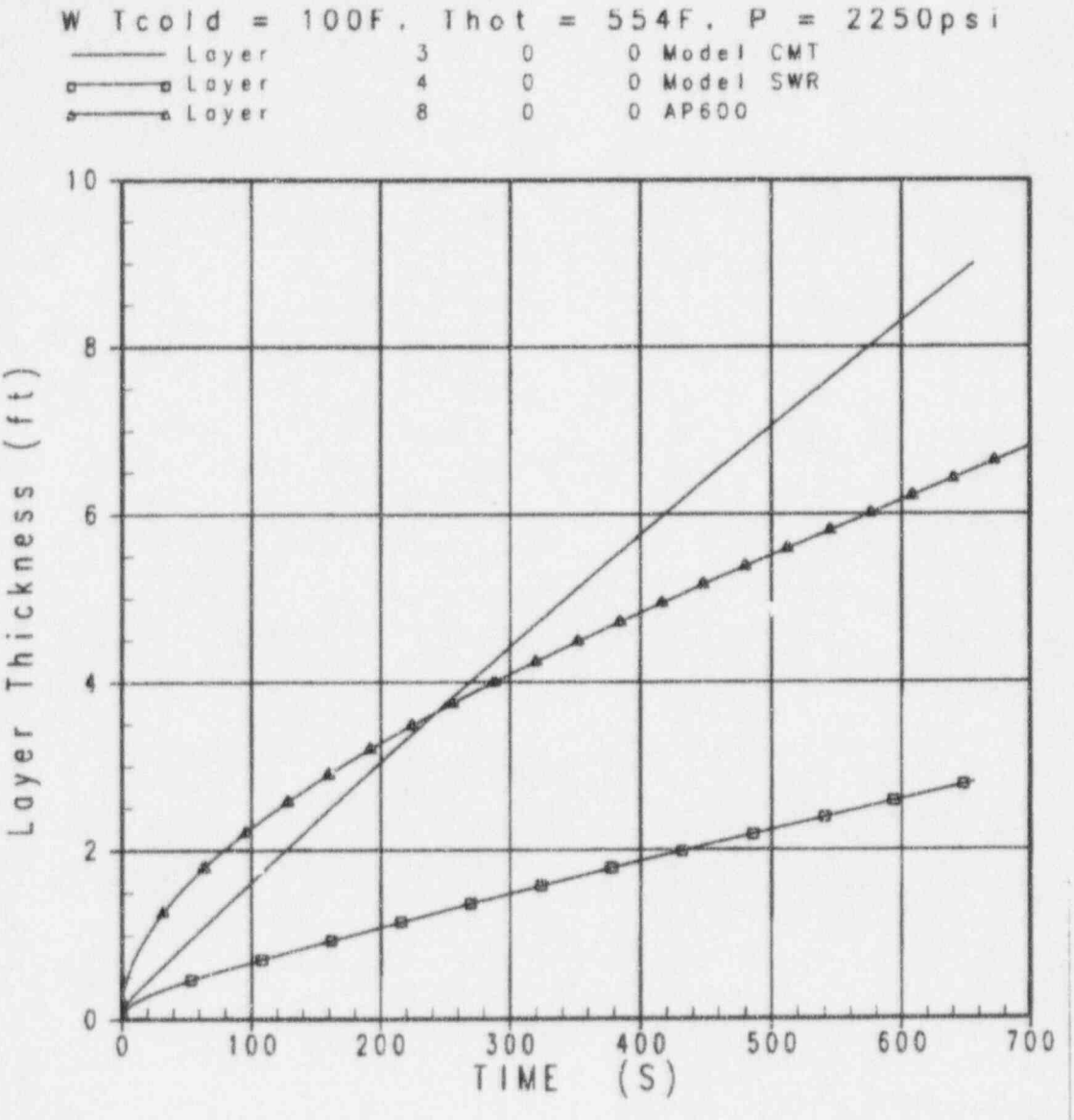

Figure 2.1-9 Comparison of the Hot Layer Thickness of the CMT Test and AP600 Plant at 2250 psia

2.2 Discussion of CMT Recirculation Scaling

Since the CMT test can simulate the full-pressure and temperature operation of the plant, the density differences are preserved. Since the heights are preserved, the buoyant expression given by the Richardson number in Equation 2.1-13 is preserved between the test and the plant, such that the Richardson number ratio $\Pi_{Ri}\big)_R \equiv 1$, as given in Equation 2.1-21. This is confirmed by the ratio of the CMT mass flux, which is near unity.

The plant resistances plant are calculated design values, not measured, which are approximated by the test. Also, the resistances in the test are dominated by frictional pressure drop, not form losses, which would make them more flow- or Reynolds-number-dependent. That is, as the flow decreases, the Reynolds number will decrease, increasing the friction factor. This effect, however, is second order, so the ratio $\Pi_{f}\big)_R \equiv 1$ between the test and the plant CMT.

A more significant effect is the buildup of the cold liquid layer in the S/WR tank in the test. There is no counterpart for this component in the AP600 reactor systems since the flow from the CMT can enter the core. In the test, the increase in the cold liquid layer in the reservoir decreases the net driving head for the test recirculation, relative to the plant. However, since the reservoir has an area that is 3.5 times as large as the CMT, the effect is small, but noticeable.

The hot liquid layer buildup in the test is also be examined from a geometric basis for the test and the plant CMT. The scaling approach used in the CMT test is to choose an inside-diameter scale ratio of:

$$\frac{19.312''}{150''} \approx 0.1287 \text{ or } \frac{1}{7.77} = S \tag{2.2-1}$$

Using this as a scale ratio, S, the areas of the inlet nozzle are preserved in the same fashion, so:

$$d_{N_m} = S\, d_{N_p} \tag{2.2-2}$$

or:

$$A_{N_m} = S^2 A_{N_p} \tag{2.2-3}$$

Since the scaling approach preserves the full pressure and full height and the line resistances are similar, the ratio of the recirculation mass flux between the CMT test and the plant is nearly unity as shown in Figure 2.1-6.

Therefore, the mass flow in the CMT test is related to the plant mass flow as:

$$\rho U)_m A_{N_m} \equiv \rho U)_p A_{N_p} S^2 \tag{2.2-4}$$

If Equation 2.2-3 is used and the derivatives are the same, the velocity scale between the test and the plant is preserved.

Since full-height simulation is used and the line resistances are similar, the time scale for the development of the heated liquid layer for the test is similar to the plant:

$$t_m = \frac{L_m}{U_m} \equiv t_p = \frac{L_p}{U_p} \tag{2.2-5}$$

at least until the CMT test, which is 10 ft. high, is filled with hot water.

Therefore, the development of the hot liquid layer in the CMT test, relative to the plant, is given as:

$$\Delta t\ \rho U A_N)_m = \rho A_m(L_m)\Delta L_m \tag{2.2-6}$$

Where $A_m(L_m)$ is the cross-sectional area of the CMT in the test head region, and ΔL_m is the layer thickness. If the tank has drained to the cylindrical portion, then the cross-sectional area is a constant. A similar expression can be written for the plant as:

$$\Delta t\ \rho U A_N)_p = \rho A_p(L_p)\Delta L_p \tag{2.2-7}$$

Since time is approximately preserved, Equations 2.2-6 and 2.2-7 can be solved for Δt and equated giving:

$$\frac{\rho A_m(L_m)\Delta L_m}{\rho U A_N)_m} = \frac{\rho A_p(L_p)\Delta L_p}{\rho U A_N)_p} \tag{2.2-8}$$

Using Equations 2.2-3 and 2.2-4, Equation 2.2-8 reduces to:

$$\frac{\Delta L_m}{\Delta L_p} = \frac{A_p(L_p)}{A_m(L_m)} \frac{\rho U)_m}{\rho U)_p} \frac{A_{N_m}}{A_{N_p}} \tag{2.2-9}$$

or:

$$\frac{\Delta L_m}{\Delta L_p} = \frac{A_p(L_p)}{S^2 A_m(L_m)} \tag{2.2-10}$$

That is, the hot layer development in the test is approximately the same as that in the plant, if the test and plant head regions are geometrically similar. Figure 2.2-1 shows the difference in the cross-sectional area of the plant CMT and the test facility. As the figure indicates, there are differences in these areas that affect the thickness of the hot water layer as it develops. In general, however, the CMT test is a reasonable approximation of the plant.

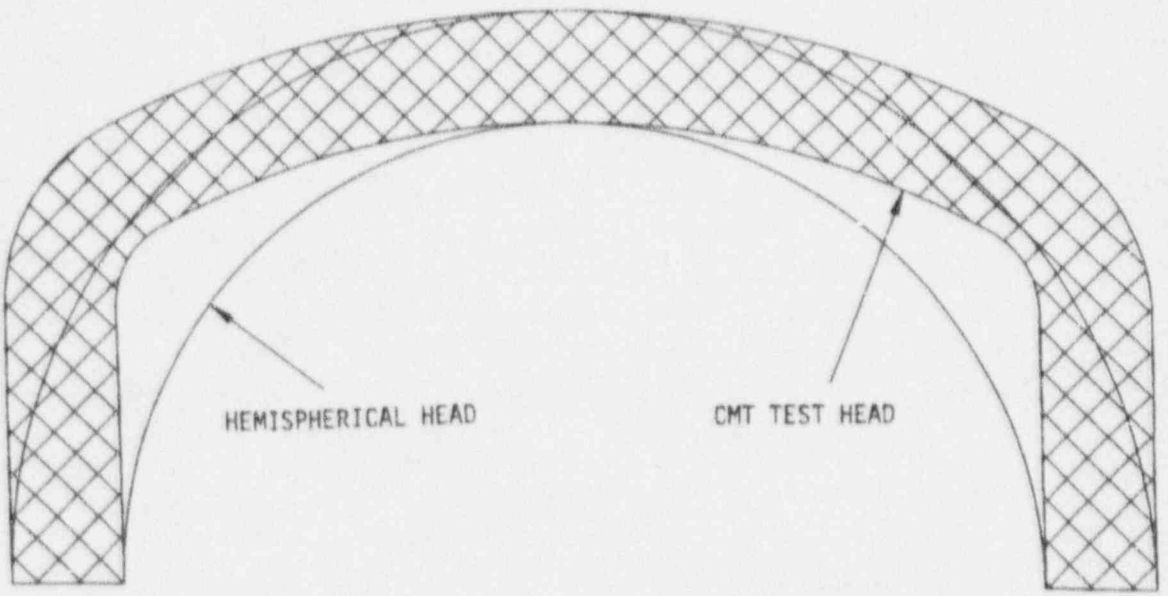

Note: Not to scale

Figure 2.2-1 Comparison of AP600 Plant Head Cross-Sectional Area and CMT Test Head Cross-Sectional Area

2.3 Heat Transfer in the CMT During Recirculation

As the CMT recirculates and hot water replaces the cold water in the tank, there will be heat transfer between the colder CMT walls and the hot water layer. The scaling effects of the wall heat transfer in the test CMT and the plant were estimated for the recirculation period. Because the CMTs are calculated to drain slowly, the convective velocity past the walls is small, approximately 0.008 to 0.016 ft./sec from the SSAR calculations, depending on whether the tank is in the recirculation or draining mode. The heat transfer at the CMT inside wall surface from the hot CMT liquid layer can be forced convection or natural convection. The heat transfer mode depends on the local fluid velocity, the temperature difference between the hot recirculated CMT liquid temperature and the CMT walls, as well as the thickness of the hot CMT liquid layer. To evaluate which mode of heat transfer dominates, the ratio:

$$\frac{Gr}{Re^2} \geq 1 \tag{2.3-1}$$

was evaluated where:

$$Gr = \frac{\beta g (T_b - T_w) Z^3}{\nu^2} \tag{2.3-2}$$

where $(T_b - T_w)$ is the temperature difference between the hot fluid temperature and the CMT inside wall temperature. If the ratio given in Equation 2.3-1 is greater than unity, then free-convection heat transfer dominates. Z is the thickness of the hot liquid layer inside the CMT. Since the hot liquid layer is estimated to be 1- to 2-ft. thick and the plant CMT is 12-ft. in diameter, the convective flow is not developed and looks like a developing boundary layer for the larger-diameter CMT.

A forced-convection heat transfer coefficient was evaluated assuming flow over a flat plate with the hot CMT liquid layer being the characteristic dimension. The correlation used is from Kreith and Bohn[4] and is given as:

$$Nu_x = 0.332 Re_x^{1/2} Pr^{1/3} \tag{2.3-3}$$

for the local heat transfer, and:

$$Nu_L = 0.664 Re_L^{1/2} Pr^{1/3} \tag{2.3-4}$$

for the average heat transfer coefficient.

The Reynolds number is given as:

$$Re = \rho UL/\mu \tag{2.3-5}$$

for the surface average heat transfer coefficient. Using the length or depth of the heated thermal layer, L, as the characteristic dimension, the Reynolds and Grashoff numbers are calculated, and the ratio of Gr/Re^2 compared for different thermal layer thicknesses. These calculations are performed for a range of CMT draining velocities, which were calculated from the AP600 SSAR analyses as well as the draining velocities that are simulated in the CMT test. The SSAR CMT draining velocities are small and range from 0.008 to 0.016 ft./sec; the CMT test draining velocities will range up to 0.127 ft./sec. The Gr/Re^2 ratio was calculated using the largest drain velocity of 0.127 ft./sec. The calculated ratios are given for different assumed thermal layer thicknesses. As the results indicate, the natural convection flow will dominate for all heated layer thicknesses.

THE CALCULATED Gr/Re^2 RATIO FOR CMT CONVECTION

Heated Layer Thickness (ft) X	Gr	Re	Gr/Re^2
0.5	3.49×10^{10}	44354.7	17.7
1.0	27.92×10^{10}	88713.94	35.5
3.0	753.9×10^{10}	266142.78	106.34

Therefore, the conclusion is that free convection dominates even for the fastest drain rates.

The free convection correlation that is used to evaluate the hot-liquid-to-wall heat transfer is the McAdams correlation,[5] which is given as:

$$Nu = \frac{0.13k_f}{L}[Gr_L\ Pr]^{.33} \tag{2.3-6}$$

where the length will cancel out when calculating the heat transfer coefficient. Using this correlation, the Π ratio for natural-convective heat transfer for the CMT test and the plant CMT becomes:

$$\Pi_{HT} = \frac{Nu_m}{Nu_p} = \frac{0.13[Gr_L\ Pr_f]_m^{.33}}{0.13[Gr_L\ Pr_f]_p^{.33}} \tag{2.3-7}$$

Since the fluid properties are preserved, the ratio of the heat transfer coefficients becomes:

$$\frac{h_m}{h_p} = \left[\frac{(T_f - T_w)_m}{(T_f - T_w)_p}\right]^{.33} \left(\frac{Z_m}{Z_p}\right) \tag{2.3-8}$$

where it has been assumed that all physical properties are the same between the test CMT and the plant CMT. Since the CMT test will experience the same wall and fluid temperature range as the plant CMT, and since the development of the hot liquid layer is very similar between the test and plant CMTs, the heat transfer coefficient ratio is:

$$\frac{h_p}{h_m} = 1.0 \tag{2.3-9}$$

which indicates that the experiment will yield natural-convective heat transfer data in the recirculation phase that is approximately the same as the plant CMT.

2.4 Conclusion on CMT Test Facility Recirculation Scaling Behavior

The system of equations that governs the CMT recirculation behavior are normalized, and the key dimensionless parameters are developed $\Pi_{R_i})_R$ and $\Pi_{F_r})_R$ for the test and plant CMT. Since full pressure and full height are preserved in the test, and the resistances are also preserved, these dimensionless ratios are near unity for the test CMT. This indicates that the CMT test preserves the recirculation thermal-hydraulic phenomena expected in the plant CMT.

In addition, a one-dimensional flow model is used to calculate the behavior of the plant CMT and the test facility during natural-circulation behavior. The calculated recirculation flows are normalized and compared between the test facility and the plant. The hot-water-layer development is also calculated and compared for both the test and the plant CMT. The comparison of the calculated recirculation flows (mass flux) and the hot water layer is very similar between the test and the plant CMT. The CMT recirculation phenomena associated with the natural circulation of the CMT and the cold leg balance line behavior is well simulated in the test so those items in the PIRT are satisfied. The CMT wall heat transfer to the CMT liquid, due to the recirculation, is also assessed showing that the test CMT yields natural-convective heat transfer coefficients similar to those expected for the plant CMT. Therefore, the water-to-CMT-wall heat transfer phenomena identified in the PIRT is addressed in the tests, and the resulting data will be available for computer code validation.

The details of the fluid-to-fluid mixing is not addressed in this portion of the scaling since only the recirculation behavior of the system was examined. While there may be local distortions between the plant and the CMT test due to mixing, the overall hydraulic effects are very similar, as the scaling analysis indicates. Since the full temperature and pressure are simulated in the experiments, the thermodynamic behavior of the test relative to the plant is similar. Since the development of the hot liquid layer is calculated to be similar between the plant and the CMT test, the fluid flashing effects is also similar. The hot liquid layer flashing is driven by the fluid temperature to saturation temperature that is determined by the depressurization rate simulated in the test. The depressurization rates are chosen to be representative of the AP600 SSAR calculations. Since the experiments will cover the full-pressure range of operation of the plant, it is expected that the flashing effect will be similar between the test and the plant, so this phenomena on the PIRT is addressed for code validation.

In conclusion, the scaling for the CMT test has shown that the same effects observed in the plant recirculation behavior can be represented adequately in the test, such that the recirculation phenomena listed in the CMT PIRT are captured in the CMT test facility.

3.0 THE CMT DRAINDOWN BEHAVIOR SCALING ASSESSMENT

3.1 Introduction

There are two aspects of the draining operation of the CMT that depend on the amount of time that the CMT has been recirculating. As the CMT recirculates, hot water flows up the cold leg balance line to the top of the CMT. As discussed in Section 1.0, as the reactor system drains, the cold leg balance line voids, and steam from the cold leg can then flow up to the CMT, condenses on the CMT walls, and mix with the CMT liquid. The amount of condensation and the rate of condensation is dependent on the time period over which recirculation has occurred. If recirculation has occurred for long time periods, which is typical of most small-break LOCAs, then a hot liquid layer will have developed at the top of the CMT. The presence of the hot liquid layer will significantly reduce the direct interfacial condensation from the steam to the CMT liquid. The hot liquid layer will also heat the initially cold CMT walls, so the wall condensation is also reduced. As the break size increases, the duration of recirculation decreases since the reactor system drains sooner. More steam will flow up the cold leg balance line as the break size increases and is condensed by both direct interfacial condensation and mixing with the CMT liquid, as well as by condensing on the colder CMT steel walls.

This section of the report concentrates on the scaling of the steam diffuser used in the AP600 plant and the CMT tests and on the condensation processes that could occur for larger break sizes. A top-down scaling analysis is also performed to assess the test pressure behavior relative to the AP600 plant CMT. The estimated response of the test facility is calculated and compared to the response of the plant CMT to verify that the thermal-hydraulic phenomena identified in the PIRT for the draining phase of the CMT operation are addressed.

3.2 Scaling of the CMT Diffuser

The hot pre-operational tests performed in the CMT test facility with steam being injected into cold CMT liquid indicated that the condensation process was violent and resulted in large vapor slugs that collapsed in the subcooled liquid. Since the process was irregular and had the potential for creating undesirable mechanical loads, a steam diffuser was developed to reduce the rapid condensation effects and promote heat-up of the liquid layer at the top of the CMT. Once the liquid layer is heated, it acts as buffer between the initially highly subcooled CMT liquid and the incoming steam from the steam line, representing the cold leg balance line.

It was recognized that the basis used for the choice of the CMT test steam distributor design had to be scalable to the plant CMT so the thermal-hydraulic phenomena associated with the diffuser observed in the tests would be scalable to the AP600 plant.

There is conflicting information in the literature on the location of the limiting heat transfer resistance for direct condensation, whether it is on the steam side of the interface or on the liquid side of the interface.[6] In this analysis, the limiting resistance is assumed to be on the liquid side since there is a

large source of steam to the CMT, and rapid condensation continues to occur until the liquid has lost most of its subcooling.

The CMT steam diffuser induces a circulatory flow pattern at the top of the CMT due to the momentum of the steam as it is injected through the diffuser and is rapidly condensed. The rapid condensation induces additional steam flow into the CMT, and also reduces the pressure at the top of the CMT so the drain flow from the tank is reduced. The liquid recirculation flow pattern continues to mix the injected steam until the liquid temperature approaches the local saturation temperature. At that time, the steam that is injected can bubble to the top of the CMT and a stable steam/water interface will be formed, and the CMT starts to drain freely.

Since it is the internal circulation or mixing of the cold CMT liquid that drives the condensation process, the approach for the scaling of the diffuser is to:

- Choose a very low CMT liquid velocity preserved at the tank wall to minimize the liquid recirculation. The liquid would heat up rapidly in the vicinity of the diffuser and condensation is reduced.

- Preserve the steam momentum flux determine the flow area in the diffuser that was needed to obtain the chosen low value of the liquid velocity at the CMT wall.

The same value of the liquid velocity at the wall was chosen for the AP600 plant, the CMT tests, and the AP600 integral systems tests at SPES and at Oregon State University so consistency would be achieved for the different CMTs used in these facilities and a rationale for comparison would exist between the test facilities and the plant.

There are other scaling considerations for the diffuser in addition to the momentum flux scaling. Small vapor jets injected into the CMT are more desirable than a single or a few large vapor jets to avoid large condensation shocks or pressure surges. Therefore, while the momentum flux scaling method resulted in a total flow area for the diffuser, the diffuser is manufactured with a large number of small holes to smooth out the condensation processes. The choice for the hole size for the AP600 plant diffuser was based on the hole size successfully tested at full scale for the ADS sparger.

Figure 3.2-1 shows the schematic of the diffuser with the liquid and steam velocity components as indicated on the figure. The velocity components and the areas are defined as:

V_{v_p} = vapor velocity in the pipe leading to the diffuser
V_{v_d} = vapor velocity flowing through the holes in the diffuser
V_{ℓ_d} = liquid velocity at the diffuser
V_{ℓ_w} = liquid velocity at the CMT wall
A_p = area of the inlet pipe to the diffuser
A_{v_d} = area of the holes in the diffuser

A_{ℓ_d} = liquid area at the diffuser

A_w = area at the CMT wall, for the same axial length as the diffuser

It is assumed that the diffuser is sufficiently porous and that the momentum effect of the steam acts to push a cylindrical region of liquid flow toward the CMT wall. The area of the liquid region at the diffuser is A_{ℓ_d} and is assumed equal to the outside area of the pipe, which contains the holes for the diffuser. This assumption implies that the steam from the individual holes in the diffuser is pushing on a cylindrical area equal to the outside area of the diffuser pipe. Preserving the momentum flux between the steam flow leaving the diffuser and the liquid at the diffuser is given as:

$$V_{v_d}^2 A_{v_d} \rho_v = V_{\ell_d}^2 A_{\ell_d} \rho_\ell \tag{3.2-1}$$

The liquid velocity at the diffuser flows radially toward the CMT wall, and the wall liquid velocity is given by continuity as:

$$\rho_\ell A_w V_{\ell_w} = \rho_\ell A_{\ell_d} V_{\ell_d} \tag{3.2-2}$$

The liquid velocity at the wall is chosen as 0.1 ft./sec to minimize the amount of recirculation in the CMT and promote the heat up of the liquid layer at the top of the CMT. This is an assumed value and is held constant for all the tests and the AP600 plant CMT diffuser. The area of the wall, A_w, is the area at the wall for the same axial length as the diffuser.

The steam flow through the diffuser is determined from the flow through the inlet pipe to the diffuser from the continuity equation as:

$$V_{v_d} = V_{v_p} \frac{A_p}{A_{v_d}} \tag{3.2-3}$$

The steam flow in the test CMT was estimated by scaling the steam flow from the SSAR calculations used to calculate V_{v_p}. Given the value for V_{v_p}, then the area ratio of A_{v_d} / A_p is solved for the given liquid velocity at the wall (0.1 ft./sec). The result is the area for the holes in the diffuser relative to the diffuser inlet pipe area. In the design of the diffuser, small holes were used, as seen in Figure 1.2-4, so the diffuser would be more porous. This supports the application of the momentum scaling approach.

Since the liquid velocity at the wall is preserved for the CMT test relative to the AP600 plant, the degree of mixing observed in the CMT test, that is, the depth of the mixing layer below the diffuser, should be the same in the test as in the plant CMT.

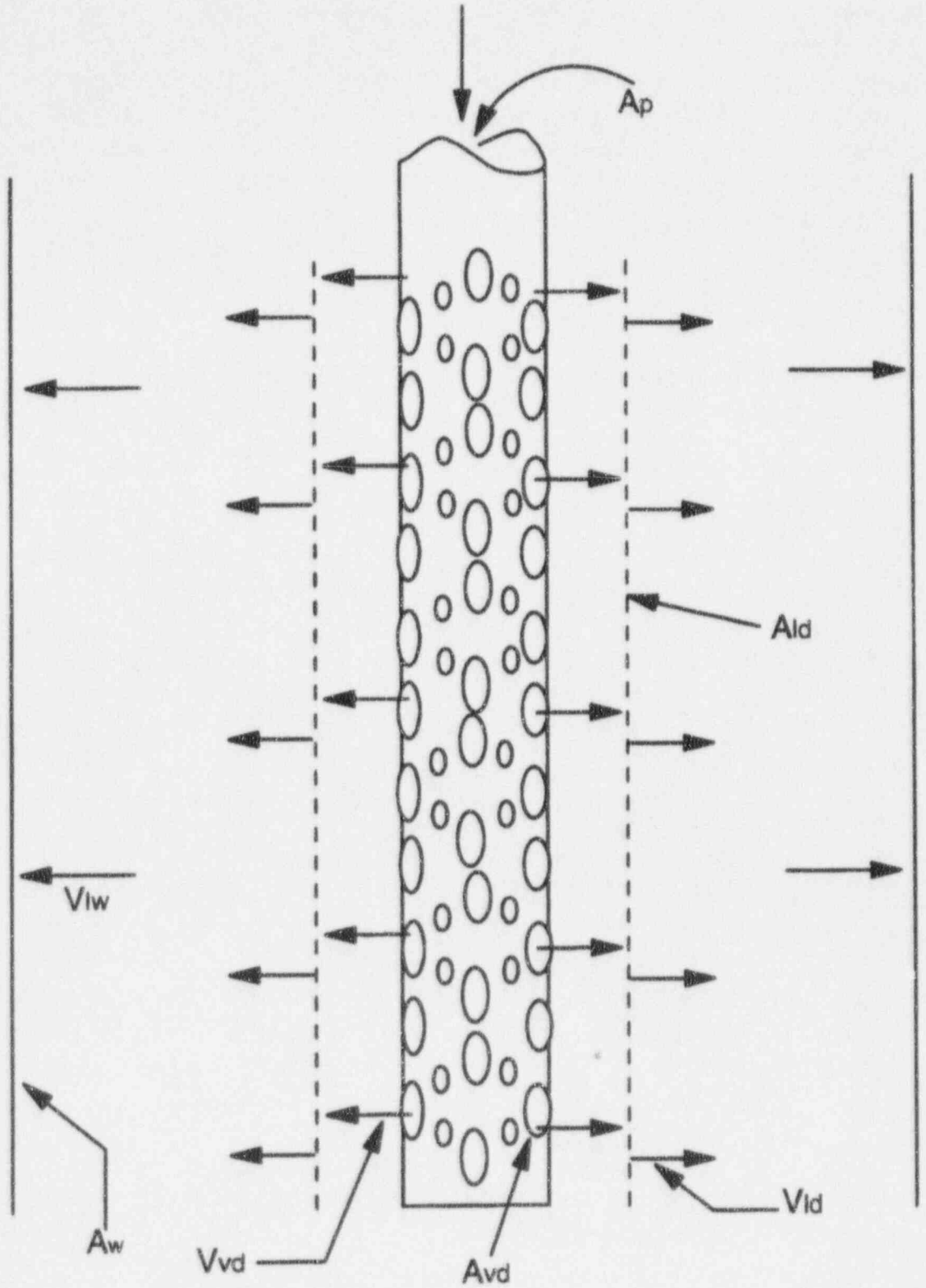

Figure 3.2-1 Model for CMT Diffuser Momentum Approach

3.3 Core Makeup Tank Pressurization Equation - Top Down Scaling Analysis

3.3.1 Introduction

As the CMT drains, steam flows from the cold leg balance line into the vapor space created at the top of the CMT. The amount of steam that flows into this vapor space is a result of the volume displacement as the liquid drains, the wall condensation, and the interfacial condensation from the steam to the liquid interface in the CMT. The bulk temperature of the liquid depends on the amount of single-phase recirculation that occurs, as well as the amount of direct condensation that occurs between the steam and the liquid layer at the top of the CMT. To estimate the CMT pressure performance, two cases are examined that bound the CMT thermal-hydraulic conditions. The first case treats a vapor space above a subcooled liquid interface so the pressure in the liquid is the same as the imposed pressure from the vapor. This case is similar to the thermal-hydraulic conditions for the CMT following a larger break in which there was very little recirculation. The second case treats the CMT as a homogenous mixture that simulates the CMT after a long period of recirculation, during which the CMT fluid is heated before the tank begins to drain.

3.3.2 Core Makeup Tank Vapor Space Pressure Equation

The CMT configuration is shown in Figure 3.3-1 with a vapor space at the top of the tank since the tank has begun to drain. Steam enters the cold leg balance line and is condensed on the cold tank walls as well as at the interface between the steam and the liquid. The vapor space represents the system volume for the mass and energy balances. The conservation of mass equation is:

$$\frac{d}{dt}\left(m_{v_{sys}}\right) = \dot{m}_{in} - \dot{m}_{out} \tag{3.3-1}$$

and the energy balance equation is:

$$\frac{d}{dt}\left[m_v e_v\right]_{sys} = \dot{m}_{in} h_{in} - \dot{m}_{out} h_{out} + q_{sys} - w_{sys} \tag{3.3-2}$$

or:

$$\frac{d}{dt}\left[m_v e_v\right]_{sys} = \dot{m}_{in} h_{in} - \dot{m}_{out} h_{out} \tag{3.3-3}$$

where heat transfer to the vapor space and work performed by the control volume is ignored.

Using the definition of the vapor enthalpy as:

$$h_v = e_v + \frac{P_v}{\rho_v} = e_v + P_v v_v \tag{3.3-4}$$

the energy equation can be written as:

$$\frac{d}{dt}\left[m_v(h_v - P_v v_v)\right]_{sys} = \dot{m}_{in}h_{in} - \dot{m}_{out}h_{out} \tag{3.3-5}$$

The left-hand side of Equation 3.3-5 can be expanded and operated on using:

$$m_{v_{sys}} = \rho_{v_{sys}} V_{v_{sys}} \tag{3.3-6}$$

so the energy equation becomes:

$$\frac{d}{dt}\left[V_v(\rho_v h_v - P_v)\right]_{sys} = \dot{m}_{in}h_{in} - \dot{m}_{out}h_{out} \tag{3.3-7}$$

Clearing the bracket term on the left hand side of the equation and expanding gives:

$$\frac{d}{dt}\left[V_v \rho_v h_v\right]_{sys} = V_{v_{sys}}\frac{dP_{v_{sys}}}{dt} + P_{v_{sys}}\frac{dV_{v_{sys}}}{dt} + \dot{m}_{in}h_{in} - \dot{m}_{out}h_{out} \tag{3.3-8}$$

Equation 3.3-8 can be non-dimensionalized using the initial conditions and the boundary conditions as:

$$\begin{aligned}
V_{v_{sys}} &= V_{v_0} V_v^* \\
\rho_{v_{sys}} &= \rho_{v_0} \rho_v^* \\
h_{v_{sys}} &= h_{v_{sys_0}} h_{v_{sys}}^* \\
P_{sys} &= P_{sys_0} P_{sys}^* \\
\dot{m}_{in} &= \dot{m}_{in_0} \dot{m}_{in}^* \\
\dot{m}_{out} &= \dot{m}_{out_0} \dot{m}_{out}^* \\
h_{in} &= h_{in_0} h_{in}^* \\
h_{out} &= h_{out_0} h_{out}^*
\end{aligned} \tag{3.3-9}$$

Using the definitions given in Equation 3.3-9 and dividing the energy equation by $h_{sys_0}\dot{m}_{in_0}$, the non-dimensional energy equation becomes:

$$\tau_0 \frac{d}{dt}\left[V_v^* \rho_v^* h_v^*\right] = \Pi_p \tau_0 \left[V_v^* \frac{dP^*}{dt} + P^* \frac{dV^*}{dt}\right] + \Pi_{h_{in}}\left(\dot{m}_{in}^* h_{in}^*\right) - \Pi_h\left(\dot{m}_{out}^* h_{out}^*\right) \tag{3.3-10}$$

where the time constant and characteristics time ratios are given as:

$$\tau_0 = \frac{\rho_{sys_0} V_{sys_0}}{\dot{m}_{in_0}} \tag{3.3-11}$$

$$\Pi_p = \frac{P_{sys_0}}{\rho_{sys_0} h_{sys_0}} \tag{3.3-12}$$

$$\Pi_{h_{in}} = \frac{h_{in_0}}{h_{sys_0}} \tag{3.3-13}$$

and:

$$\Pi_h = \frac{\dot{m}_{out_0} h_{out_0}}{\dot{m}_{in_0} h_{sys_0}} \tag{3.3-14}$$

The inlet mass flow of vapor is used to non-dimensionalize the energy equations, since this mass flow can be directly related to the condensation that occurs on the CMT walls and the liquid surface, as well as the volume displacement as the CMT drains. As seen in Section 3.5, since the CMT drains slowly, the volume change is small compared to the mass flow into the system so the time derivative of the vapor volume can be neglected, and the mass flow into the CMT is then directly related to the condensation. If there is a small pressure drop between the inlet and the vapor control volume, the $\Pi_{h_{in}}$ group can be assumed to be unity.

Equation 3.3-10 is also valid for the AP600 CMT so the ratios of the characteristic times and the time constant can be compared. The system time constant τ_0, is dependent on the inlet mass flow, $\dot{m}_{in_0}$, which means the condensation rate in the AP600 CMT is relative to the condensation rate in the CMT test. Comparisons of these rates are made in Section 4.0 for quasi-steady-state conditions.

The Π_p group is only a function of the initial conditions. Since the CMT test is designed to cover the full pressure and temperature conditions for the AP600, this ratio is unity. Therefore, the difference in the rate of condensation between the CMT test and the plant CMT influences the system time constant τ_0.

3.3.3 Core Makeup Tank Homogeneous Mixture Pressure Equation

After the CMT has recirculated for an extended time period, the liquid in the tank is very hot and may be near or at the local saturation temperature. A top-down scaling analysis for the tank in this condition can be performed in a similar fashion as that performed in Section 5.0 of the Oregon State University Scaling Report.[2]

The objective of the system level scaling analysis is to examine the similarity criteria to scale the system depressurization. The governing equations are presented in Equations 3.3-15 and 3.3-16 for the CMT fluid mass:

$$\frac{d}{dt}(\rho_{sys} V_{sys}) = \Delta[\rho Q] \tag{3.3-15}$$

and for the CMT fluid energy:

$$\frac{d}{dt}(\rho_{sys} e_{sys} V_{sys}) = \Delta\left[\rho Q\left(e+\frac{P}{\rho}\right)\right] + q_{sys} - w_s \tag{3.3-16}$$

The control volume for this analysis is the entire CMT depicted as a single control volume. Equations 3.3-15 and 3.3-16, are the fluid conservation equations for the system. In these equations:

ρ_{sys}	is the average CMT fluid density
V_{sys}	is the CMT fluid volume
$\Delta[\rho Q]$	is the net rate of fluid mass entering the CMT volume (through the cold leg balance line) or leaving (through the CMT drain line)
q_{sys}	is the net heat rate into the control volume, assumed equal to zero
w_s	is the shaft work done by the fluid, and assumed equal to zero
e_{sys}	is the average system fluid energy per unit mass. It consists of internal energy, kinetic energy and potential energy components as follows:

$$e_{sys} = e_{int} + \frac{U^2}{2g_c} + \frac{gz}{g_c} \tag{3.3-17}$$

The term:

$$\Delta\left[\rho Q\left(e + \frac{P}{\rho}\right)\right] \tag{3.3-18}$$

is the net rate of fluid energy entering the CMT volume (through injection) or leaving (through draining). It includes the work done by pressure on mass flowing across the control surface boundaries.

Equations 3.3-15 and 3.3-16 can be simplified by recognizing that the mass flow rates can be written as:

$$\dot{m} = \rho Q \tag{3.3-19}$$

Thus, Equations 3.3-15 and 3.3-16 can be written as:

$$\frac{d}{dt}\rho_{sys}V_{sys} = \dot{m}_{in} - \dot{m}_{out} \tag{3.3-20}$$

$$\frac{d}{dt}(\rho_{sys}V_{sys}e_{sys}) = \left[\dot{m}\left(e + \frac{P}{\rho}\right)\right]_{in} - \left[\dot{m}\left(e + \frac{P}{\rho}\right)\right]_{out} \tag{3.3-21}$$

Substituting Equation 3.3-17 into Equation 3.3-21 yields:

$$\frac{d}{dt}\left[\rho_{sys}V_{sys}\left(e_{int} + \frac{U^2}{2g_c} + \frac{gz}{g_c}\right)_{sys}\right] = \left[\dot{m}\left(e + \frac{P}{\rho}\right)\right]_{in} - \left[\dot{m}\left(e + \frac{P}{\rho}\right)\right]_{out} \tag{3.3-22}$$

Simplifying assumptions:

a. Changes in kinetic and potential energy, internal to the fluid, are negligible.
b. Fluid kinetic and potential energy associated with the injection and drain flows are negligible.

Applying these assumptions to the fluid energy Equation 3.3-22 yields:

$$\frac{d}{dt}(\rho_{sys}V_{sys}e_{int}) = \left[\dot{m}\left(e_{int} + \frac{P}{\rho}\right)\right]_{in} - \left[\dot{m}\left(e_{int} + \frac{P}{\rho}\right)\right]_{out} \tag{3.3-23}$$

Using the definition of enthalpy, h:

$$h = e_{int} + \frac{P}{\rho} \tag{3.3-24}$$

Equation 3.3-23 can be written as:

$$\frac{d}{dt}\left[\rho_{sys} V_{sys}\left(h_{sys} - \frac{P_{sys}}{\rho_{sys}}\right)\right] = (\dot{m}h)_{in} - (\dot{m}h)_{out} \tag{3.3-25}$$

Noting that V_{sys}, the total CMT volume, is constant allows Equation 3.3-25 to be written as:

$$\frac{d}{dt}(\rho_{sys} h_{sys}) = \frac{dP_{sys}}{dt} + \frac{1}{V_{sys}}\left[(\dot{m}h)_{in} - (\dot{m}h)_{out} + q_{sys}\right] \tag{3.3-26}$$

Furthermore, for homogeneous equilibrium conditions, h_{out} will be equal to the average system enthalpy, h_{sys}. Thus:

$$(\dot{m}h)_{out} = h_{sys}\dot{m}_{out} \tag{3.3-27}$$

Substituting Equation 3.3-27 into 3.3-26 and ignoring the heat transferred to the system yields:

$$\frac{d}{dt}(\rho_{sys} h_{sys}) = \frac{dP_{sys}}{dt} + \frac{1}{V_{sys}}\left[(\dot{m}h)_{in} - h_{sys}\dot{m}_{out}\right] \tag{3.3-28}$$

The mass simplified energy equations can be expressed in terms of dimensionless quantities using the initial and boundary conditions given as:

$$\rho_{sys} = \rho_{sys,0}\rho^{*}_{sys}$$

$$V_{sys} = V_{sys,0}V^{*}_{sys}$$

$$\dot{m}_{in} = (\dot{m}_{in})_0\,\dot{m}^{*}_{in}$$

$$P_{sys} = P_{sys,0}P^{*}_{sys} \tag{3.3-29}$$

$$\dot{m}_{out} \propto (\dot{m}_{out})_0\,\dot{m}^{*}_{out}$$

$$(\dot{m}h)_{in} = (\dot{m}h)_{in,0}(\dot{m}h)^*_{in}$$

$$h_{sys} = h_{sys,0}h^*_{sys}$$

The resulting dimensionless continuity and energy equations are given in Equations 3.3-30 and 3.3-31 as:

$$\tau_0 \frac{d}{dt}\left(\rho^*_{sys} V^*_{sys}\right) = \Pi_m \dot{m}^*_{in} - \dot{m}^*_{out} \tag{3.3-30}$$

System fluid energy:

$$\tau_0 \frac{d}{dt}\left(\rho^*_{sys} h^*_{sys}\right) = \Pi_p \tau_0 \frac{dP^*_{sys}}{dt} + \frac{1}{V^*_{sys}}\left[\Pi_h (\dot{m}h)^*_{in} - h^*_{sys}\dot{m}^*_{out}\right] \tag{3.3-31}$$

Where the residence time and characteristic time ratios are given as:

Fluid residence time:

$$\tau_0 = \frac{\rho_{sys,0} V_{sys,0}}{\dot{m}_{out,0}} \tag{3.3-32}$$

Characteristic time ratios:

$$\Pi_m = \frac{\dot{m}_{in,0}}{\dot{m}_{out,0}} \qquad \text{System flow rate ratio} \tag{3.3-33}$$

$$\Pi_p = \frac{P_{sys,0}}{\rho_{sys,0} h_{sys,0}} \qquad \text{System pressure ratio} \tag{3.3-34}$$

$$\Pi_h = \frac{(\dot{m}h)_{in,0}}{h_{sys,0}\dot{m}_{out,0}} \qquad \text{System enthalpy ratio} \tag{3.3-35}$$

Examining the fluid residence time and the characteristic time ratios for the CMT test relative to the plant CMT for the fluid residence time, the ratio of the CMT test to the AP600 test facility is given as:

$$\Pi_R = \frac{\tau_0\rangle_{CMT_{test}}}{\tau_0\rangle_{CMT_{plant}}} = \frac{\left.\dfrac{\rho_{sys,0} V_{sys,0}}{\dot{m}_{out,0}}\right]_{test}}{\left.\dfrac{\rho_{sys,0} V_{sys,0}}{\dot{m}_{out,0}}\right]_{plant}} \qquad (3.3\text{-}36)$$

The SSAR calculations indicate that the recirculation flow rate is 50 lbm/sec for the plant CMTs when in single-phase recirculation. Since recirculation is a constant volume process and the volume of the plant CMT is 2000 ft.^{3}, the fluid residence time is calculated to be 1823 seconds using the saturated density of liquid at 1100 psia. For the CMT tests, the fluid volume is given as 18 ft.^{3} from the Facility Description Report.[7] Since the drain flow rate can be controlled over a range of 2 to 26 gpm, the fluid time constant for the AP600 plant can be simulated in the test.

The system flow rate ratio, given as Π_m in Equation 3.3-33, depends on the modeling of the system hydraulic resistances. As seen in Section 2.0, the CMT test does represent the hydraulic resistances expected for the plant CMT flow path from the cold leg through the tank to the injection line. Therefore, this ratio would be unity for the test relative to the AP600 plant CMT.

The system pressure ratio is only a function of the pressure level simulated in the test relative to the plant CMT. Since the test facility can simulate full AP600 pressure and temperature conditions, this Π ratio would be unity.

The system enthalpy ratio is a function of pressure and the mass flow rate ratio. The pressure effects would be the same in the test as in the plant CMT since the test is full pressure and full temperature. Also, since the hydraulic circuit is preserved between the test and the plant, as seen in Section 2.0, this ratio is at or near unity.

Therefore, the CMT test simulates the conditions needed to represent the depressurization behavior of the plant CMT.

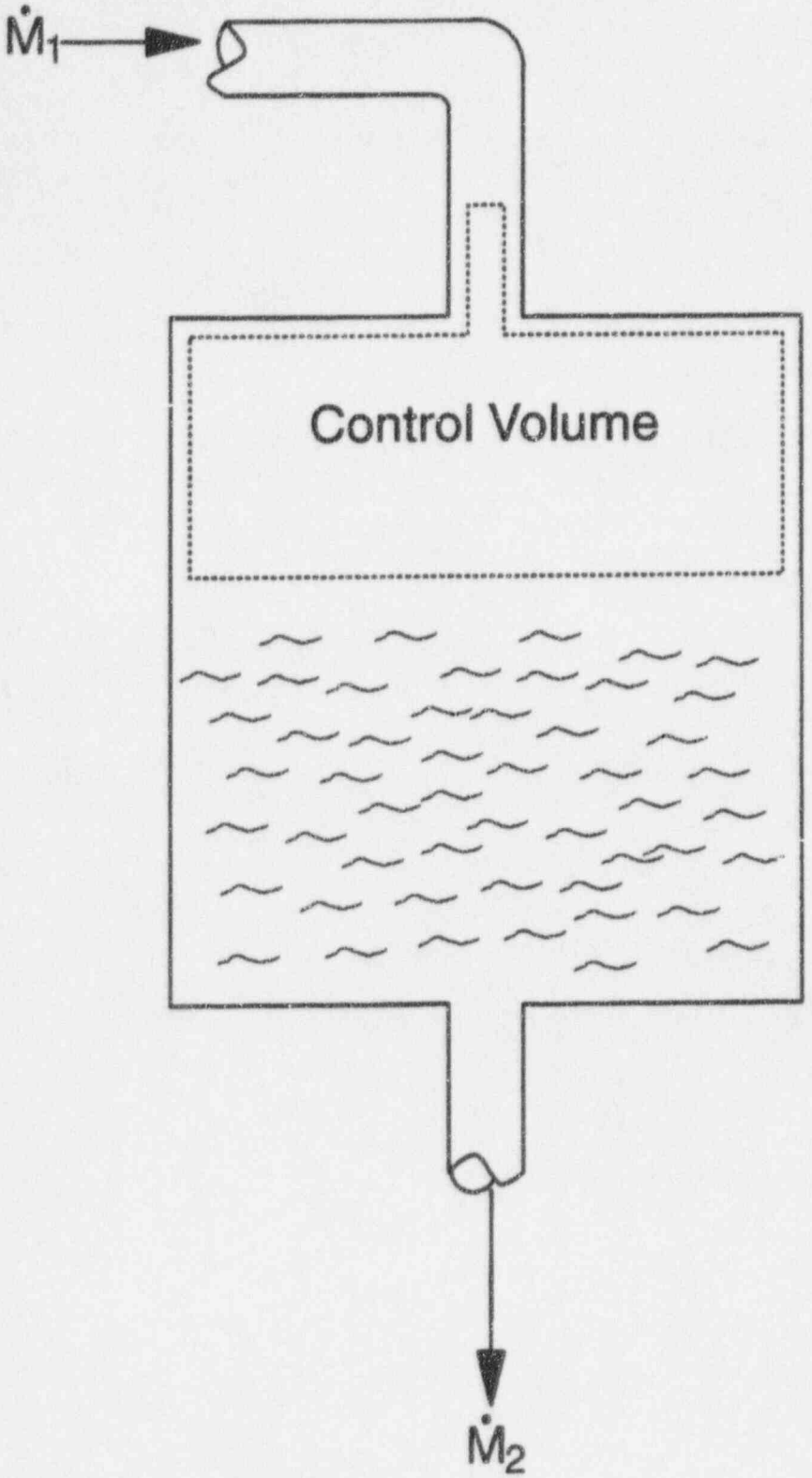

Figure 3.3-1 Control Volume Boundaries for CMT Draining Analysis

3.4 CMT Draining Processes at Constant Pressure

3.4.1 Introduction

This section examines the draining process at constant pressure for the CMT. The top-down scaling analysis given in Section 3.3 indicates that the large size of the CMT, combined with modest drain rates, makes the draining process quasi-steady. Before the ADS valves open, there is an extended period after recirculation in which the CMT continues to deliver water to the reactor vessel and begins to drain. The conditions at the top of the CMT vary depending on the size of the break. For small breaks, CMT recirculation heats up the liquid layer at the top of the CMT, so wall and interfacial condensation is reduced. For larger break sizes, there is less time for recirculation, so the CMT walls and the liquid are colder and condensation can occur.

Two aspects of the draining process are examined. The first analysis examines the situation in which the CMT remains full and there has been no recirculation, so the CMT liquid is initially very subcooled. This is the situation for a large-break LOCA or a very large small-break LOCA. The objective in these calculations is to examine the thermal-hydraulic effects of the CMT diffuser for the test and the AP600 plant.

The second series of calculations simulates the CMT after some initial drainage, so there is a level in the tank with a vapor space at the top of the tank; there is wall condensation as well as interfacial condensation at the steam/liquid interface. The recirculation behavior of the vapor flow is approximated for the plant CMT as well as the CMT test to estimate the interfacial heat transfer.

3.4.2 Governing Equations for Constant-Pressure CMT Draining Process

The energy and continuity equations from Section 3.3 are simplified to examine the constant-pressure draining process for the CMT. A set of balance equations and dimensionless groups, applicable to draining processes in general, is developed. Figure 3.3-1 defines the control volume boundaries for the CMT. The system of equations that represent the CMT and its draining are given as:

Liquid mass:

$$\frac{d}{dt}(\rho_\ell V_\ell) = \Delta[\rho Q] \tag{3.4-1}$$

Liquid energy:

$$\frac{d}{dt}(\rho_\ell e_\ell V_\ell) = \Delta\left[\rho Q\left(e_\ell + \frac{P}{\rho}\right)\right] + q_i - W_i \tag{3.4-2}$$

Solid structure energy:

$$\frac{d}{dt}(\rho_s V_s C_{vs} T_s) = H_{si}(T_s - T_\ell)a_{si} - H_{sa}(T_s - T_{amb})a_{sa} \tag{3.4-3}$$

Equations 3.4-1 and 3.4-2 are the liquid conservation equations for the CMT where:

ρ_ℓ = density of the liquid inside the control volume

V_ℓ = volume of liquid inside the control volume

$\Delta[\rho Q]$ = net rate of fluid mass entering or leaving the control volume

q_t = net heat loss to the ambient

W_t = shaft work done by the liquid

e_ℓ = average liquid energy per unit mass

The liquid energy, e_ℓ, consists of internal energy, kinetic energy, and potential energy as follows:

$$e_\ell = e_{int} + \frac{U^2}{2g_c} + \frac{gz}{g_c} \tag{3.4-4}$$

The term:

$$\Delta\left[\rho Q\left(e_\ell + \frac{P}{\rho}\right)\right] \tag{3.4-5}$$

is the net rate of liquid energy entering or leaving the control volume. It includes the work done by pressure on liquid flowing across the control surface boundaries. Equations 3.4-1 and 3.4-2 describe the average liquid mass and energy transfer for the liquid portion of the control volume.

Equation 3.4-3 is the solid structure energy conservation equation. It is a lumped parameter description of the solid structure that encloses the control volume. It assumes a uniform temperature throughout the solid. This equation is replaced by a more complete one-dimensional conduction equation in subsequent sections to more accurately calculate the heat transfer to the CMT walls. H_{st} is the coefficient for convective heat transfer from the surface to the liquid inside the CMT, and H_{sa} is the coefficient for the convective heat transfer from the surface to the ambient.

The following assumptions are applied to the governing equations:

- The liquid inside the control volume is inviscid and incompressible
- There is no work done by the liquid
- Changes in kinetic and potential energy internal to the liquid inside the control volume are small compared to its internal energy

The liquid volume inside a tank having a constant cross-sectional area, A_{TANK}, over the entire height of liquid, $L_\ell(t)$, is given by:

$$V_\ell = A_{TANK} L_\ell(t) \tag{3.4-6}$$

This particular assumption is modified when analyzing the plant CMT since a large fraction of the surface area and tank volume is contained within the heads of the tank.

Substituting Equation 3.4-6 into Equation 3.4-1 yields:

$$\frac{d}{dt}(\rho_\ell A_{TANK} L_\ell) = \Delta[\rho Q] \tag{3.4-7}$$

Recognizing that the mass flow rate, $\dot{m}$, equals ρQ, Equation 3.4-7 becomes:

$$\frac{d}{dt}(\rho_\ell A_{TANK} L_\ell) = \dot{m}_1 - \dot{m}_2 \tag{3.4-8}$$

Locations 1 and 2 are shown on Figure 3.3-1.

Applying the assumptions stated above to the liquid energy Equation 3.4-2 yields:

$$\frac{d}{dt}(\rho_\ell A_{TANK} C_{v\ell} T_\ell L_\ell) = (\dot{m}h)_1 - (\dot{m}h)_2 + q_{si} \tag{3.4-9}$$

These simplified equations are summarized in Table 3.4-1 and can be expressed in terms of dimensionless quantities using the initial and boundary conditions presented in Table 3.4-2.

Substituting the dimensionless quantities into Equations 3.4-3, 3.4-8, and 3.4-9 and dividing the liquid mass conservation equation by $(\dot{m}_2)_0$, the liquid energy conservation equation by $(\dot{m}_2 h_2)_0$, and the solid structure energy equation by $(H_{sa} a_{si} T_{amb})_0$, yields the non-dimensionalized balance equations listed in Table 3.4-3.

3.4.3 Application of the Governing Equations for CMT Draining

This section presents a more detailed analysis for the CMTs, using the system equation derived in subsection 3.4.2.

The phenomena of interest during the CMT draining process are given in the Table 1.4-1 and are:

- Condensation on cold steel surfaces
- Transient conduction in CMT walls
- Interfacial condensation on CMT liquid surface
- Dynamic effects of steam injection and mixing, with the CMT diffuser
- Thermal stratification and mixing of condensate with colder CMT water

TABLE 3.4-1
TOP-DOWN SUBSYSTEM LEVEL SCALING ANALYSIS: CONTROL VOLUME BALANCE EQUATIONS FOR CORE MAKEUP TANK DRAINING (WITH SIMPLIFYING ASSUMPTIONS)

Liquid Mass:

$$\frac{d}{dt}(\rho_\ell A_{TANK} L_\ell) = \dot{m}_1 - \dot{m}_2 \qquad (3.4\text{-}8)$$

Liquid Energy:

$$\frac{d}{dt}(\rho_\ell A_{TANK} L_\ell C_{v\ell} T_\ell) = (\dot{m}h)_1 - (\dot{m}h)_2 + q_t \qquad (3.4\text{-}9)$$

Solid Structure Energy:

$$\frac{d}{dt}(\rho_s V_s C_{vs} T_s) = H_{st}(T_s - T_\ell)a_{si} - H_{sa}(T_s - T_{amb})a_{sa} \qquad (3.4\text{-}3)$$

TABLE 3.4-2
SET OF INITIAL AND BOUNDARY CONDITIONS USED TO NON-DIMENSIONALIZE THE CORE MAKEUP TANK BALANCE EQUATIONS

$$(\rho_\ell A_{TANK}) = (\rho_\ell A_{TANK})_0 \, \rho_\ell^* A_{TANK}^*$$

$$\dot{m}_1 = (\dot{m}_1)_0 \, \dot{m}_1^*$$

$$\dot{m}_2 = (\dot{m}_2)_0 \, \dot{m}_2^*$$

$$L = (L_0) L^*$$

$$\rho_\ell A_{TANK} C_{v\ell} T_\ell = (\rho_\ell A_{TANK} C_{v\ell} T_\ell)_0 \, \rho_\ell^* A_{TANK}^* C_{v\ell}^* T_\ell^*$$

$$(\dot{m}h)_1 = (\dot{m}h)_{1,0} (\dot{m}h)_1^*$$

$$h_2 = h_{2,0} h_2^*$$

$$q_t = q_{t0} q_t^*$$

$$\rho_s V_s C_{vs} T_s = (\rho_s V_{vs} T_s)_0 \, \rho_s^* V_s^* C_{vs}^* T_s^*$$

$$H_{SP} a_{si} = (H_{SP} a_{si})_0 \, H_{SP}^* a_{si}^*$$

$$(T_s - T_\ell) = (T_s - T_\ell)_0 (T_s - T_\ell)^*$$

$$(T_s - T_{amb}) = (T_s - T_{amb})_0 (T_s - T_{amb})^*$$

$$H_{sa} a_{s0} = (H_{sa} a_{s0})_0 H_{sa}^* a_{sa}^*$$

TABLE 3.4-3
NON-DIMENSIONALIZED BALANCE EQUATIONS FOR CMT CONSTANT PRESSURE DRAINING

Liquid Mass:

$$\tau_0 \frac{d}{dt}\left(\rho_\ell^* A_{TANK}^* L_\ell^*\right) = \prod_m \dot{m}_1^* - \dot{m}_2^* \tag{3.4-10}$$

Liquid Energy:

$$\tau_0 \prod_e \frac{d}{dt}\left(\rho_\ell^* A_{TANK}^* L_\ell^* C_{v\ell}^* T_\ell^*\right) = \prod_h (\dot{m}h)_1^* - \dot{m}_2^* h_2^* + \prod_q q_t^* \tag{3.4-11}$$

Solid Structure Energy:

$$\tau_s \frac{d}{dt}\left(\rho_s^* V_s^* C_{vs}^* T_s^*\right) = -H_{st}^* a_{si}^* (T_s - T_\ell)^* \Theta_s - \prod_H H_{sa}^* a_{so}^* (T_s - T_{amb})^* \Theta_{sa} \tag{3.4-12}$$

Time Constant, Solid Specific Frequency and Characteristic Time Ratios

Drain Rate Time Constant:

$$\tau_0 = \left[\frac{\rho_\ell A_{TANK} L_\ell}{\dot{m}_2}\right]_0 \tag{3.4-13}$$

Solid Structure Specific Frequency:

$$\frac{1}{\tau_s} = \left[\frac{H_{st} a_{si}}{\rho_s V_s C_{vs}}\right]_0 \tag{3.4-14}$$

Characteristic Time Ratios:

$$\prod_m = \left[\frac{\dot{m}_1}{\dot{m}_2}\right]_0 \quad \text{Flow Rate Ratio} \tag{3.4-15}$$

$$\prod_e = \left[\frac{C_{v\ell} T_\ell}{h_2}\right]_0 \quad \text{Energy Ratio} \tag{3.4-16}$$

$$\prod_h = \left[\frac{(\dot{m}h)_1}{h_2 \dot{m}_2}\right]_0 \quad \text{Enthalpy Ratio} \tag{3.4-17}$$

$$\prod_q = \left[\frac{q_t}{h_2 \dot{m}_2}\right]_0 \quad \text{Heat Loss Ratio} \tag{3.4-18}$$

$$\prod_H = \left[\frac{H_{sa} a_{so}}{H_{si} a_{si}}\right]_0 \quad \text{Surface Heat Transfer Ratio} \tag{3.4-19}$$

$$\Theta_{et} = \left[\frac{T_s - T_\ell}{T_s}\right]_0 \quad \text{Dimensionless Liquid Temperature Ratio} \tag{3.4-20}$$

$$\Theta_{sa} = \left[\frac{T_s - T_{amb}}{T_s}\right]_0 \quad \text{Dimensionless Ambient Temperature Ratio} \tag{3.4-21}$$

The CMT test facility parameters that have to be assessed to address the phenomena of interest to the AP600 plant CMT draining process are as follows:

- Metal mass
- Internal volume
- Length
- Diameter
- Heat transfer time constant

Other parameters that affect the CMT test facility recirculation behavior are discussed in Section 2.1.

This section assesses the similar criteria and characteristic time ratios needed to scale the various processes occurring in the CMT during both modes of draining. The general balance equations presented in Table 3.4-1 are now made specific for the CMTs, and additional detail is added to the original equations to more accurately calculate the thick wall condensation and heat-up effects.

For the CMTs, the inlet flow rate is given by $\dot{m}_{BAL}$, the steam mass flow rate through the cold leg balance line. The flow leaving the CMTs is given by $\dot{m}_{CMT}$, the CMT discharge mass flow rate. Thus, Equation 3.4-8, the liquid mass balance equation, can be written as:

$$\frac{d}{dt}(\rho_f A_t L_f) = \dot{m}_{BAL} - \dot{m}_{CMT} \qquad (3.4\text{-}22)$$

where A_t is the horizontal liquid surface area in the cylindrical portion of the CMT where the tank is filled to some level L_f. To evaluate $\dot{m}_{BAL}$, it is necessary to perform an energy balance on the steam entering the CMT head.

There are two condensation periods in the CMT as it starts to drain. During the first period, the CMT is full, and the steam exits the diffuser and is directly condensed in the CMT liquid if sufficient subcooling exists. As the steam is condensed in the liquid, the liquid heats up, and eventually the condensation in the liquid ceases and the CMT drains. The second period of condensation occurs as the tank drains; the colder CMT walls are exposed and wall condensation occurs. The relative amounts of wall condensation or direct condensation on the CMT liquid depend on the liquid level in the CMT and the temperature conditions of the liquid and walls when steam enters the cold leg balance line.

Figures 3.4-1 and 3.4-2 depict an idealized view of the condensation processes within the CMT for the two different condensation periods. As seen in Figure 3.4-1, a full CMT with the diffuser models the condensation process as submerged jets where the individual holes in the diffuser are releasing the steam into the subcooled CMT water. In this mode of operation, the condensation is occurring directly in the CMT liquid, and there is no CMT wall condensation. The steam that is entering the

CMT is assumed to be saturated at the system pressure, and the CMT liquid is assumed to be initially at 100°F.

The CMT liquid level after the tank has partially drained is shown in Figure 3.4-2. In this configuration, there is wall condensation as well as direct condensation on the CMT liquid. It is assumed that steam enters the CMT at saturated conditions. Direct steam condensation in the CMT liquid and wall condensate film develops a thermal layer at the steam-liquid interface. The thickness and temperature of this layer affects the liquid surface condensation rate. Writing an energy balance for the steam in terms of these two condensation mechanisms yields:

$$\dot{m}_{BAL} h_{fg} = q_{WS} + q_{LS} \tag{3.4-23}$$

where it is assumed that the steam gives up only its latent heat, h_{fg}. In this equation, q_{WS} is the energy transferred to the condensate film on the CMT walls, and q_{LS} is the energy directly transferred to the cold CMT liquid as the steam flows out of the diffuser and is condensed. The amount of energy transferred to the liquid film on the CMT walls is given by:

$$q_{WS} = H_{LF} a_{ws} (T_d - T_{ws}) \tag{3.4-24}$$

where H_{LF} is a heat transfer coefficient for condensation of steam on vertical surfaces. This coefficient is obtained in the bottom-up scaling analysis. The total CMT wall surface area exposed to the steam is a_{ws}, and $(T_d - T_{ws})$ is the temperature difference across the condensate film, as depicted in Figure 3.4-2, and depends on the liquid level in the tank.

Early in the transient when the CMT is initially filled, no wall area is exposed, such that $q_{ws} = 0$ and the steam is directly condensed in the subcooled CMT liquid at the diffuser. The amount of energy directly transferred to the CMT liquid, q_{LS}, can be estimated by:

$$q_{LS} = H_{LS_i} A_I (T_d - T_l) \tag{3.4-25}$$

where H_{LS_i} is the interfacial condensation heat transfer coefficient that depends on the diffuser geometry and the steam flow rates into the diffuser, and A_I is the interfacial area between the steam and CMT liquid.

In this situation, the flow rate in the balance line is equal to the condensation rate occurring at the diffuser. Therefore, the balance line flow is given as:

$$\dot{m}_{BAL} = \frac{H_{LS_i} A_I (T_d - T_l)}{h_{fg}} \tag{3.4-26}$$

and the continuity equation for the CMT becomes:

$$\frac{d}{dt}\left(\rho_\ell A_t L_\ell\right) = \frac{H_{LS_i} A_i \left(T_d - T_\ell\right)}{h_{fg}} - \dot{m}_{CMT} \qquad (3.4\text{-}27)$$

Since the CMT does not drain and remains full, the left hand side of this equation is zero.

This equation directly relates to the draining rate of the CMT to the condensation that is occurring at the diffuser in the CMT for the initial condensation and draining period.

As the top liquid layer around the diffuser is heated by condensation, the CMT begins to drain and the diffuser becomes uncovered. Condensation can now occur on the CMT walls as well as on the interface between the steam space and the CMT liquid in the tank; therefore, the steam flow in the balance line must now equal the sum of wall and liquid condensation rate.

Substituting Equations 3.4-24 and 3.4-25 into 3.4-23 and solving for the balance line mass flow rate yields:

$$\dot{m}_{BAL} = \frac{H_{LP} a_{ws}\left(T_d - T_{ws}\right)}{h_{fg}} + \left[H_{LS}\right] \frac{\left(T_d - T_\ell\right) A_t}{h_{fg}} \qquad (3.4\text{-}28)$$

where the conduction effects into the CMT liquid are ignored.

Substituting Equation 3.4-28 into 3.4-22 yields:

$$\frac{d}{dt}\left(\rho_\ell A_t L_\ell\right) = \frac{H_{LP} a_{ws}\left(T_d - T_{ws}\right)}{h_{fg}} + \left[H_{LS}\right] \frac{\left(T_d - T_\ell\right) A_t}{h_{fg}} - \dot{m}_{CMT} \qquad (3.4\text{-}29)$$

where H_{LS} is the condensation coefficient on the liquid surface once the CMT has begun to drain, and A_t is the steam/liquid surface area for a given tank level.

This equation directly relates the rate of change (draining) of the CMT to the condensation processes on the walls and surfaces for a partially drained CMT.

Equations 3.4-27 and 3.4-29 are part of the governing equations for CMT scaling.

The liquid energy equation, Equation 3.4-9, can also be made specific to the CMT draining mode by implementing the definition of $\dot{m}_{BAL}$ provided by either Equation 3.4-26 or 3.4-28, depending if the CMT is full and condensation is only at the diffuser, or if the CMT had started to drain and condensation was occurring at the walls and the steam/water interface. Thus, the CMT liquid energy equation becomes:

$$\frac{d}{dt}\left(\rho_\ell A_t L_\ell C_{v\ell} T_\ell\right) = (\dot{m}h)_{BAL} - (\dot{m}h)_{CMT} \qquad (3.4\text{-}30)$$

where the heat loss from the tank, q_t, is assumed to be negligible.

If the condensation is only occurring at the steam diffuser and the CMT level has not begun to decrease, then Equation 3.4-26 can be substituted into the liquid energy equation, Equation 3.4-30, and a convective heat loss term can be added to give:

$$\frac{d}{dt}\left(\rho_\ell A_t L_\ell C_{v\ell} T_\ell\right) = h_{BAL}\left[\frac{H_{LS_i} A_t (T_d - T_\ell)}{h_{fg}}\right] - (\dot{m}h)_{CMT} - h_{CONV} A_{CONV}\left(T_\ell - \bar{T}_s\right) \qquad (3.4\text{-}31)$$

The level of the CMT is assumed to be full since the effects of the wall condensation have been ignored in this case. For the cases in which the CMT stays full and condensation is only occurring at the diffuser, a convection heat loss term to the initially cold CMT wall is added. For this calculation, the wall is assumed to be a lumped thermal mass, and the heat transfer is from the heated water layer by natural convection using the McAdams correlation described in Section 2.0. The area term used in the calculation, A_{CONV}, is the area associated with the mixing layer chosen for the calculation. The value $\bar{T}_s$ is the average wall temperature for the convection calculation. While this is less precise, the convection heat transfer to the walls is much smaller than the energy being added from the steam flow into the CMT.

Once the tank begins to drain and the diffuser is uncovered, then the liquid energy equation is given by substituting Equation 3.4-28 into 3.4-30 to give:

$$\frac{d}{dt}\left(\rho_\ell A_t L_\ell C_{v\ell} T_\ell\right) = h_{BAL}\left[\frac{H_{LF} a_{ws}(T_d - T_{ws})}{h_{fg}} + [H_{LS}]\frac{(T_d - T_\ell)A_t}{h_{fg}}\right] - (\dot{m}h)_{CMT} \qquad (3.4\text{-}32)$$

Because the CMT walls are thick structures and are initially at ambient conditions, a more detailed solid structure energy equation is considered for the wall condensation. For the CMTs, the structure energy equation is written as follows:

$$\frac{\partial}{\partial t}\left(\rho_s V_s C_{vs} T_s\right) = \frac{1}{r}\frac{\partial}{\partial r}\left(r k_s \frac{\partial T_s}{\partial r}\right) \tag{3.4-33}$$

which assumes one-dimensional heat transfer in the CMT wall. The boundary conditions become:

$$k_s \frac{\partial T_s}{\partial r})_{r=R_i} = H_{LF}\,(T_d - T_{ws}) \tag{3.4-34}$$

at the inner surface where condensation is occurring with the transient wall surface temperature T_{ws}. The outer wall boundary condition is:

$$k_s \frac{\partial T_s}{\partial r})_{r=R_o} = 0 \tag{3.4-35}$$

where it is assumed that the heat transfer from the outer surface of the tank is assumed to be sufficiently small, so the tank is adiabatic.

The use of the one-dimensional conduction equation permits a more accurate assessment of the wall heat up and condensation effects and, therefore, the draining behavior of the CMT. This is particularly important because the plant CMT has a 7.78-in. wall thickness, while the test CMT has a wall thickness of 2.32 in. Cylindrical coordinates are used for the CMT wall conduction calculation, spherical coordinates are used for the plant CMT head, and a modified spherical coordinate system is used for the ellipsoidal head of the test CMT to calculate the wall and head heat-up rates.

It should be noted that the CMT wall surface participating in the energy exchange process is limited to that section of the tank that has its inner wall surface exposed to steam. As the CMT drains, more surface is exposed and, hence, condensation on the walls should increase.

Equations 3.4-27, 3.4-29, 3.4-31, and 3.4-32 forms the basis of the top-down scaling analysis. These equations are listed in Table 3.4-4 for purposes of future reference for both CMT condensation modes.

Equations 3.4-27, 3.4-29, 3.4-31, and 3.4-32 are made dimensionless using the CMT boundary, initial, and geometry conditions given in Table 3.4-5. Applying these conditions and dividing the liquid mass equation by $(\dot{m}_{CMT})_0$ and the energy equation by $(\dot{m}_{CMT} h_{fg})_0$, yields the dimensionless equations presented in Table 3.4-6. The dimensionless equations in Table 3.4-6 and 3.4-7 cover the case with the condensation at the diffuser. Tables 3.4-8 and 3.4-9 provide the dimensionless equations when a level exists in the CMT and condensation occurs on the walls and liquid surface. The structure

conduction equations used in Tables 3.4-8 and 3.4-9 can be put into a dimensionless form, as given in Table 3.4-7, which yields the Biot number and the Fourier number defined as:

$$B_i = \frac{H_{LF}L}{k_s} = \frac{H_{LF}\left(R_o - R_i\right)}{k_s} \tag{3.4-36}$$

and

$$F_o = \frac{k_s t}{\rho_s C_{vs} L^2} = \frac{\alpha t}{\left(R_o - R_i\right)^2} \tag{3.4-37}$$

which characterizes the conduction process in the CMT wall and dome.

Tables 3.4-7 and 3.4-9 list the CMT drain time constant, the solid structure specific frequency, and the characteristic time ratios for the different modes of CMT draining.

TABLE 3.4-4
BALANCE EQUATIONS FOR TOP-DOWN SCALING ANALYSIS OF THE CMTS

Liquid Mass:

$$\frac{d}{dt}(\rho_\ell A_t L_\ell) = \frac{H_{LS_i} A_t (T_d - T_\ell)}{h_{fg}} - \dot{m}_{CMT} \tag{3.4-27}$$

(Condensation at the diffuser)

$$\frac{d}{dt}(\rho_\ell A_t L_\ell) = \frac{H_{LF} a_{ws} (T_d - T_{ws})}{h_{fg}} + [H_{LS}] \frac{(T_d - T_\ell) A_t}{h_{fg}} - \dot{m}_{CMT} \tag{3.4-29}$$

(Condensation on walls and liquid surface)

Liquid Energy:

$$\frac{d}{dt}(\rho_\ell A_t L_\ell C_{v\ell} T_\ell) = h_{BAL} \left[\frac{H_{LS_i} A_t (T_d - T_\ell)}{h_{fg}} \right] - (\dot{m}h)_{CMT} - A_{CONV} h_{CONV} \left(T_\ell - \bar{T}_s \right) \tag{3.4-31}$$

(Condensation at the diffuser)

$$\frac{d}{dt}(\rho_\ell A_t L_\ell C_{v\ell} T_\ell) = \frac{h_{BAL} H_{LF} a_{ws} (T_d - T_{ws})}{h_{fg}} + \frac{h_{BAL} [H_{LS}] (T_d - T_\ell) A_t}{h_{fg}} - (\dot{m}h)_{CMT} \tag{3.4-32}$$

(Condensation on wall and liquid surface

Solid Structure Energy:

$$\frac{d}{dt} \left(M_S C_{V_s} \bar{T}_s \right) = A_{CONV} h_{CONV} \left(T_\ell - \bar{T}_s \right)$$

(Condensation at the diffuser)

$$\frac{\partial}{\partial t} (\rho_s V_s C_{vs} T_s) = \frac{1}{r} \frac{\partial}{\partial r} \left[(r k_s \frac{\partial T_s}{\partial r}) \right] \tag{3.4-33}$$

(Condensation on the wall and surface)

Where the boundary conditions are:

$$k_s \frac{\partial T_s}{\partial r})_{r=R_i} = H_{LF} (T_d - T_{ws}) \tag{3.4-34}$$

and

$$k_s \frac{\partial T_s}{\partial r})_{r=R_o} = 0 \tag{3.4-35}$$

TABLE 3.4-5
CMT BOUNDARY AND INITIAL CONDITIONS

$$\rho_\ell A_t L_\ell = (\rho_{\ell 0} A_{t0} L_{t0})\ \rho_\ell^* A_t^* L_\ell^*$$

$$H_{LF} a_{ws} = (H_{LF0} a_{ws0})\ H_{LF}^* a_{ws}^*$$

$$H_{LS_i} A_I = (H_{LS_i} A_I)_0\ H_{LS_i}^* A_I^*$$

$$\frac{k_\ell}{\delta_T} A_t = \left(\frac{k_{\ell 0} A_{t0}}{\delta_{T0}}\right) \frac{k_\ell^* A_t^*}{\delta_T^*}$$

$$H_{LS} A_t = (H_{LS0} A_{t0}) H_{LS}^* A_t^*$$

$$h_{fg} = h_{fg0} H_{fg}^* \qquad (3.4\text{-}38)$$

$$C_{v\ell} T_\ell = (C_{v\ell} T_\ell)_0 C_{v\ell}^* T_\ell^*$$

$$h_{BAL} = (h_{BAL})_0 h_{BAL}^*$$

$$q_t = (q_t)_0 q_t^*$$

$$\dot{m}_{CMT} = (\dot{m}_{CMT})_0\ \dot{m}_{CMT}^*$$

$$A_{CONV} h_{CONV} = (A_{CONV} h_{CONV})_0 A_{CONV}^* h_{CONV}^*$$

$$\left(T_\ell - \overline{T}_w\right) = \left(T_\ell - \overline{T}_w\right)_0 \left(T_\ell^* - \overline{T}_w^*\right)$$

$$M_s C_{vs} T_s = (M_s C_{vs} T_s)_0\ M_s^* C_{vs}^* T_s^*$$

$$\Theta = \frac{T_d - T_s}{(T_d - T_s)_0} \qquad (3.4\text{-}39)$$

$$B_i = \frac{H_{LF}(R_o - R_i)}{k_s} \qquad (3.4\text{-}40)$$

$$F_0 = \frac{\alpha t}{(R_o - R_i)^2} \qquad (3.4\text{-}41)$$

TABLE 3.4-6
DIMENSIONLESS BALANCE EQUATIONS FOR TOP-DOWN SCALING OF THE CMTS, WHEN CONDENSATION OCCURS AT THE DIFFUSER

Liquid Mass:

$$\tau_{CMT}\frac{d}{dt}\left(\rho_l^* A_t^*\right)L_l^* = \prod_{lcond}\left(H_{LS_i}^*\right)\frac{A_I^*\left(T_d - T_l\right)^*}{h_{fg}^*} - \dot{m}_{CMT}^* \qquad (3.4\text{-}42)$$

Liquid Energy:

$$\tau_{CMT}\prod_{e,CMT}\frac{d}{dt}\left(\rho_l^* A_t^* L_l^* C_{vl}^* T_l^*\right)$$

$$= \prod_{h,CMT}\prod_{lcond} h_{BAL}^*\left(H_{LS_i}^*\right)\frac{A_I^*\left(T_d - T_l\right)^*}{h_{fg}} - (\dot{m}h)_{CMT} \qquad (3.4\text{-}43)$$

$$+ \prod_{CONV}\left(A_{CONV}^* h_{CONV}^*\right)\left(T_l^* - \overline{T}_S^*\right)$$

Solid Structure Energy:

$$\prod_S \frac{d}{dt}\left(M_S^* C_{V_s}^* \overline{T}_S^*\right) = A_{CONV}^* h_{CONV}^*\left(T_l^* - \overline{T}_S^*\right) \qquad (3.4\text{-}44)$$

TABLE 3.4-7
CMT TIME CONSTANT, SPECIFIC FREQUENCY,
CHARACTERISTIC TIME RATIOS
WHEN CONDENSATION OCCURS AT THE DIFFUSER

Drain Rate Time Constant:

$$\tau_{CMT} = \left(\frac{\rho_\ell A_t L_\ell}{\dot{m}_{CMT}} \right)_0 \tag{3.4-45}$$

Solid Structure Specific Frequency:

$$\tau_{S,CMT} = \left(\frac{M_s \, C_{vs}}{H_{LF} \, a_{ws}} \right)_0 \tag{3.4-46}$$

Characteristic Time Ratios:

$$\Pi_{\dot{m}cond} = \left[\left(H_{LS_i} \right) \frac{A_i (T_d - T_\ell)}{\dot{m}_{CMT} h_{fg}} \right]_0$$ Diffuser Condensation Rate Ratio (3.4-47)

$$\Pi_{c,CMT} = \left[\frac{C_{v\ell} T_\ell}{h_{CMT}} \right]_0$$ Energy Ratio (3.4-48)

$$\Pi_{h,CMT} = \left[\frac{h_{BAL}}{h_{CMT}} \right]_0$$ Enthalpy Ratio (3.4-49)

$$\Pi_{CONV} = \left[\frac{\left(A_{CONV} h_{CONV} \right) \left(T_\ell - \bar{T}_S \right)}{\dot{m}_{CMT} h_{fg}} \right]_0$$ Convective Ratio (3.4-50)

$$\Pi_S = \frac{\left(M_S C_{V_s} \bar{T}_S \right)_0}{\left(A_{CONV} h_{CONV} \right)_0 \left(T_\ell - \bar{T}_S \right)_0}$$ Structure Time Constant (3.4-51)

TABLE 3.4-8
DIMENSIONLESS BALANCE EQUATIONS FOR TOP-DOWN SCALING OF THE CMTS, WHEN A LEVEL EXISTS IN THE CMT

Liquid Mass:

$$\tau_{CMT}\frac{d}{dt}\left(\rho_{\ell}^{*}A_{t}^{*}\right)L_{\ell}^{*} = \prod_{wcond}\frac{H_{LP}^{*}a_{ws}^{*}\left(T_{d}-T_{ws}\right)^{*}}{h_{fg}^{*}} + \prod_{lcond}\left(H_{LS}^{*}\right)\frac{A_{t}^{*}\left(T_{d}-T_{\ell}\right)^{*}}{h_{fg}^{*}} - \dot{m}_{CMT}^{*} \quad (3.4\text{-}52)$$

Liquid Energy:

$$\tau_{CMT}\prod_{c,CMT}\frac{d}{dt}\left(\rho_{\ell}^{*}A_{t}^{*}L_{\ell}^{*}\ C_{v\ell}^{*}T_{\ell}^{*}\right) = \prod_{h,CMT}\prod_{wcond}\frac{H_{BAL}^{*}h_{LP}^{*}a_{ws}^{*}\left(T_{d}-T_{ws}\right)^{*}}{h_{fg}^{*}} + \prod_{h,CMT}\prod_{\ell cond}h_{BAL}^{*}\left(H_{LS}^{*}\right)\frac{A_{t}^{*}\left(T_{d}-T_{\ell}\right)^{*}}{h_{fg}} - \left(\dot{m}*h*\right)_{CMT} + \prod_{q,CMT}q_{t}^{*} \quad (3.4\text{-}53)$$

Solid Structure Energy:

$$\frac{\partial\Theta}{\partial F_{o}} = \frac{1}{\eta}\frac{\partial}{\partial\eta}\left(\eta\frac{\partial\Theta}{\partial\eta}\right) \quad (3.4\text{-}54)$$

Where $F_{o} = \frac{\alpha t}{L^{2}}$ where $L = R_{o} - R_{i}$ and the boundary condition becomes:

$$\left.\frac{\partial\Theta}{\partial\eta}\right)_{\eta=\eta_{i}} = \left.\frac{H_{LP}L}{k_{S}}\Theta\right)_{\eta=\eta_{i}} = B_{i}\Theta)_{\eta=\eta_{i}} \quad (3.4\text{-}55)$$

TABLE 3.4-9
CMT TIME CONSTANT, SPECIFIC FREQUENCY,
CHARACTERISTIC TIME RATIOS
WHEN LEVEL EXISTS IN THE CMT

Drain Rate Time Constant:

$$\tau_{CMT} = \left(\frac{\rho_\ell A_t L_\ell}{\dot{m}_{CMT}} \right)_0 \tag{3.4-56}$$

Solid Structure Specific Frequency:

$$\tau_{S,CMT} = \left(\frac{M_s \, C_{vs}}{H_{LF} \, a_{ws}} \right)_0 \tag{3.4-57}$$

Characteristic Time Ratios:

$$\Pi_{wcond} = \left(\frac{H_{LF} a_{ws} (T_d - T_{ws})}{\dot{m}_{CMT} h_{fg}} \right)_0$$ Wall Condensation Rate Ratio (3.4-58)

$$\Pi_{\ell cond} = \left[(H_{LS}) \frac{A_\ell (T_d - T_\ell)}{\dot{m}_{CMT} h_{fg}} \right]_0$$ Liquid Condensation Rate Ratio (3.4-59)

$$\Pi_{c,CMT} = \left[\frac{C_{v\ell} T_\ell}{h_{CMT}} \right]_0$$ Energy Ratio (3.4-60)

$$\Pi_{h,CMT} = \left[\frac{h_{BAL}}{h_{CMT}} \right]_0$$ Enthalpy Ratio (3.4-61)

$$B_i = \frac{H_{LF} (R_o - R_i)}{k_S}$$ Biot Number (3.4-62)

$$F_o = \frac{\alpha t}{(R_o - R_i)^2}$$ Fourier Number (3.4-63)

The CMT liquid balance equations implement the same time scale, $\tau_{CMT,0}$. This permits direct comparisons of the Π groups. The time scale for the solid energy equation, $\tau_{s,CMT}$, differs from the CMT liquid time scale. The ratio of these time scales is written as follows:

$$\varepsilon_{CMT,t} = \frac{\tau_{CMT,0}}{\tau_{s,CMT}} = \frac{M_f H_{LF} a_{ws}}{\dot{m}_{CMT} M_s C_{vs}} \qquad (3.4\text{-}64)$$

When $\varepsilon_{CMT,t} << 1$, the CMT liquid variables change more rapidly than those of the solid, that is, the CMT drains before the CMT walls are significantly affected. When $\varepsilon_{CMT,t} >> 1$, the solid variables change more rapidly than those of the liquid because the draining rate is so slow that the CMT walls are directly affected. Thus, the time scale ratio presented in Equation 3.4-64 indicates the degree of coupling between the liquid transport phenomena and the heat transport phenomena in the CMT walls.

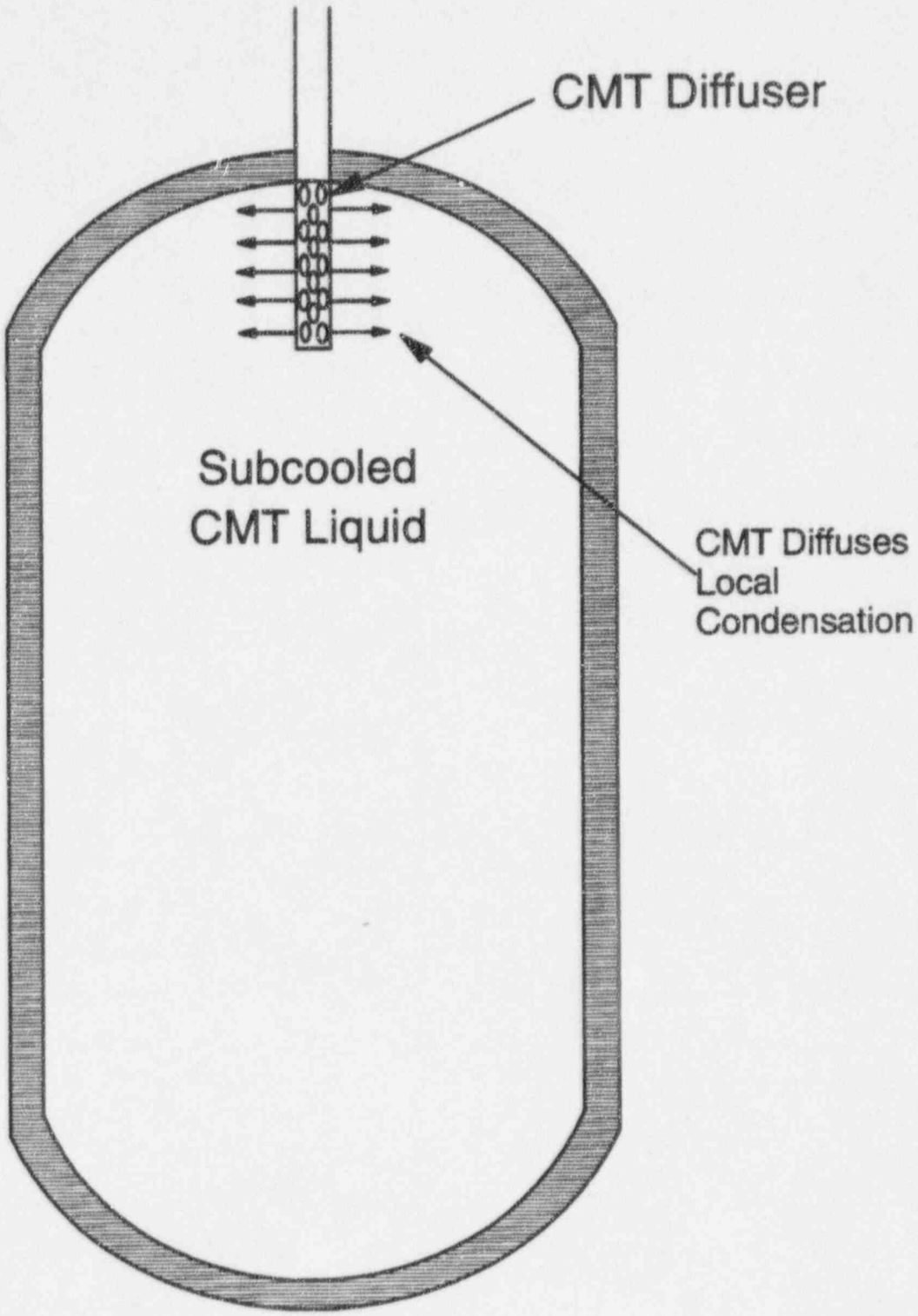

Figure 3.4-1 Diffuser Steam Condensation Behavior for a Full CMT

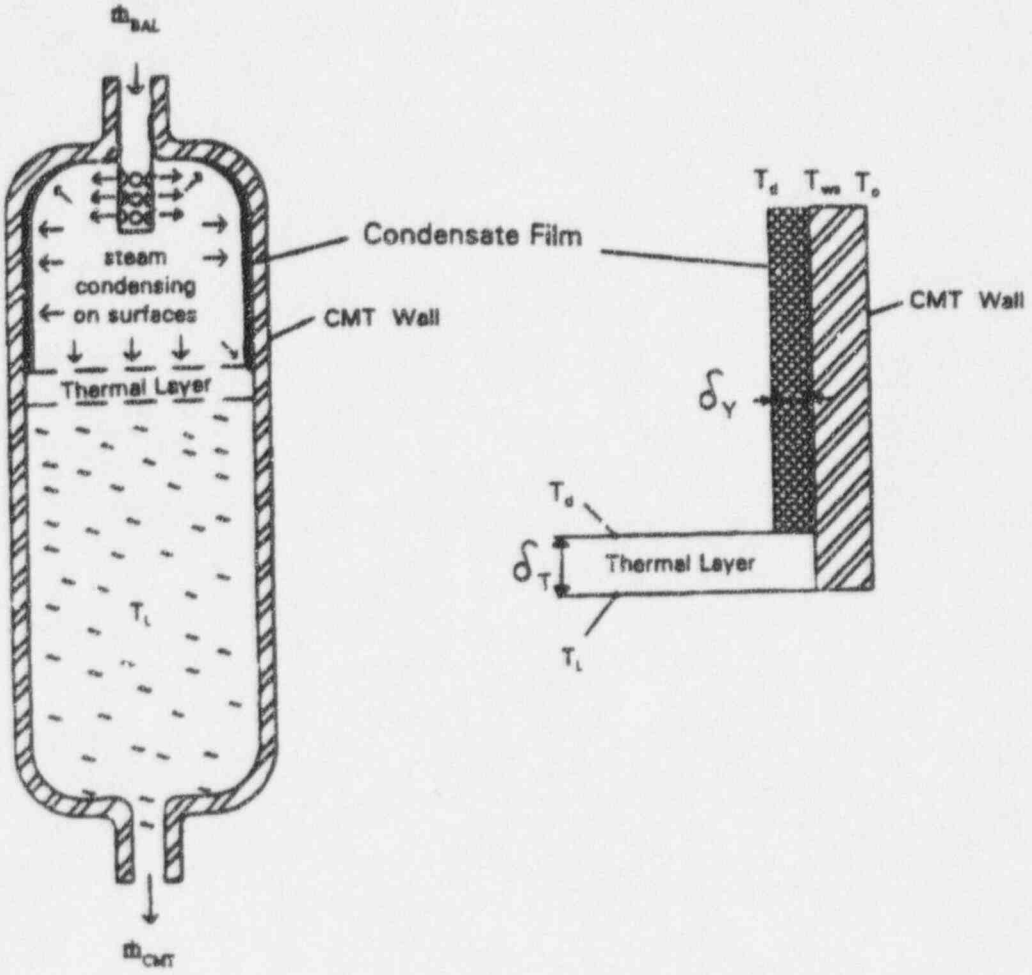

Figure 3.4-2 Idealized Model for Scaling CMT Condensation Behavior with a Level in the CMT

3.5 Bottom-Up Scaling Analysis for CMT Transient Processes

The CMT systems equations provided in Table 3.4-4 give the thermal-hydraulic response of the CMT for the different condensation modes of operation. The heat transfer coefficients are key ingredients and are assumed for the wall condensation and the direct condensation on the liquid surface.

3.5.1 Condensation on CMT Walls

It is assumed that film condensation exists on the CMT walls. The condensation heat transfer coefficient is a function of the film Reynolds number defined as:

$$Re_{\Gamma} = \frac{4\Gamma}{\mu_f} \tag{3.5-1}$$

where Γ is the film flow per unit width. The wall condensation model used in the CMT scaling analysis uses the Nusselt[8] laminar film condensation coefficient for $Re_{\Gamma} \leq 2000$; given as (see Reference 9):

$$\bar{H}_{LF} = 0.94 \left[\frac{\rho_\ell g h_{fg} k_f^3}{\mu_f L \left(T_d - T_{ws}\right)} \right]^{1/4} \tag{3.5-2}$$

where:

$$T_d = \frac{T_{ws} + T_{sat}}{2} \tag{3.5-3}$$

such that:

$$T_d - T_{ws} = \frac{1}{2} \left(T_{sat} - T_{ws}\right) \tag{3.5-4}$$

where T_{ws} is the surface temperature that is calculated from the one-dimensional CMT wall conduction solution. For turbulent film condensation, the modified Colburn[10] correlation is used, as recommended by Kreith. The correlation is given as:

$$H_{LF} = 0.056 \left(\frac{4\Gamma_c}{\mu_f} \right)^2 \left(\frac{k_f^3 \rho_\ell^2 g}{\mu_f^2} \right)^{\frac{1}{3}} Pr_f^{\frac{1}{2}} \tag{3.5-5}$$

This is a local correlation since Γ_c is the local film flow. However, in the CMT heat transfer analysis, an average film flow is calculated separately for the dome region and for the combined dome and cylindrical wall region. Therefore, the Γ_c in Equation 3.5-5 represents the average film flow, so the heat transfer coefficient is also taken as an average, over these regions.

3.5.2 Interfacial Condensation at the CMT Diffuser

As mentioned earlier, interfacial condensation can occur in the CMT by two different mechanisms depending on the level in the CMT. When the CMT is full, the diffuser is submerged in the subcooled CMT liquid. If the LOCA break size is large, then the cold leg balance line will void quickly before significant recirculation has occurred. Therefore, the CMT liquid is subcooled and rapid condensation occurs at the CMT diffuser. The small holes in the diffuser will create small vapor jets, which are quickly condensed by the subcooled liquid that is driven in a recirculation pattern by the steam momentum. The condensation process is limited by the circulation of the subcooled CMT liquid and its resulting temperature.

The condensation heat transfer of vapor jets into subcooled water has been examined by several authors.[6, 11, 12, 13, 14] To model the jet condensing processes, the appropriate interfacial heat transfer area, A_I, and the local heat transfer coefficient that corresponds to the interfacial area must be determined. The ORNL data from Reference 14, can be used to estimate the jet surface area for a condensing jet in subcooled water; however, the report by Catton et al., made detailed measurements on the interfacial area for the jet condensing and determined that the true interfacial area is significantly larger than the conical jet areas estimated in the ORNL data. The data from Catton et al., are used to estimate the condensation interfacial area, A_I, that could be expected to occur from the steam diffuser in the CMT. The area data for the largest subcooling are normalized on the exit jet area from their experiments and averaged over the range of flow rates. The high subcooling data is used since the initial CMT liquid temperature is highly subcooled.

For subcooled liquid, the interfacial heat transfer coefficient is calculated using a fit to Catton et al, data as a function of liquid subcooling as:

$$h_I = 635.1\ (T_{sat} - T_\ell) \left(\frac{\text{Btu}}{\text{hr. ft.}^2\text{°F}} \right) \qquad (3.5\text{-}6)$$

with a maximum value set at:

$$h_I = 100{,}000 \left(\frac{\text{Btu}}{\text{hr. ft.}^2\text{°F}} \right)$$

In addition to the Catton et al., data for jet condensation, the data from Cumo[11] and Young[12] are also used in a sensitivity study to calculate an interfacial heat transfer coefficient, h_I. The interfacial area for these sensitivity calculations is the same as that for the Catton calculations since Catton's

interfacial area data are believed to be the most accurate source of information. However, there may be double accounting of the total heat transfer using the Cumo and Young correlations with the area as determined by Catton's experiments.

When the calculations are made to examine the diffuser behavior, the CMT is liquid solid so there is no wall condensation. As the liquid layer surrounding the diffuser heats up, the hotter liquid will transfer some of its heat to the colder CMT walls by convection. The McAdams natural convection correlation, which is given in Section 2.0, is suitable for this portion of the calculation.

Once the liquid layer is heated and the CMT begins to drain, then the diffuser is uncovered and the interfacial heat transfer occurs on the liquid surface in the CMT.

3.5.3 Interfacial Condensation When the CMT has Drained and a Level Exists

A correlation for the liquid surface condensation, proposed by Bankoff,[15] is used for steam flowing countercurrent to a liquid flow on a flat channel. This particular correlation represents condensation as a hydrodynamically controlled process so that as the steam flow increases, the surface condensation increases, and it will draw in more steam flow into the CMT and further increase the condensation heat transfer coefficient. Once the CMT begins to drain and a level is established in the tank, the steam from the diffuser exits radially, flows to the CMT walls, and recirculates within the CMT. It is postulated that the steam flows parallel to the CMT liquid level and creates waves on the liquid surface, depending on the steam flow rate and the location of the liquid level to the diffuser. As the tank continues to drain, the steam recirculation flow becomes weaker since the volume of vapor space above the liquid level increases. At some point, the interfacial condensation heat transfer degenerates to condensation from stagnant steam to a liquid surface that is at or near the saturation temperature. In the limit, the heat transfer becomes conduction-limited to the liquid surface from the steam as conduction into a semi-infinite slab.

Bankoff's correlation is given as:

$$H_{LS} = 0.061 \frac{k_f}{\eta} Re_t^{1.12} Pr^{\frac{1}{2}} \qquad (3.5\text{-}7)$$

where η is the maximum interfacial wave amplitude, and the Reynold's number is given by:

$$Re_t = \frac{U_f \eta}{\nu_f} \qquad (3.5\text{-}8)$$

where U_f is the steam friction velocity for flow parallel to the liquid surface.

It is hypothesized that when the level has dropped, there is a recirculating steam flow, which is developed as the steam exits the diffuser in a radial direction and then contacts the CMT walls and

flows downward toward the liquid surface, as shown in Figure 3.5-1. Since the diffuser has a finite length, it is postulated that the downward vapor flow along the CMT walls is in the form of an annulus with a thickness equal to the length of the hole region of the diffuser. This assumption permits the calculation of the vapor velocity at the edge of the tank from the inlet steam flow rate by continuity. This model for the recirculation also ignores the wall condensation that reduces the vapor flow downward along the wall. Therefore, this model over-estimates the interfacial heat transfer on the liquid surface of a partially drained CMT. This is compensated by the liquid at the top of the CMT already heated by the steam condensation from the diffuser or from the CMT recirculation.

The calculation of the steam velocity at the edge of the CMT is used to calculate the size of the waves generated on the CMT surface by the annular jet that flows down the sides of the CMT. Also, since the steam must turn and flow parallel to the surface, the jet velocity is used to estimate the velocity flowing parallel to the CMT liquid surface to calculate the interfacial heat transfer from Equation 3.5-7.

For an incompressible, inviscid liquid, impinged upon by a steam jet, Lamb's[16] analysis of the wave height at the radial boundary of the disturbance is determined by the following force balance:

$$\rho_\ell g\eta = \frac{1}{2}\rho_j u_j^2 \tag{3.5-9}$$

where surface tension has been neglected, and η is the height of the wave formed at the edge of the disturbance, ρ_ℓ is the liquid density, ρ_j is the steam density, and u_j is the velocity of the jet. Rearranging this equation and writing it in terms of the wave height yields:

$$\eta = \left[\frac{\rho_j u_j^2}{2\rho_\ell g}\right] \tag{3.5-10}$$

This equation can also be written in terms of the mass flow rate through the balance lines as follows:

$$\eta = \left[\frac{\dot{m}_{BAL}^2}{2\rho_j\rho_\ell a_j^2 g}\right] \tag{3.5-11}$$

where a_j is the cross-sectional flow area of the steam jet at the point of impact with the fluid surface. It should be noted that the wall condensation increases the $\dot{m}_{BAL}$ flow, which enhances the liquid surface condensation.

Equation 3.5-7 uses a friction velocity to calculate the Reynolds number, as given in Equation 3.5-8. The friction velocity is defined as:

$$U_f = \frac{\sqrt{\tau_w g_c}}{\rho_v} \tag{3.5-12}$$

using:

$$\tau_w = \frac{fL}{D} \frac{\rho_v U^2}{2g_c} \tag{3.5-13}$$

for the shear stress. Assuming that a constant friction factor of f = 0.02 and L/D is unity, the friction velocity can be expressed in terms of the annular steam jet velocity as:

$$U_f = 0.1\ U_j \tag{3.5-16}$$

which is used in the calculation of the Reynolds number for the Bankoff interfacial heat transfer correlation given in Equation 3.5-7. The interfacial area used in this calculation is the cross-sectional area of the CMT.

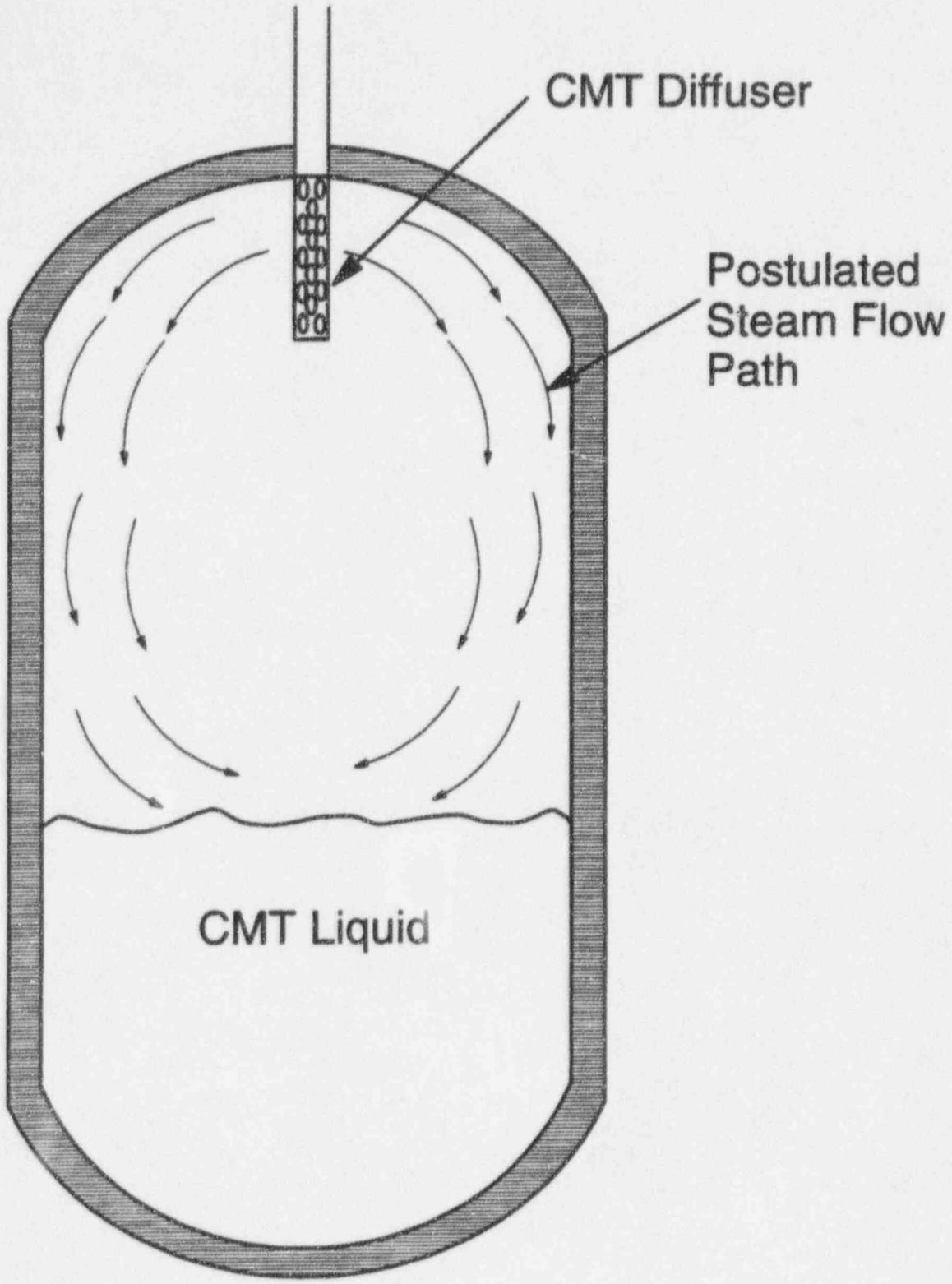

Figure 3.5-1 Postulated Steam Recirculation Flow Pattern for Partially Drained CMT

4.0 COMPARISON CALCULATIONS OF THE AP600 PLANT CMT DRAINING BEHAVIOR AND THE CMT TEST DRAINING BEHAVIOR

4.1 Introduction and Approach

The equations that describe the CMT draining behavior are provided in Table 3.4-4. The dimensionless versions of these equations are provided in Tables 3.4-6 to 3.4-9 and indicate the dimensionless Π groups that are preserved between the test and the plant. These equations are programmed and solved to estimate the plant and test CMT behavior for both modes of CMT draining. Calculations are performed considering that the CMT was liquid-filled and the inlet steam was condensed at the diffuser, and then separate calculations are performed for the case in which a level existed in the CMT and condensation could occur on both the CMT walls and the steam/liquid interface. Several assumptions are made in solving the system of equations:

1) Calculations are performed with a full CMT to evaluate the diffuser condensation. For calculations with the full CMT, the transient term in the mass continuity equation in Table 3.4-4 becomes zero, and the mass of steam into the CMT equals the mass of condensate out of the CMT.

2) Calculations are also performed at a fixed CMT water level that simulated a quasi-steady-state CMT draining behavior. This is valid since the CMT drain rates are small. This approach fixed the amount of CMT wall surface area and liquid surface area exposed to the incoming steam flow.

3) The wall condensation coefficient is assumed to be an average value on the dome or on the cylindrical walls of the CMT. The film flow is calculated from the condensation and used to choose either a laminar or turbulent coefficient.

4) The conduction in the dome and the cylindrical portion of the tank is calculated separately using ... transient, one-dimensional conduction equation and the specific geometry of the component.

5) The liquid energy equation provided in Table 3.4-4 solves for the transient liquid temperature in the CMT water. The CMT mixing depth is varied, in a parametric fashion in the calculations, to examine its effect on the liquid surface condensation and the overall plant and test CMT response. As the condensation heat transfer occurs on the liquid surface, a stratified hot liquid layer develops and the local fluid temperature approaches the saturation temperature. As the liquid temperature increases, the condensation heat transfer to the liquid decreases. Using different thicknesses of the liquid layer changes the relative importance of the liquid surface condensation.

4.2 Calculated Results for Condensation at the CMT Diffuser for the AP600 Plant and the CMT Test

The equations given in Table 3.4-4 are programmed using the assumptions given in Section 4.1 to calculate the heat transfer performance for the CMT when the tank is full and condensation occurs at the diffuser. Two pressures are examined for both the plant CMT and the CMT test. A pressure of 1100 psia is used to capture the thermal-hydraulic behavior of the CMT at a typical small-break pressure level; and a pressure of 60 psia is used to model the CMT behavior for large-break LOCA conditions. In both of these calculations, the CMT is full, so there is no wall condensation effect. The calculations are performed for a mixing layer thickness of 0.5, 1.0, 1.5, and 3.0 ft. below the diffuser. The mixing layer thickness is an input quantity to the calculation and cannot be explicitly calculated from the equations given in Table 3.4-4.

4.2.1 Calculated Results at 1100 psia for Different Mixing Depths

Calculations are performed for a full CMT for both the plant and the CMT test. The calculations for the CMT test are presented followed by the calculations for the AP600 plant. Comparisons are then made between the sets of calculations.

Figures 4.2-1 and 4.2-2 show the CMT test liquid layer temperature for the different mixing depths at different pressures. The mixing depth is defined as the distance below the bottom of the diffuser. As expected, as the mixing depth increases, the time to reach the saturation temperature increases since there is more subcooled liquid that must be heated by the condensation process. The liquid that is above the bottom of the diffuser is also included in the mixing layer. Figure 4.2-3 shows the calculated interfacial heat transfer coefficient used in the calculations based on the Catton et al., data and is a function of the CMT subcooling as seen in Equation 3.5-6. As the figure indicates, the interfacial heat transfer coefficient is large initially, resulting in a large condensation rate, which induces a large mass flow into the CMT diffuser. For the full CMT cases, the induced steam flow equals the condensation rate at the diffuser. The larger interfacial heat transfer coefficient for 1100 psia is due to the larger initial subcooling. Also, the thicker mixing depth retains the liquid subcooling for longer times, so the heat transfer is higher. As the CMT liquid temperature increases, the condensation rate decreases, which then decreases the inlet mass flow into the diffuser. Figures 4.2-4 and 4.2-5 show the condensation flow rate for the different mixing depths. As the mixing depth increases, the condensate mass flow increases as expected.

Similar plots for the plant CMT are shown in Figures 4.2-6 to 4.2-10. The same trends are seen for the plant calculation as in the test calculations. As the mixing depth increases, the amount of induced steam flow into the diffuser increases, and the time to heat the thicker water layer also increases. The heat transfer coefficient behavior is the same between the test and the plant and depends on the condensation-induced steam flow into the diffuser.

The CMT test calculations can be compared to the plant CMT calculation. The calculated condensate flow rate, which is a measure of the heat transfer that is occurring at the diffuser, is normalized by the

diffuser flow area to obtain a condensate mass flux for both the plant CMT and the test CMT. The ratio of the CMT test condensate mass flux to the AP600 plant condensate mass flux is shown in Figure 4.2-11 and 4.2-12 for the different assumed mixing depths at the different pressures.

The relatively good agreement between the plant and the CMT test for the condensate mass flux indicates that the scaling logic used for the plant CMT diffuser and the test CMT diffuser is consistent. The agreement also indicates that the test captures the diffuser condensation effects in the plant. The normalized time constant for the diffuser condensation, given as Equation 3.4-47 in Table 3.4-7, has a value of unity for both the plant and the test CMT since the condensation is normalized on the energy rate out of the CMT. Therefore, this ratio is always unity for the plant and the test. Since this is the case, the best comparison is the ratio of the condensate mass fluxes as shown in Figures 4.2-11 and 4.2-12.

A sensitivity study is also performed by varying the condensation heat transfer coefficient for the diffuser. The heat transfer coefficients, as given by Cumo and Young, are programmed into the calculation model and calculations are performed at 1100 psia for the different mixing depths. Figure 4.2-13 shows the comparisons of the different heat transfer coefficients for a mixing depth of 1.5 ft. for the AP600 plant case at 1100 psia. As the figure indicates, the Cumo correlation gives higher interfacial heat transfer than the other correlations and heats the liquid layer faster. Figure 4.2-14 shows the calculated heat up of the liquid layer for the test using the Cumo heat transfer correlation for the different mixing depths, and Figure 4.2-15 shows the same calculation using Young correlation for the same conditions. The reason that the plot for the Cumo heat transfer correlation is so short in Figure 4.2-13 is that at a mixing depth of 1.5 ft., the liquid is quickly heated to nearly the saturation temperature, as seen in Figure 4.2-14. As the layer approaches the saturation temperature, the interfacial heat transfer approaches zero and the steam is no longer condensed. As indicated above, the higher interfacial heat transfer coefficient calculated by the Cumo correlation results in a more rapid heatup of the liquid layer at the top of the CMT as compared to the interfacial heat transfer correlation by Catton et al., or by Young. The same trends are also seen for calculations for the CMT test facility.

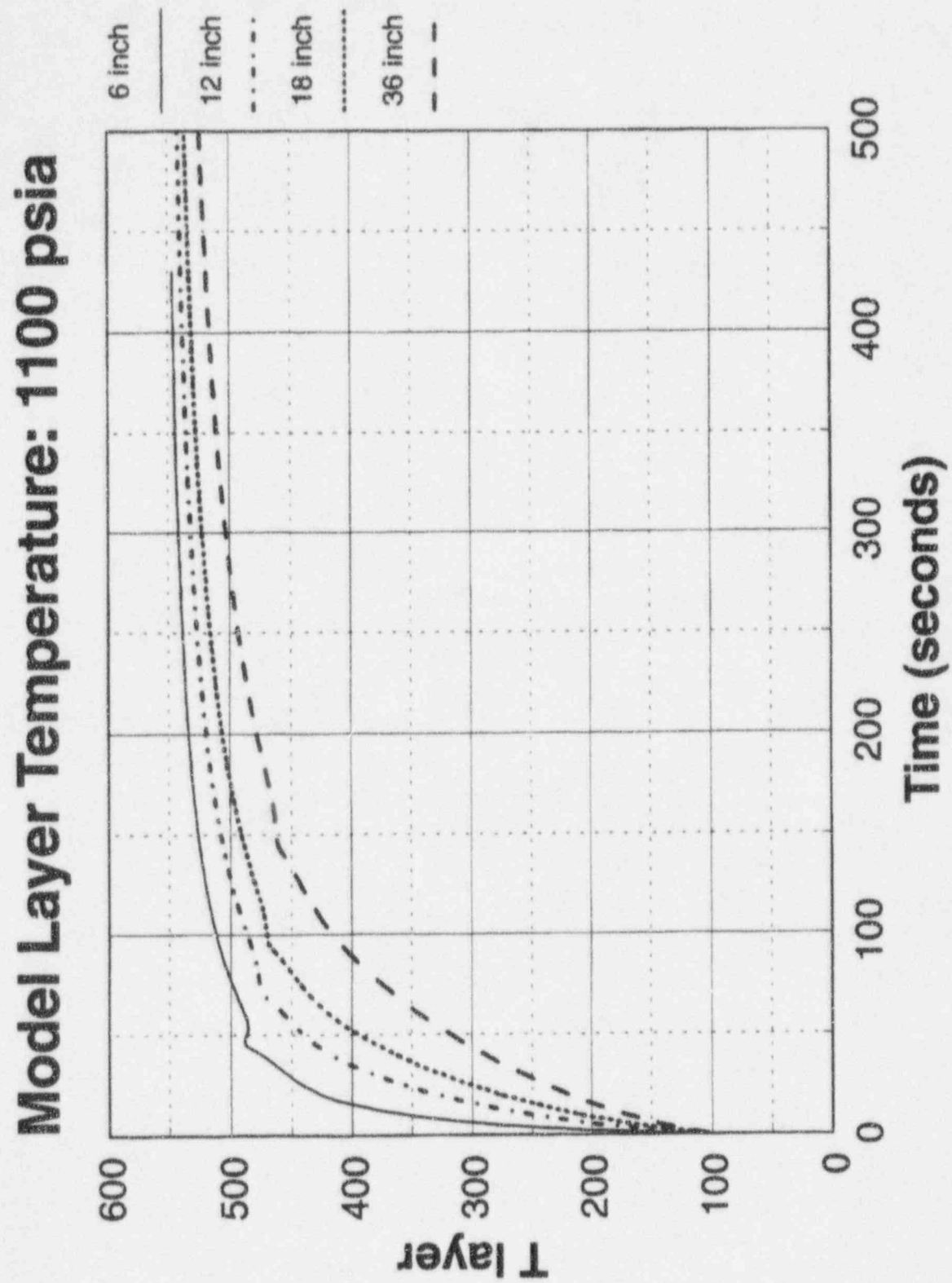

Figure 4.2-1 Calculated CMT Test Liquid Layer Temperature (°F) for Different Mixing Depths at 1100 psia for Diffuser Condensation

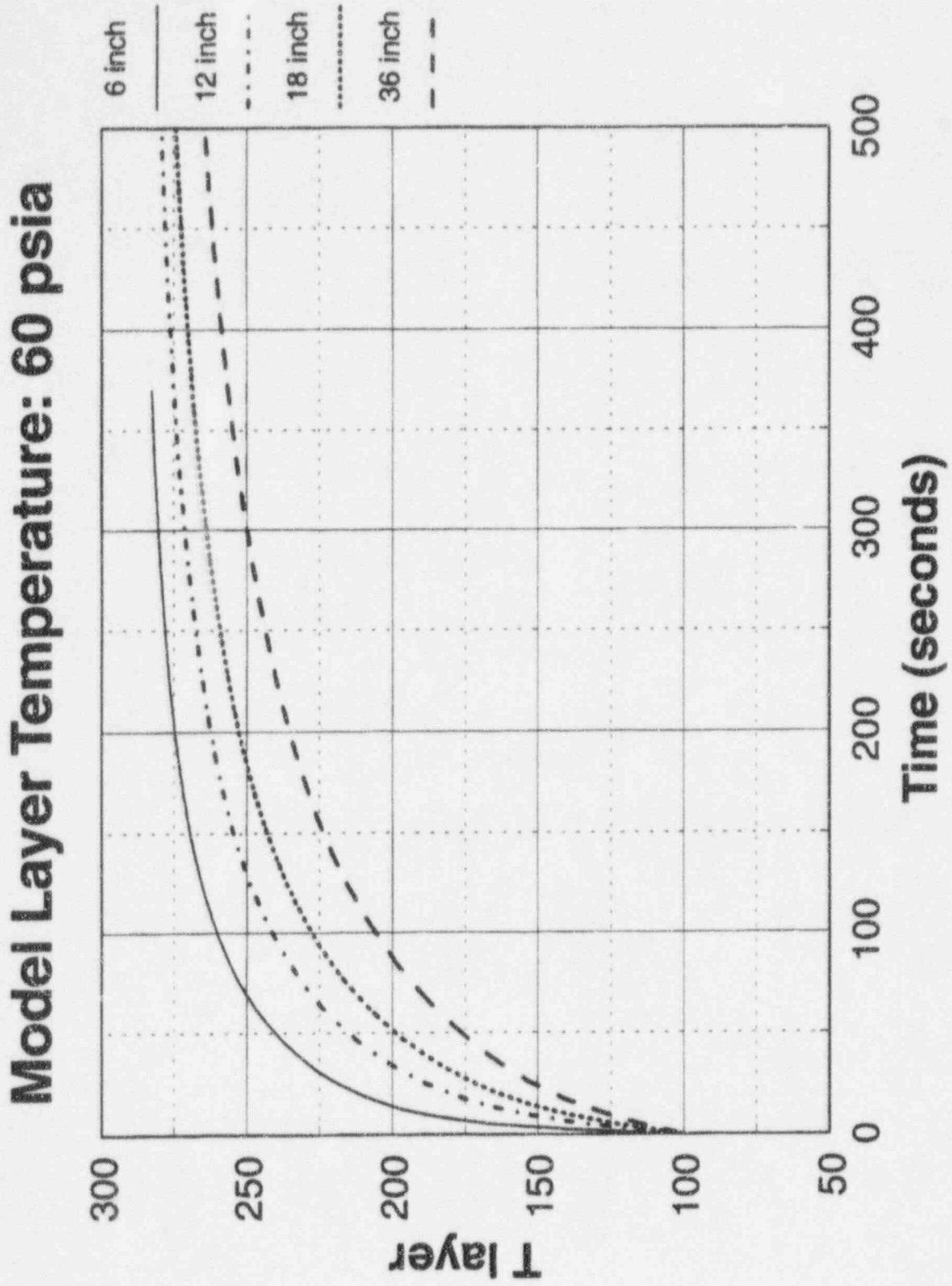

Figure 4.2-2 Calculated CMT Test Liquid Layer Temperature (°F) for Different Mixing Depths at 60 psia for Diffuser Condensation

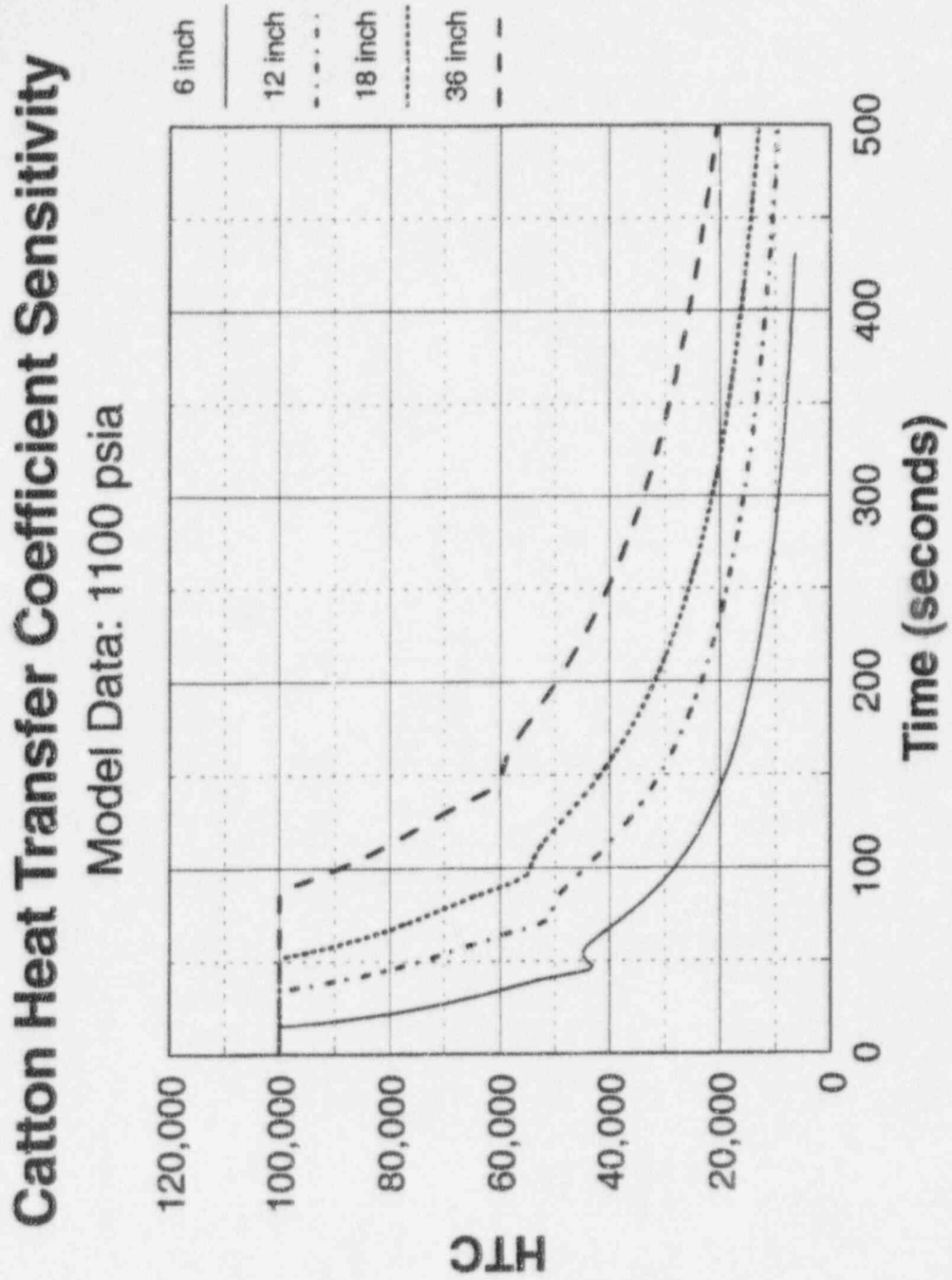

Figure 4.2-3 Calculated Interfacial Condensation Heat Transfer Coefficient (Btu/hr-ft^2-°F) from Catton et al., for Different Mixing Depths for the CMT Test at 1100 psia for full CMT

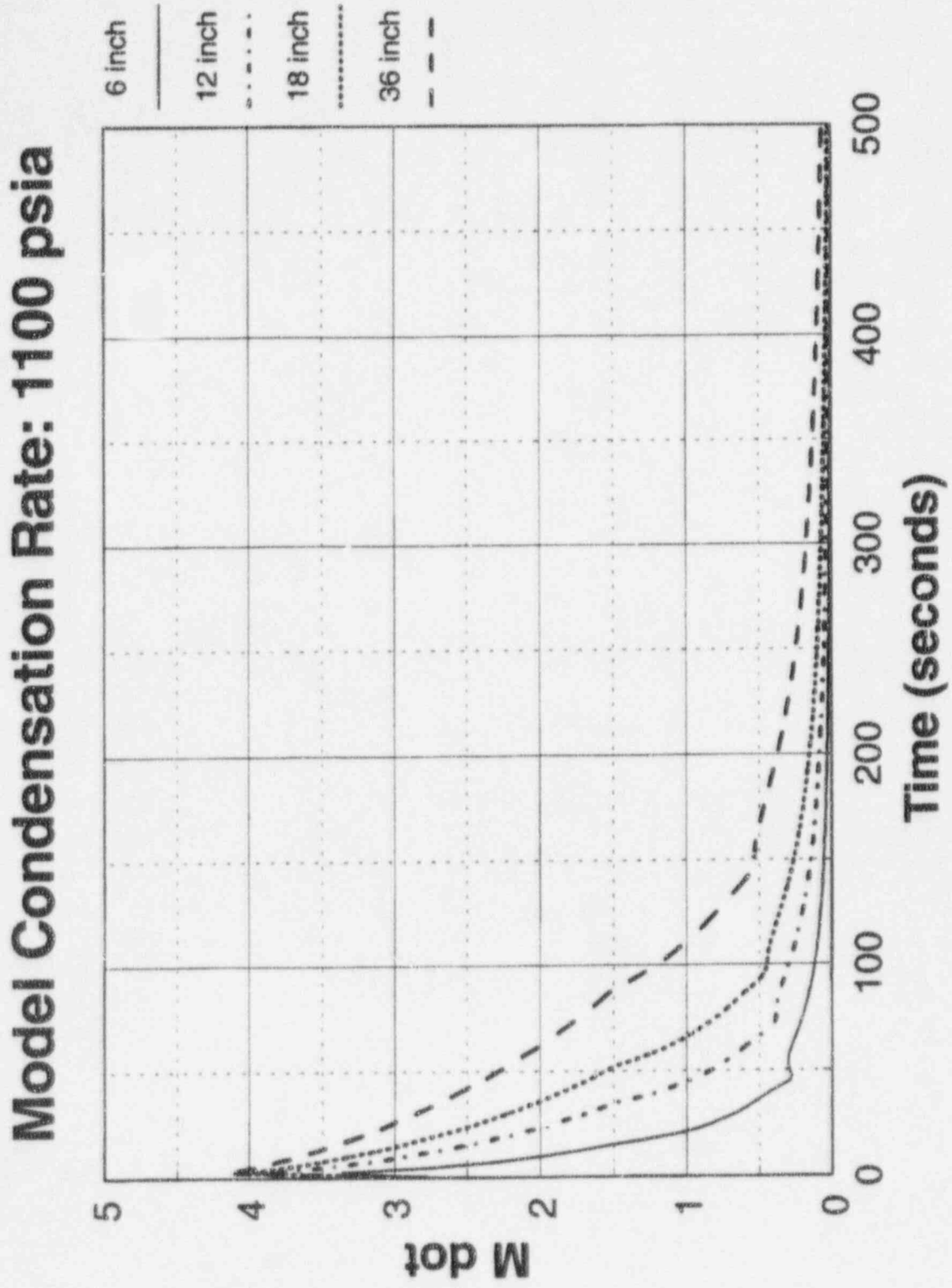

Figure 4.2-4 Calculated CMT Test Condensation Rate (lbm/sec) at 1100 psia for Different Mixing Depths

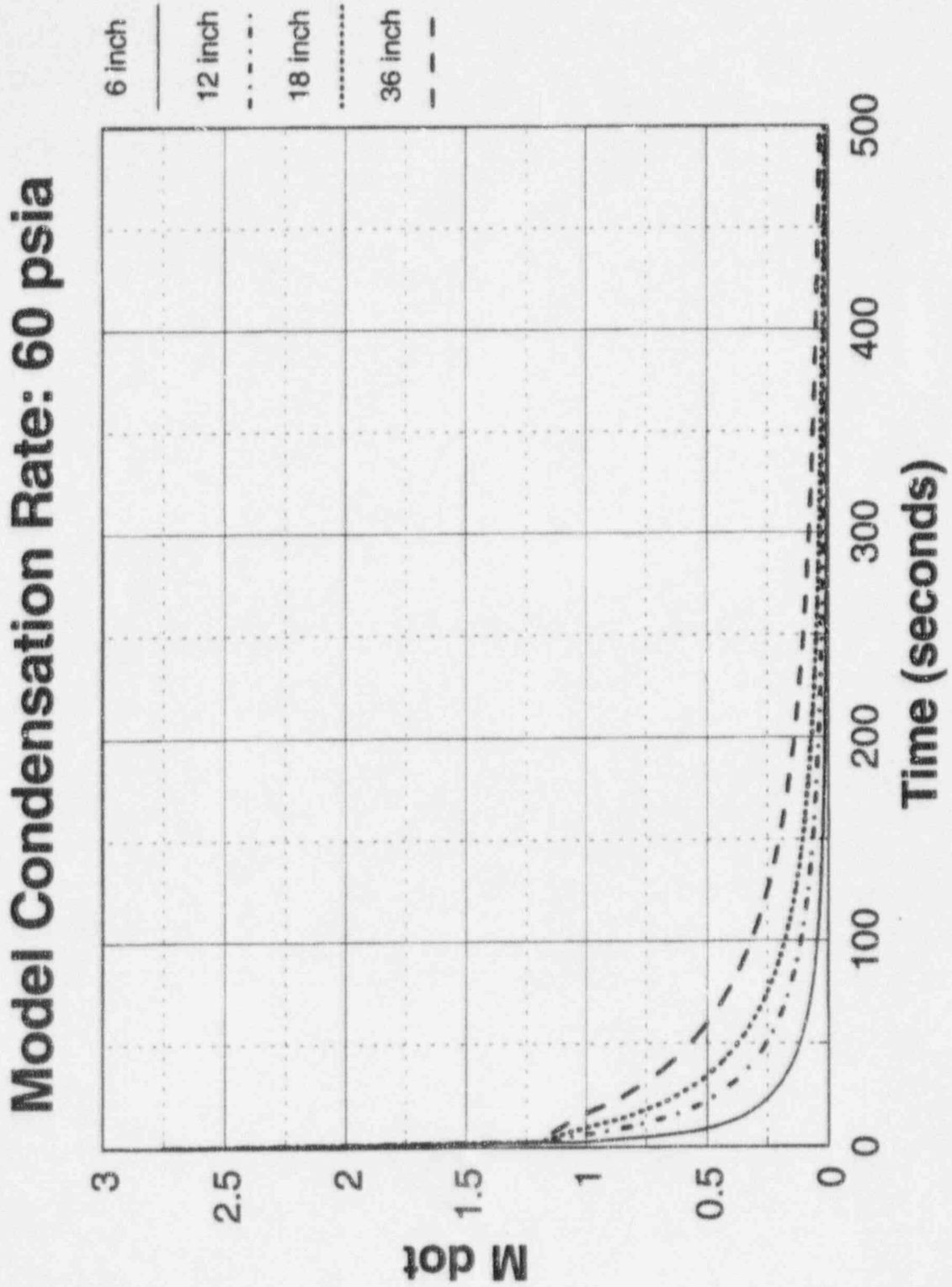

Figure 4.2-5 Calculated CMT Test Condensation Rates (lbm/sec) at 60 psia for Different Mixing Depths

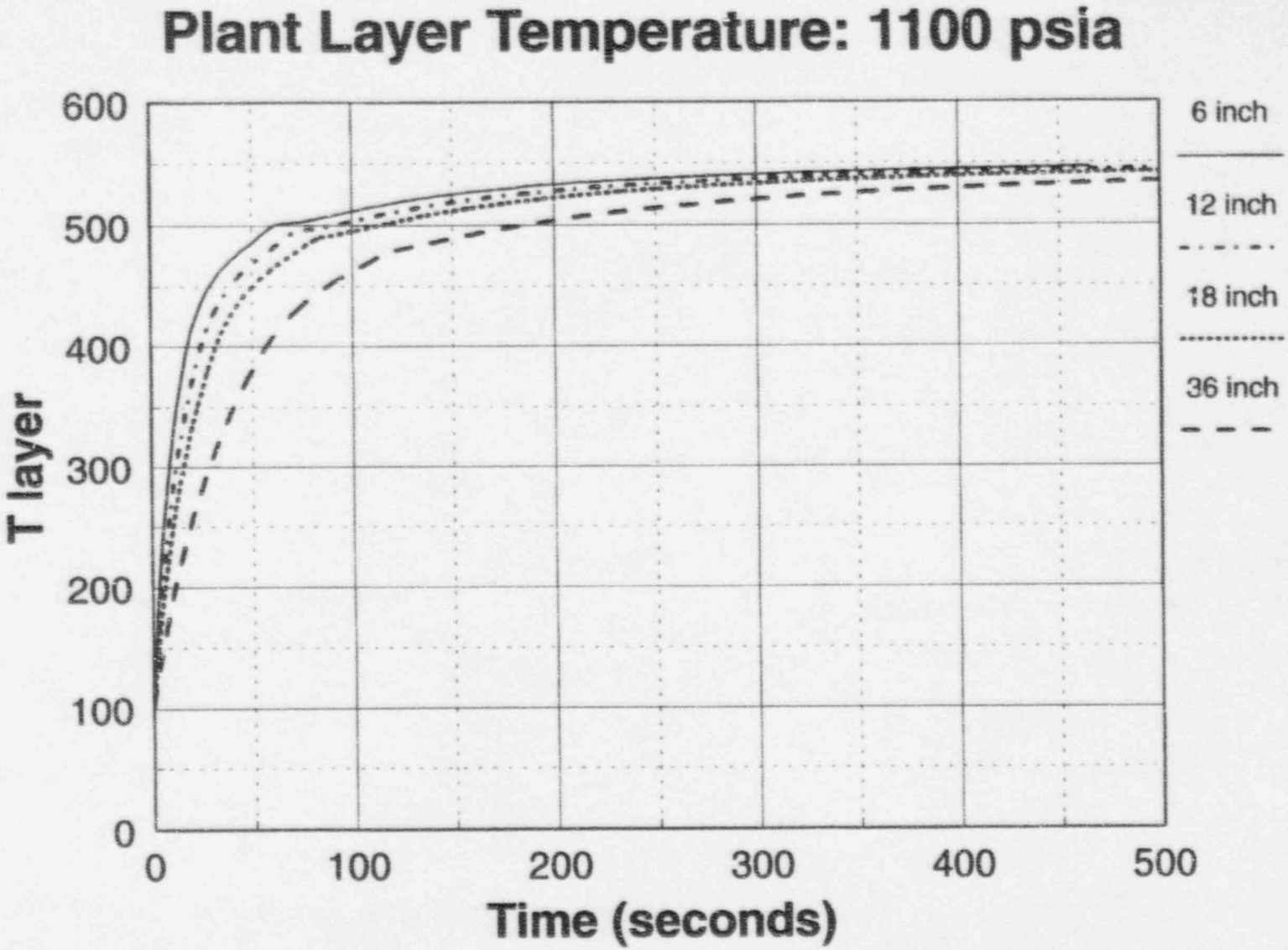

Figure 4.2-6 Calculated Plant Liquid Layer Temperature (°F) for Different Mixing Depths at 1100 psia for Diffuser Condensation

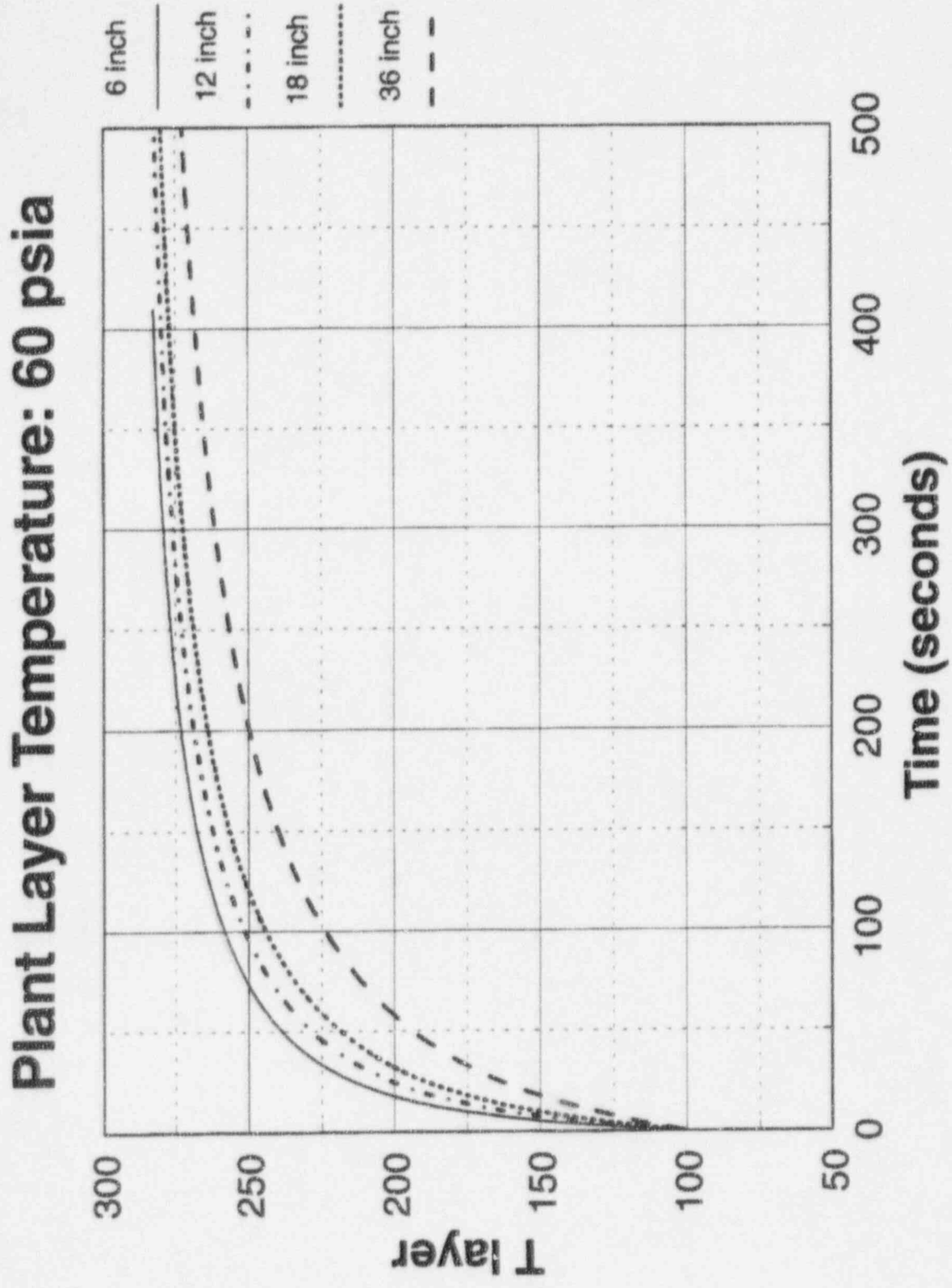

Figure 4.2-7 Calculated Plant Layer Temperature (°F) for Different Mixing Depths at 60 psia for Diffuser Condensation

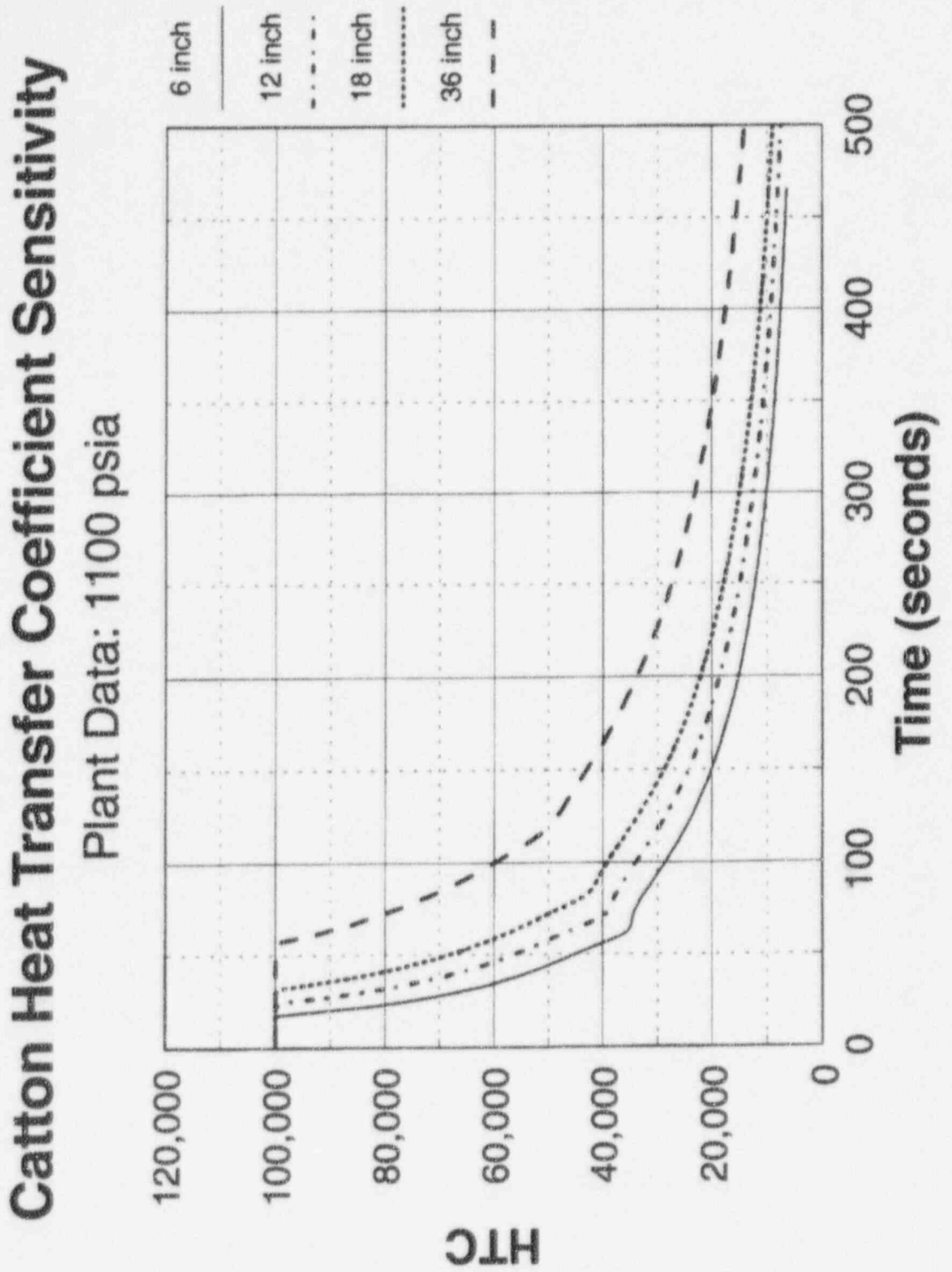

Figure 4.2-8 **Calculated Plant Interfacial Condensation Heat Transfer Coefficient (Btu/hr-ft^2-°F) from Catton et al., for Different Mixing Depths at 1100 psia for full CMT**

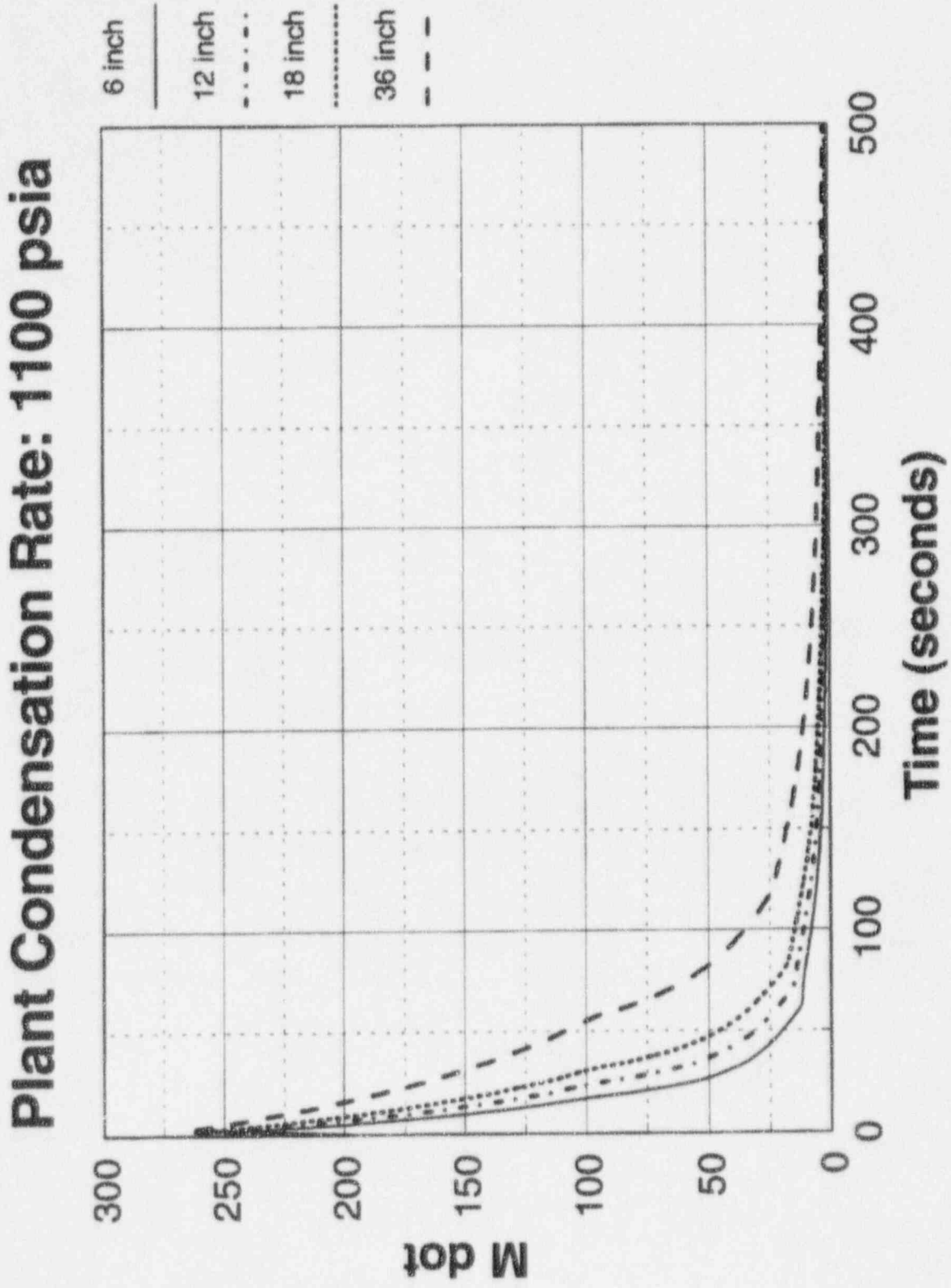

Figure 4.2-9 **Calculated Plant Condensation Rates (lbm/sec) at 1100 psia for Different Mixing Depths**

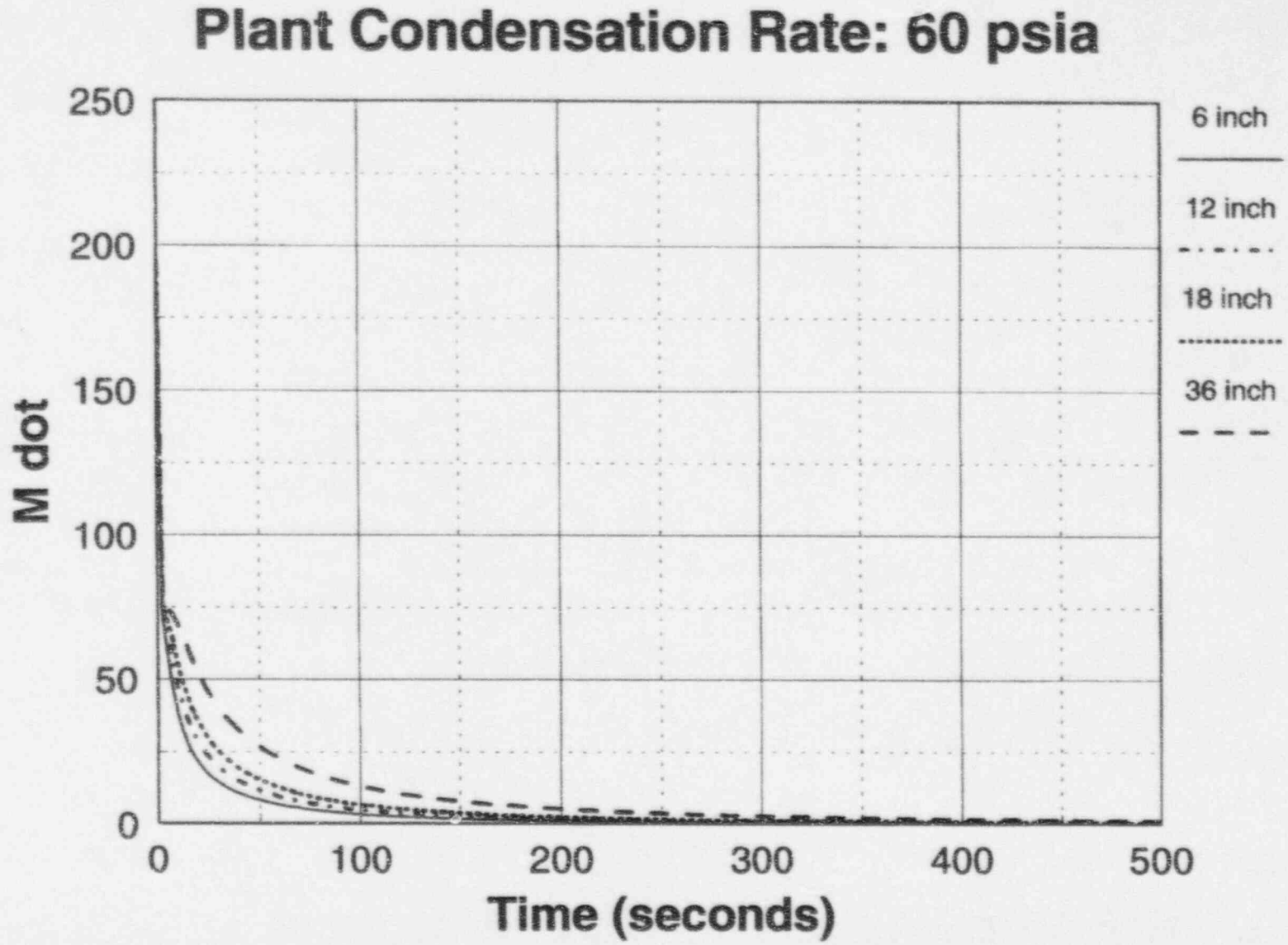

Figure 4.2-10 Calculated Plant Condensation Rates (lbm/sec) at 60 psia for Different Mixing Depths

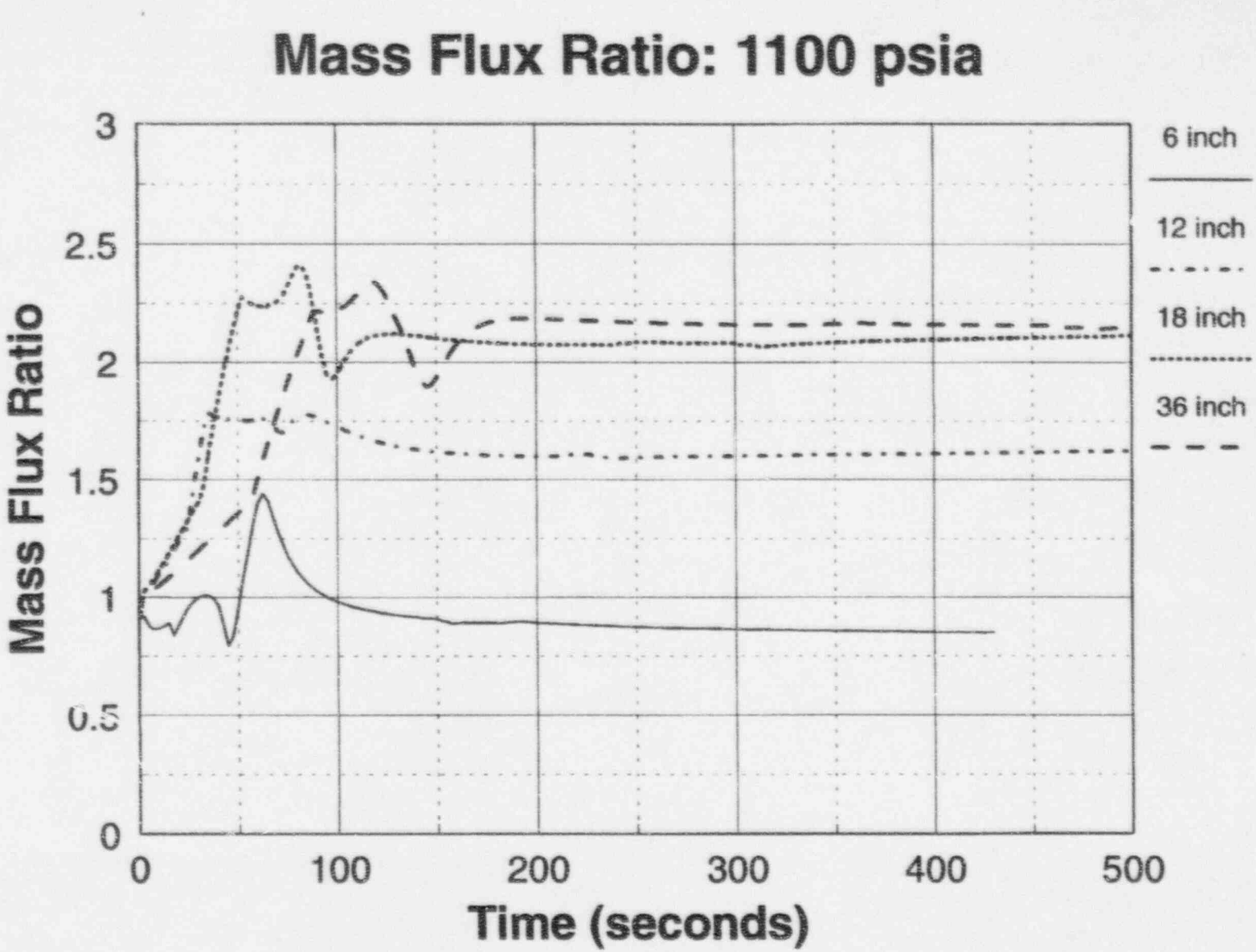

Figure 4.2-11 Calculated Condensate Mass Flux Ratio at 1100 psia

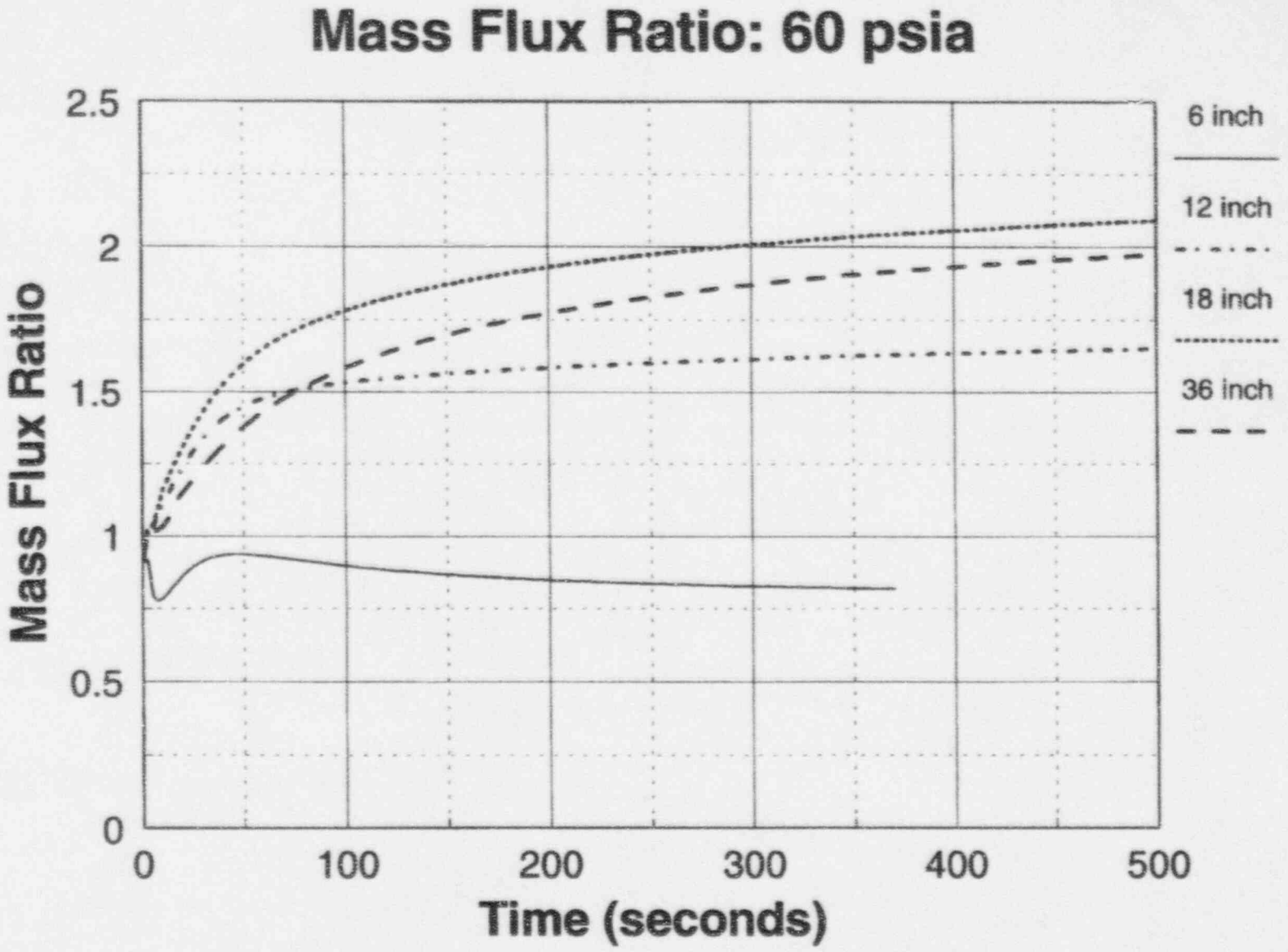

Figure 4.2-12 Calculated Condensate Mass Flux Ratio at 60 psia

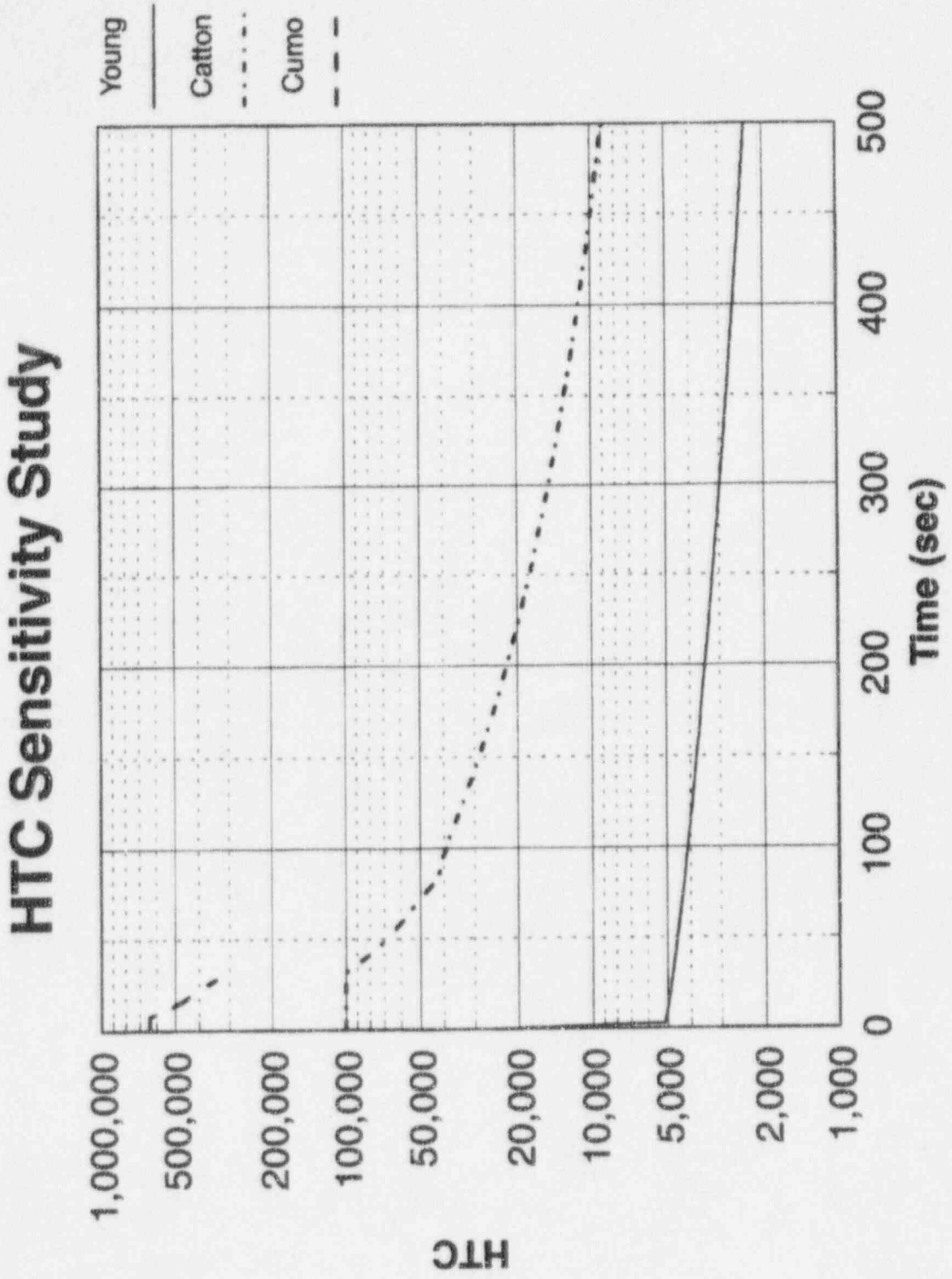

Figure 4.2-13 Comparison of Different Interfacial Heat Transfer Condensation Coefficients (Btu/hr-ft^2-°F) for 1100 psia and a Mixing Depth of 1.5 ft. for the Plant

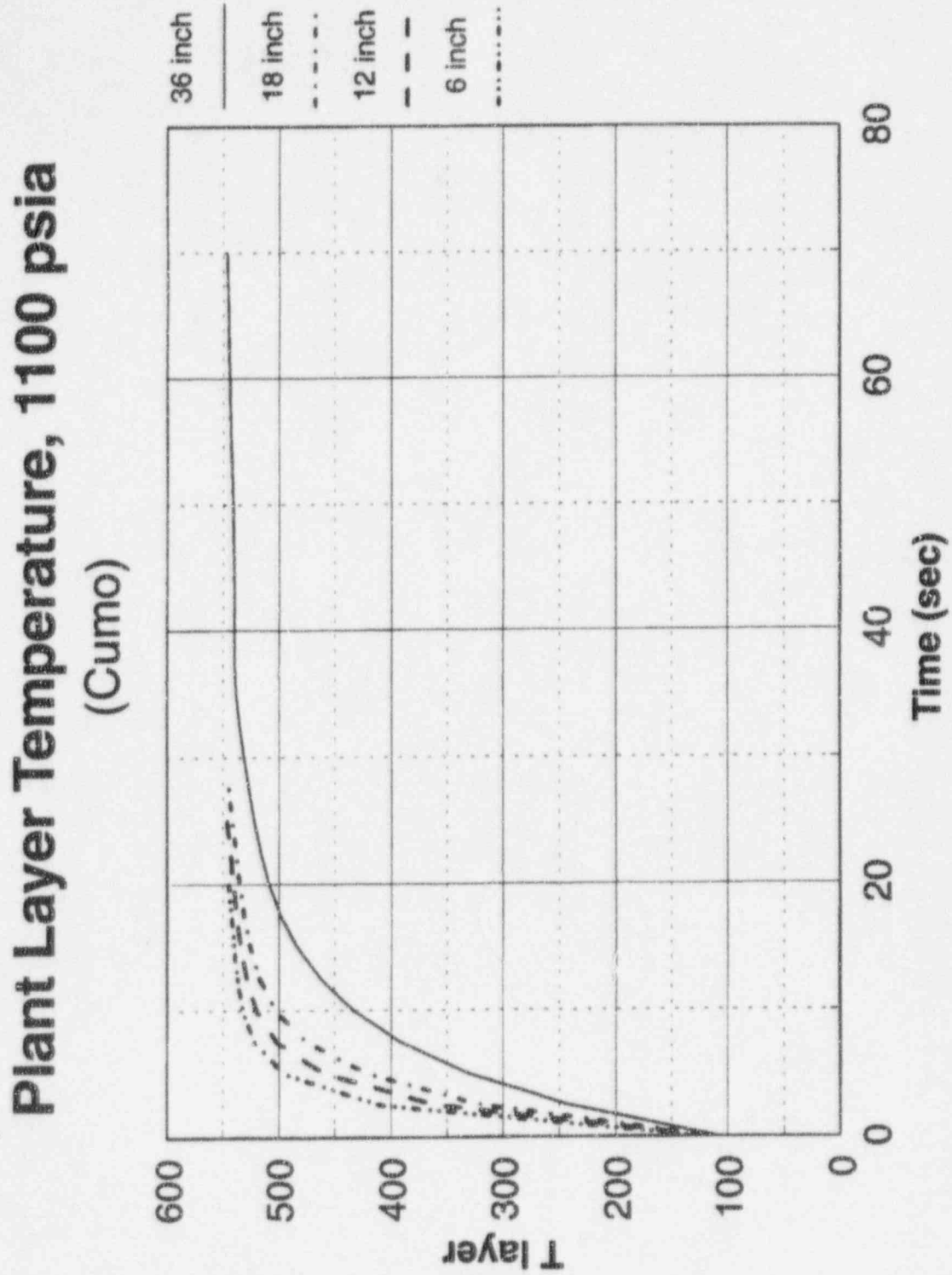

Figure 4.2-14 Calculated Plant Liquid Layer Temperature (°F) for Different Mixing Depths at 1100 psia Using Cumo Heat Transfer Correlation

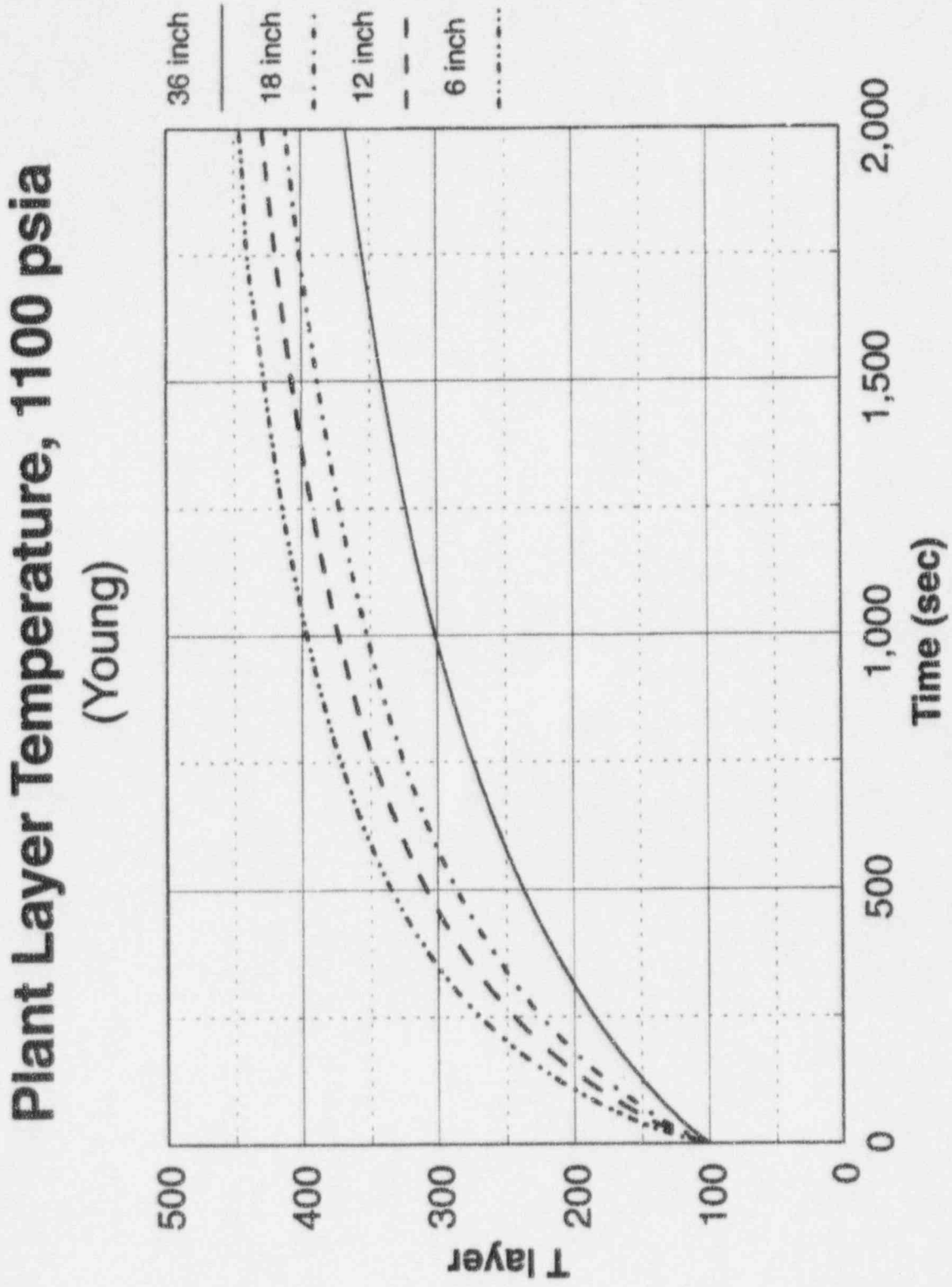

Figure 4.2-15 Calculated Plant Liquid Layer Temperature (°F) for Different Mixing Depths at 1100 psia Using Young Heat Transfer Correlation

4.3 Calculated Results for Wall and Surface Condensation Behavior for the AP600 CMT and the Test CMT When the CMT is Partially Drained

The calculations for the partially drained CMT are performed at liquid levels of 95 percent, 90 percent, and 50 percent at two pressures of 1100 psia and 60 psia. The mixing depth is kept constant at 1.5 ft. Calculations are performed with initial CMT wall and liquid conditions of 300°F for the 1100-psia cases and 150°F for the 60-psia cases. The initially higher temperatures reflect the effects of the initial liquid and wall heatup that might be expected from a period of CMT recirculation.

Figures 4.3-1 and 4.3-2 show the calculated wall and dome surface temperatures for the different liquid levels at the two different pressures for the CMT test facility. The 95 percent level point is in the dome for both the test and plant CMTs. The 90 percent level point is also in the dome for the plant CMT, but not for the test CMT. Similar plots are shown in Figures 4.3-3 and 4.3-4 for the plant CMT for the same two pressures. The figures all indicate that the metal surface heats quickly due to the condensation rate with the test metal surface heat up being slightly faster.

Figures 4.3-5 and 4.3-6 show the average wall and dome temperatures for the CMT test for the two different pressures. The average temperature is calculated from the one-dimensional transient conduction equation across the metal wall thickness. The average temperatures respond more slowly to the condensation heat transfer at the wall. Since the test dome has a thicker wall than the cylindrical portion, it heats slower than the walls. Figures 4.3-7 and 4.3-8 show the same plots for the plant CMT average wall temperature. The plant average wall temperature calculations take longer to heat up due to its increased wall thickness (7.78 in.) compared to the test (2.34 in.). Therefore, a time scale, as given in Table 3.4-6 exists for the test relative to the plant due to the difference in the wall thickness. Also, in the plant, the dome is thinner than the side walls, as seen in Figure 1.2-2, so it heats faster.

Figure 4.3-9 shows the calculated wall condensation coefficient for the plant CMT at different levels at 1100 psia. The heat transfer is initially large, then decreases as the CMT dome and wall temperatures increase. For the first 1500 seconds, the condensation heat transfer is in the turbulent regime for both the dome and the cylindrical walls. After 1500 seconds, the dome has heated sufficiently that the condensation film flow is in the laminar regime, and the correlation changes to Nusselt laminar film condensation. A similar behavior can be observed in the literature from Kreith, as seen in Figure 4.3-10. A similar plot of the test CMT wall condensation heat transfer coefficient is shown in Figure 4.3-11 at 1100 psia. The trends are the same between the plant and the test CMT, except that the cylindrical walls heat up faster in the test, so the condensation model changes from turbulent film condensation to laminar condensation over the entire vessel after 500 seconds. Again, this is a consequence of the test CMT walls being thinner than the walls for the plant CMT.

Figure 4.3-12 shows the plant wall condensation mass flow rates for different water levels in the CMT at 1100 psia. Figure 4.3-13 shows the plant CMT wall condensation flow rates at 60 psia for different water levels. As the figures indicate, the more surface area that is exposed, the larger the condensate flow rate. All values decrease with time as the structure heats up. Figures 4.3-14 and 4.3-15 show the

test CMT wall condensate flow rates at different water levels in the tank for the same pressures as the plant. The same trend as seen with the model condensate flow rates are seen in the plant, except that in the test CMT, the condensate mass flows decrease faster because the thinner walls heat up faster.

As shown in Table 3.4-9, the dimensionless parameters that characterize the CMT wall thermal response are given by the Biot and Fourier numbers. One method of assessing the differences between the plant CMT wall condensation behavior and the test CMT wall condensation behavior is to examine the ratio of the product of the Biot and Fourier numbers for each CMT. That is, define a new Π group as:

$$\Pi_{cond} = \frac{B_i F_o)_m}{B_i F_o)_p} \tag{4.3-1}$$

The product of $B_i F_o$ is used for solving transient conduction problems, where the internal conduction resistance is negligible and the average structure temperature can be used. In the plant CMT and test CMT, the internal conduction cannot be neglected; however, the product of the dimensionless numbers can be used to examine the difference in the time constant for the two CMTs. This will help explain the differences observed in the CMT wall condensation rate and heat-up time.

Equation 4.3-1 can be written as:

$$\Pi_{cond} = \frac{\left.\frac{H_{HL}(R_o-R_i)}{k_s}\,\frac{\alpha t}{(R_o-R_i)^2}\right)_m}{\left.\frac{H_{HL}(R_o-R_i)}{k_s}\,\frac{\alpha t}{(R_o-R_i)^2}\right)_p} \tag{4.3-2}$$

and we assume that $\Pi_{cond} = 1$.

If we assume that the heat transfer coefficient is similar, the materials are the same, and R_o-R_i is the wall thickness, then Equation 4.3-2 reduces to:

$$\frac{\left.\frac{t}{R_o-R_i}\right)_m}{\left.\frac{t}{R_o-R_i}\right)_p} = 1 \tag{4.3-3}$$

Using the dimensions for the plant and the test CMT, the time scale for the wall condensation in the test is approximately one third of that for the plant, due to the wall thickness difference. Therefore, wall condensation in the test CMT will diminish approximately three times faster than wall condensation in the plant CMT, as illustrated in the previous figures.

The heat transfer to the CMT liquid surface was also calculated for both the plant CMT and the test CMT, assuming a 1.5-ft. mixing depth and using the Bankoff correlation for surface condensation, as discussed in Section 3.0. The assumption of the 1.5-ft. depth is chosen as being representative of the CMT pre-operational test results. The assumption of a mixing depth affects the calculated CMT water temperature, which, in turn, affects the heat transfer from the steam to the water. Figures 4.3-16 and 4.3-17 show the calculated liquid temperature for the plant CMT for different water levels at 1100 psia but the same mixing depth (1.5 ft.). Similar plots are shown for the CMT test in Figures 4.3-18 and 4.3-19.

The most important parameter is the assumed mixing depth because this fixes the amount of CMT water that can interact with the steam. As seen in Figure 4.3-16, the liquid temperature approaches a near steady-state temperature as the interfacial heat transfer decreases due to the reduced steam flow into the tank. The liquid temperatures are slightly higher for the lower liquid levels since there is an increase in the total wall condensate (due to the increase in the wall area at lower water levels) that flows into the original CMT liquid and mixes; thereby more quickly heating it to higher temperatures. These calculations indicate that the liquid layer would remain subcooled. This is a direct result of choosing a layer thickness of 1.5 ft. Thinner layers would heat up closer to saturation. Also, the direct heat transfer to the liquid now depends on the steam flow rate into the CMT. As the wall condensation decreases, it will decrease the liquid surface condensation heat transfer as well.

A sensitivity study was performed to examine the effects of the assumed liquid layer thickness at the top of the partially drained CMT. The reference case uses a liquid layer that is 1.5-ft. thick and does not completely heat to the saturation temperature. A sensitivity study was performed using a liquid layer thickness of 3-in. for the different CMT levels. As seen in Figure 4.3-20, the thinner liquid layer heats to the saturation temperature much faster, as expected. The long delay in heating the thicker liquid layer is due to the reduced interfacial condensation heat transfer coefficient calculated by the Bankoff convective condensation correlation.

As discussed earlier, the magnitude of the convective condensation coefficient is dependent on the total steam flow into the CMT. Early in time, the steam flow is quite large since the CMT walls and liquid surfaces are cold and no initial temperature gradients have been established in the structures. Once the walls and the liquid layer begin to heat up, the steam flow diminishes and the corresponding Bankoff heat transfer coefficient also decreases, so that an assumed thick liquid layer is calculated to not reach the saturation temperature. However, for a more realistic calculation, the liquid layer is thinner and there will be sufficient heat transfer to heat the layer to the saturation temperature.

The calculated heat transfer coefficients for the condensation on the CMT liquid surface is shown in Figures 4.3-21 and 4.3-22 for the plant CMT at 1100 psia and 60 psia. As the figures indicate, the

decrease in the level in the CMT increases the wall condensation and the steam flow into the CMT. This, in turn, increases the condensation heat transfer on the liquid surface. The condensation heat transfer coefficients initially are large since the inlet steam flow into the CMT is large. As the CMT walls heat up and the liquid layer heats, the inlet steam flow decreases and the resulting condensation heat transfer coefficient also decreases. This is the expected trend from the Bankoff correlation since it is a convection-driven model. Figures 4.3-23 and 4.3-24 show the calculated condensation heat transfer coefficients for the CMT tests. As these figures indicate, the same trends are observed for the tests as for the plant CMT. The 60-psia calculated condensation heat transfer coefficients are larger than the 1100-psia cases due to the increased steam velocity at the lower pressures.

Figures 4.3-25 and 4.3-26 show the calculated condensation flow rates on the liquid surface for the plant at 1100 psia and 60 psia for the different liquid levels in the CMT. As these figures indicate, the behavior is consistent with the condensation heat transfer coefficients, where the condensate flow rates are large at the beginning of the transient, then decrease as the liquid layer heats up. The liquid surface condensate is larger at the lower pressure (60 psia) because of the higher condensation (convection) coefficient, calculated by the Bankoff correlation. This is a direct result of the lower system pressure, which increases the vapor velocity and resulting heat transfer coefficient. The same trends are seen for the condensate flow rates for the CMT test as seen in Figures 4.3-27 and 4.3-28 for the same two pressures. All these calculations are performed for the same mixing depth below the diffuser of 1.5 ft. If a larger mixing depth is chosen, the liquid condensate is larger and remains larger for a longer period of time since the liquid is a larger heat sink for condensation.

If the plant CMT wall condensate flow rates are compared to the plant CMT liquid condensate flow rates (compare Figures 4.3-12 and 4.3-13 to Figures 4.3-25 and 4.3-26), it can be seen that the wall condensation dominates the total condensation. As the liquid level decreases, the difference between the wall condensation and the liquid condensation decreases; however, the wall condensation is still larger. Comparing the test CMT wall condensate flow to the liquid condensate flow (comparing Figures 4.3-14 and 4.3-15 to Figures 4.3-27 and 4.3-28) indicates the same trends as the plant CMT calculations, except that the liquid surface condensation is larger earlier in time due to the larger surface condensation heat transfer coefficient. The wall condensation still dominates the total condensation since the test liquid surface condensate is smaller then the wall condensate. At the 50-percent level, the liquid condensate becomes larger due to the larger steam flow into the CMT, which increases the surface heat transfer coefficient.

To determine the behavior of the CMT test relative to the plant CMT, the relationships given by Equations 3.4-58 to 3.4-61 were examined. The energy and enthalpy Π groups given in Equations 3.4-60 and 3.4-61 are essentially in unity since the test is at full system pressure and temperature. The wall and liquid condensation Π groups are given in Equation 3.4-58 for the wall condensation and in Equation 3.4-59 for liquid or water surface condensation. The denominator in each equation is given as:

$$\dot{m}_{CMT} h_{fg} \qquad (4.3\text{-}4)$$

which represents the energy of the drain flow out of the CMT. However, since the calculations are assuming a constant liquid level in the CMT, the drain rate is nearly equal to the CMT balance line flow, as given by Equation 3.4-26. For these calculations, the balance line flow is the total steam flow rate into the CMT.

Two approaches are used to compare the CMT test to the plant CMT. The first approach is to normalize the condensate flow rates on the surface areas of the plant and test CMT and to compare the calculated condensate fluxes. The second approach is to directly calculate the wall and liquid surface Π groups and take the ratio to compare the test to the plant CMT.

4.3.1 Normalized Condensate Comparisons

In the first approach, the calculated wall surface condensate rate, shown in Figures 4.3-12 to 4.3-15, is divided by the exposed wall surface area (for the different assumed liquid levels) to obtain a wall condensate mass flux for both the plant and the CMT test. This normalizes the condensation heat transfer on the actual surface area and permits comparisons between the CMT test and the plant CMT. A similar approach is used for the water surface condensate rate given in Figures 4.3-25 to 4.3-28, except that the water surface cross-sectional area is used to divide the condensate mass flow for the plant and the test.

The ratio of the test wall condensate mass flux to the plant wall condensate mass flux is plotted in Figures 4.3-29 and 4.3-30 for the different CMT levels at the two pressures. As Figure 4.3-29 indicates, the wall condensate mass flux ratio is slightly less than unity for the first 500 seconds at the 90 and 95 percent levels of the calculation. The calculation for the 50 percent level is initially greater than unity, then decreases below one as the test wall condensate mass flux decreases after 500 seconds. At 60 psia, the condensate mass ratio is less than unity for most of the transient due to the larger wall condensation in the plant relative to the test. The decrease of the test wall condensate flux is a result of the thinner test CMT wall. The test CMT wall average temperature heats up faster than the plant CMT, resulting in a decease in the condensate mass flux. This behavior is observed in the average wall temperature calculations for the plant and test and is consistent with the test-to-plant CMT Biot-Fourier number ratio given in Equation 4.3-2. At a CMT water level of 90 or 95 percent, the surface area of the plant is significantly larger, due to the hemispherical head relative to the ellipsoidal head used in the test. Therefore, the plant wall condensate flux is lower than the test, resulting in ratios that can be greater than unity.

The ratio of the test water surface condensate mass flux to the plant water surface mass flux is plotted in Figures 4.3-31 and 4.3-32. Figure 4.3-31 indicates that the plant water surface condensate mass flux is larger than the test water surface condensate mass flux for the 50-percent CMT level, so the ratio is less than unity. The ratios for CMT levels of 90- and 95-percent values become inaccurate at times greater than 500 seconds since the condensate mass flows are so small.

The trend of the normalized liquid surface condensate ratios between the plant and the test is also due to the use of the Bankoff correlation for the interfacial heat transfer. This correlation is scale-

independent as compared to the liquid surface condensate calculation used in Revision 0 of this report, which used the Grigull [17] correlation that used the tank diameter as the characteristic dimension. The Bankoff correlation uses the wave height as the characteristic dimension, which is a local parameter, independent of scale, but does depend on the steam flow into the CMT.

4.3.2 Condensation Π Groups and Their Ratios

The second method of comparing the test CMT condensation behavior to the plant CMT condensation behavior is to directly calculate the Π groups from the dimensionless equations.

The condensation Π groups are defined in Equations 3.4-58 and 3.4-59 in Table 3.4-9. The comparisons made in subsection 4.3.1 of the normalized condensate mass flux ratios for the test CMT to the plant CMT indicate that the test captures the condensation phenomena of interest for the plant CMT. The Π groups given in Equations 3.4-58 and 3.4-59 have been normalized on the CMT drain rate energy, $\dot{m}_{CMT}h_{fg}$. This is approximately correct when the level in the CMT is constant, and the temperature effects on the liquid density are small.

Figures 4.3-33 to 4.3-36 show the calculated wall condensation Π_{Wcond} group for both the CMT test and the AP600 CMT for a mixing depth of 1.5 ft. and different CMT levels at 1100 psia and 60 psia. The calculated Π_{wcond} group is the ratio of the condensate mass flow from the walls to the total condensate mass flow from both the walls and the liquid surface. As the plots for the plant CMT indicate, the wall condensate is a larger portion of the total condensate flow compared to the test, particularly later in the transient. As the wall and the liquid surface condensation decreases, the wall condensate becomes an even larger portion of the total condensate flow, even as the total flow decreases. Therefore, particularly later in time, the plant wall condensation is a larger fraction of the total condensation as compared to the test.

Figures 4.3-37 and 4.3-38 show the calculated ratio of the CMT test wall condensation Π_{wcond} to the plant wall condensation Π_{wcond} group for a mixing depth of 1.5 ft. and different CMT levels. As Figures 4.3-37 and 4.3-38 indicate, the agreement is good for all the levels. This comparison indicates that, in spite of the thinner walls, the test CMT will adequately model the wall condensation phenomena associated with the plant CMT.

The liquid surface condensation Π group for both the CMT test and the plant CMT is shown in Figures 4.3-39 to 4.3-42, using the Bankoff correlation for different CMT levels and a 1.5 ft. mixing depth at 1100 psia and 60 psia.

As Figure 3.4-40 indicates, at low pressure, the surface condensation can be a relatively large fraction of the total condensation early in the transient due to the induced high interfacial heat transfer coefficient. However, once the wall begins to heat and the steam flow into the CMT decreases, the surface condensation also quickly decreases and the total condensation becomes dominated by the wall condensation.

The $\Pi_{g_{cond}}$ group for the plant CMT indicates that the liquid surface condensation is a smaller fraction of the total condensation for the plant, as compared to the test for both pressures. Clearly, the wall condensation dominates for the plant due to the thicker walls. The liquid surface condensation is a significant fraction of the total condensation at 60 psia for both the plant and the test, due to the larger interfacial heat transfer coefficients at the lower pressure.

The ratio of the test CMT to the plant liquid condensation Π group is shown in Figures 4.3-43 and 4.3-44. The $\Pi_{g_{cond}}$ ratio indicates that the test CMT will experience larger surface condensation relative to the plant CMT. However, the condensation phenomena at the surface of the test CMT will be sufficiently similar to the expected condensation phenomena for the plant CMT, so the CMT tests can be used to evaluate and assess this phenomena.

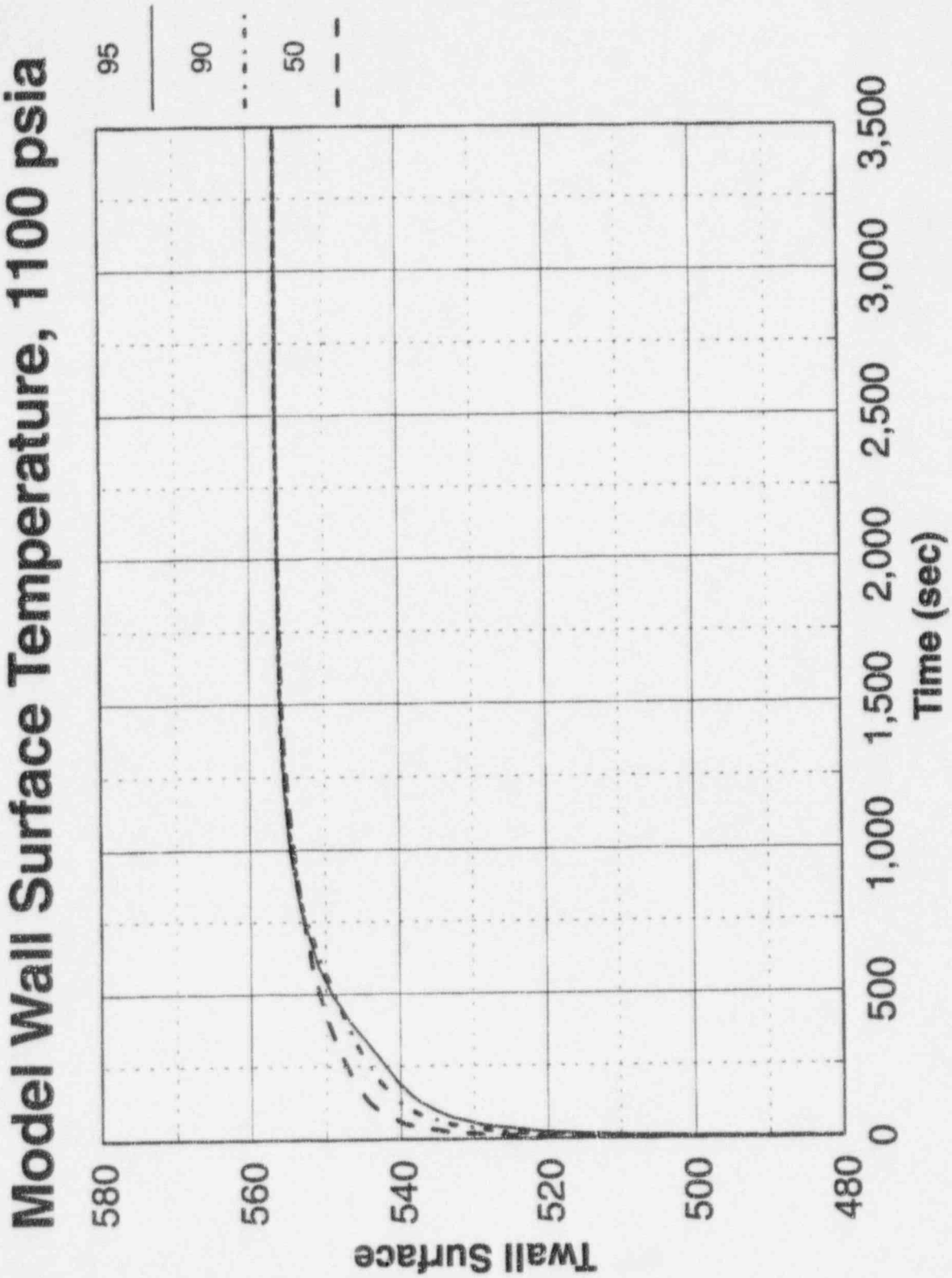

Figure 4.3-1 Calculated CMT Test Wall and Dome Surface Temperatures (°F) for Different Liquid Levels at 1100 psia

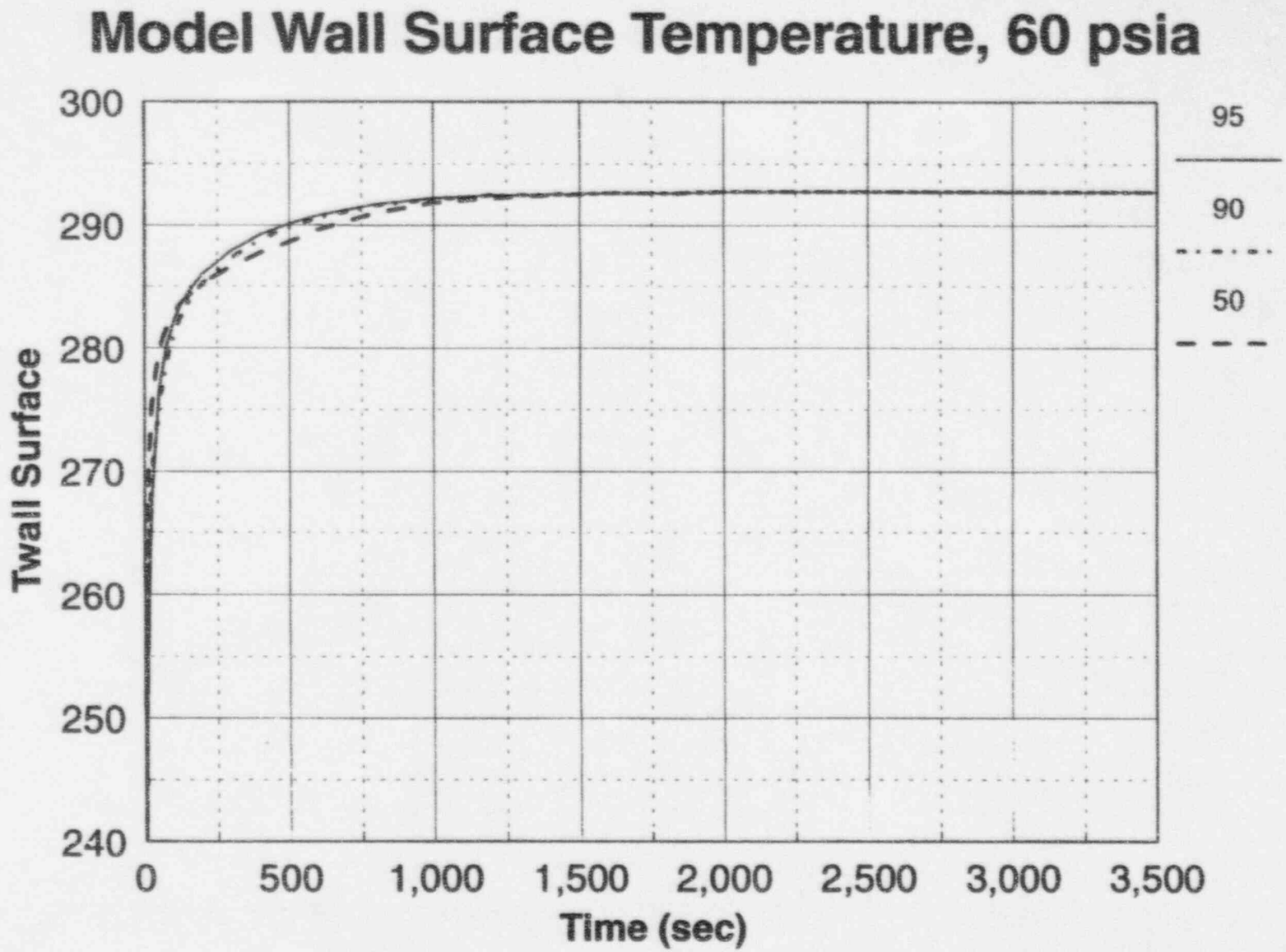

Figure 4.3-2 Calculated CMT Test Wall and Dome Surface Temperatures (°F) for Different Liquid Levels at 60 psia

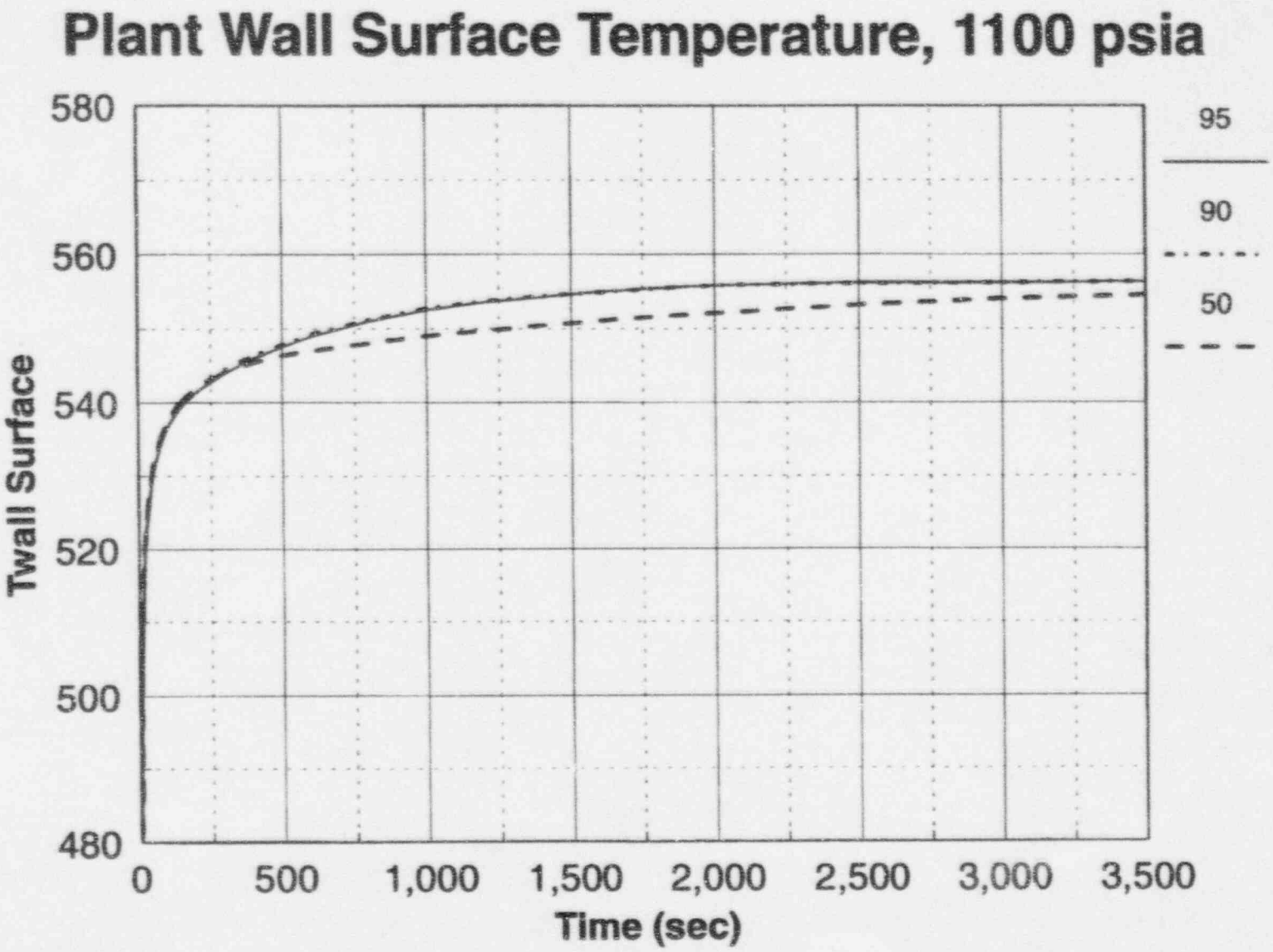

Figure 4.3-3 Calculated Plant Wall and Dome Surface Temperatures (°F) for Different Liquid Levels at 1100 psia

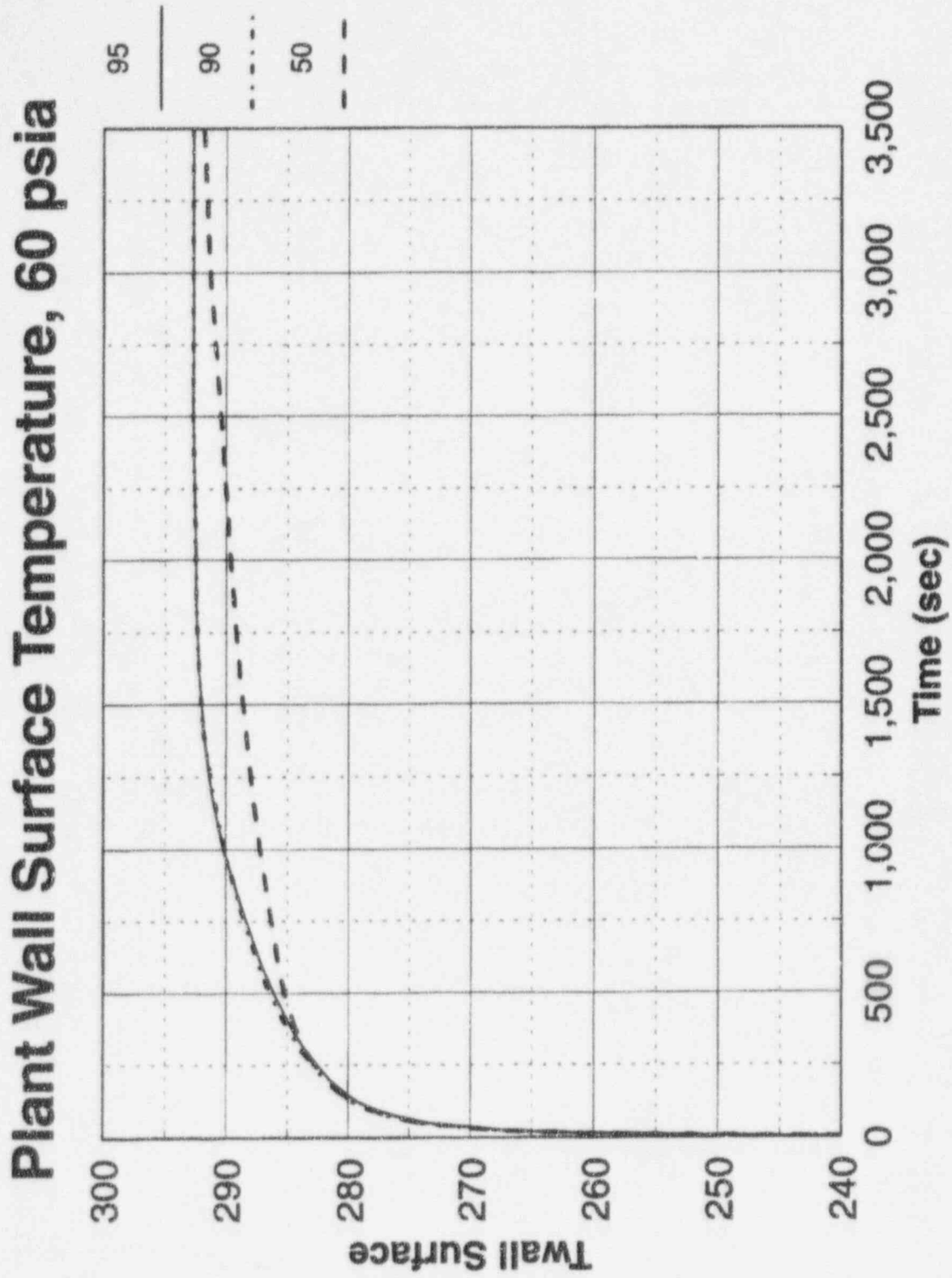

Figure 4.3-4 Calculated Plant Wall and Dome Surface Temperatures (°F) for Different Liquid Levels at 60 psia

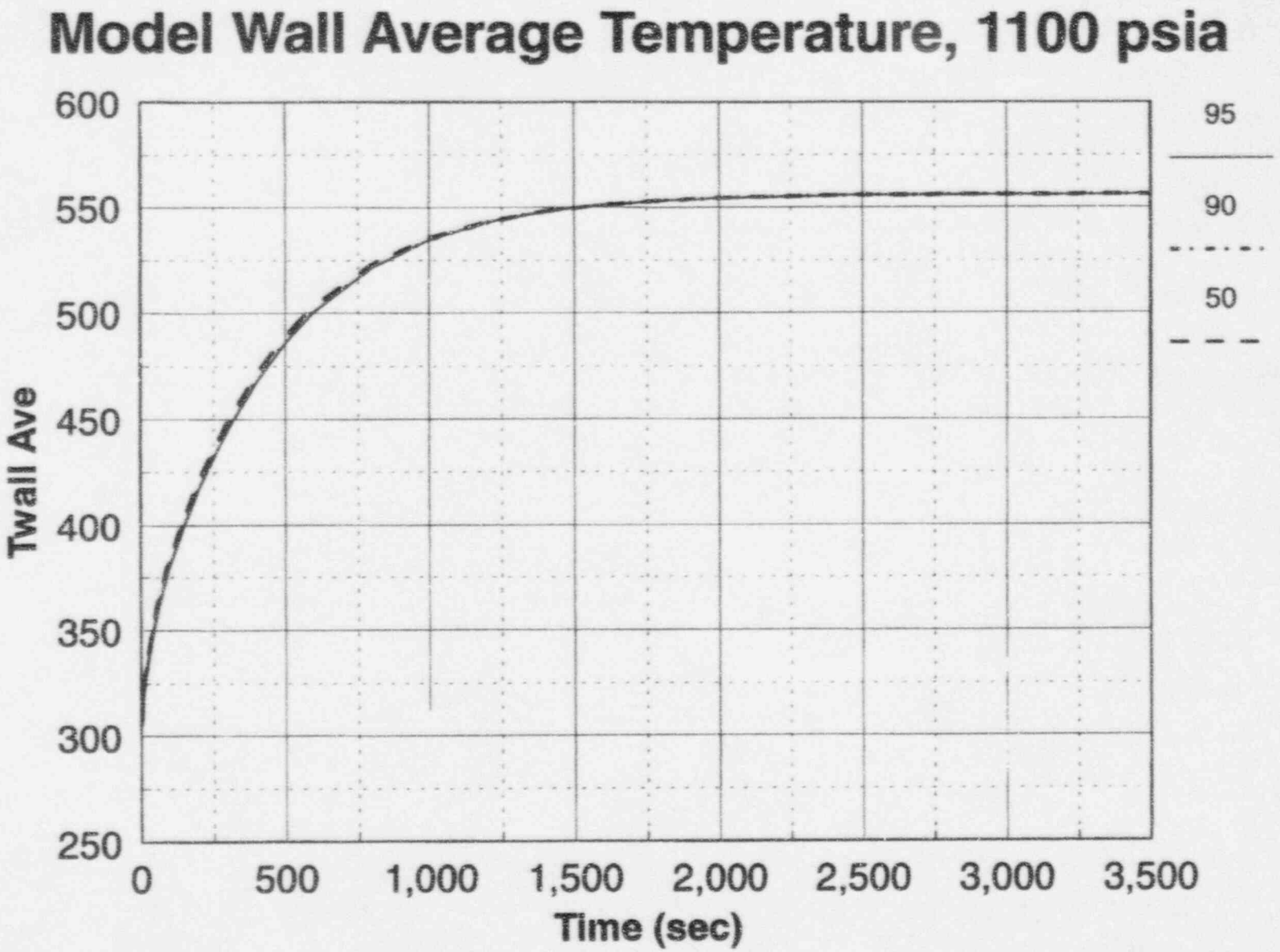

Figure 4.3-5 Average CMT Test Wall and Dome Temperatures (°F) for Different Liquid Levels at 1100 psia

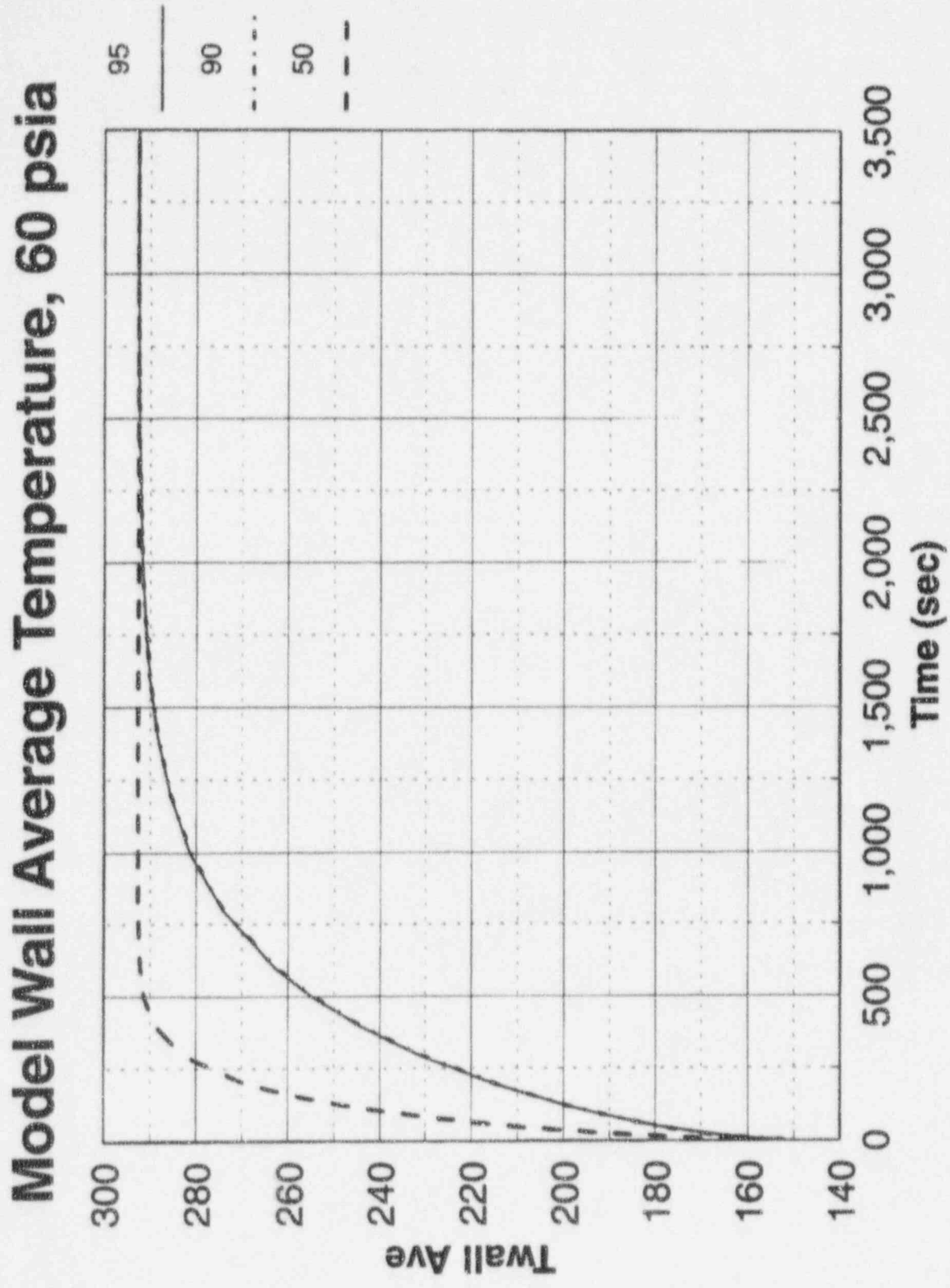

Figure 4.3-6 Average CMT Test Wall and Dome Temperatures (°F) for Different Liquid Levels at 60 psia

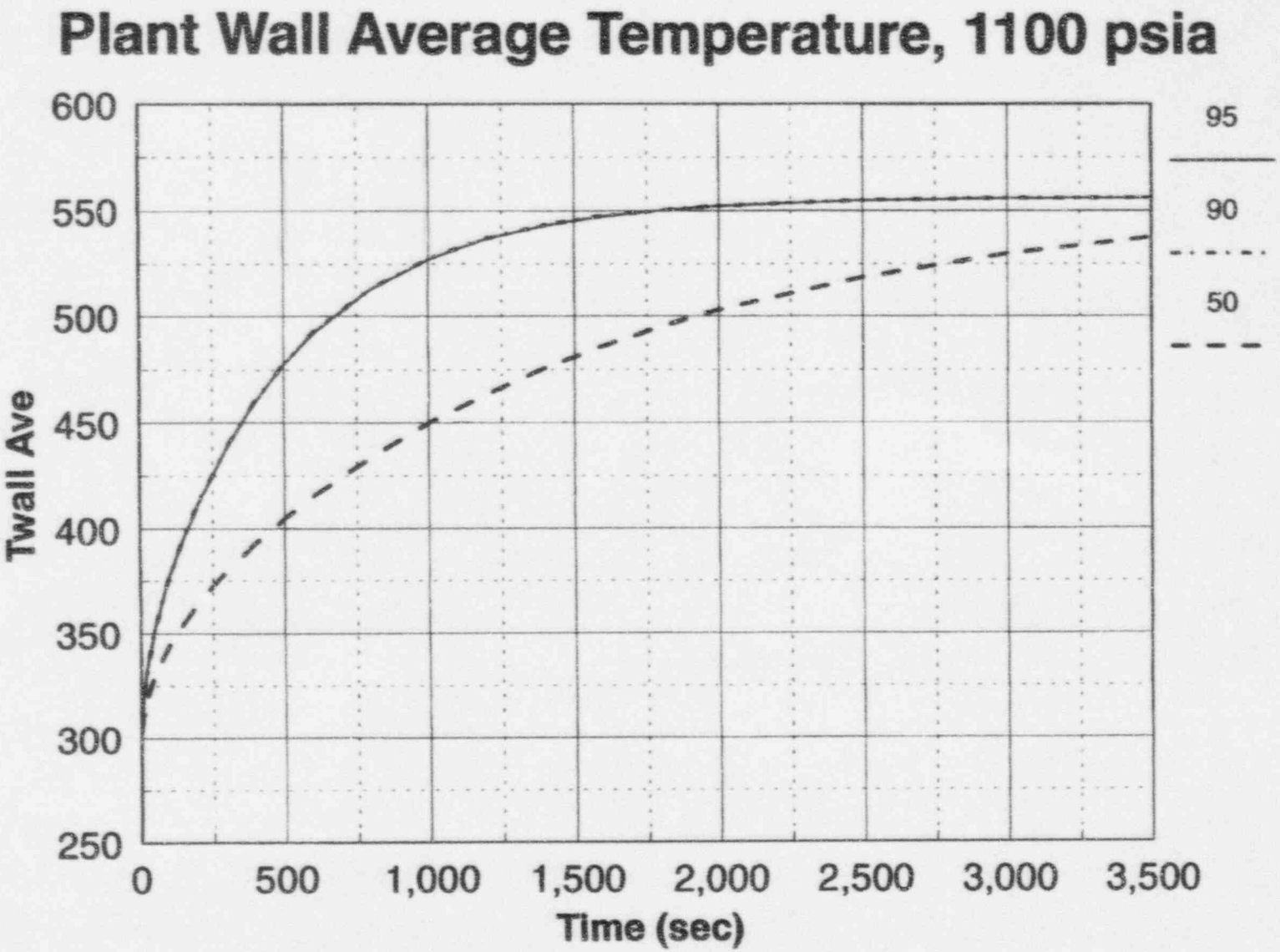

Figure 4.3-7 Average Plant Wall and Dome Surface Temperatures (°F) for Different Liquid Levels at 1100 psia

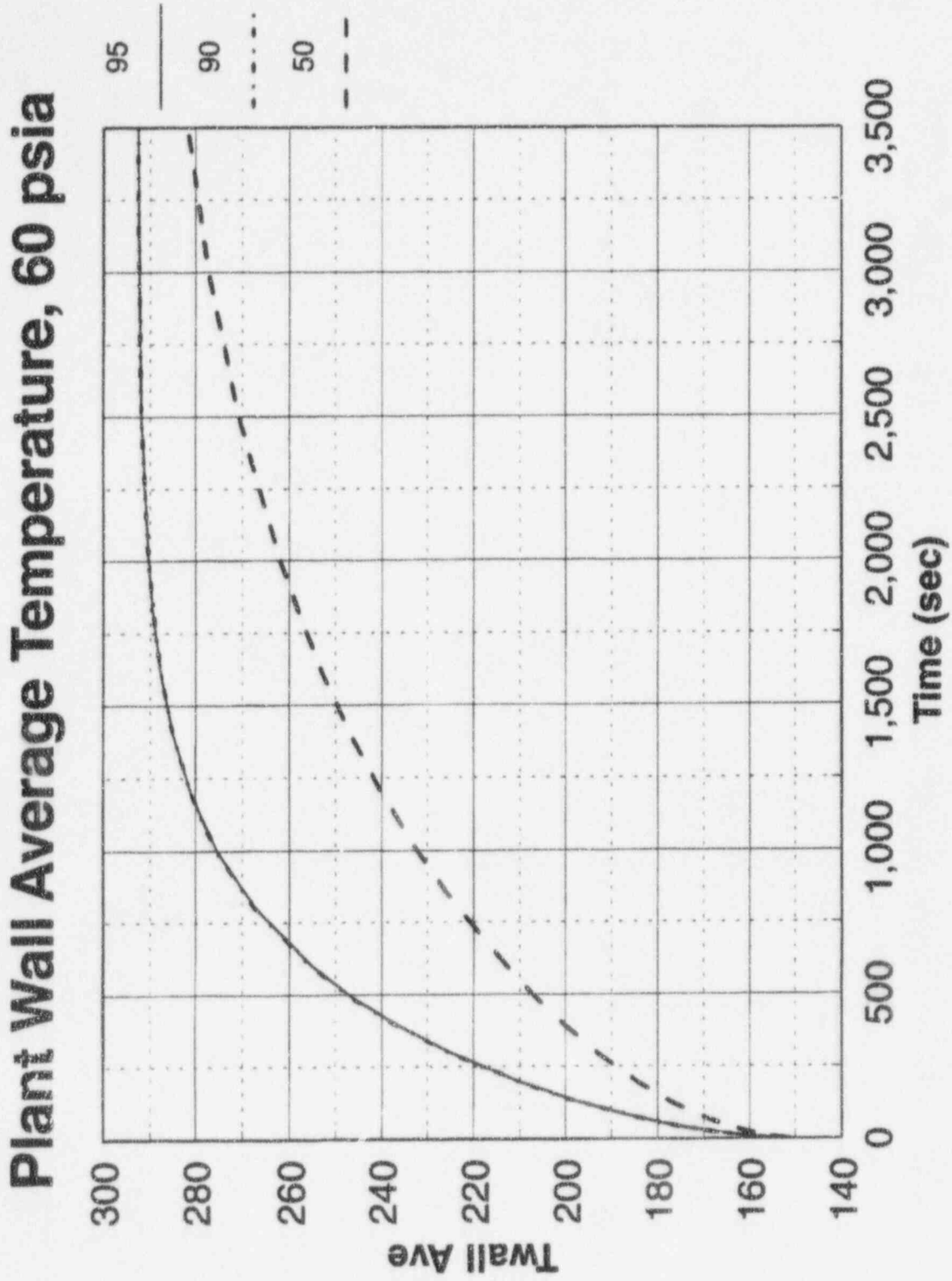

Figure 4.3-8 Average Plant Wall and Dome Temperatures (°F) for Different Liquid Levels at 60 psia

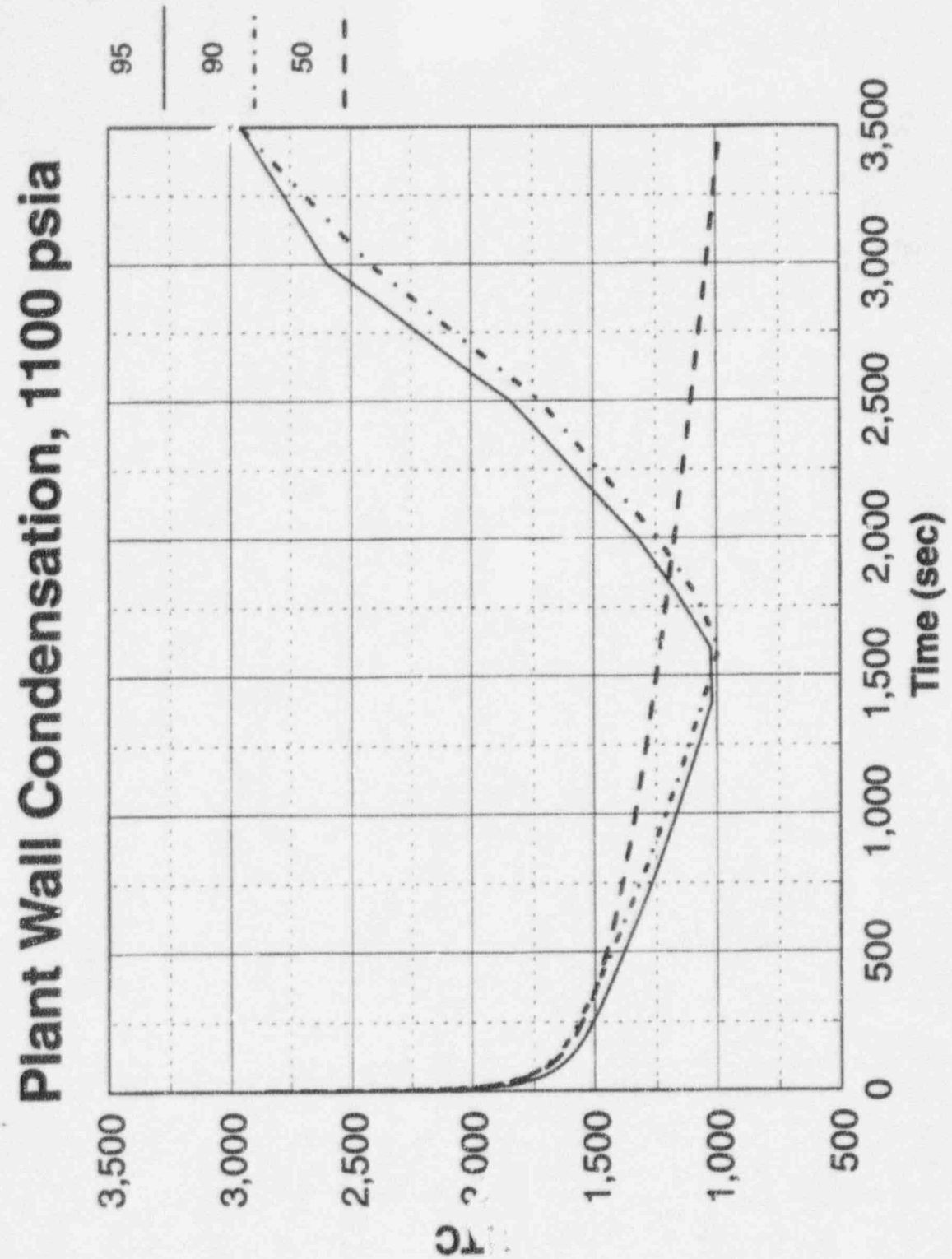

Figure 4.3-9 Calculated Plant Wall Condensation Coefficient (Btu/hr-ft^2-°F) for Different Liquid Levels at 1100 psia

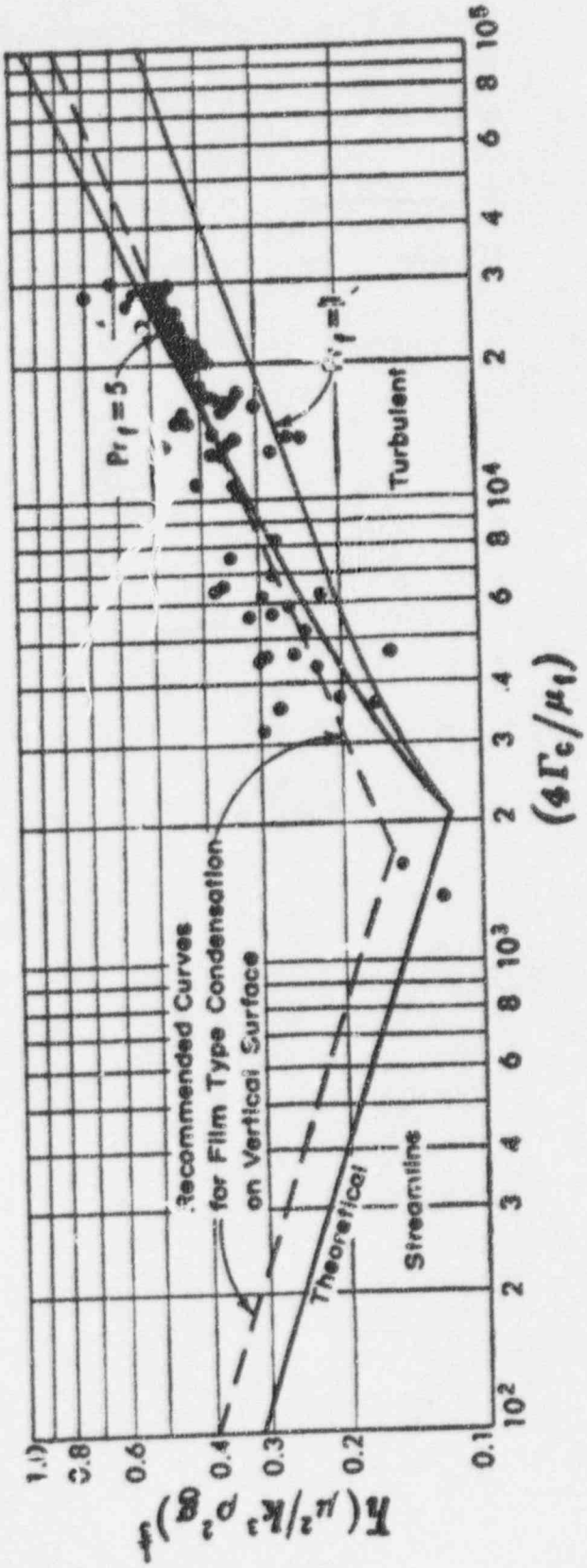

Figure 4.3-10 Normalized Laminar and Turbulent Film Condensation Heat Transfer Coefficients[9]

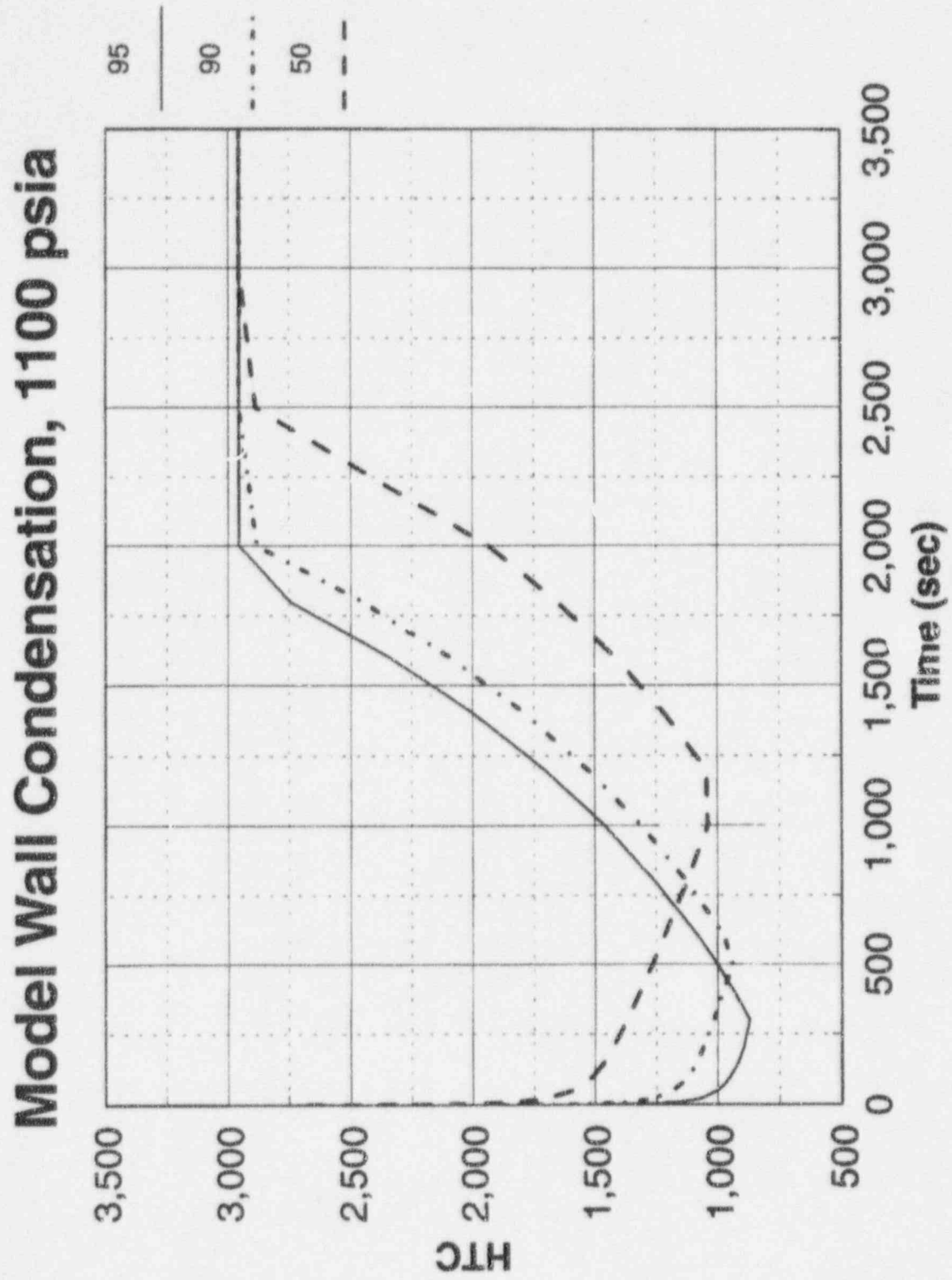

Figure 4.3-11 Calculated CMT Test Wall Condensation Coefficient (Btu/hr-ft^2-°F) for Different Liquid Levels at 1100 psia

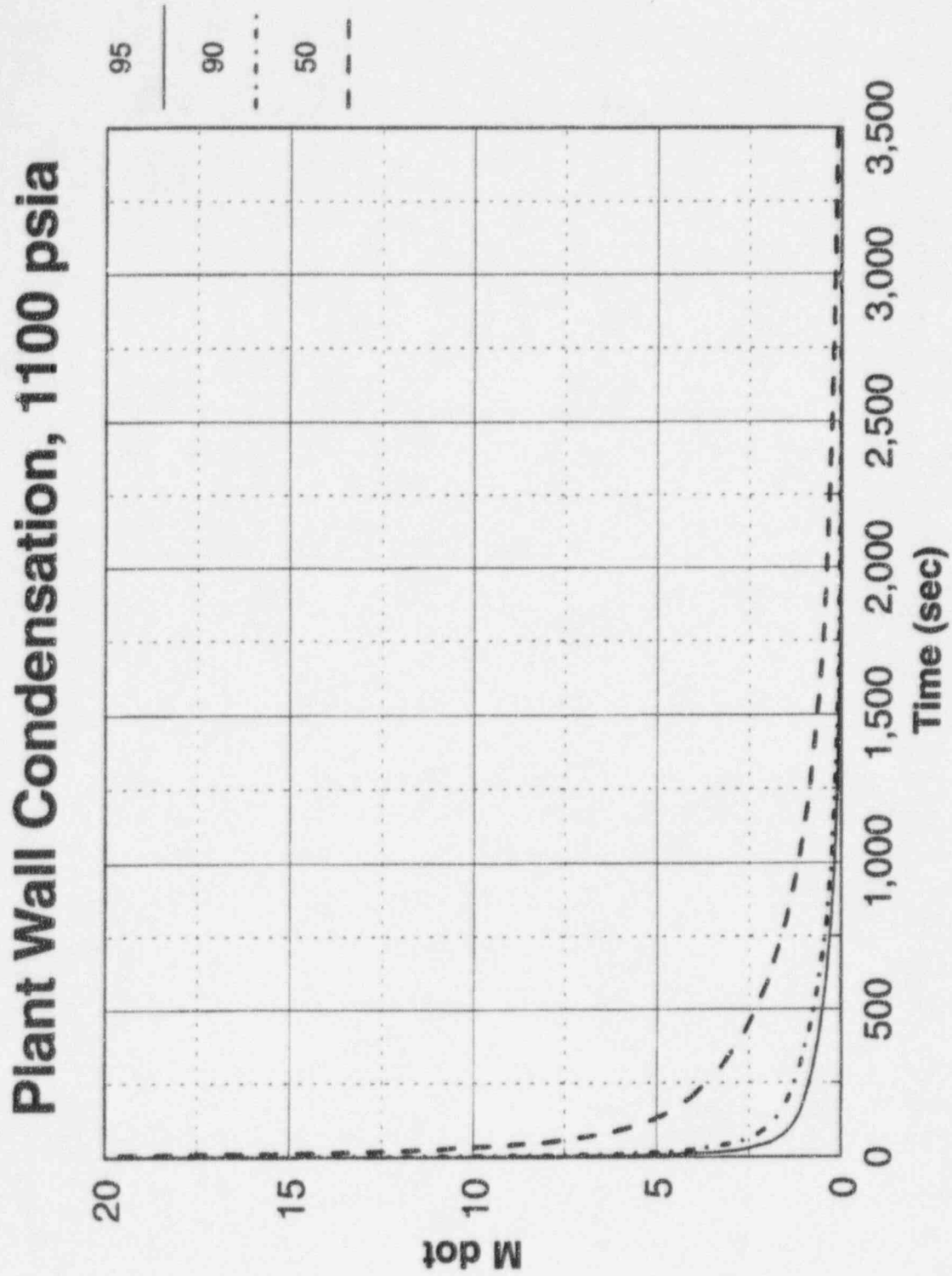

Figure 4.3-12 Calculated Plant Wall Condensation Mass Flow Rates (lbm/sec) for Different Liquid Levels at 1100 psia

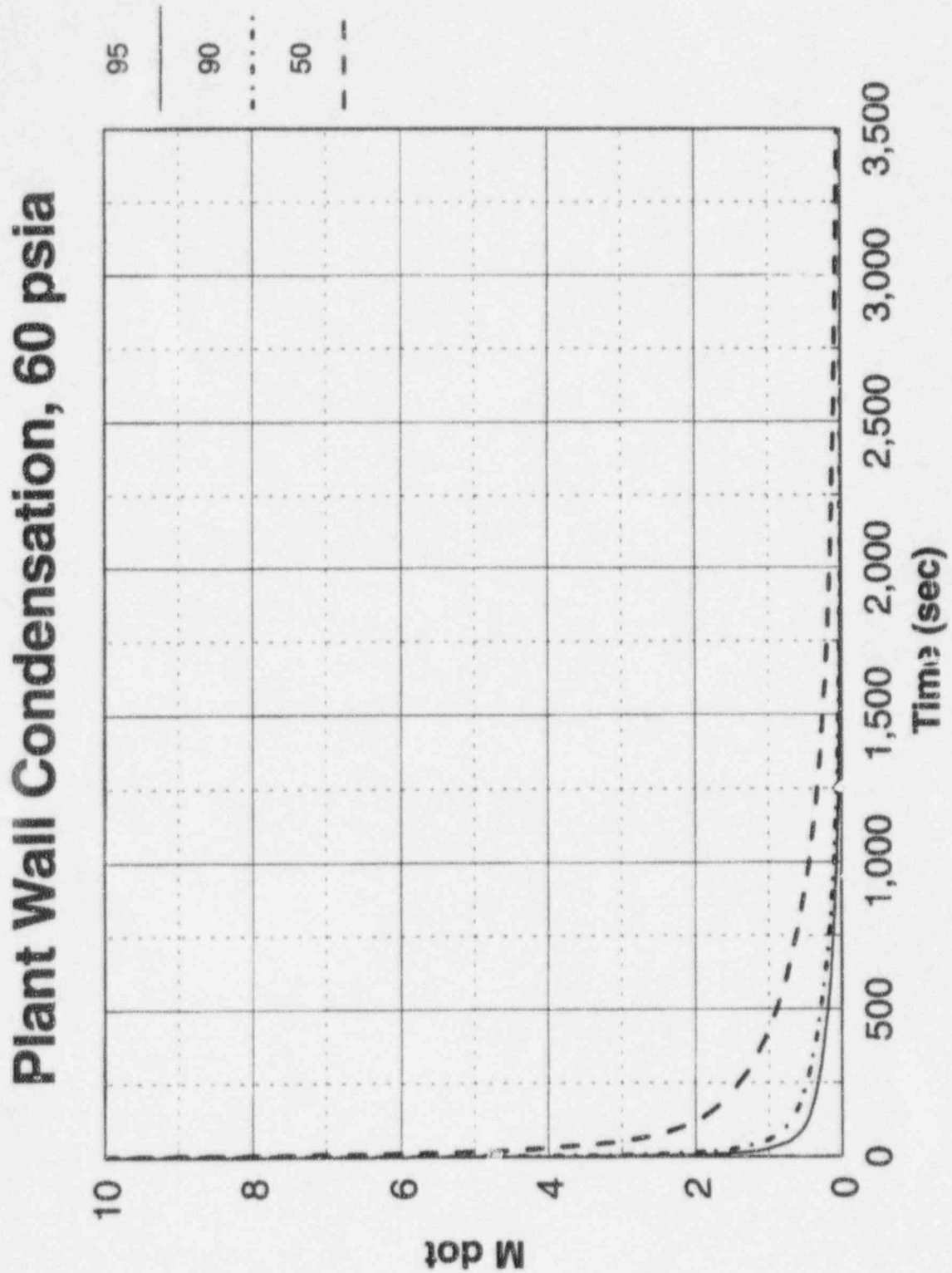

Figure 4.3-13 Calculated Plant Wall Condensation Mass Flow Rates (lbm/sec) for Different Liquid Levels at 60 psia

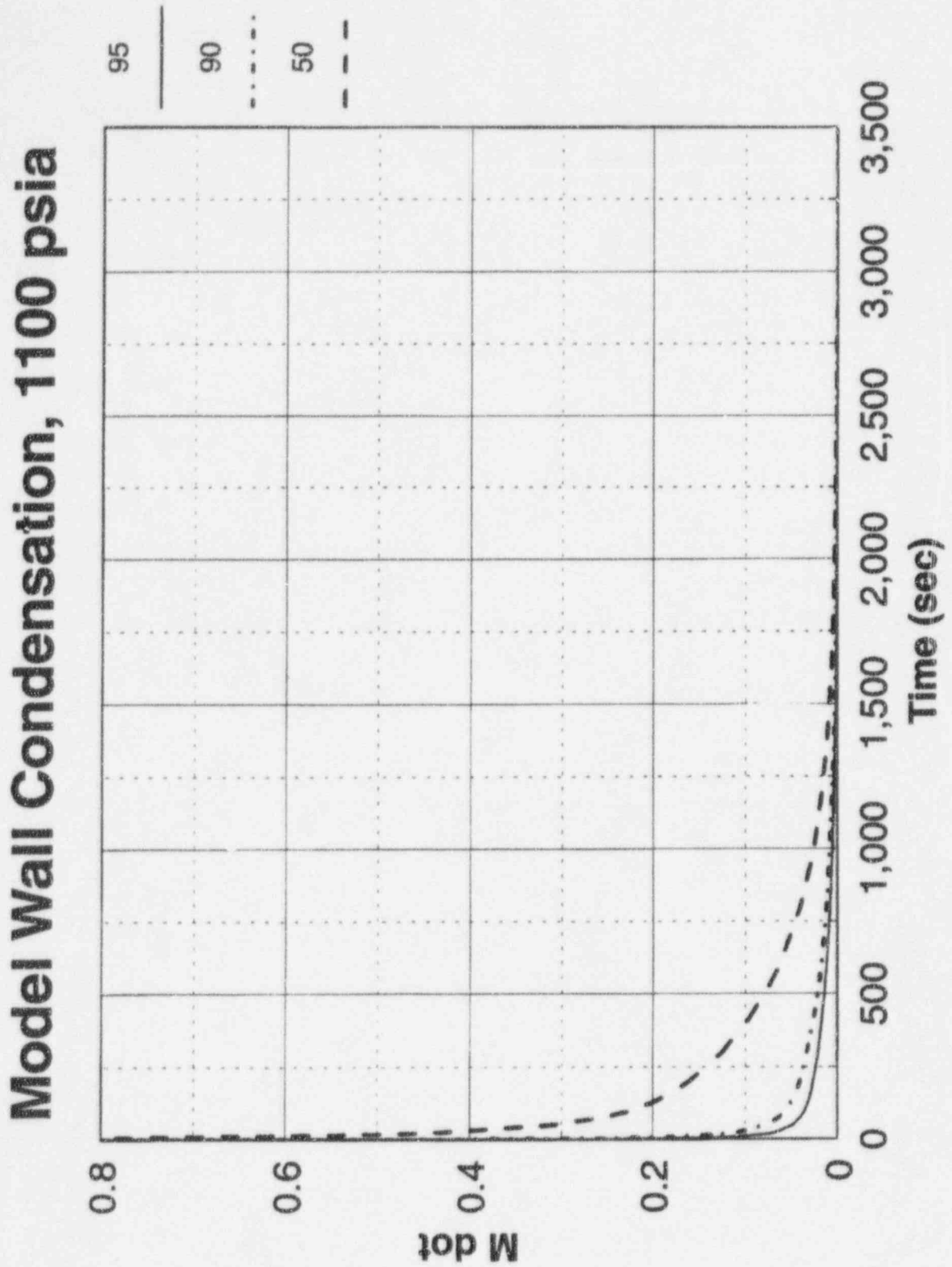

Figure 4.3-14 Calculated CMT Test Wall Condensation Mass Flow Rates (lbm/sec) for Different Liquid Levels at 1100 psia

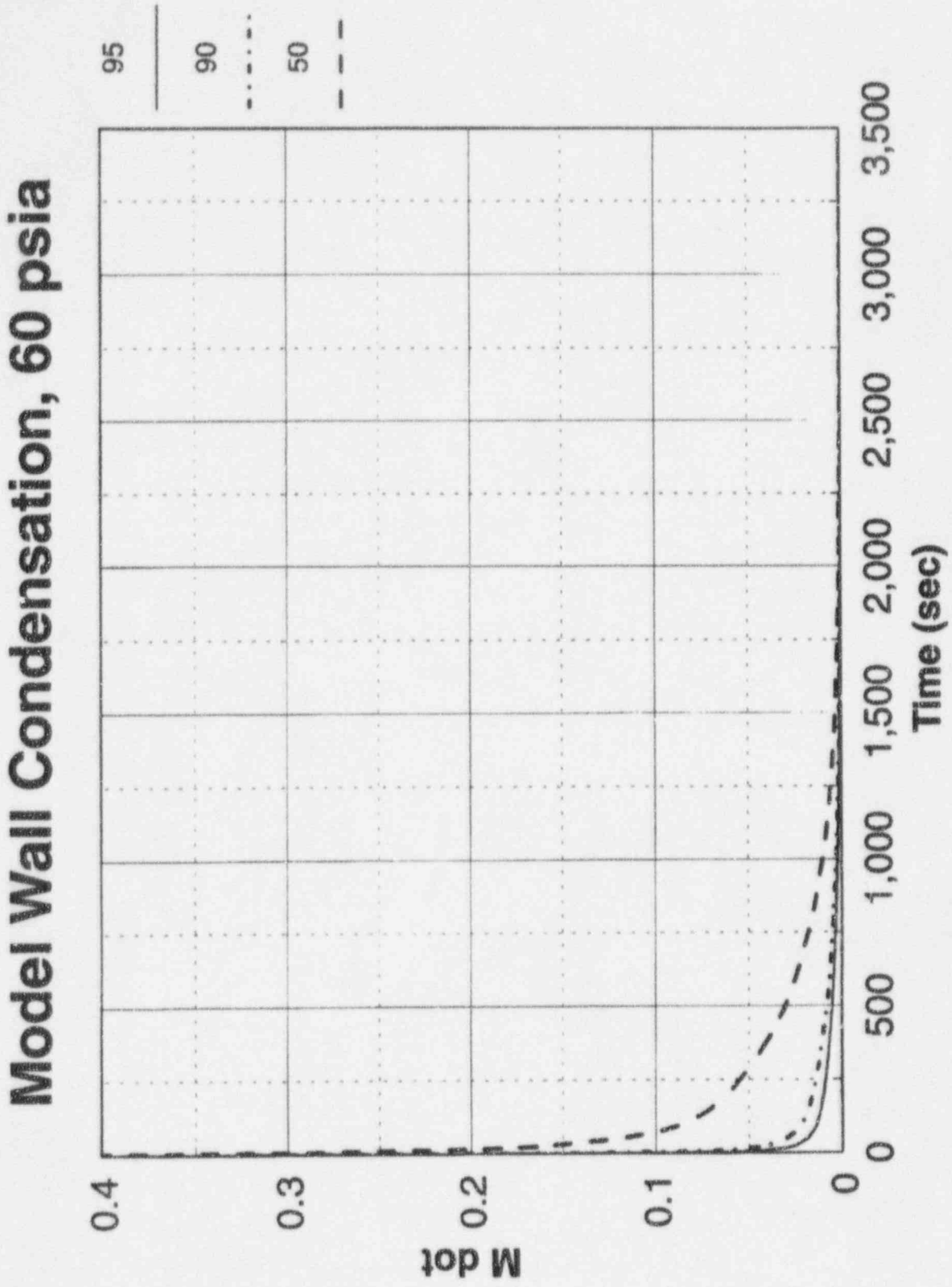

Figure 4.3-15 Calculated CMT Test Wall Condensation Mass Flow Rates (lbm/sec) for Different Liquid Levels at 60 psia

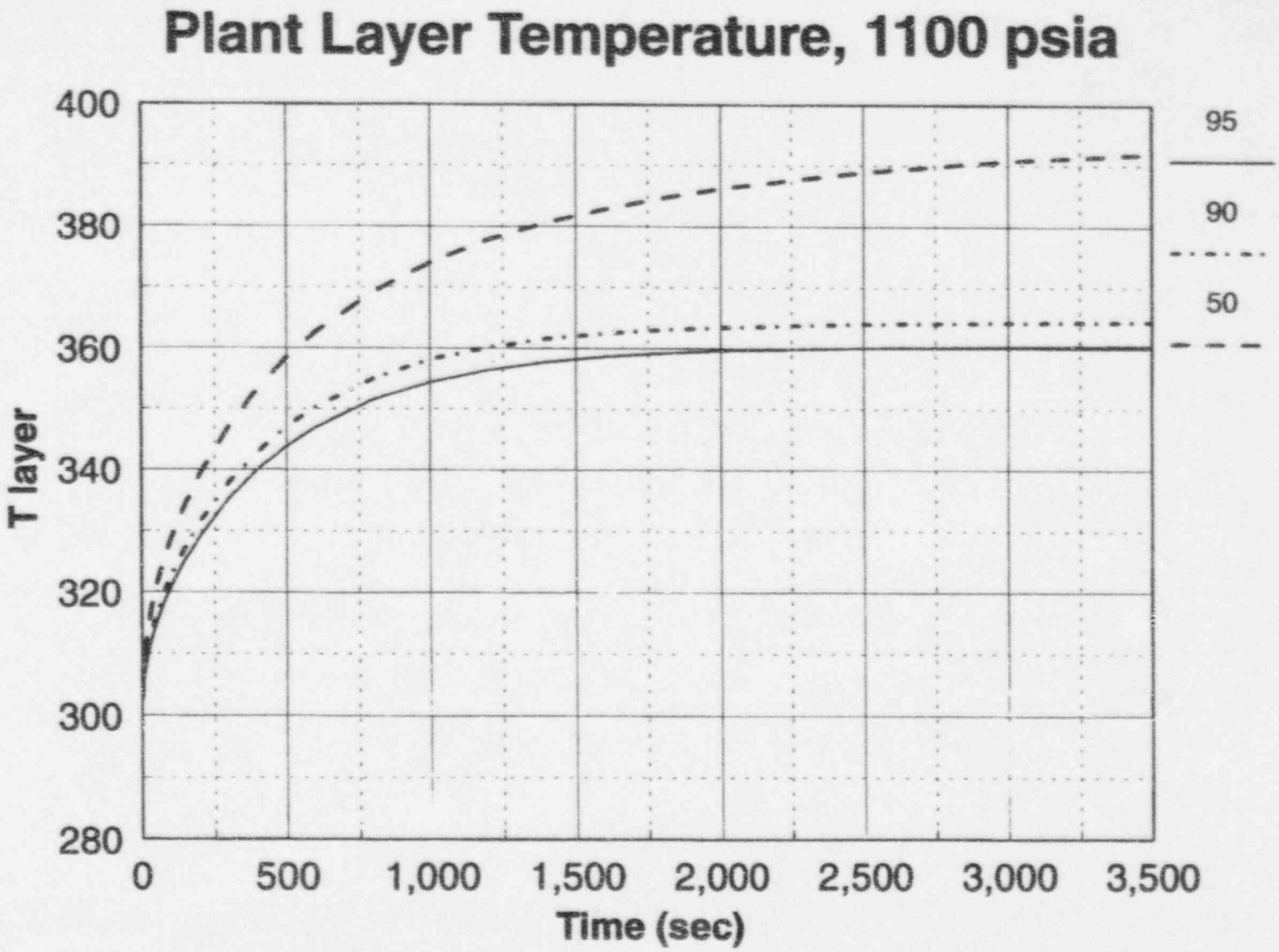

Figure 4.3-16 Calculated Plant Liquid Temperatures (°F) for Different Liquid Levels at 1100 psia and a Mixing Depth of 1.5 ft.

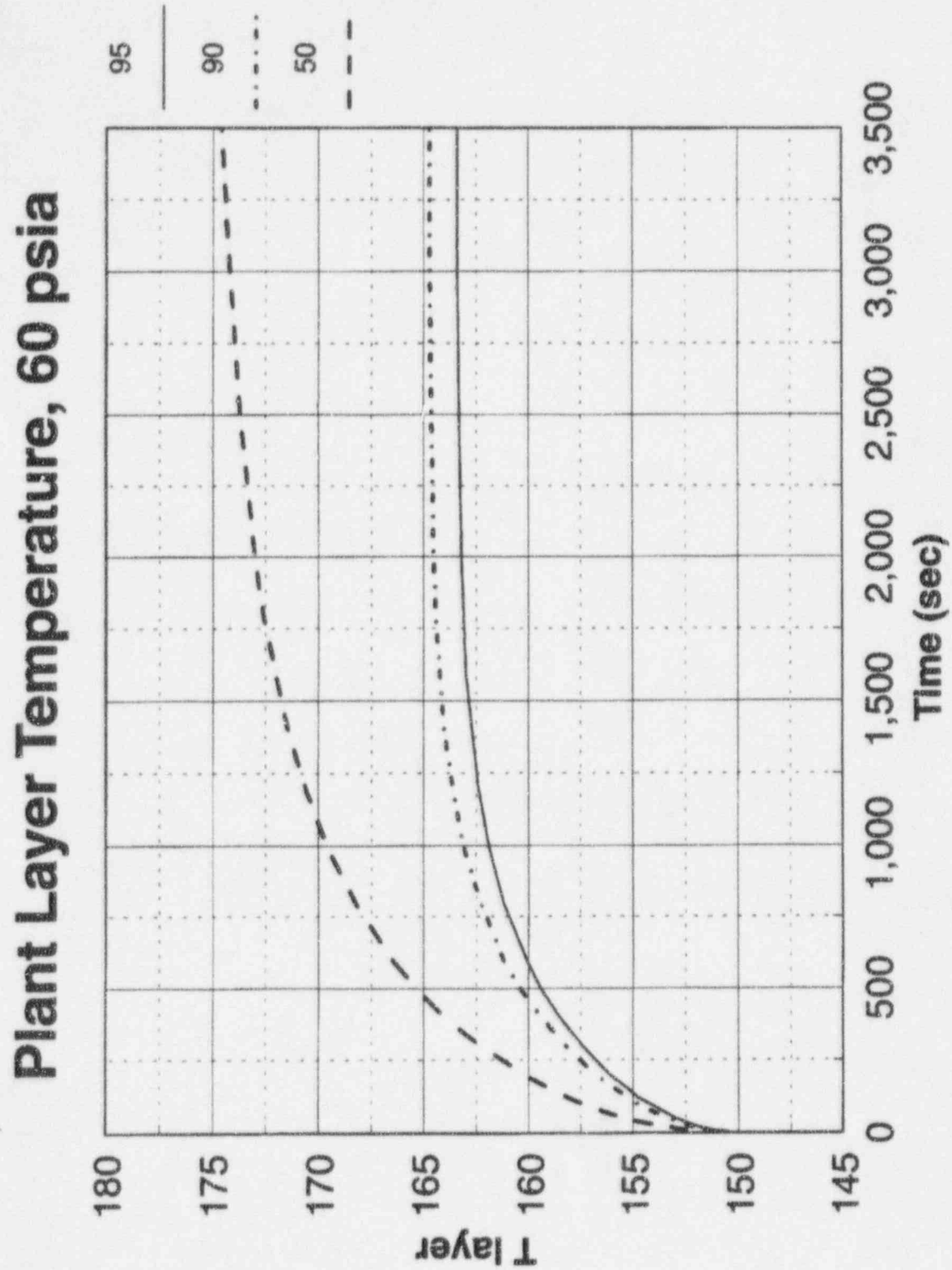

Figure 4.3-17 Calculated Plant Liquid Temperatures (°F) for Different Liquid Levels at 60 psia and a Mixing Depth of 1.5 ft.

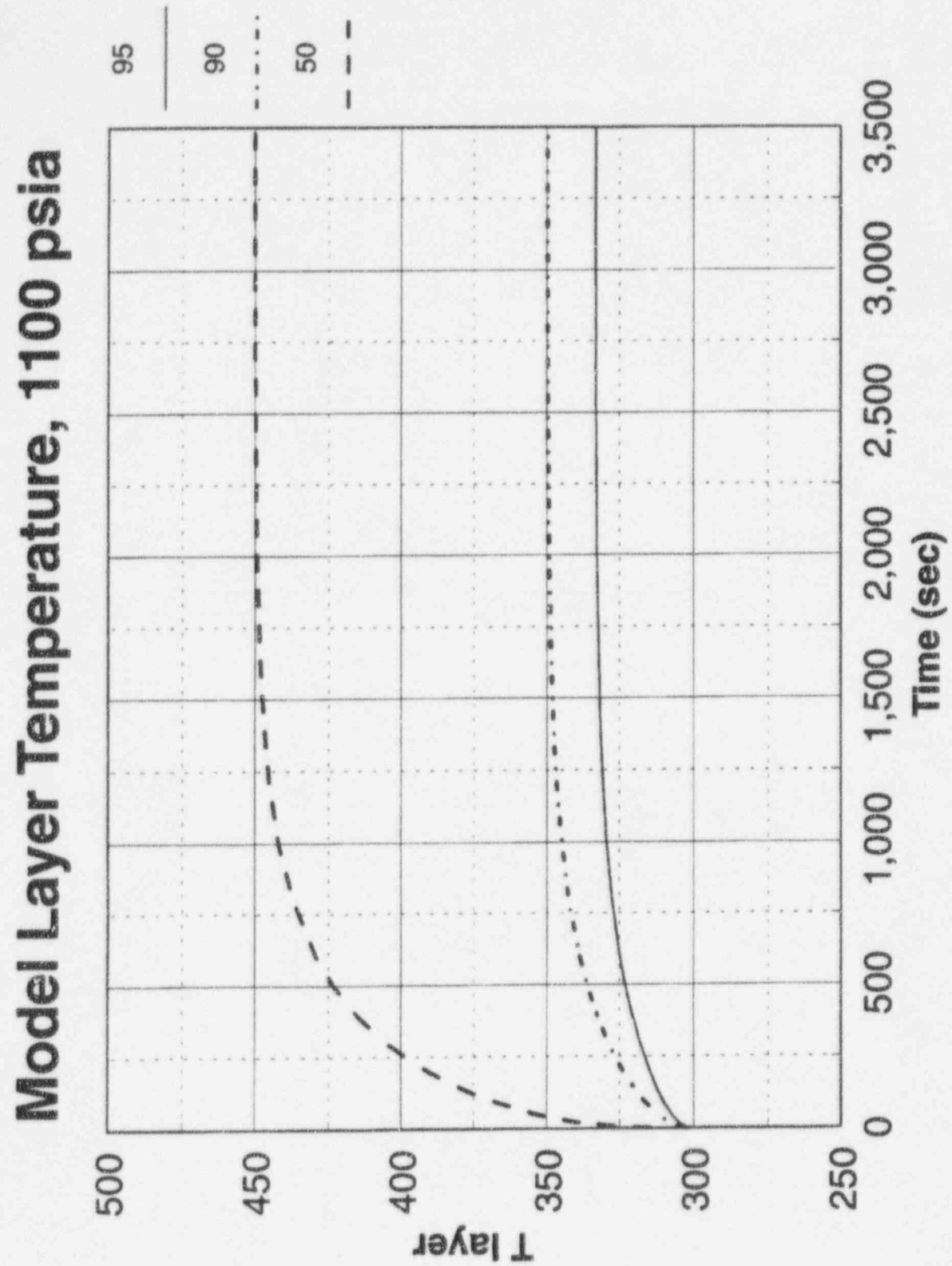

Figure 4.3-18 Calculated CMT Test Liquid Temperatures (°F) for Different Liquid Levels at 1100 psia and a Mixing Depth of 1.5 ft.

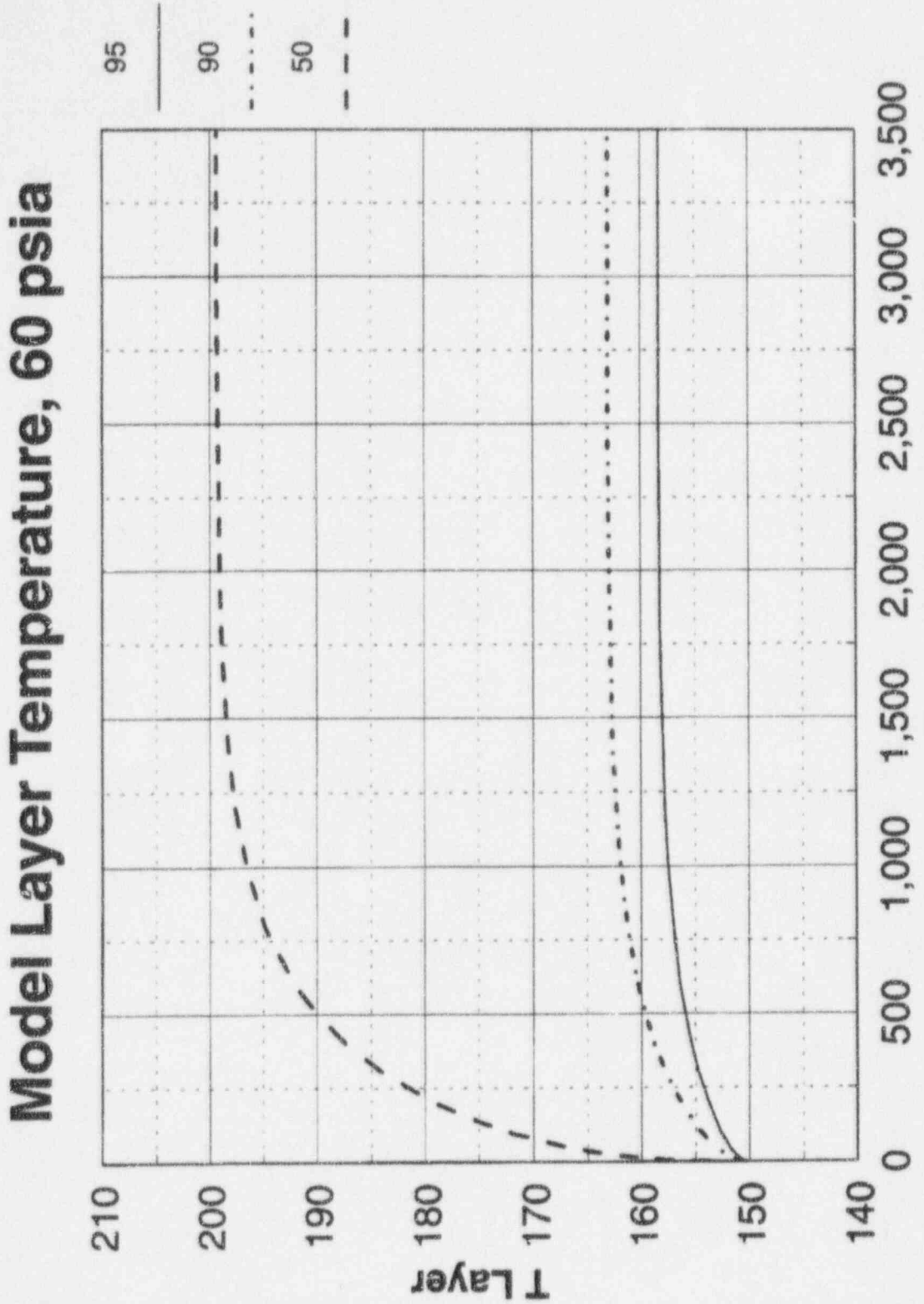

Figure 4.3-19 Calculated CMT Test Liquid Temperatures (°F) for Different Liquid Levels at 60 psia and a Mixing Depth of 1.5 ft.

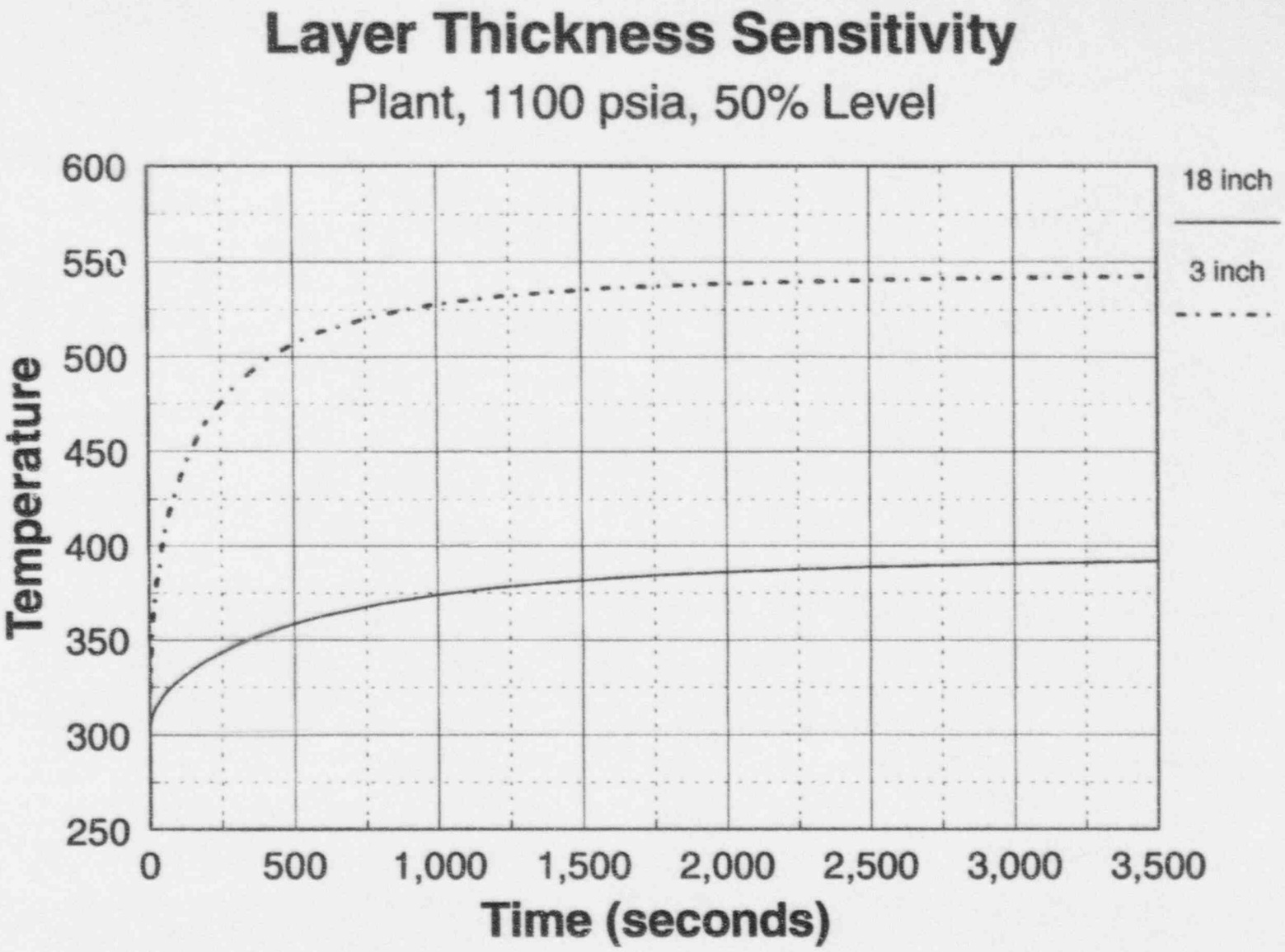

Figure 4.3-20 Sensitivity Study to the Assumed Liquid Layer Thickness for the Plant CMT at 1100 psia, Temperature in °F

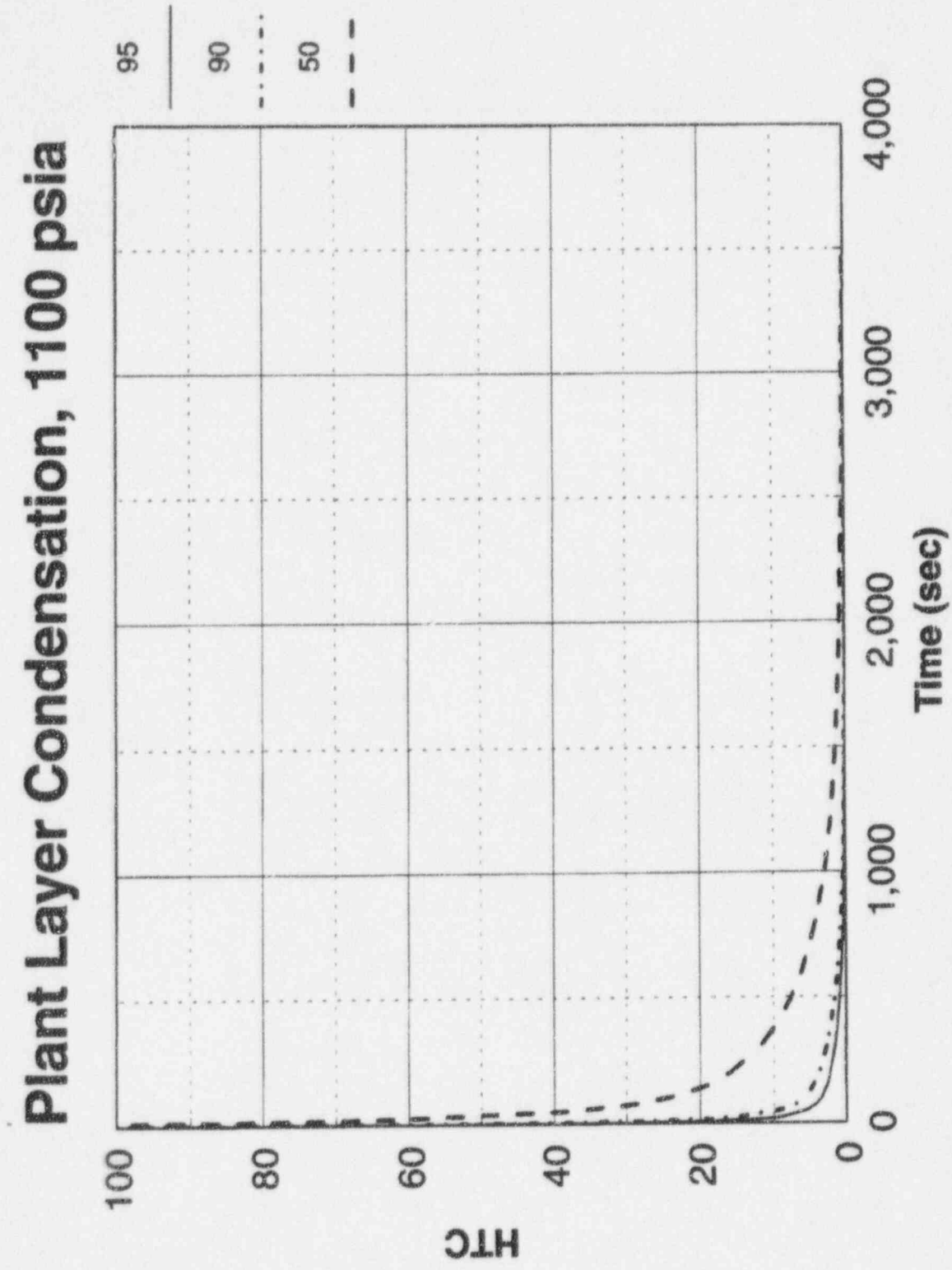

Figure 4.3-21 Calculated Plant Condensation Heat Transfer Coefficients (Btu/hr-ft^2-°F) on the CMT Liquid Surface at 1100 psia

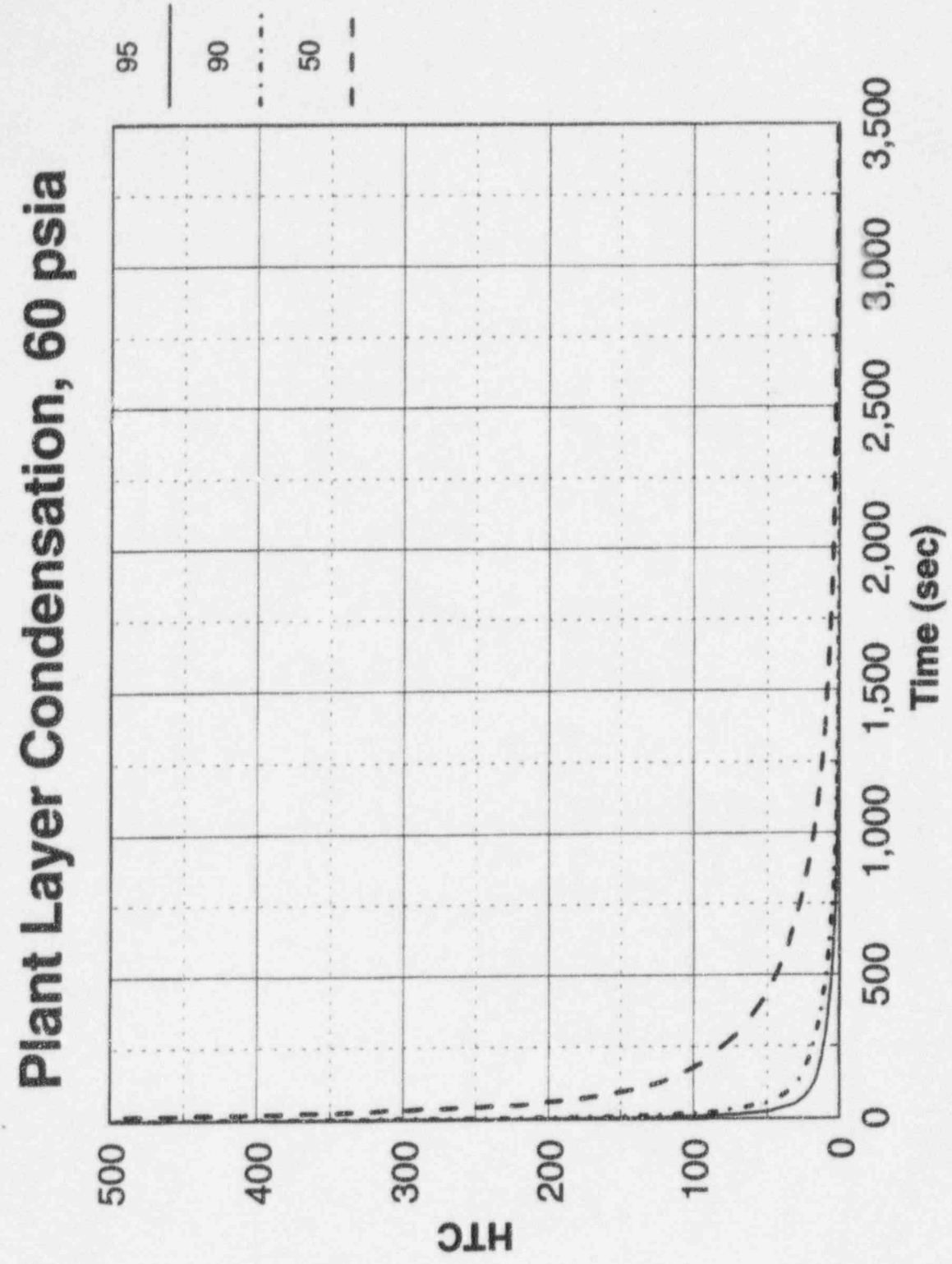

Figure 4.3-22 Calculated Plant Condensation Heat Transfer Coefficients (Btu/hr-ft^2-°F) on the CMT Liquid Surface at 60 psia

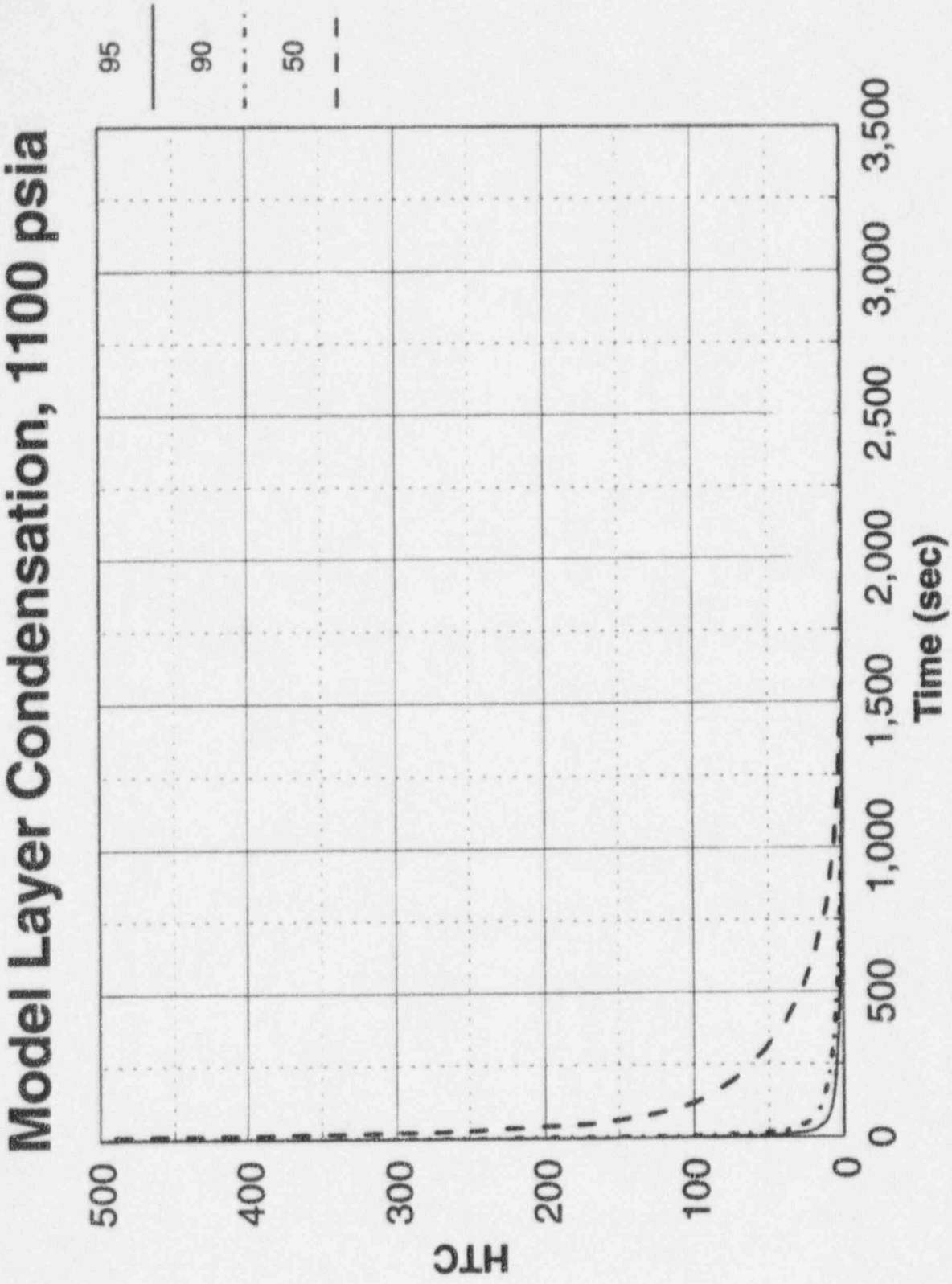

Figure 4.3-23 Calculated CMT Test Condensation Heat Transfer Coefficients (Btu/hr-ft^2-°F) on the Liquid Surface at 1100 psia

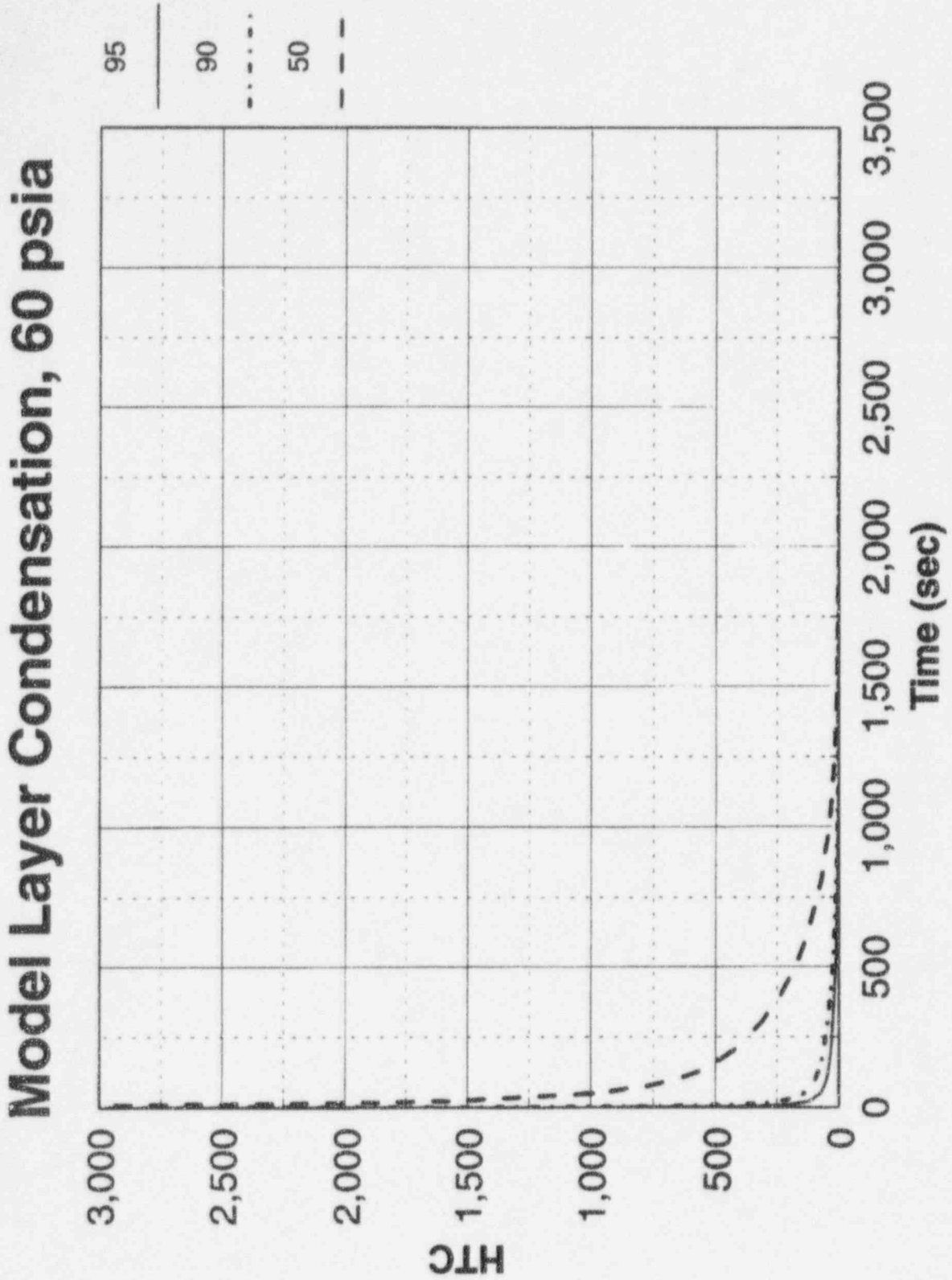

Figure 4.3-24 Calculated CMT Test Condensation Heat Transfer Coefficients (Btu/hr-ft^2-°F) on the Liquid Surface at 60 psia

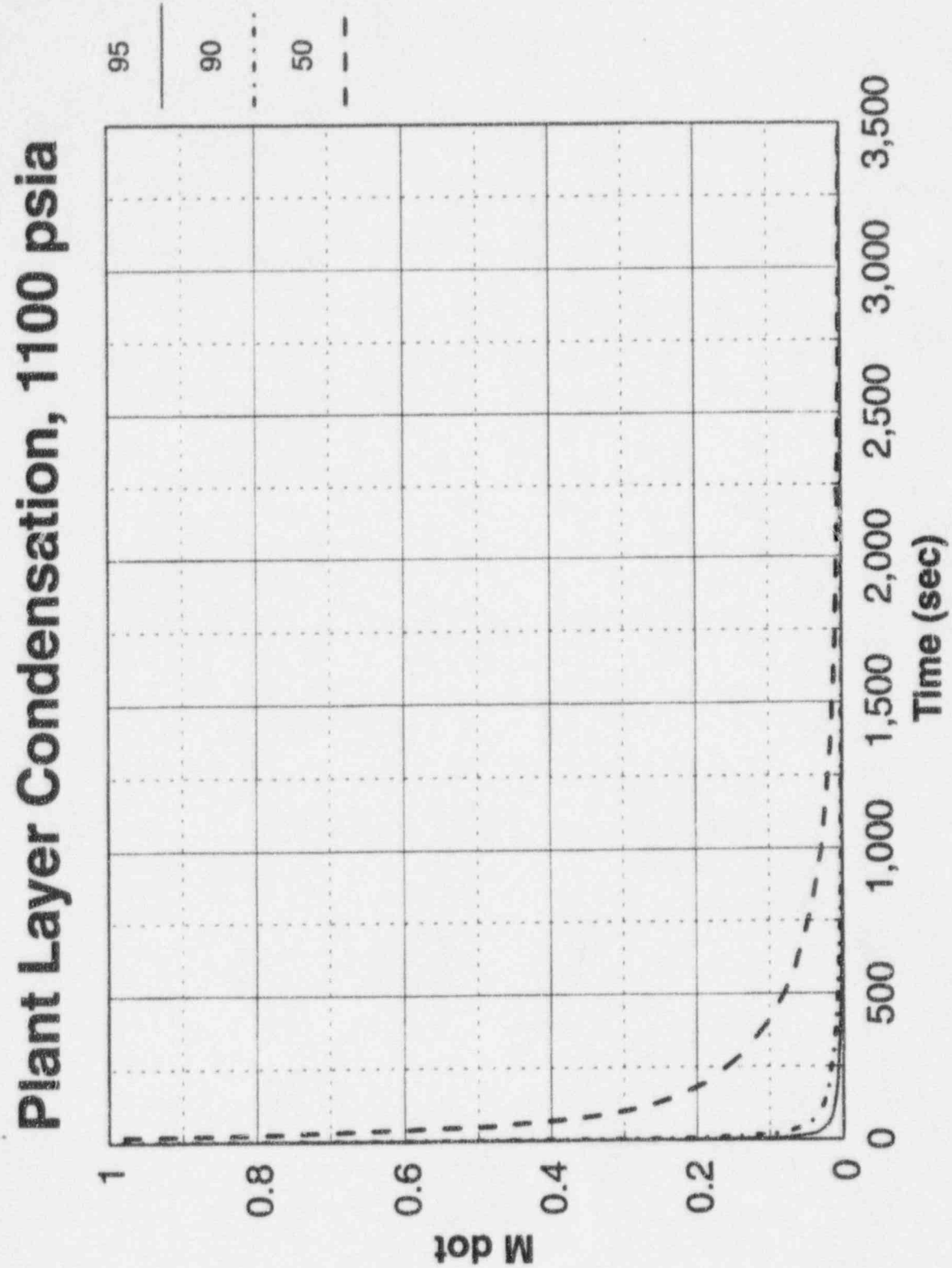

Figure 4.3-25 Calculated Plant Condensation Flow Rates (lbm/sec) on the Liquid Surface at 1100 psia

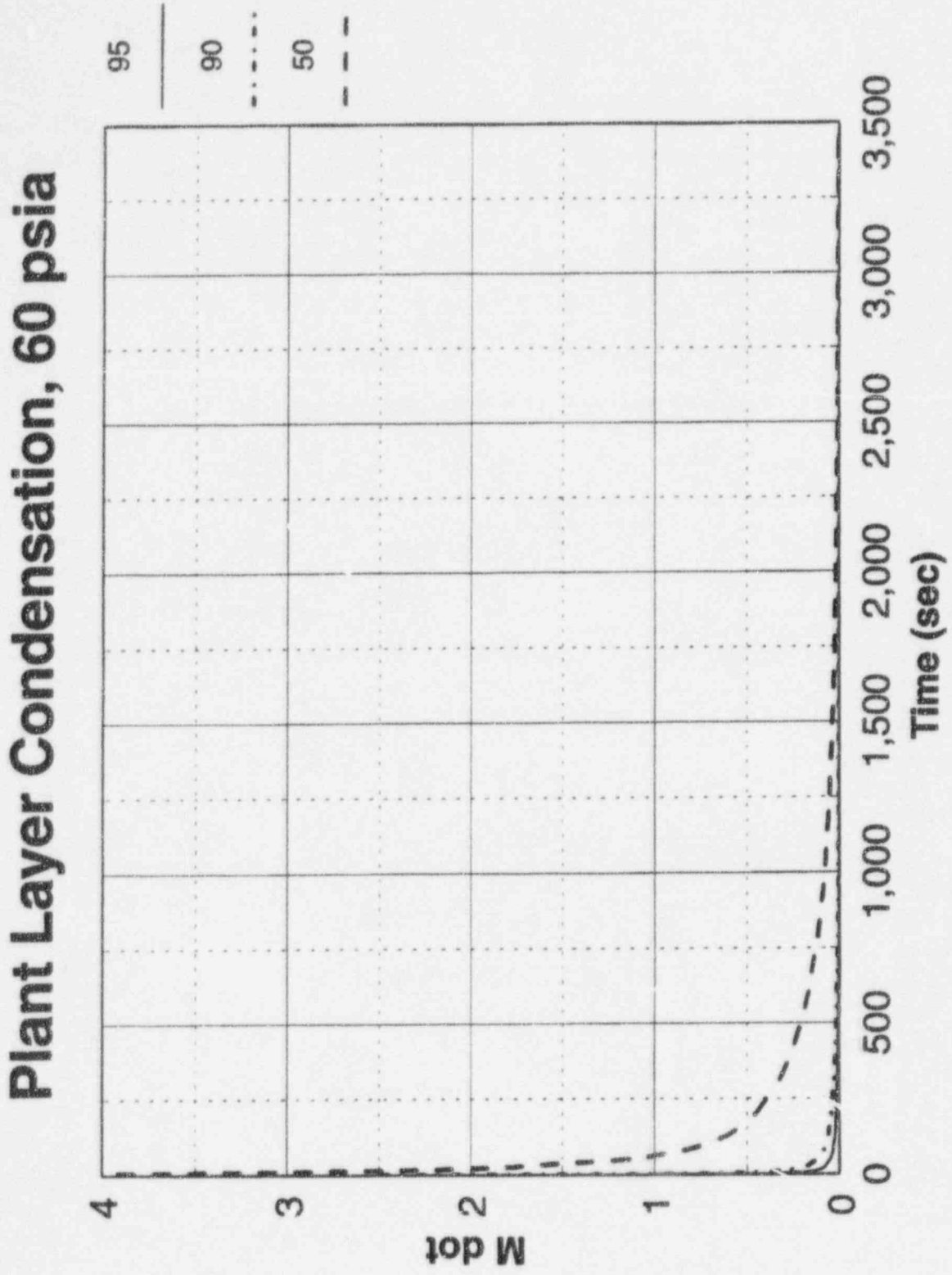

Figure 4.3-26 Calculated Plant Condensation Flow Rates (lbm/sec) on the Liquid Surface at 60 psia

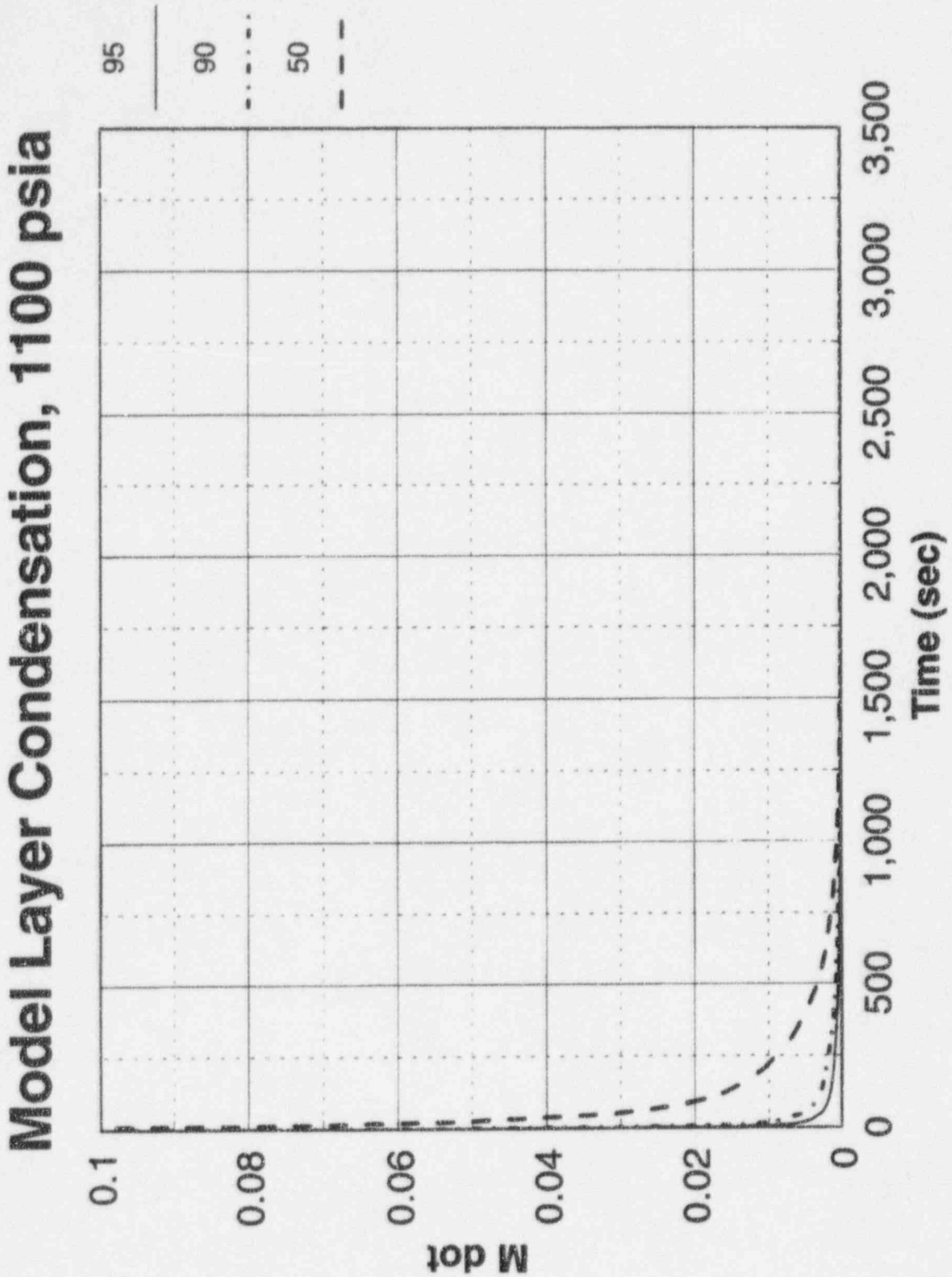

Figure 4.3-27 Calculated CMT Test Condensation Flow Rates (lbm/sec) on the Liquid Surface at 1100 psia

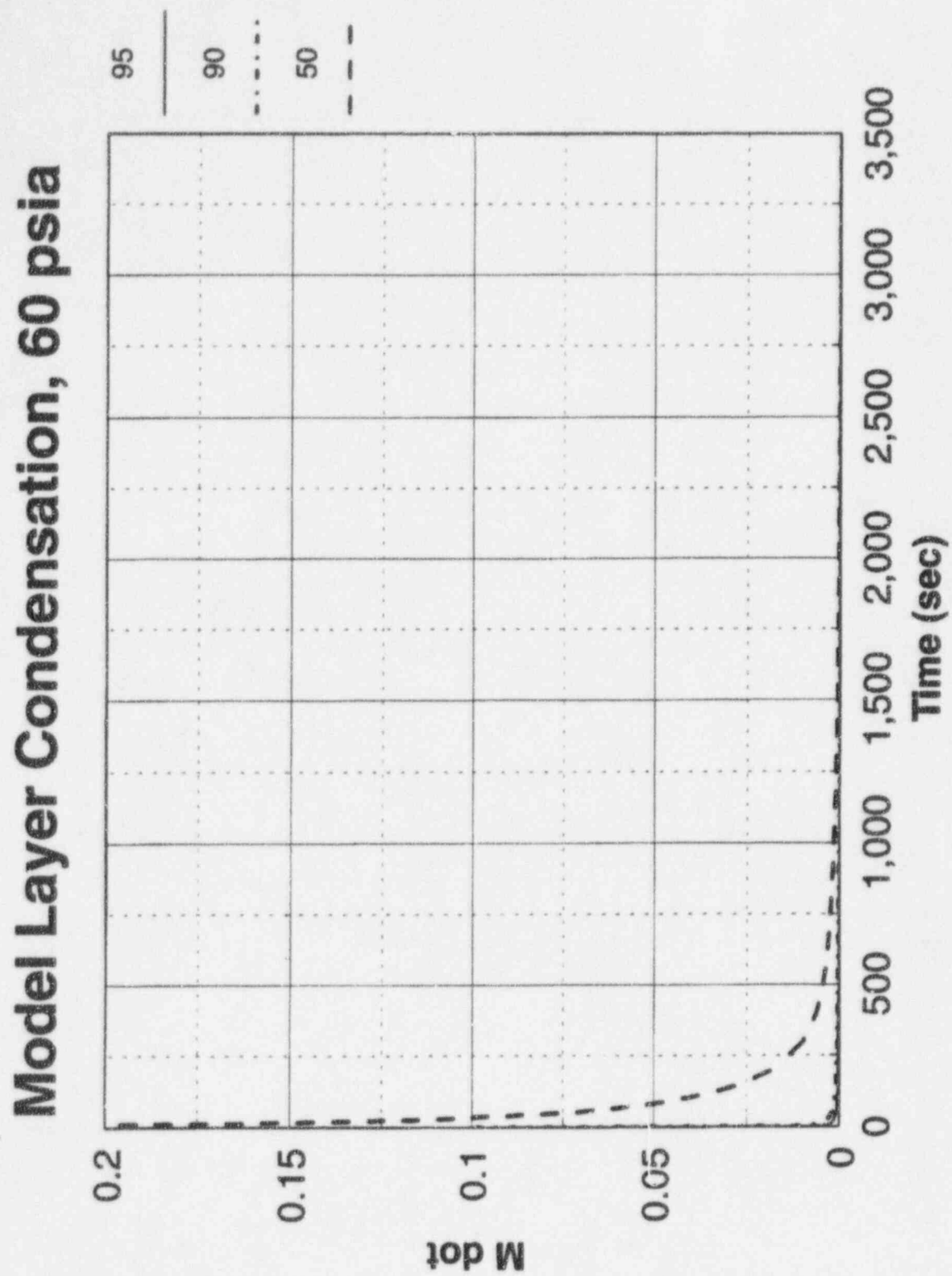

Figure 4.3-28 Calculated CMT Test Condensation Flow Rates (lbm/sec) on the Liquid Surface at 60 psia

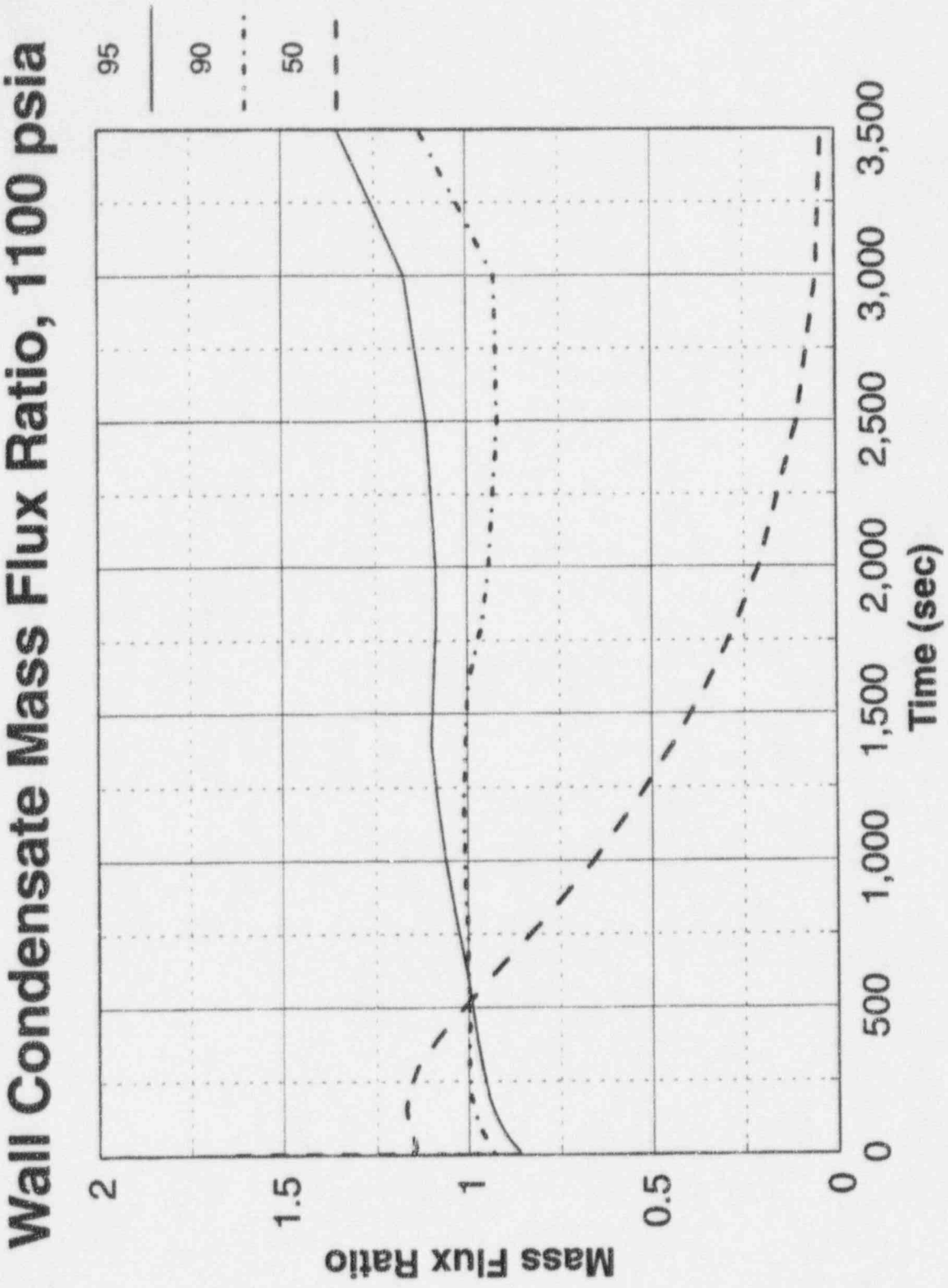

Figure 4.3-29 Ratio of the CMT Test Wall Condensate Mass Flux to the Plant Condensate Mass Flux for Different CMT Levels at 1100 psia

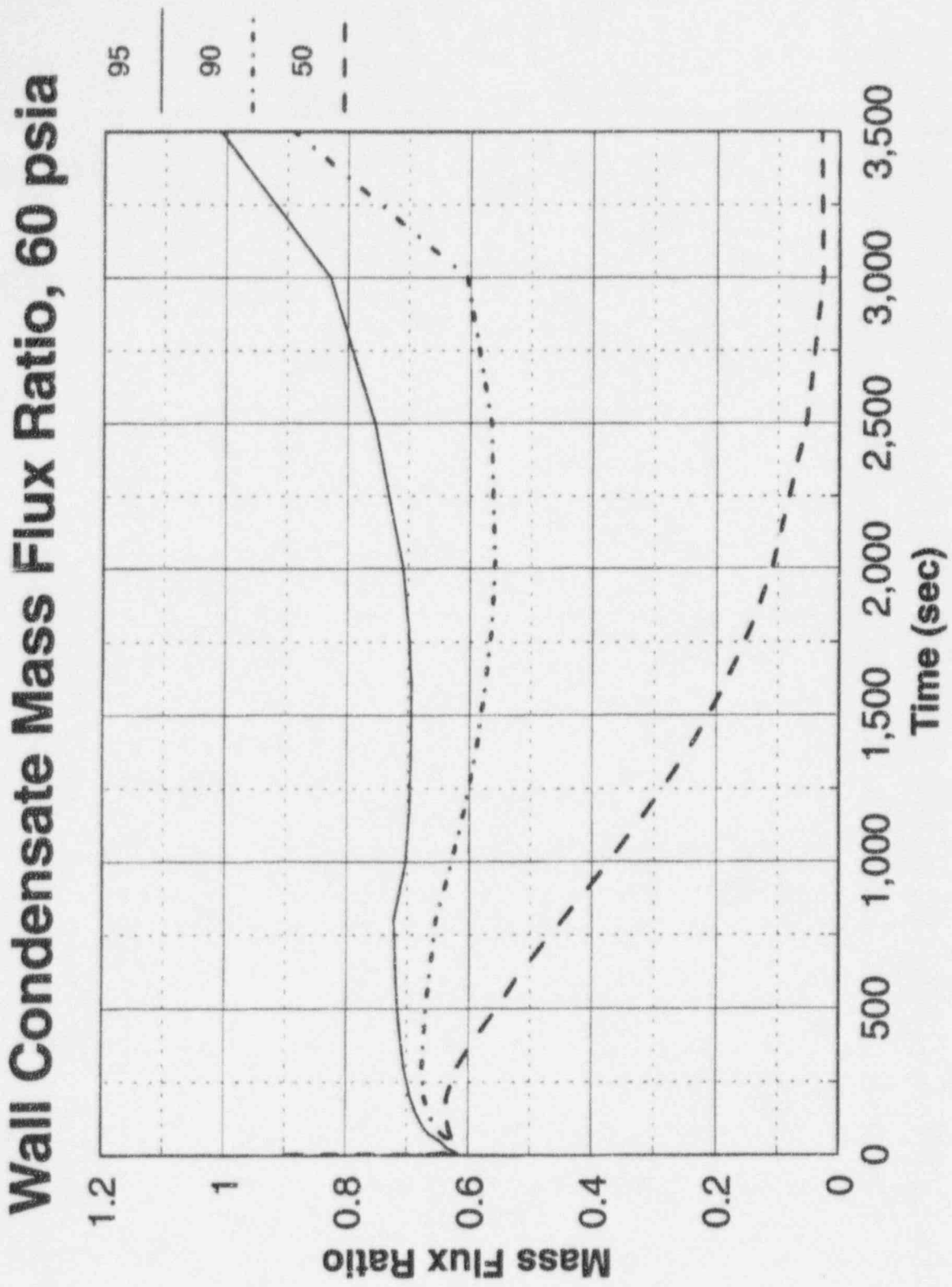

Figure 4.3-30 Ratio of the CMT Test Wall Condensate Mass Flux to the Plant Condensate Mass Flux for Different CMT Levels at 60 psia

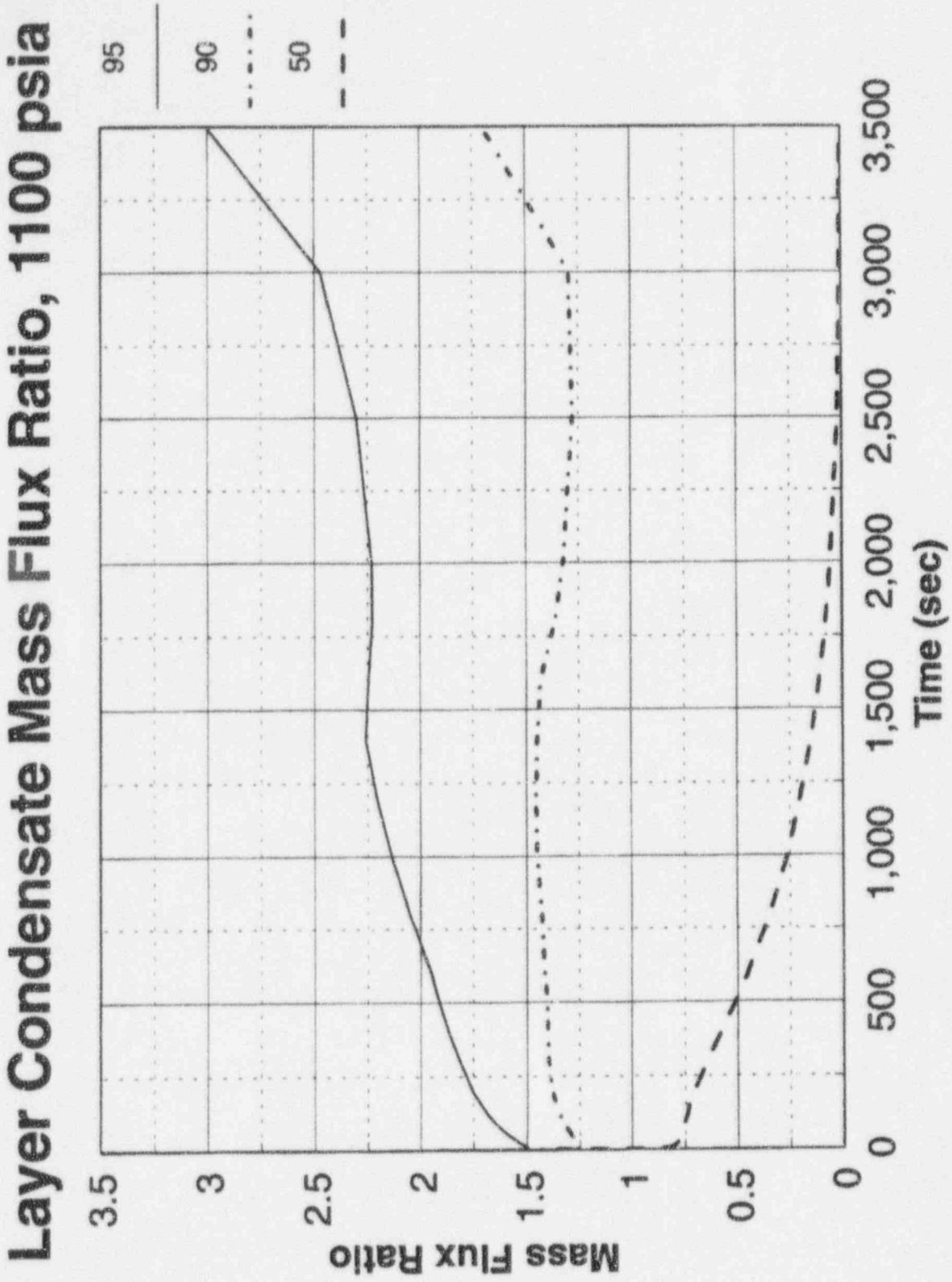

Figure 4.3-31 Ratio of the CMT Test Water Surface Condensate Mass Flux to the Plant Water Surface Condensate Mass Flux or 1100 psia

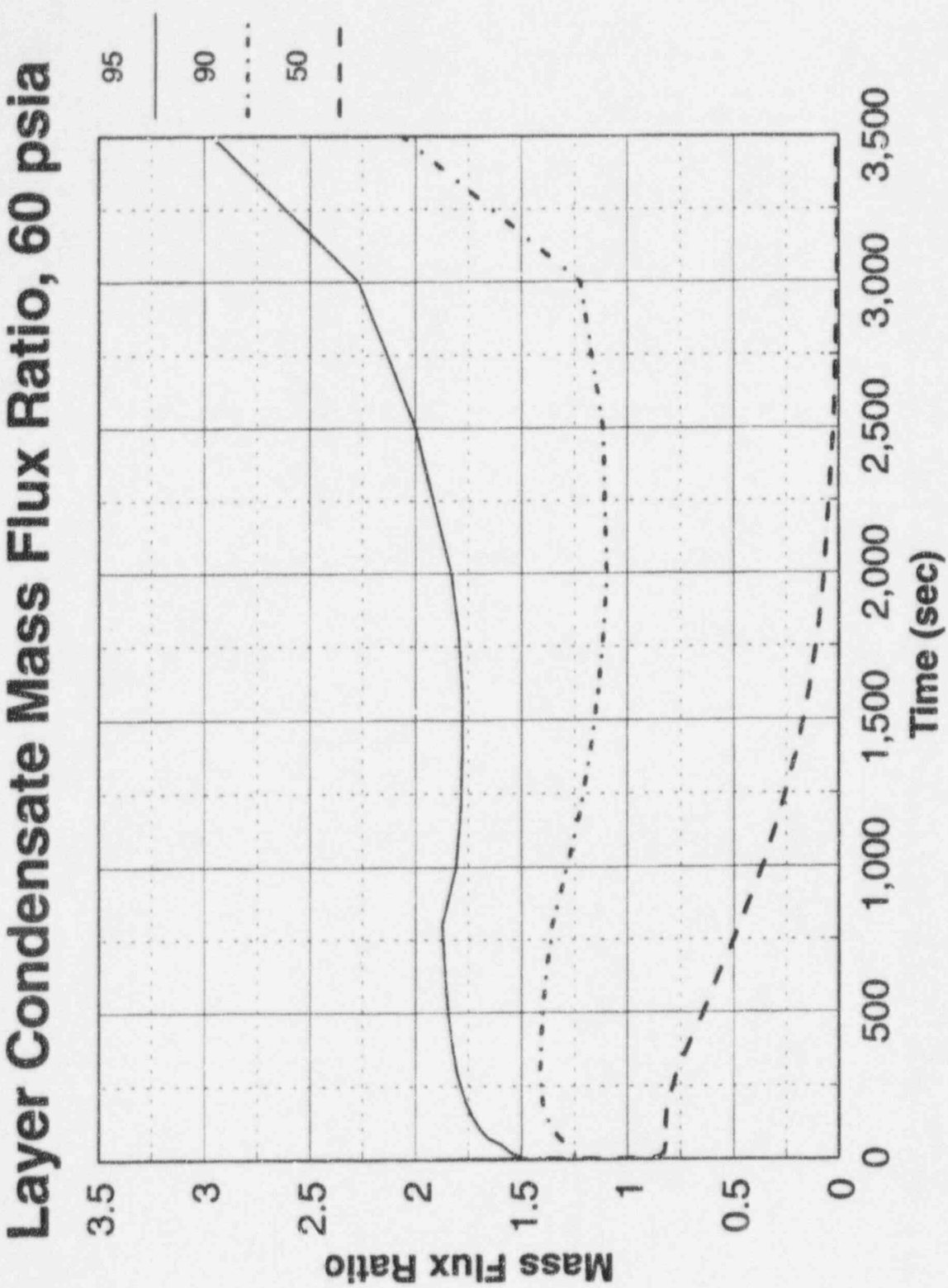

Figure 4.3-32 Ratio of the CMT Test Water Surface Condensate Mass Flux to the Plant Water Surface Condensate Mass Flux at 60 psia

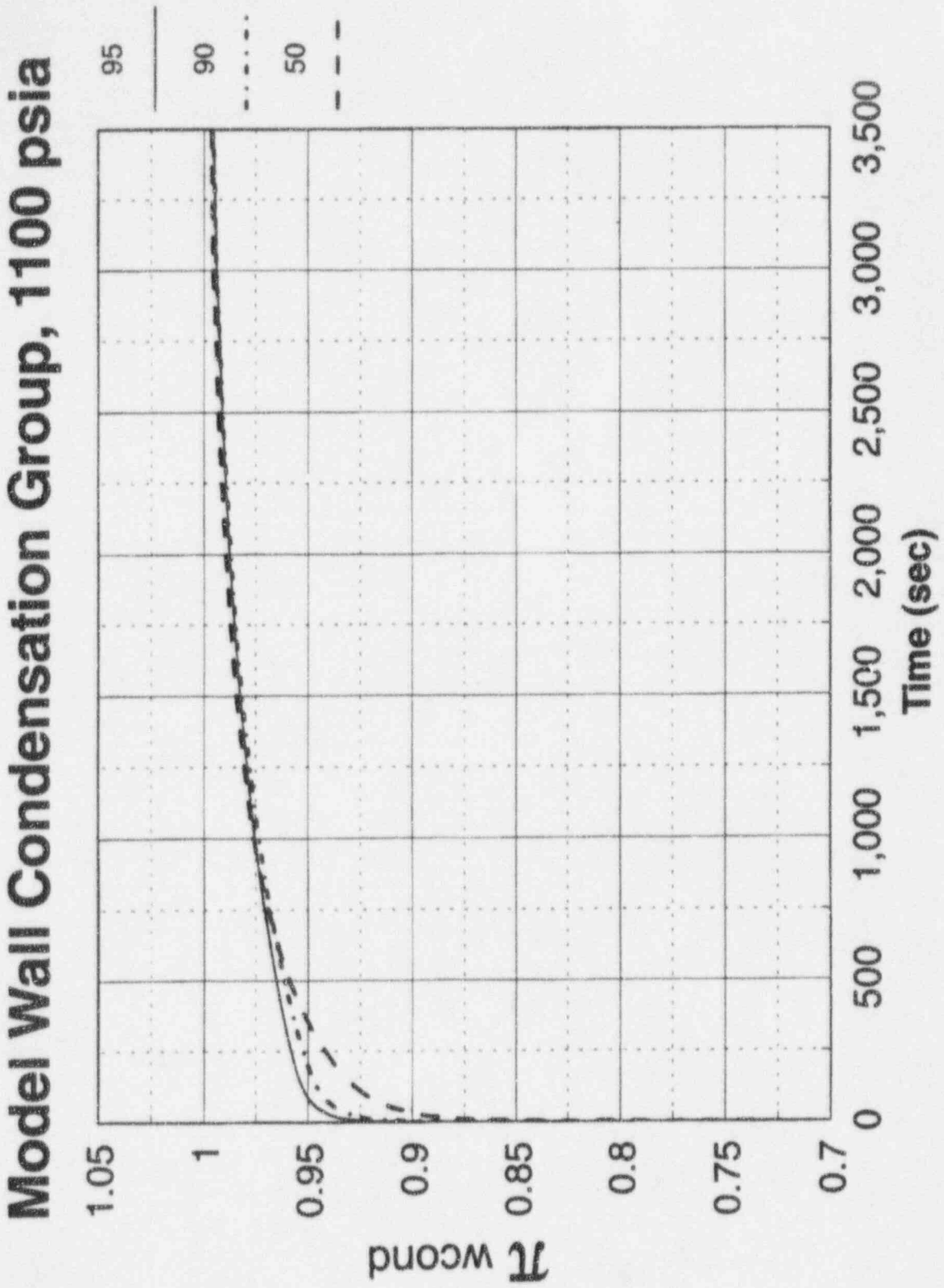

Figure 4.3-33 Calculated CMT Test Π_{wcond} Group for Different Liquid Levels at 1100 psia and a Mixing Depth of 1.5 ft.

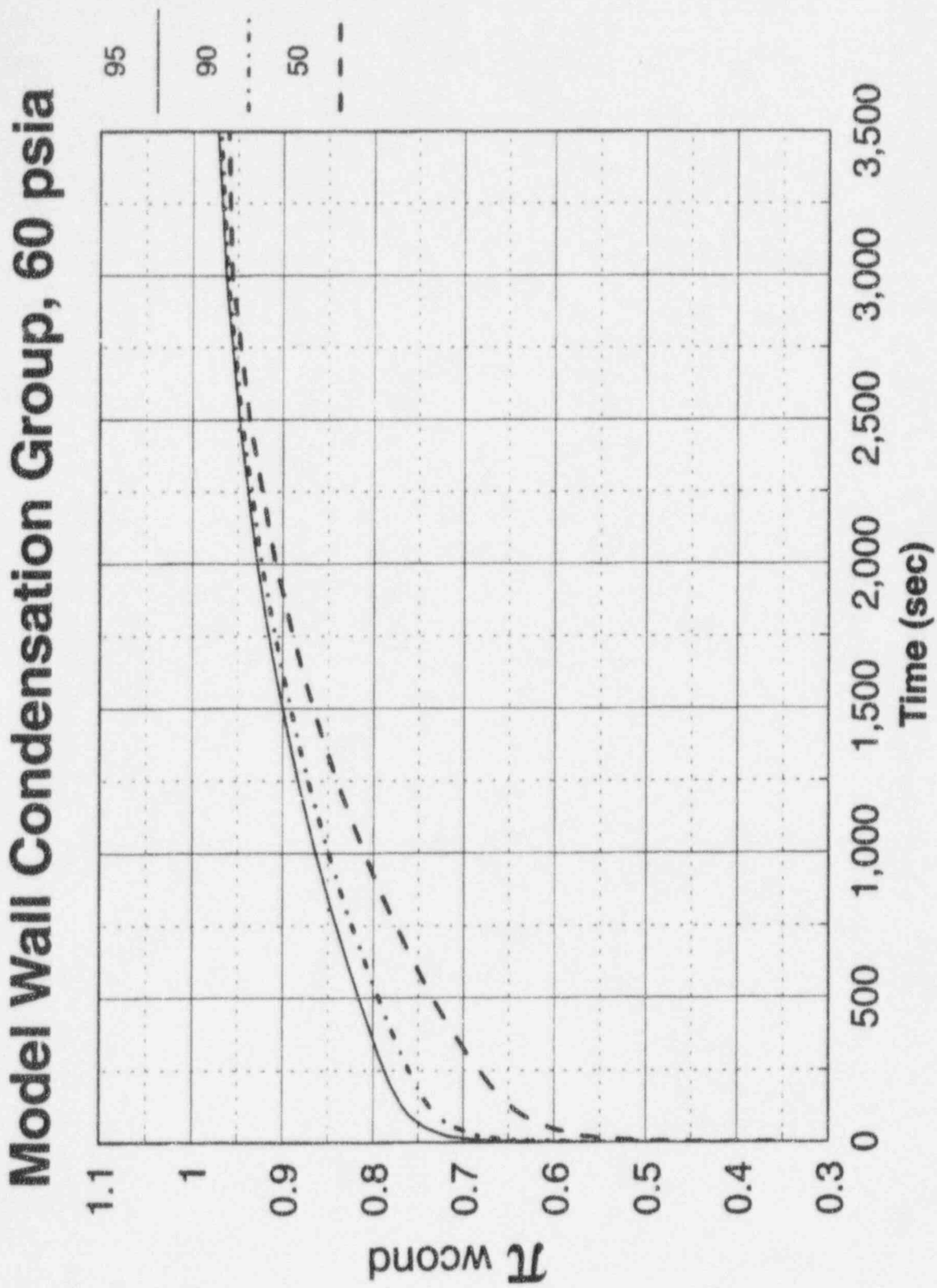

Figure 4.3-34 Calculated CMT Test Π_{wcond} Group for Different Liquid Levels at 60 psia and a Mixing Depth of 1.5 ft.

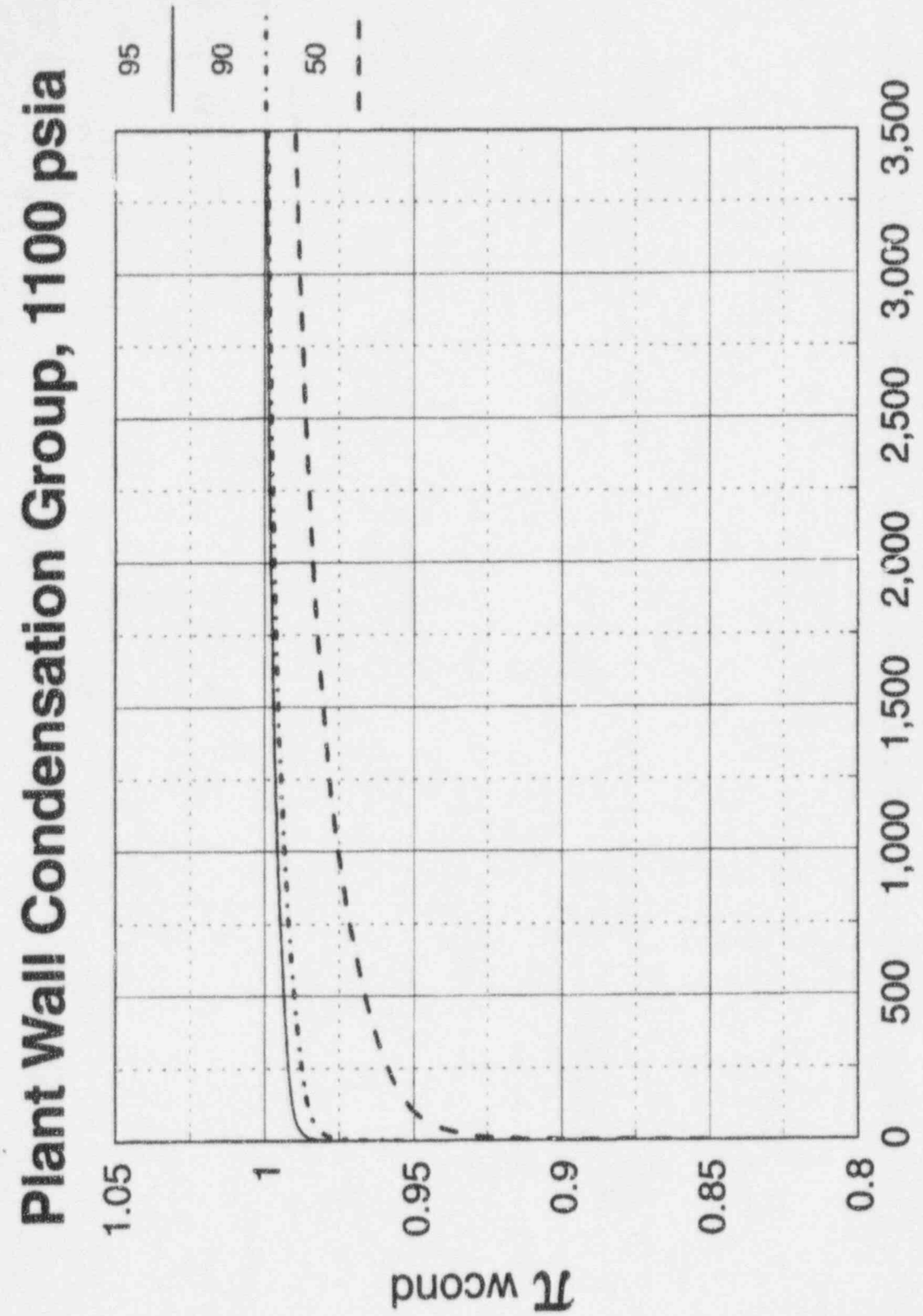

Figure 4.3-35 Calculated Plant Π_{wcond} Group for Different Liquid Levels at 1100 psia and a Mixing Depth of 1.5 ft.

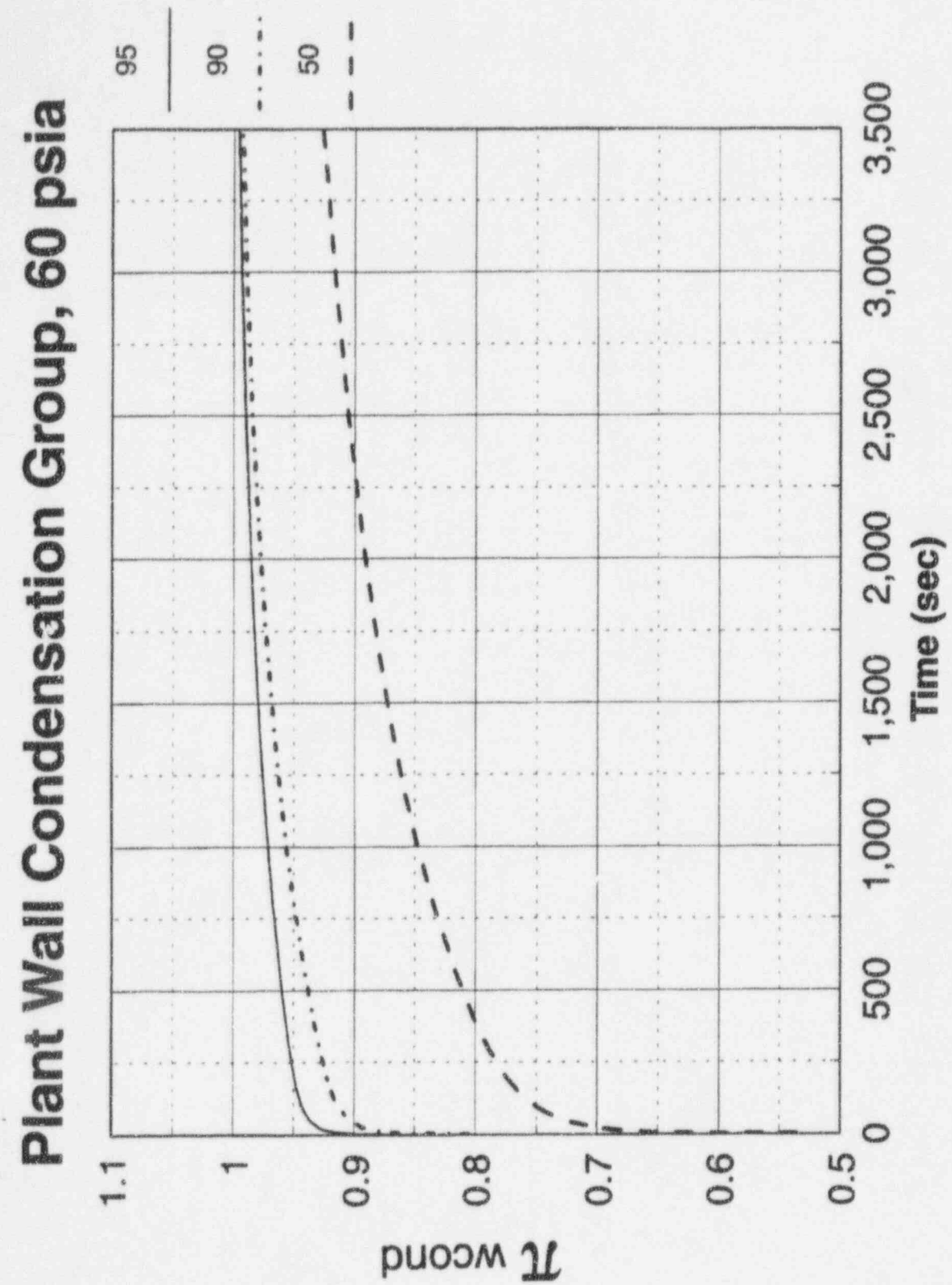

Figure 4.3-36 Calculated Plant Π_{wcond} Group for Different Liquid Levels at 60 psia and a Mixing Depth of 1.5 ft.

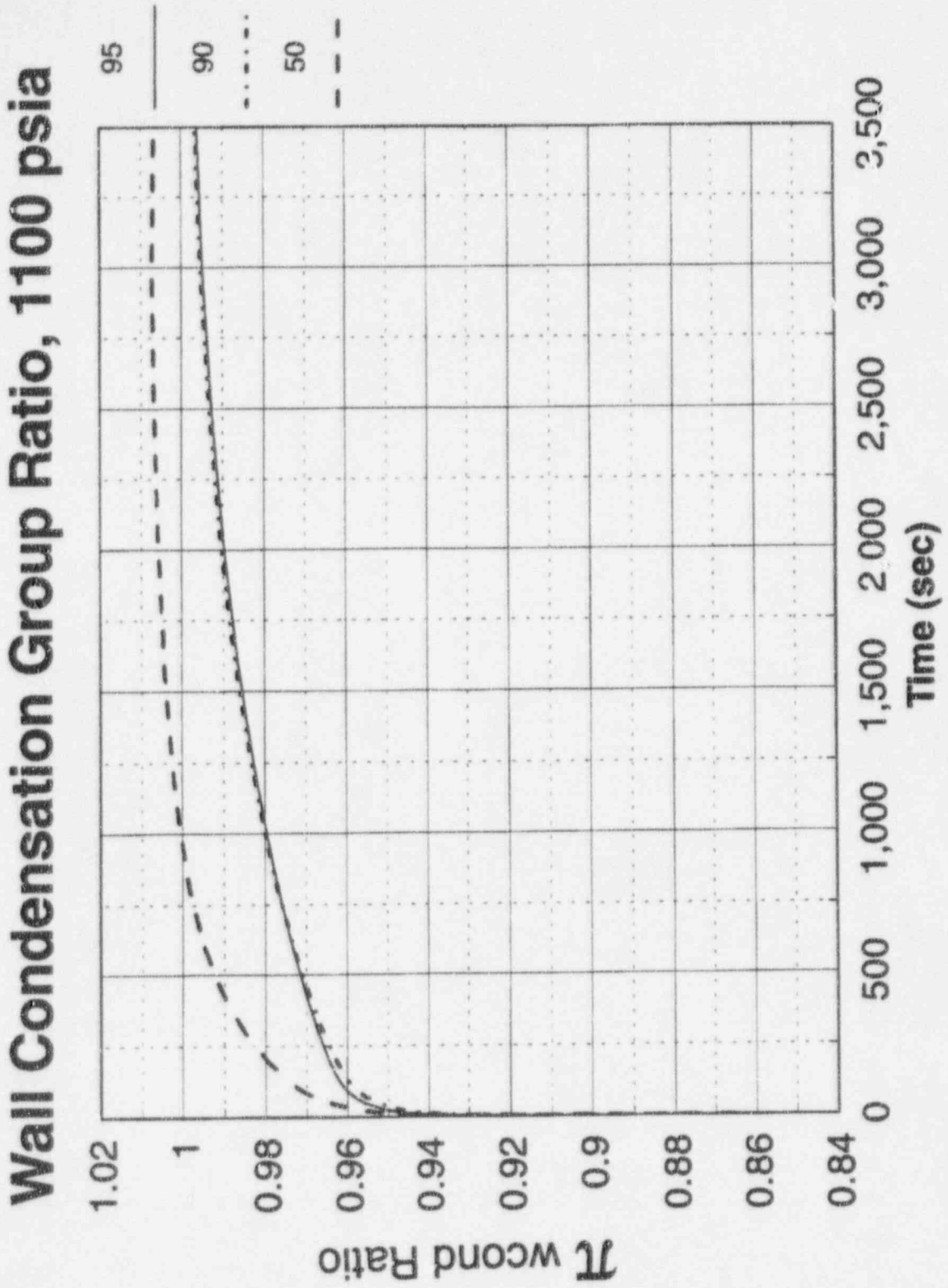

Figure 4.3-37 Calculated Ratio of the CMT Test Π_{wcond} Group to the Plant CMT Π_{cond} Group for Different Liquid Levels at 1100 psia and a Mixing Depth of 1.5 ft.

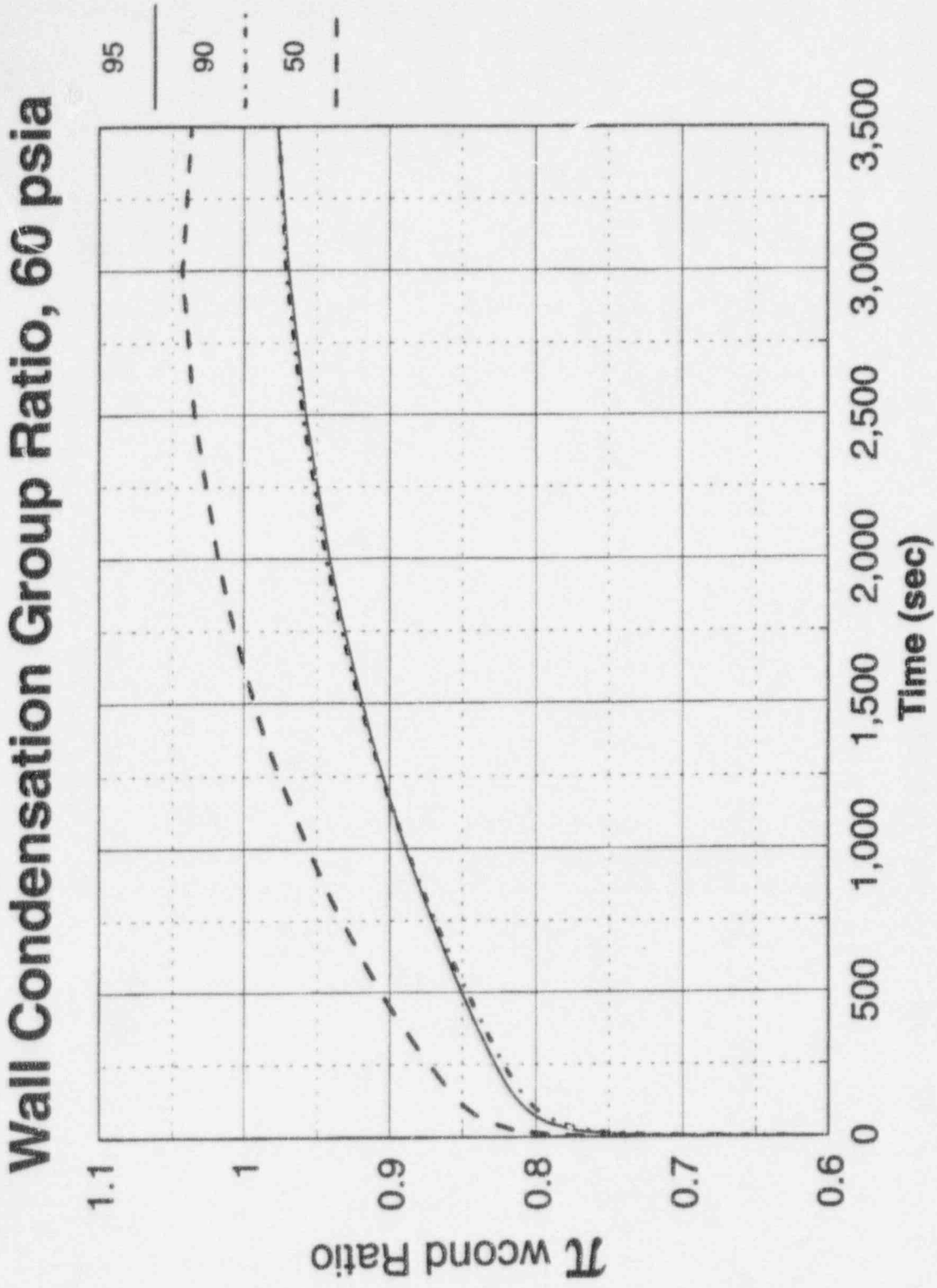

Figure 4.3-38 Calculated Ratio of the CMT Test Π_{wcond} Group to the Plant CMT Π_{cond} group for Different Liquid Levels at 60 psia and a Mixing Depth of 1.5 ft.

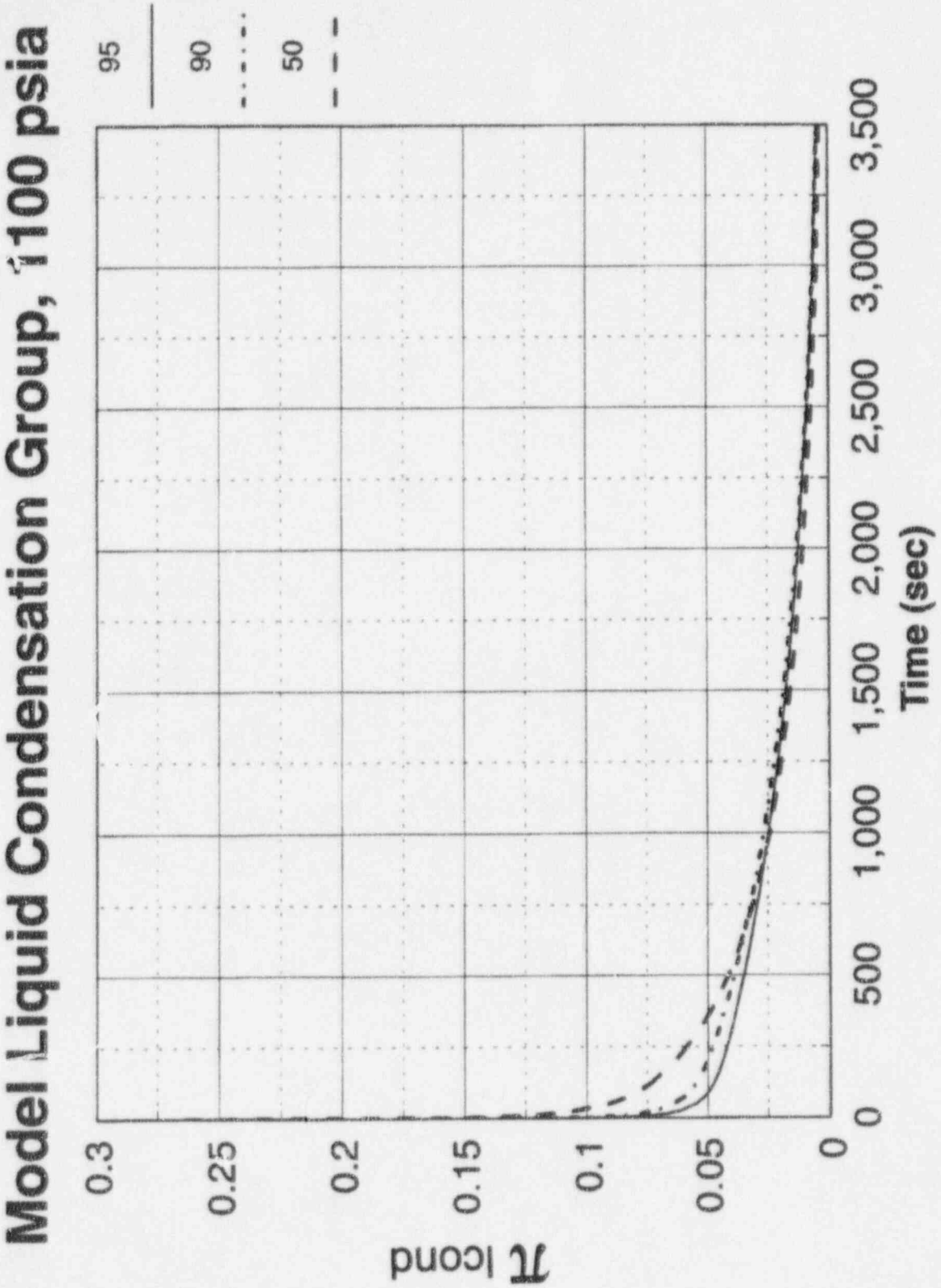

Figure 4.3-39 Calculated CMT Test $\Pi_{t_{cond}}$ Group for Different Liquid Levels at 1100 psia and a Mixing Depth of 1.5 ft.

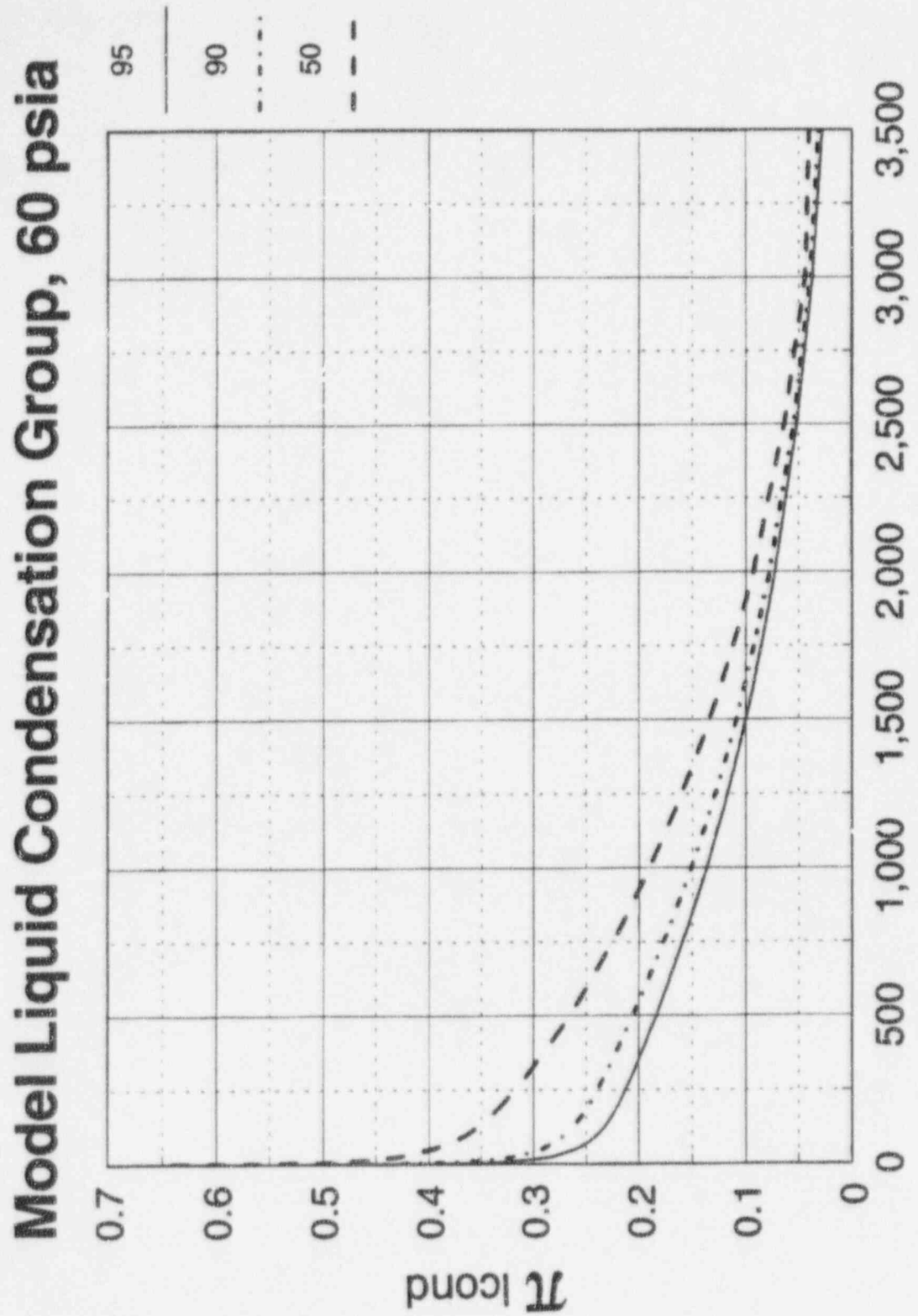

Figure 4.3-40 Calculated CMT Test Π_{lcond} Group for Different Liquid Levels at 60 psia and a Mixing Depth of 1.5 ft.

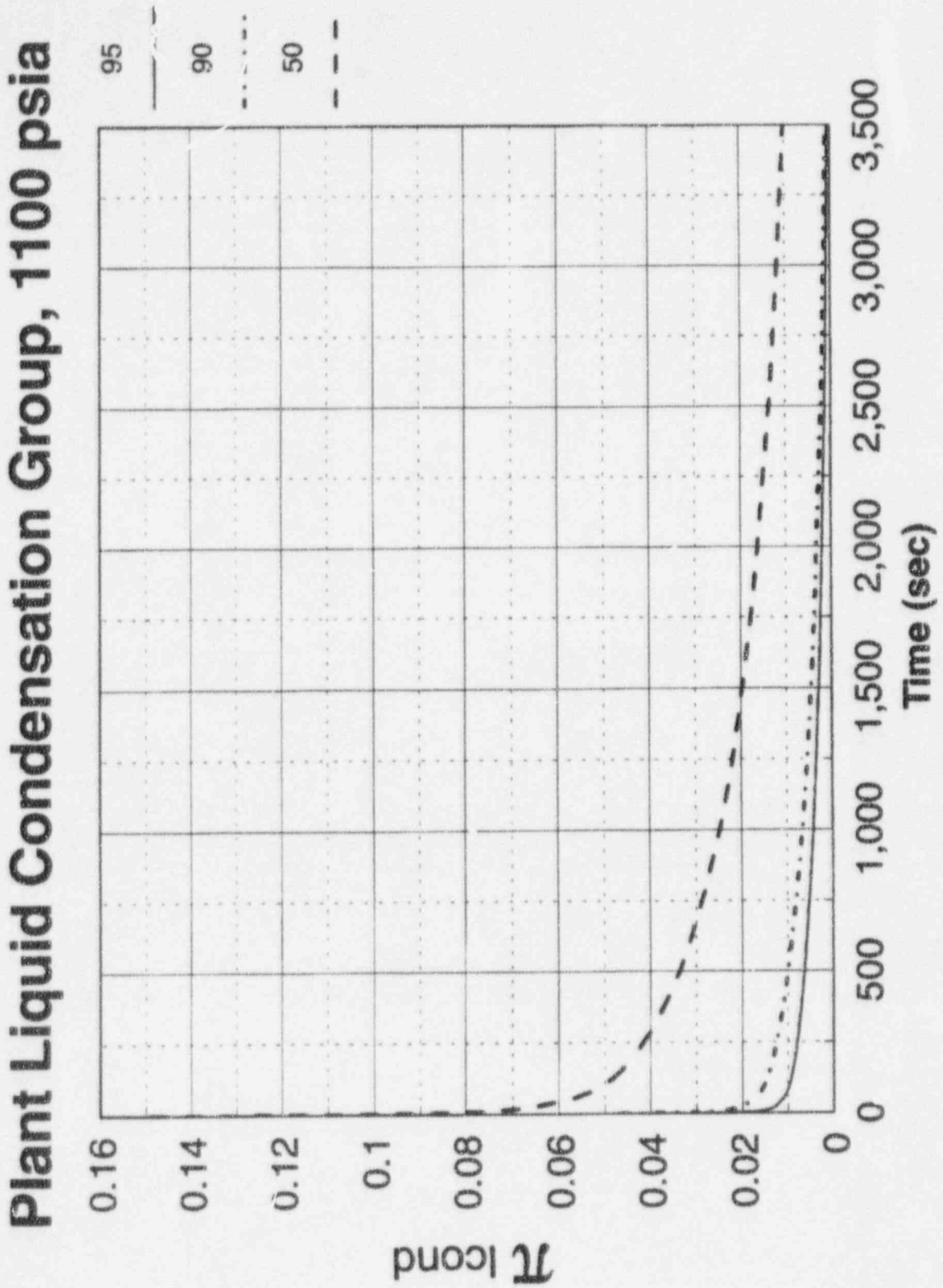

Figure 4.3-41 **Calculated Plant Π_{lcond} Group for Different Liquid Levels at 1100 psia and a Mixing Depth of 1.5 ft.**

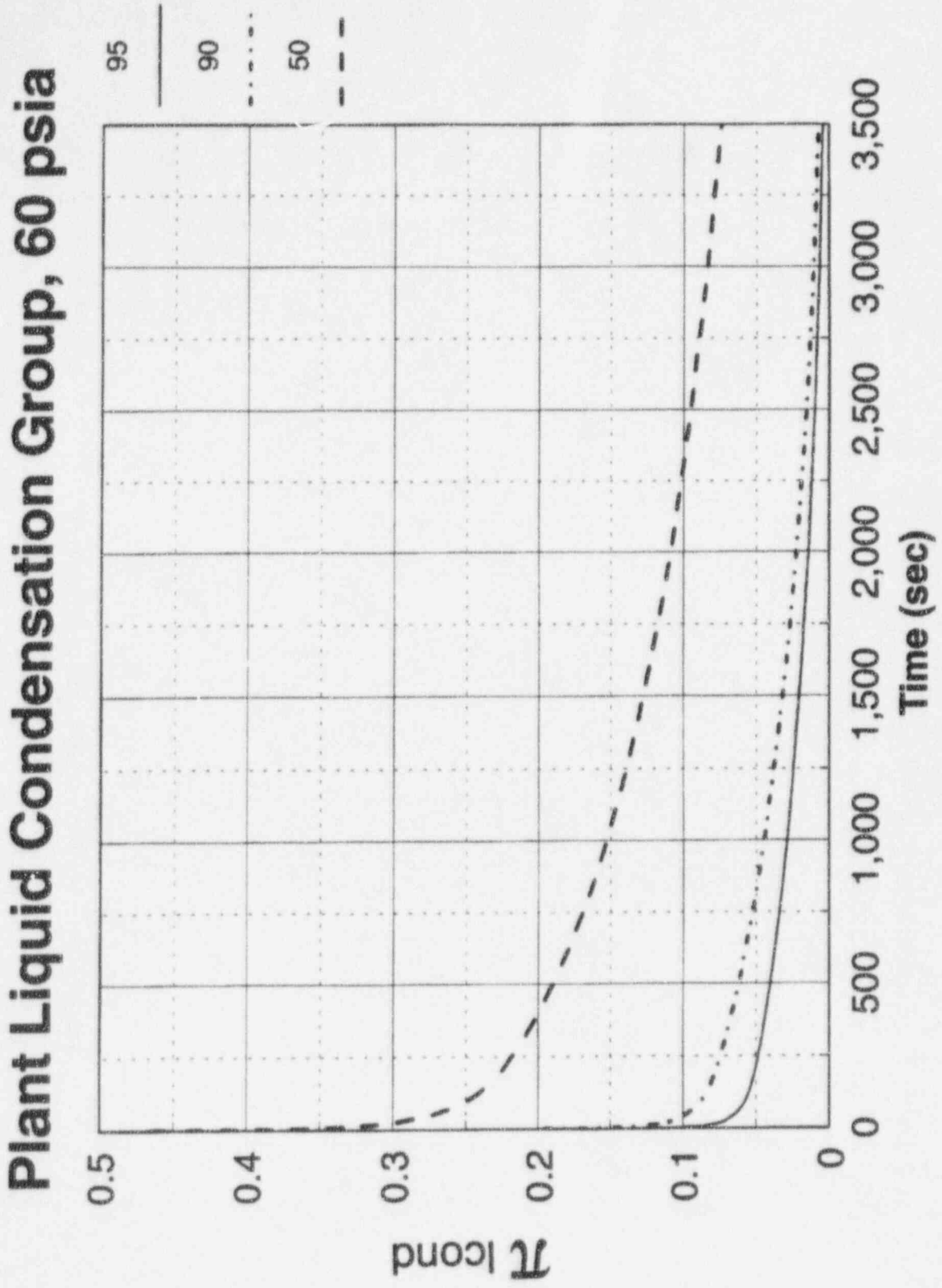

Figure 4.3-42 Calculated Plant Π_{lcond} Group for Different Liquid Levels at 60 psia and a Mixing Depth of 1.5 ft.

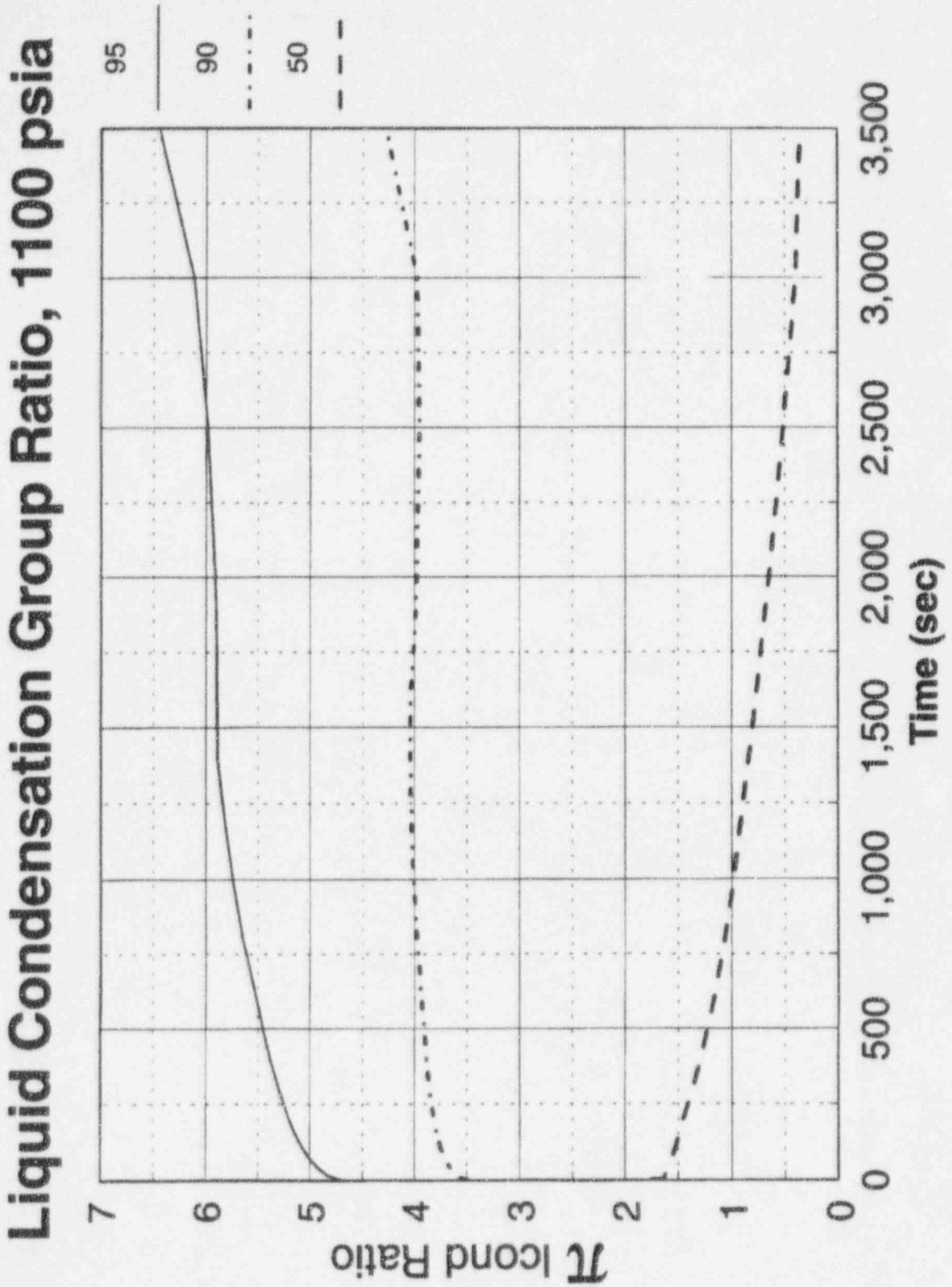

Figure 4.3-43 Calculated Ratio of the CMT Test Π_{cond} Group to the Plant Π_{cond} Group for Different Liquid Levels at 1100 psia and a Mixing Depth of 1.5 ft.

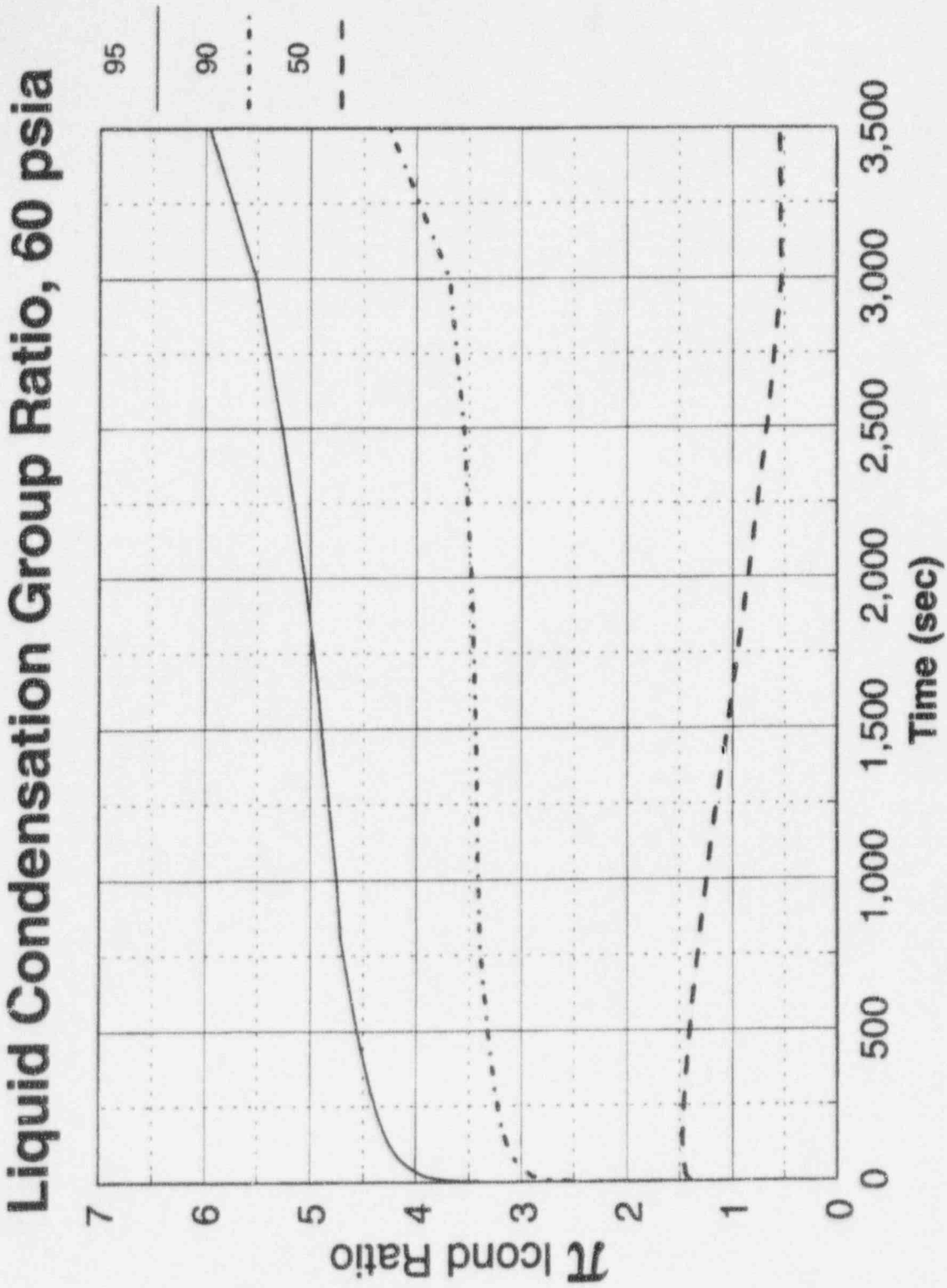

Figure 4.3-44 Calculated Ratio of the CMT Test Π_{cond} Group to the Plant Π_{cond} Group for Different Liquid Levels at 60 psia and a Mixing Depth of 1.5 ft.

5.0 CMT TEST MATRIX

Introduction

In the original CMT scaling report, the proposed CMT test matrix is examined to ensure that the tests would obtain data on the key thermal-hydraulic parameters identified in the PIRT, Table 1.4-1. Design changes have occurred in the AP600 that affect the CMT layout and balance lines, which can have an effect on the CMT performance. These changes are reflected in the CMT test design and test matrix.

5.1 Pre-Operational Tests

The cold and hot pre-operational tests were used to characterize the test facility and provide basic data that can be used to help model and interpret the test matrix. One cold pre-operational test characterized the loop resistance so the recirculation flow can be calculated. Other cold pre-operational tests characterized the draindown rate of the facility and the volumes in the test facility.

Initial hot pre-operational tests examined the thick wall condensation with an empty and initially evacuated CMT. This test provided data on the wall condensation heat transfer that were used as a basis to evaluate matrix tests. Wall condensation tests were also performed in the test matrix with and without the presence of noncondensibles to assess their effects on the wall condensation.

There were also CMT draindown experiments used to calibrate the drain line resistances and draindown rate for different tank levels. The hot pre-operational tests also examined the effects of the steam entering the CMT and the impact on the condensation on the CMT liquid surface. Specific tests examined the effect of the steam CMT liquid surface interaction and determined that a steam distributor or diffuser was needed to reduce the condensation and mixing. There were also recirculation pre-operational tests to verify how to initiate recirculation tests.

5.2 Test Matrix

The test matrix is shown in Table 5.2-1 and is structured to increase the complexity with each test series until, at the end of the matrix, the CMT is operated in a systems-effects manner. Each test series is now discussed and related to the key phenomena identified in Table 1.4-1. Table 5.2-2 shows the CMT PIRT from Section 1.0 and identifies which matrix tests address the key thermal-hydraulic phenomena identified on this PIRT.

Tests 101 to 111 examine the effects of wall condensation alone, with and without noncondensible gases present, over a range of pressures. The CMT does not maintain a water level and the condensate is drained to obtain only the wall condensation effects.

Tests 201 to 214 examine wall and liquid surface condensation at different fixed water levels in the CMT. By fixing the water level at different values, the wall condensation is separated from the liquid

surface condensation so each effect can be calculated from the test data. The wall condensation tests (101 to 111, described above) provide additional data on wall condensation alone, which help to interpret the fixed CMT level experiments. The design change to eliminate the pressurizer balance line significantly reduces the probability that steam could be introduced into the CMT when the liquid is cold. Also, the addition of the steam diffuser, which would limit the current steam/water mixing that could occur in the CMT, eliminates the need for the 200-series tests. These experiments are deleted from the test matrix and additional 300-series and 500-series tests are added.

Tests 301 to 316 simulate the CMT draindown at a constant pressure. The draindown rates and the tank pressure are varied. These tests provide additional transient data on the CMT wall condensation effect as well as the interfacial heat transfer to the liquid surface over a range of draindowns and pressures and provide data on the CMT steam injection, mixing, and thermal stratification within the CMT, with the diffuser.

Tests 401 to 404 are also draindowns, but the tank is allowed to depressurize. These tests provide data on the flashing behavior of the heated condensate layer and the effects of flashing on the CMT delivery rate.

Tests 501 to 506 are experiments that investigate the natural recirculation behavior of the CMT and the cold leg balance lines. The CMT develops a hot liquid layer because it is heated by the recirculating flow. The test facility is then depressurized and allowed to drain down. These tests allow the CMT to recirculate until the liquid in the CMT is approximately 20 percent, one-half, and nearly completely hot. The tests are then depressurized.

As Table 5.2-2 indicates, the matrix tests capture the key CMT thermal-hydraulic phenomena are identified in the initial PIRT in Section 1.0. Therefore, the tests, as performed, provide the necessary data identified in the PIRT for computer code model development and validation.

TABLE 5.2-1 (Sheet 1 of 2)
AP600 CMT TEST MATRIX

Test No.	Test Type	CMT Drain Rate (gpm)	Steam Supply Pressure (psig)	Comments
101-105	CMT wall condensation with and without noncondensible gases	N/A CMT drain rate based on steam condensation rate and drain capability	10/135/685/1085/2235, with subsequent depressurization	CMT initially contains no water and is evacuated (no air).
106-108			10	CMT initially evacuated and then pressurized with air (or N_2) to 0.236, 1.13, and 2.13 psia, respectively.
201-214	CMT wall and water surface condensation			This test series deleted due to AP600 design change that eliminated the pressurizer to CMT balance line.
301-312	CMT draindown at constant pressure	6/11/16/MAX	10/135/1085	Supply line no. 1 utilized; drain rate controlled by discharge line resistance.
317-319		6/11/16	45	
320-323		6/11/16/MAX	685	
401	CMT draindown during depressurization	16	1085 followed by depressurization to 20	Initial CMT water level is full. Depressurization rate of 1 psi/second.
402-404			685 followed by depressurization to 20	Initial CMT water level is 2 in. (nominal) below PDT3 top tap. Depressurization rates of 1, 2, and 0.5 psi/sec.

TABLE 5.2-1 (Sheet 2 of 2)
AP600 CMT TEST MATRIX

Test No.	Test Type	CMT Drain Rate (gpm)	Steam Supply Pressure (psig)	Comments
501-502	Natural circulation followed by draindown and depressurization	Discharge line resistance set for 6/16-gpm drain rate	1085 followed by depressurization to 20	Reservoir water level is "HI," reservoir water saturated. Steam line no. 2 and CMT drain valve are opened to initiate natural circulation until one-fifth of CMT is heated. Then, drain valve and steam line no. 2 are closed, steam line no. 1 is opened, and reservoir is drained sufficiently to allow full CMT drain. CMT drain valve is then opened to initiate CMT draining. When CMT water level reaches 97 in., depressurization is initiated by reducing the steam supply set pressure and venting the reservoir.
[illegible]4				Repeat with natural circulation until 0.50 of CMT heated.
505-506				Repeat with natural circulation until CMT is completely heated.
507-509		Discharge line resistance set for either 6-gpm or 16-gpm drain rate, to be determined by results of tests 501-506	1835 followed by depressurization to 20	Repeat with natural circulation until 0.20, 0.50, and complete CMT is heated.

TABLE 5.2-2
PHENOMENA IDENTIFICATION AND RANKING TABLE FOR THE AP600 CMT COMPARED TO THE TEST MATRIX

PIRT					Proposed Matrix Tests or Pre-Operational Tests which Provide Data
Phenomena	Large-Break LOCA	Small-Break LOCA	MSLB	SGTR	
CMT Draining Effects					
Condensation on cold thick steel surfaces	H	H	L	L	100-, 300-series
Transient conduction in CMT walls	H	H	L	L	100-, 300-series
Interfacial condensation on CMT water surface	H	H	M	M	300-, 400-, 500-series
Dynamic effects of steam injection and mixing with CMT liquid and condensate	H	H	M	M	300-series
Thermal stratification and mixing of warmer condensate with colder CMT water	H	H	M	M	300-, 400-, 500-series
CMT Recirculation					
Natural circulation of CMT and CL balance leg	L	H	H	H	500-series
Liquid mixing of CL balance leg, condensate, and CMT liquid	L	H	H	H	500-series
Flashing effects of hot CMT liquid la[illegible]	L	H	L	L	400-, 500-series
CMT wall heat transfer to liquid	L	M	M	M	300-, 500-series

Notes:
L = low importance
M = medium importance
H = high importance

6.0 CONCLUSIONS

The scaling of the AP600 CMT test facility is assessed relative to the AP600 plant CMT and the PIRT. The PIRT identifies the key thermal-hydraulic data needed to develop and verify the CMT test. The dimensionless scaling groups are developed and compared for the test CMT and the plant CMT over a range of pressures at which the CMT would operate. Both the recirculation and two different draining modes are examined for the CMT test and are compared to the plant CMT.

The Π groups for the recirculation mode of operation of the CMT are well-scaled since the heights and the line resistances are nearly preserved. The mass flux ratio of the test to the plant is approximately 0.9, and the development of the heated layers in the test and plant CMT are similar. One effect that was observed is that head geometry differences between the test and plant can make some differences, since the recirculation phase is a volume replacement calculation with hot liquid replacing the cold liquid in the tank. The CMT test facility does have distortion in the recirculation mode relative to the plant CMT; the test steam/water reservoir will develop a layer of cold water as the test recirculates, which acts to decrease the driving head in the test faster than in the plant, where there is no reservoir effect. However, these effects are small, and the recirculation mode can be adequately modelled in the test.

A top-down scaling analysis is performed to determine the CMT pressure dependence for two specific cases: with a vapor space at the top of the CMT as draining begins; and when the CMT has recirculated for a long period of time and is full of hot liquid. An evaluation of the Π groups from the pressure equations indicate that the CMT test can maintain similarity for depressurization transients.

The scaling basis for the steam diffuser used in the CMT tests and its relationship to the AP600 plant is developed, and comparisons are made between the expected performance of the CMT tests and the AP600 CMT with a diffuser. The comparisons show that the condensation behavior for the diffuser used in the CMT tests capture the expected condensation performance for the diffuser in the AP600 CMT.

The bottom-up scaling for the CMT draining develops the governing equations for the draindown mode of the plant and CMT test, as well as the dimensionless Π parameters that govern the wall and liquid surface condensation. The structural similarity between the plant CMT and the test CMT is also assessed. There is distortion of the wall conduction and condensation effects in which the thinner test CMT wall has a time constant that is approximately one third of that of the plant. This means that the test tank wall temperature becomes saturated more quickly than the plant for the same draindown times. The Π ratio for the wall condensation effects indicate that the CMT test can represent the plant wall condensation for the initial period (500 seconds) of a transient. After this time, the test walls are much hotter than the plant walls.

The liquid surface heat transfer and the effects of the steam diffuser are investigated. Two specific draindown modes are examined: when the tank is initially cold and the diffuser is submerged in subcooled liquid; and when the tank has drained and the tank level is below the diffuser. The liquid

surface condensation is estimated and the Π groups for wall condensation and liquid surface condensation are calculated for the plant CMT and the CMT test. The ratio of the Π groups are examined. The Π ratios indicate that the diffuser condensation effects scale reasonably well, with the ratio varying between 1 to 6 over the transient time for the cases examined. An examination of the CMT water surface effects, due to the circulation flow pattern of steam into the CMT from the diffuser, indicates that the CMT test will exhibit higher interfacial heat transfer coefficients for a drained CMT as compared to the plant CMT. However, in spite of this distortion, the test CMT captures the thermal-hydraulic phenomena of interest for the plant CMT.

As the Π group ratios indicate, the test models the CMT recirculation and different draindown behavior in a reasonable fashion so the key thermal-hydraulic phenomena for recirculation, CMT water heat up, liquid surface condensation, wall condensation, stratification during recirculation, and flashing is captured in the CMT test. Therefore, the AP600 CMT test provides valid data for development and verification of the CMT computer model.

7.0 REFERENCES

1. Fisher, J. E., T. J. Boncher and J. M. Cozznol, "Evaluation of Westinghouse CMT Test Facility and Test Matrix for Relap 5/Mod 3 Code Assessment," Letter Report transmitted from J. M. Cozznol to Dr. F. Odar U.S. NRC, May 28, 1993.

2. Reyes, J., et al, *AP600 Low Pressure Integral Systems Test at Oregon State University - Facility Scaling Report*, WCAP-14270, January 1995.

3. Bennett, C. O. and J. E. Meyer, *Momentum, Heat, and Mass Transfer*, McGraw-Hill, New York, New York, 1960.

4. Kreith, F., and M. S. Bohn, *Principles of Heat Transfer*, Fourth Edition, Harper and Row Publishers, 1986, pg. 217.

5. McAdams, W. H., *Heat Transmission*, McGraw-Hill, Inc., New York, 1954.

6. Catton, I., C. K. Chan, V. K. Dhir, and M. Simpson, "Hydrodynamics of a Vapor Test in Subcooled Liquid," NUREG-CR-1632, 1980.

7. Deiose, F., *Facility Description Report for AP600 Core Makeup Tank (CMT) Test Program Facility Description Report*, WCAP-14132, July 1994.

8. Nusselt, W., "Die Oberflächenkcondensatiin des Wasserdampfes," Z. Ver. Deutsch, Ing. Vol 80, pg 541, 569, 1916.

9. Kreith, F., *Principles of Heat Transfer*, International Textbook Company, Scranton, Pennsylvania, 1962.

10. Colburn, A. P., "The Calculation of Condensation Where a Portion of the Condensate Layer is in Turbulent Flow," Trans Am. Inst. Chem. Engrs., Vol. 30, pg 187, 1933.

11. Cumo, M., G. E. Farello, and G. Ferrari, "Direct Heat Transfer in Pressure Suppression Systems," Sixth International Heat Transfer Conference, Toronto, Volume 5, 1978.

12. Young, R. J., K. T. Yang, and J. L. Novotry, "Vapor-Liquid Interaction in a High Velocity Vapor Jet Condensing in a Coaxial Water Flow," Proceedings of the Fifth International Heat Transfer Conference, Tokyo Vol. III, 1974.

13. Kerney, P. J., G. M. Faeth, and D. R. Olson, "Penetration Characteristics of a Submerged Jet," AICHE Journal, Vol. 18, No. 3, 1972.

14. Cottrell, W. B., Nuclear Safety Program Annual Progress Report, ORNL-4374, 1969.

15. Bankoff, S. G., H. J. Kim, R. S. Tankin, and M. C. Yuen, "Counter-Current Steam-Water Flow in a Flat Plate," NUREG-CR-2783, 1982.

16. Lamb, H. *Hydrodynamics*, Dover Publications, New York, New York, 1932.

17. Grigull, U., Forsch. Ing. Wes. Vol 13, pg 49-57, Z. Ver Deutch Ingr. Vol 86, pg 444-445, 1942.

8.0 NOMENCLATURE

8.1 Nomenclature for Section 2.0

$\dot{m}(t)$	mass flow into CMT
β_T	coefficient of volume expansion
β_{T0}	coefficient of volume expansion
δ	metal wall thickness conduction depth (area/wetted perimeter)
ΔT	axial fluid temperature difference across the length of the core
μ	fluid dynamic viscosity
ρ	fluid density
ρ_1	hot RCS and balance line flow
ρ_2	Cold CMT fluid density state
ρ_ℓ	liquid density
A_{BL}	area balance line
a_c	cross-sectional flow area of CMT
A_{CL}	area cold leg
A_{CMT}	CMT cross-sectional area
A_{DVI}	area DVI line
A_{N_p}, A_{N_m}	CMT nozzle area for prototype (p) and model (m)
A_s	heat transfer surface area
$C_{p\ell}$	liquid specific heat at constant pressure
C_{vs}	solid specific heat
$C_{v\ell}$	liquid specific heat at constant volume
D	diameter of piping (CL, DVI, CLBL)
D_h	hydraulic diameter of the heated subchannel
d_{N_p}, d_{N_m}	CMT nozzle diameter for prototype (p) and test (m)
f	Darcy friction factor
g	gravitational acceleration
g_c	Newton's law conversion factor
h_m	test CMT convective heat transfer coefficient
h_p	plant CMT convective heat transfer coefficient
H_s	average convective heat transfer coefficient over the heated length
K	loss coefficient
K_{CKV}	CMT discharge line check valve loss coefficients
K_{CL_N}	cold leg nozzle loss coefficient
$K_{CMT_{EX}}$	CMT outlet nozzle loss coefficient
K_{CMT_N}	CMT inlet nozzle loss coefficient
K_{DVI_N}	DVI nozzle loss coefficients
k_s	solid thermal conductivity
K_T	cold leg-to-cold leg balance line tee
k_ℓ	liquid thermal conductivity
L	height of driving head for CMT flow
L_1	height of less dense liquid ρ_1
L_f	frictional lengths in cold leg, balance line and DVI line
L_m	CMT model heated liquid layer
L_p	plant CMT heated liquid layer
P	fluid pressure
Pr	Prandtl Number
q_s	heat loss
Q_ℓ	volumetric flow rate

S	scale factor
T_0	initial axial fluid temperature difference
T_b	bulk fluid temperature
t_p, t_m	time for prototype (p) and model (m)
T_s	surface temperature
T_s-T_ℓ	average temperature difference over the heated length
T_w	wall temperature
T_ℓ	liquid temperature
U_0	initial velocity
U_b	bulk fluid velocity
U_{CL}, U_{BL}, U_{DVI}	average liquid velocities in cold leg, balance line and DVI line
U_m	liquid velocity in test CMT
U_p	liquid velocity in plant CMT
U_ℓ	liquid velocity
v	fluid kinematic viscosity
V_S	metal volume
V_ℓ	liquid volume
x	distance in solid structure
Z	thickness of the hot liquid layer inside the CMT
ℓ	heated length of the CMT

q_{sys}	heat transfer to vapor space
q_t	is the heat loss to the ambient
q_{WS}	condensation on the CMT walls
r	radial position within CMT wall
R_i	inside radius of the CMT
R_o	outside radius of the CMT
t	wall thickness
T_{amb}	ambient temperature
T_d	condensate interface temperature
T_s	structure temperature
T_{sat}	saturation temperature
T_{WS}	inner CMT wall temperature with a condensate film
T_ℓ	fluid temperature
u	velocity
U	fluid velocity
V_s	structure volume
V_t	CMT volume
V_v	vapor volume
V_ℓ	is the volume of liquid inside the control volume
w_{sys}	work performed by vapor space
W_t	is the shaft work done by the liquid
z	height

8.2 Nomenclature for Section 3.0

α	CMT wall thermal diffusivity
$\Delta[PQ]$	is the net rate of fluid mass entering or leaving the control volume
v_v	vapor specific volume
ρ_v	vapor density
ρ_ℓ	is the density of the liquid inside the control volume
a_{sa}	CMT outside surface area
a_{si}	CMT inside surface area
A_{tank}	CMT tank cross section area
a_{ws}	CMT metal wall surfaces exposed to steam
Cp_ℓ	liquid specific heat at constant pressure
C_{vs}	structure specific heat
$C_{v\ell}$	specific heat of the liquid
e	energy flowing across central surfaces
e_{int}	internal energy
e_v	vapor internal energy
e_ℓ	is the average liquid energy per unit mass
g	gravitational acceleration
g_c	gravitational constant
h	enthalpy
h_{bal}	enthalpy of the balance line fluid
h_{conv}	convective heat transfer coefficient from hot CMT water to wall
h_{in}	inlet enthalpy
H_{LF}	condensation of steam on metal surfaces
H_{LS}	condensation of steam on CMT liquid surface
h_{out}	outlet enthalpy
H_{sa}	CMT outside convective heat transfer coefficient to ambient
H_{sf}	surface heat transfer coefficient
H_{st}	CMT inside convective heat transfer coefficient
h_v	vapor enthalpy
$\dot{m}_{in}$	mass flow into CMT
k_s	CMT wall thermal conductivity
$L_\ell(t)$	level in CMT
$M_{v_{sys}}$	mass of vapor in the system
$\dot{m}_{out}$	mass flow out of the CMT
ρ_s	structure density
P_{sys}	system pressure
P_v	vapor pressure
Q	volumetric flow
q_{LS}	condensation on the CMT water surface